Dynamic Helical Assemblies with Chiroptical Functionality: A Supramolecular Chiral Auxiliary Approach

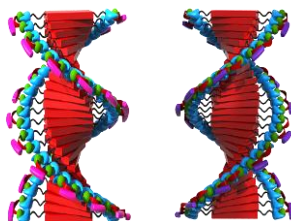A Thesis Submitted for the Degree of

Doctor of Philosophy

By

Mohit Kumar

New Chemistry Unit

Jawaharlal Nehru Centre for Advanced Scientific Research

(A Deemed University)

Bangalore - 560064 (INDIA)

JULY 2014

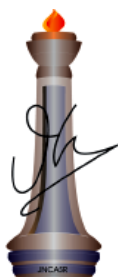# Dynamic Helical Assemblies with Chiroptical Functionality: A Supramolecular Chiral Auxiliary Approach

A Thesis Submitted for the Degree of

Doctor of Philosophy

By

Mohit Kumar

UNDER THE SUPERVISION OF

Prof. SUBI J. GEORGE

New Chemistry Unit

Jawaharlal Nehru Centre for Advanced Scientific Research

(A Deemed University)

Bangalore-560064 (INDIA)

JULY 2014

DEDICATED TO MY PARENTS

DECLARATION

I hereby declare that the thesis entitled "*Dynamic Helical Assemblies with Chiroptical Functionality: A Supramolecular Chiral Auxiliary Approach*" is an authentic record of research work carried out by me at the New Chemistry Unit, Jawaharlal Nehru Centre for Advanced Scientific Research, Bangalore, India under the supervision of **Prof. Subi J. George** and that it has not been submitted elsewhere for the award of any degree or diploma.

In keeping with the general practice in reporting scientific observations, due acknowledgment has been made whenever the work described is based on the findings of other investigators. Any omission that might have occurred due to oversight or error in judgment is regretted.

Mohit Kumar

Jawaharlal Nehru Centre for Advanced Scientific Research

Prof. Subi J. George
New Chemistry Unit
Jawaharlal Nehru Centre for Advanced
Scientific Research (JNCASR)
Bangalore-560064,India
Phone : +91 80 2208 2964
Fax: + 91 80 22082627
E-mail: george@jncasr.ac.in

Date

July 18, 2014

CERTIFICATE

I hereby certify that the work described in this thesis titled "*Dynamic Helical Assemblies with Chiroptical Functionality: A Supramolecular Chiral Auxiliary Approach*" has been carried out by **Mohit Kumar** at the New Chemistry Unit, Jawaharlal Nehru Centre for Advanced Scientific Research, Bangalore, India under my supervision and it has not been submitted elsewhere for the award of any degree or diploma.

Subi J. George

(Research Supervisor)

ACKNOWLEDGEMENTS

Mohit

Preface

This thesis presents the design, synthesis and properties of helical supramolecular polymers of π-conjugated chromophores for their chiroptical functionalities.

The thesis is majorly divided into six Chapters.

Chapter 1 introduces the field of asymmetric non-covalent synthesis of supramolecular polymers through chiral auxiliary approach. The major emphasis is given to various design strategies employed for the guest induced helicity in self-assembly of π-conjugated chromophores. An overview of the important developments in this field along with its potential chiroptical functionality based applications is presented.

Chapter 2 presents the molecular design strategy wherein various diimide based π-conjugated molecules are functionalized with dipicolylethylenediamine–zinc complex (DPA) as the positively charged molecular recognition unit, which upon interaction with negatively charged chiral adenosine phosphates (chiral auxiliary) induces helicity into their assembly. DPA functionalization is central to the design of this thesis and here we established its importance. DPA functionalized naphthalenediimide (NDPA) and perylenebisimide (PDPA) derivatives were synthesized, which showed adenosine phosphate recognition induced assembly. We show that adenosine triphosphate (ATP) induces right-handed assembly, whereas binding to adenosine mono and di phosphate (AMP/ADP) show left-handedness. We have also shown a novel strategy for the dynamic helix reversal in supramolecular assemblies, based on competitive binding of the guest molecules.

Having shown the opposite handedness in assembly of NDPA on binding with ATP when compared with ADP/AMP**, Chapter 3** explores the possibility of utilizing this dynamic helical assembly for monitoring real time reaction kinetics. Here we present a unique supramolecular system which show differential signaling along with stimuli dependent fast stereomutations upon ATP-ADP/AMP interconversion. This has been capitalized to probe the reaction kinetics of enzymatic hydrolysis of bound ATPs. Detailed chiroptical analysis has provided mechanistic insights into the enzymatic hydrolysis and various intermediate steps. This *in situ* method could probe the concentration fluctuation of Adenosine phosphates which dictate the energy economy of various living organisms. Thus a unique "all-in-one" dynamic helical assembly to monitor the real time reaction processes via its stimuli-responsive chiroptical signaling is conceptualized.

Chapter 4 is divided into two parts. Ist part deals with the self-assembly of DPA functionalized

coronenebisimide (ZnCPA) leading to construction of self-assembled multivalent scaffold for phosphate recognition. 2nd part demonstrates a chaperoning effect in stabilizing the kinetically trapped state, leading to imprinted chiral memory in ZnCPA assemblies. ZnCPA molecules self-assemble in presence of water, whereas binding to ADP induces helical bias into their organization. Interestingly, we show that by using a negatively charged protein we can competitively replace ADP through multivalent interactions. Through chiroptical probing, kinetics of helical memory was investigated and an intra-stack racemization mechanism was established. Control over the strength of memory could be easily achieved just by changing the solvent medium.

Chapter 5 presents a biomimetic design for allosteric control over supramolecular helicity of molecular assemblies. We have functionalized perylenebisimide with molecular recognition unit (PDPA) which respond to biologically relevant chiral guests like ATP thereby inducing chirality into achiral assembly in a highly allosteric fashion. Allosteric effect could be achieved by using helically dormant ATP bound chromophoric assembly, which shows turn on helicity in a cooperative manner either by further addition of chiral ATP or other diphosphates like pyrophosphate (PPi), ADP leading to homotropic and heterotropic allosteric regulation, respectively. Thus, the present system can be a unique artificial analogue of various allosterically regulated events in biological systems.

Chapter 6 deals with the functional properties of such molecular recognition driven self-assembly. It is further divided into two parts. 1st part reports the guest induced chirality for circularly polarized luminescence (CPL) in various fluorophores. DPA functionalized molecules, on binding to adenosine phosphates not only show ground state helicity as seen from circular dichroism signal, but they retain supramolecular chirality in the excited state as well. Interestingly, upon removal of chiral information, they are seen to retain CPL in a so called chiral memory in the excited state. To our knowledge, this is the only report of guest induced CPL induction and its chiral memory in π conjugated systems. 2nd part describes a novel supramolecular clipping design for influencing the photo-physical properties of functional molecular assemblies, by the pre-organization (clipping) of chromophores. Chromophores like naphthalenediimide and dialkoxynaphthalene were functionalized with DPA units, which upon clipping with adenosine phosphates allows ground state pre-organization of chromophores, leading to formation of pre-associated excimer. Interestingly, mixing of these two chromophores form charge transfer complex only in presence of adenosine phosphates, establishing the crucial role of molecular clippers in controlling the supramolecular interactions.

TABLE OF CONTENTS

CHAPTER-1

Introduction

1

Helical Supramolecular Polymers by Chiral Auxiliary Approach

CHAPTER-2

Molecular Recognition Driven Helical Assembly with Tunable Handedness

CHAPTER-3

Dynamic Helical Supramolecular Polymer with Stimuli Responsive Handedness: In situ probing of Enzymatic ATP Hydrolysis

CHAPTER-4

Self-assembly of Coronene Bisimide Bolaamphiphile

CHAPTER-5

Homotropic and Heterotropic Allosteric Regulation of Supramolecular Chirality

CHAPTER-6

Towards Chiroptical Functionality

~ 1 ~

CHAPTER-1

Introduction

Helical Supramolecular Polymers by

Chiral Auxiliary Approach

Chapter-1 (Introduction)

Helical Supramolecular Polymers by Chiral Auxiliary Approach

Abstract

Supramolecular helical polymers, constructed by self-assembly of chiral monomers have been well investigated for understanding chiral amplification and various chiroptical functionalities. In this regard, helical assembly of achiral molecules obtained by non-covalent interaction with chiral auxiliaries (guest) holds greater potential. This chapter presents a comprehensive review of various design principles that have been utilized for guest induced helicity into one-dimensional assembly of achiral chromophores and their potential applications. The chapter is divided into two main parts. First part deals with variety of approaches used for induced helicity and the type of non-covalent forces involved between the host and guest molecules. This is further categorized based on the type of chiral auxiliaries employed. The second part mainly focuses on the construction of metastable enantiomeric stacks of achiral monomers (chiral / helical memory) state by post synthetic removal of chiral auxiliaries. The major emphasis is on the rational approach for tunable strength of memory and various applications. Furthermore, we have presented the challenges ahead and the greater scope of this field leading to the thesis work.
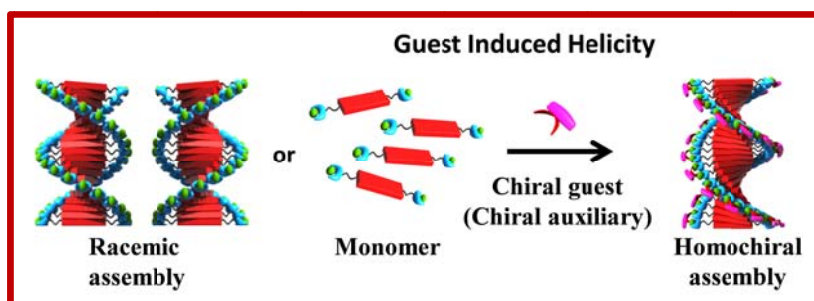
1.1 Introduction

Chirality as a concept is very much central to the efficient functioning of biological systems.[1] Most intriguing among them is the origin of homochirality, wherein nature shows preferential synthesis of one enantiomeric pure building block for construction of biopolymers. For example, the preference for L-amino acids when compared to their mirror image form, for the synthesis of proteins. Interestingly, the molecular level chirality can be easily expressed in their hierarchical organization with biased handedness like in α-helix of protein, right-handed DNA double helical structure etc. In the synthetic world, Louis Pasteur demonstrated the spontaneous resolution of tartaric acid salts upon crystallization from the racemic solution into enantiomeric pure form.[2] He could successfully distinguish crystals of opposite chirality by observing them under optical microscope. Thus, it confirms that the molecular chirality can be expressed into their higher level of organization, even in non-biological systems.

a) Helical Polymer (repeating unit)
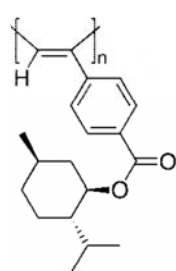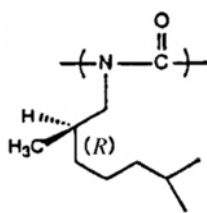
Polyacetylene   Polyisocyanate   Polysilane   Polyisocyanide
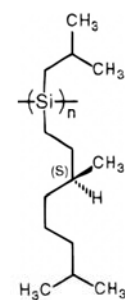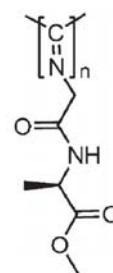
b) Helical Supramolecular Polymer (monomeric unit)
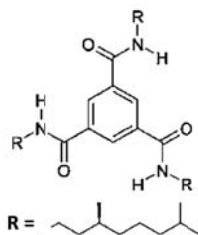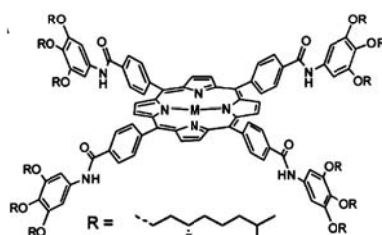
Benzene-1,3,5-tricarboxamides   *meso*-tetraphenylporphyrins   Oligo(*p*-phenylenevinylenes)
(BTA)   (OPV)
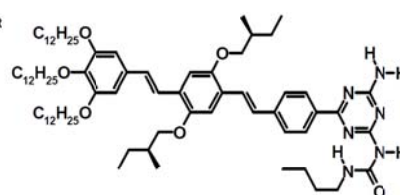
Figure 1.1. *Chemical structures of a) conventional helical polymers and b) chiral monomeric self-assembling units for helical supramolecular polymers (Reproduced with permission from ref. 3c, 4b, 31a, 55, 57).*

In the field of material chemistry, polymers have been well investigated for their chiral ordering, leading to a variety of chirotechnological applications.[3] Great amount of research has gone into synthesis of conventional helical polymers, obtained by covalent linking of chiral

monomeric units. Chiral polymers like polyacetylenes, polyisocyanates, polysilanes, polyisocyanides etc. (Figure 1.1a) were extensively utilized to show chiral amplification following "sergeant and soldiers" and "majority rule" principles.[3] Molecular chirality in such systems is usually expressed in their organization into either a left- or right-handed helix.[4] Apart from the conventional helical polymers, another class of chiral macromolecules can be constructed by non-covalent self-assembly of small molecules leading to "helical supramolecular polymers".[4e-j,] These are also synthesized by the chiral monomeric units like chiral derivatives of benzene-1,3,5-tricarboxamides (BTA), oligo(*p*-phenylenevinylenes) (OPV), porphyrins, 3,4,9,10-perylenetetracarboxylic diimides etc. (Figure 1.1b), which self-assemble to form helical aggregates. Asymmetric preferences in these systems also provide insights into the probable mechanism of homochirality in nature.

Synthetic polymers composed of chiral monomeric unit self-assemble into helix, whose handedness is mainly governed by the configuration of the chiral centre in the monomers. Moreover, it has been shown in polymers (covalent and supramolecular), that the simplest chiral perturbation created by isotopic substitution of hydrogen with deuterium in their monomers can amplify their homochiral helical organization.[5] However, one of the major limitation of such systems is their inability to switch its handedness, which can only be achieved by synthesizing the monomers of opposite chirality (which is synthetically challenging). Therefore, another novel design for creating helical bias into the assembly of achiral molecule is by "chiral auxiliary" approach.[6] Chiral auxiliaries are optically active and enantiomerically pure guest molecules, which upon non-covalent interaction with the achiral molecules induces a helical bias into the assembly of host molecules. With this design, the assembly of opposite handedness can be easily constructed just by changing the chirality of the guest molecules, thereby circumventing the challenge of separately synthesizing the two enantiomers of host molecules.

For most applications, helical polymers are functionalized with chromophores, which provide a chiroptical probe to monitor their chiral self-assembly. The helical organization of chromophores are mainly characterized by circular dichroism (CD), based on the "exciton chirality method".[7] When two identical chromophores (i and j, Figure 1.2a) interact to constitute a chiral organization, their electronic transition dipoles couple with each other. This results in splitting of the excited state energy levels into a lower and higher energy states.[8] As a consequence, the absorption signal splits into two component spectra, one blue shifted (β-transition) and the other one red shifted (α-transition), but with the same sign (Figure 1.2b). The resultant two absorption signal usually appear as a single absorption band, however strongly coupled dipoles with high energy difference between the α and β energy levels does create two well separated absorption bands. Interestingly, the CD signal corresponding to α- and β-

transitions are opposite in sign, depending upon the orientation of transition dipoles (either clockwise or counter clockwise direction). Thus, a negative bisignated or split CD signal is obtained, with negative and positive cotton effect at higher and lower wavelengths respectively, which is characteristic of left-handed helical organization. Similarly, right-handed helical organization is characterized by a positive bisignated CD signal (Figure 1.2c).
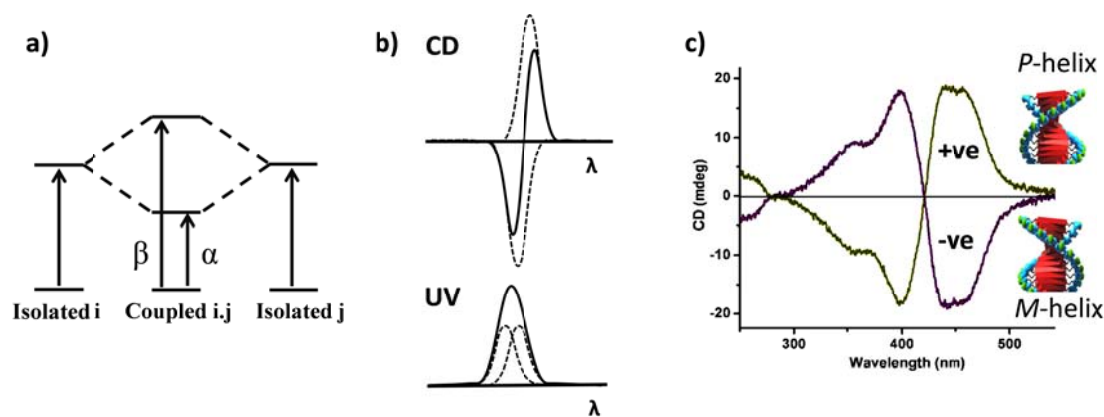
Figure 1.2. *a) Splitting of the electronic excited state upon exciton coupling between two identical chromophores, whereas b) shows the corresponding absorption and CD signal. c) Representative CD spectra showing positive and negative bisignated signal and their respective helical organization (Reproduced with permission from ref. 7a, 57).*

Thus, such a design of guest induced helical assembly of chromophores and their chiroptical readout have been utilized for various applications like determining the enantiomeric purity of samples, absolution chirality of natural products, drug molecules etc.[9] Another interesting aspect is the retention of helical conformation in a metastable state, obtained by the removal of chiral auxiliary (Figure 1.3a).[10] Retention of CD signal in such an assembly of achiral polymer is termed as "chiral memory" and is due to kinetic inertness of the assembly. These assemblies can provide useful insights into the mechanism of aggregation-deaggregation, stereomutation kinetics and offer chirotechnological applications. For example, yashima *et al.* have utilized guest responsive achiral polyacetylene (**1**) derivatives as stationary phase of chiral HPLC, whose helix handedness can be tuned even in the solid phase.[11] Interaction of stationary phase with chiral alcohol induces helicity into polymeric backbone, which retained its handedness even after removal of chiral alcohol due to imprinted memory (Figure 1.3b-c). This stationary phase with memorized chirality could be used to separate the enantiomers of trans-stilbene oxide. Interestingly, the order of elution among two enantiomers could be easily reversed by dynamically switching the chirality of stationary phase, which was achieved by treatment of column with alcohol of opposite chirality. Thus, it demonstrates an unprecedented example of reversible switching of elution order in a chiral HPLC.
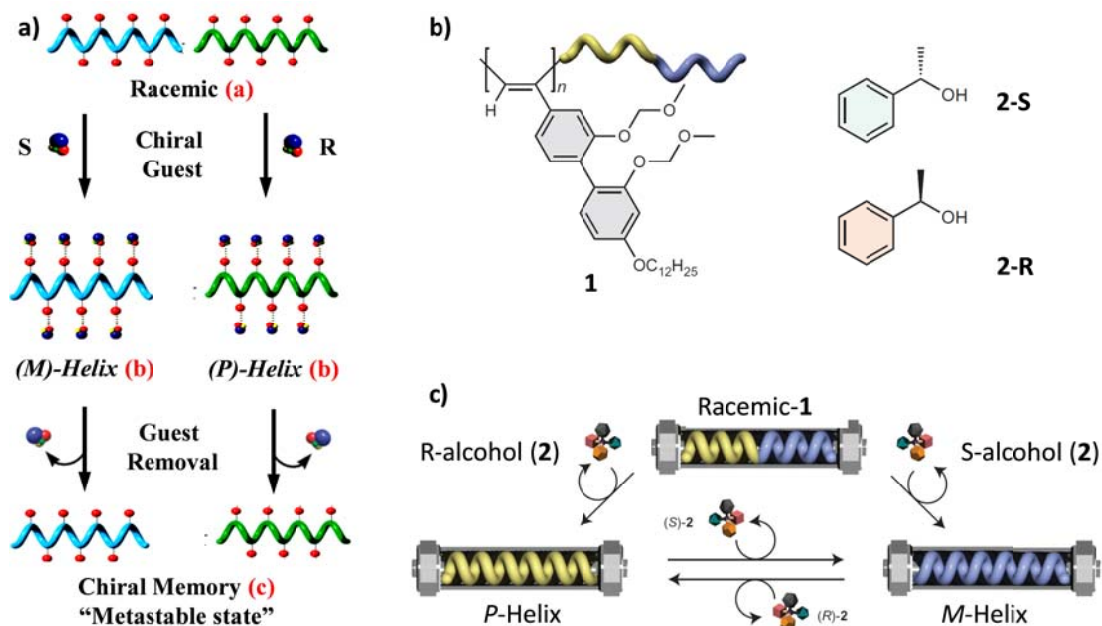
Figure 1.3. *a) Schematic representation of guest induced helicity and chiral memory in racemic polymeric assembly. b) Chemical structure of (**1**) and c) pictorial representation of chiral HPLC made from imprinted helicity in polyacetylene (**1**) with switchable handedness. (Reproduced with permission from ref. 3a, 11).*

Although guest induced helical assembly and chiral memory are well studied topics in conventional helical polymers, their translation into non-covalent supramolecular polymers require special design strategy, mainly because of the weak intermolecular interactions and highly dynamic nature, wherein the assembly can be adversely affected by guest addition and their removal. This chapter will deal with various design strategies employed for the construction of helical assemblies using a chiral auxiliary approach. The focus will be on the induction of helicity and chiral memory into the assembly of achiral molecules. Although, there are a few reports of these processes in discrete assemblies and molecular complexes, it is beyond the scope of this thesis and readers are directed to the excellent literature in this regard.[12]

This chapter is divided into two main parts:

a) **Chirality Induction in Supramolecular Polymers**: This section deals with induction of chirality into assembly of achiral chromophores. Various chiral auxiliary approaches utilized for the non-covalent synthesis of extended helical architectures and their enantiospecific functionality will be discussed.

b) **Supramolecular Chiral Memory**: This part will deal with the construction of metastable homochiral assemblies of achiral molecules, by post synthetic removal of chiral guest,

termed as "chiral memory". Detailed analysis of various design strategies utilized for the non-invasive removal of guest molecules and stabilization of the resultant kinetic assemblies will be discussed.

1.2 Chirality Induction in Supramolecular Polymers

Chiral preferences can be created into the assembly of achiral molecules by interaction with optically active guests. Here we describe various design strategies that have been employed for transfer of chirality from dissymmetric guest molecules into extended assembly of achiral chromophoress. This section is divided into three parts based on the type of guest and its interactions with the host.

1.2.1 Electrostatic and Hydrogen Bonding Interactions
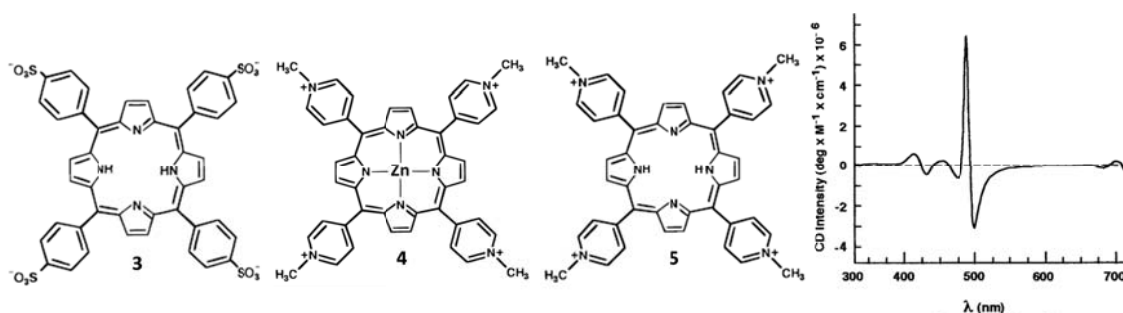
Figure 1.4. *Chemical structure of anionic (**3**) and various cationic (**4, 5**) porphyrin and the ICD of heteroassembly **4**+**3** in presence of poly-L-glutamate (Reproduced with permission from ref. 14, 15).*

One of the earliest known example of induced circular dichroism (ICD) in assembly of achiral π-conjugated systems was shown by Purrello *et al.* in positively charged porphyrins (**4-5,** Figure 1.4). These molecules which does not self-associate due to intermolecular electrostatic repulsions, tend to aggregate in presence of oppositely charged polymeric templates like DNA and RNA. The chiral nature of these templates induces a helical organization into the assembly of porphyrin. For example, when polyadenylicacid (PolyA) – polyuridylic acid (polyU) were mixed in presence of **5**, it resulted in the formation of poly(A.A.U) based triple helix under conditions which do not allow such assemblies in absence of **5**.[13] Interestingly, this assembly showed an ICD signal at the porphyrin absorption band, indicating formation of chiral assembly. Detailed investigation revealed the role of molecular recognition along with electrostatic interactions between the template and chromophores being responsible for such an effect. This design strategy could be extend to heteroaggregates in a ternary mixture. The same group demonstrated the formation of chiral assemblies of anionic porphyrin (**3**) on negatively charged poly-L-glutamic acid upon heteroaggregation with cationic

porphyrin (**4**).[14, 15] CD spectrum of the ternary mixture shows an intense bisignated CD signal. Moreover, these spectra show a mirror image relationship upon addition of poly-glutamic acid with opposite chirality, confirming the induction of helicity from chiral polymer to chromophoric assembly.

Similar examples of induced chirality in porphyrin derivatives were reported with small chiral auxiliaries as well. For example, dendritic macromolecules functionalized with zinc porphyrin units show strong ICD in presence of chiral ligating agents.[16] Presence of multiple Zinc porphyrin unit in the dendrimer resulted in highly cooperative binding of asymmetric ligands with enantiospecific chiroptical sensing and enhanced sensitivity. Shinkai *et al.* could demonstrate ICD in neutral porphyrin bearing four urea groups at its periphery.[17] These formed high aspect ratio one dimensional aggregates, which upon interaction with chiral urea derivatives show bisignated CD signal, indicating a helical twist in their supramolecular ordering.
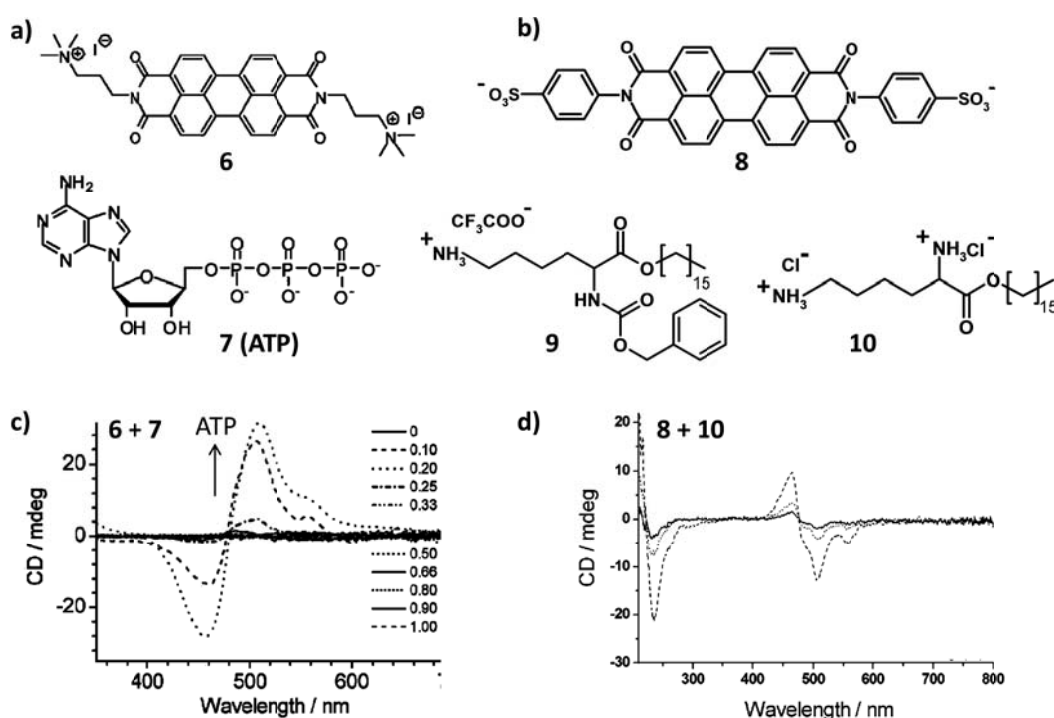
Figure 1.5. *Chemical structure of a) cationic and b) anionic perylenebisimide along with their oppositely charged chiral auxiliaries used for ICD. CD spectra of solution containing c)* **6**+**7** *and d)* **8**+**10** *showing bisignated spectra confirms chiral organization. (Reproduced with permission from ref. 18, 20).*

Apart from DNA and other related polynucleotides, smaller nucleotides like adenosine triphosphate have been utilized as chiral guest molecules. Water soluble dicationic perylenebisimide (PBI, **6**, Figure 1.5a) molecules show strong intermolecular interaction in

presence of anions like ATP (**7**).[18] Binding of this homochiral guest shows a strong ICD with a positive bisignated CD signal, indicating efficient transfer of molecular chirality into right-handed helical assembly (Figure 1.5c). Detailed solvent dependent study revealed that a balance of good and poor solvent is necessary for transfer of chirality into their organization. Similar cationic PBI derivatives also interact with synthetic chiral phosphate based surfactant molecules leading to ionic self-assembly with ICD.[19] These complexes show liquid crystalline ordering with a columnar mesophase. Having shown the induction of chirality into the assembly of cationic PBI, it could be extended to anionic counterpart as well. PBI molecules substituted with benzenesulfonic acid salt (**8**) act as negatively charged chromophores (Figure 1.5b), which show ionic self-assembly in presence of positively charged lysine based chiral surfactant (**9**, **10**).[20] Presence of (**10**) induces a left-handed helical organization of (**8**), as evident from the negative bisignated CD signal, both in solution and in bulk solid state (Figure 1.5d).
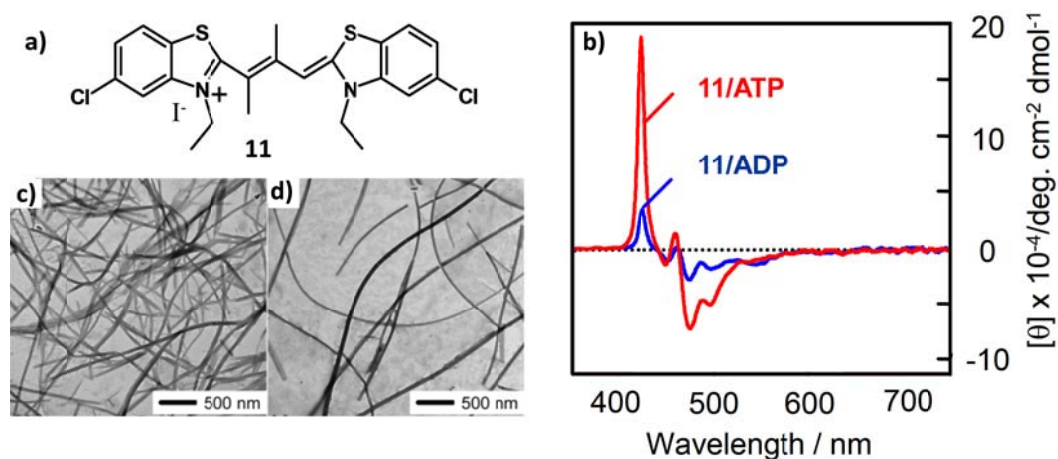
Figure 1.6. *Molecular structure of cationic cyanine dye (a) and its induced CD signal (b) upon binding to homochiral adenosine phosphates. TEM images of nanofibers formed by self-assembly of **11** in presence of ATP at c) 25 °C and d) upon thermal annealing (Reproduced with permission from ref. 21).*

Adenosine phosphate as a homochiral guest was shown (Figure 1.5, Figure 1.6) to be highly versatile auxiliary for inducing chirality into the assemblies of achiral chromophores. Due to their non-specific electrostatic interactions, they show efficient binding with a wide variety of cationic dyes. Kimizuka *et al.* have used ATP for the organization of cationic cyanine dyes (**11**), which resulted in an H-aggregate along with negative bisignated ICD signal, indicating excitonic coupling of parallel oriented chromophores.[21] They also show that binding to ATP result in most efficient ICD when compared with ADP and AMP binding, mainly due to number of negative charges affecting the electrostatic interactions. **11**–ATP complex formed one dimensional nanowires assisted by the acquired amphiphilicity upon interaction with ATP,

which showed enhanced regularity upon thermal annealing (Figure 1.6 c, d). In their quest to study dye-biomolecules interactions, they investigated the interaction of a redox responsive coenzyme β-nicotinamide adenine dinucleotide (NAD$^+$) with modified cyanine dye having naphthothiazole rings.[22] Binding to NADH induced a positive bisignated CD signal, whereas its interaction with NAD$^+$ showed distinct spectral features. Such differential signalling were assigned to variation in supramolecular ordering leading to H and J aggregation of cyanine dyes upon complexation with NADH and NAD$^+$ respectively. This confirms that the redox states of the coenzyme can greatly influence the molecular organization of dyes, which can be useful in biosensory applications.
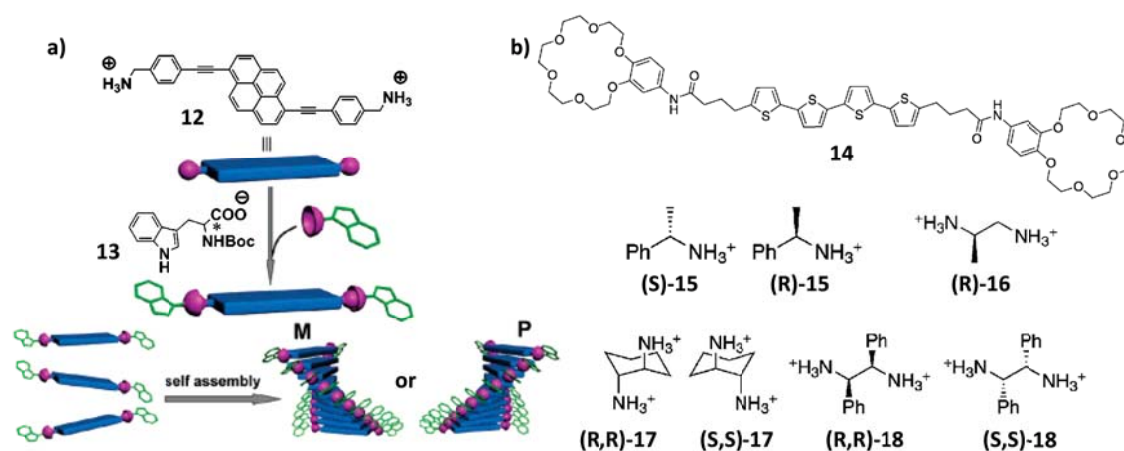
Figure 1.7. *Molecular recognition driven helical assembly of a) pyrene based cationic amphiphile (**12**) which self-assembles in presence of optically active tryptophan (**13**) leading to helical assemblies as represented in the schematics. b) Chemical structure of crown ether appended oligothiophene (**14**) and various quaternary ammonium derivatives as guest molecules (Reproduced with permission from ref. 23, 25).*

Molecular recognition driven chirality induction were also demonstrated with various amino acids. An amphiphilic pyrene molecule (**12**) substituted with quaternary ammonium group shows ICD upon interaction with chiral tryptophan (**13**), confirming helical organization (Figure 1.7a).[23] The electrostatic nature of the interaction leading to **12-13** complex was confirmed by the CD measurements done in solution with high ionic strength, which showed a decrease in CD signal at higher concentration of NaCl. Similarly, phosphonic acid appended naphthalenediimide (NDI) self-assembly in presence of L- and D-arginine resulted in efficient chirality induction.[24] Shinkai *et al.* have used host-guest interactions between crown ether and ammonium cation for induced helicity. Oligothiophene connected to crown ether group (**14**) form organogels, wherein the helical organization of fibrous assembly was driven by the configuration at the asymmetric 1,2 bisammonium (**15-18**) guest molecules (Figure 1.7b).[25]
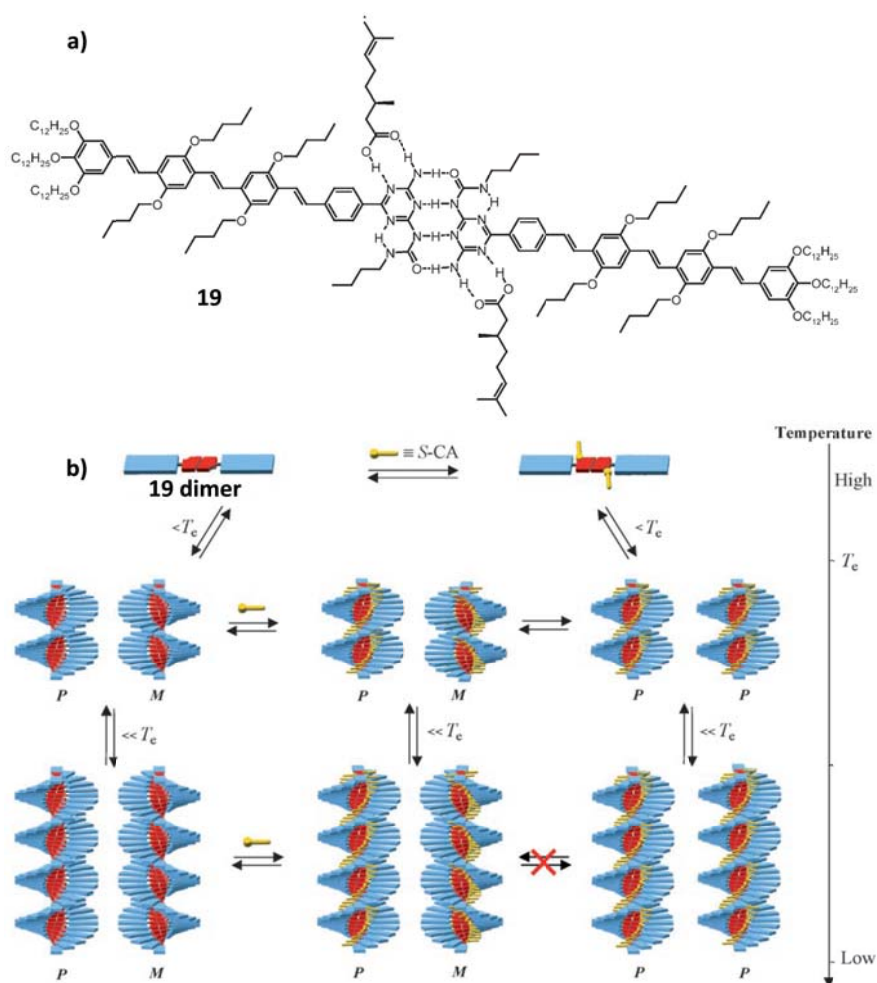
Figure 1.8. *a) Chemical structure of ureidotriazine appended OPV molecules along with its hydrogen bonded dimeric structure (**19**) and their non-covalent interactions with chiral citronellic acids (**CA**) leading to ICD. Schematic in b) depicts the process of **CA** binding induced helical organization and the crucial role of temperature in controlling the degree of self-assembly and the chirality induction process (Reproduced with permission from ref. 26).*

Oligo(*p*-phenylenevinylene) (OPV) is another class of well studied dye molecules which have been investigated for its self-assembly and helical ordering. First report of guest induced chirality was shown in achiral OPV end capped with mono-ureidotriazine (UT) (**19**).[26] These molecules show hierarchical organization, first forming dimers due to self-complementary quadruple hydrogen bonding interactions, which further π-stack to result in an extended assembly (Figure 1.8). This motif show strong interaction with carboxylic acid group of **CA**, which binds to UT moiety of **19** through orthogonal two point hydrogen bonding interactions as shown in Figure 1.8a. Thus, homochiral citronellic acids (**CA**) were used as a chiral guest, which induced a preferred helical assembly of **19**, with tunable handedness depending upon the chirality of the bound **CA**. The ICD showed strong bisignated signal, characteristic of excitonically coupled chromophores with biased handedness in their assembly.

Through detailed spectroscopic investigations, role of hydrogen bonding between **CA** and **19** was confirmed and concluded that chirality induction happens only at certain degree of self-assembly as shown in Figure 1.8b. Finally, they report an unprecedented chiral amplification in assembly of achiral **19** in a majority rule (by varying enantiomeric excess of chiral auxiliary), sergeant and soldiers experiment (by varying percentage of chiral **CA** in a mixture with their achiral analogue). The versatility of **19** was evident from the induction of helicity in presence of a number of chiral carboxylic acid and phosphoric acid derivatives.[27] These were utilized as a chiroptical sensor to estimate the absolute chirality and enantiomeric excess (*ee*) of unknown samples.

Molecular recognition based ICD was also demonstrated in systems that show aggregation induced emission (AIE) property.[28] Silole unit functionalized with chiral phenylethanamine do not show any CD signal upon aggregation.[28] But, upon interaction with enantiopure mandelic acid, efficient chirality transfer was observed. This was confirmed from the CD signal as well as circularly polarized luminescence due to helical organization in the electronic excited state.

1.2.2 Chiral Solvation
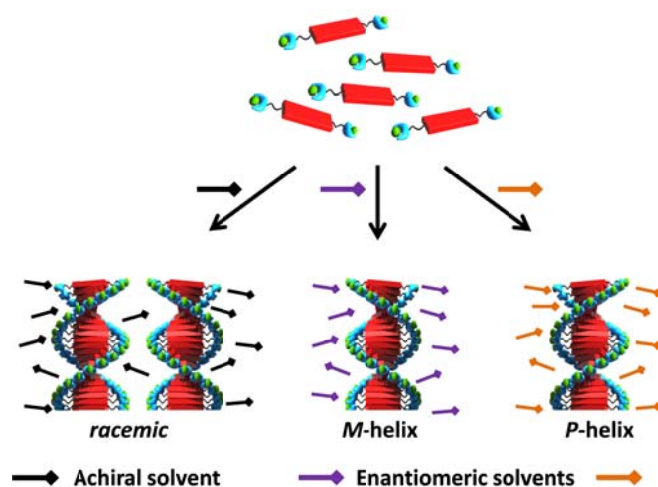
Figure 1.9. *Schematic representation of the chiral solvation method for induced helicity with preferred handedness.*

Chiral solvent induced helical structure in achiral systems have been well studied in polymeric systems.[29] As seen in Figure 1.9, the chirality of the solvent molecules govern the handedness of the resultant aggregate. Such observations have been attributed to either specific interaction with the chiral solvent molecules or by formation of asymmetric solvent sheath around the assembly. This strategy could be utilized as a probe to investigate preferential solvation of polymers in mixed solvent systems.[30] However, to obtain such solvent driven

preferred handedness in supramolecular polymers is a challenge, due to their highly dynamic nature.

One of the initial study of solvent dependent helical organization in self-assembly of small molecules was shown in disc shaped C_3 symmetric benzene-1,3,5-tricarboxamide (BTA) derivatives (Figure 1.10a).[31] The UV and CD spectra of achiral (**20**) in presence of optically active (*R*)-2,6-dimethyloctane as solvent was identical to their chiral analogue in achiral solvents. This suggests a chiral solvation induced helical organization into assembly of achiral molecules. Similarly, carbocyanine dye (**21**) also show a mirror image bisignated CD signal in presence of enantiomeric pure (*R*) or (*S*)-2-octanol as solvent (Figure 1.10b).[32] The induction of opposite helical organization was also reflected in their higher order assembly, which show preferred right- and left-handed twist of helical bundles in presence of (*S*)- and (*R*)-2-octanol respectively (Figure 1.10 c, d).
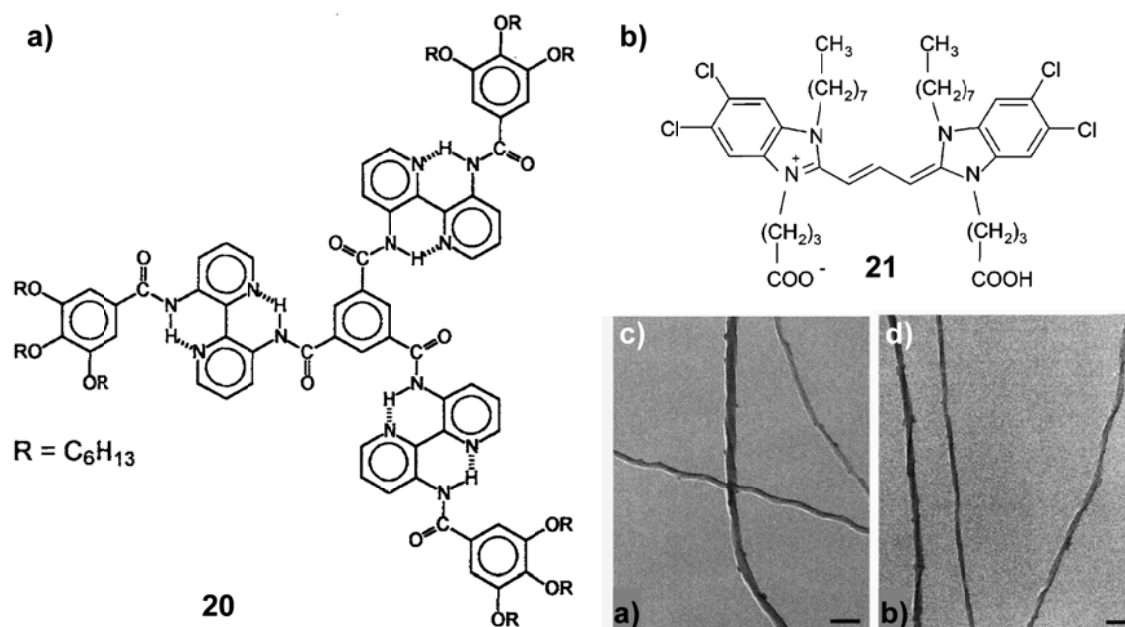
Figure 1.10. *a) Molecular structure of C_3 symmetric achiral BTA derivative (**20**) which show ICD in presence of chiral 2,6-dimethyloctane. b) Carbocyanine dye (**21**) and its self-assembled nanostructures as seen in TEM micrographs in presence of chiral solvent c) (R)-2-octanol, d) (S)-2-octanol showing left and right-handed twist, respectively (scale bar = 200 nm) (Reproduced with permission from ref. 31b, 32).*

Limonene is another class of chiral solvent that has been utilized for ICD. Würthner *et al.* have studied the self-assembly of achiral perylenebisimide (PBI, **22,** Figure 1.11a) in presence of (*R*)- and (*S*)- limonene.[33] Detailed spectroscopic investigations revealed almost 100% enantiomeric selectivity of the helical assembly, whose handedness is governed by the

configuration of limonene solvent. Such efficient chirality transfer could be expressed in their helical organization of one-dimensional nanofibers (Figure 1.11 c), however with lower *ee* compared to the solution state, due to the kinetic self-assembly process of these fibrillar network at high concentrations. These optically active limonene were also used as solvent for ICD in racemic bisurea derivatives (**23**, Figure 1.11b).[34] These formed helical nanotubes in presence of chiral solvent, where the CD signal was comparable to the assembly of enantiomeric bisurea in achiral solvents.
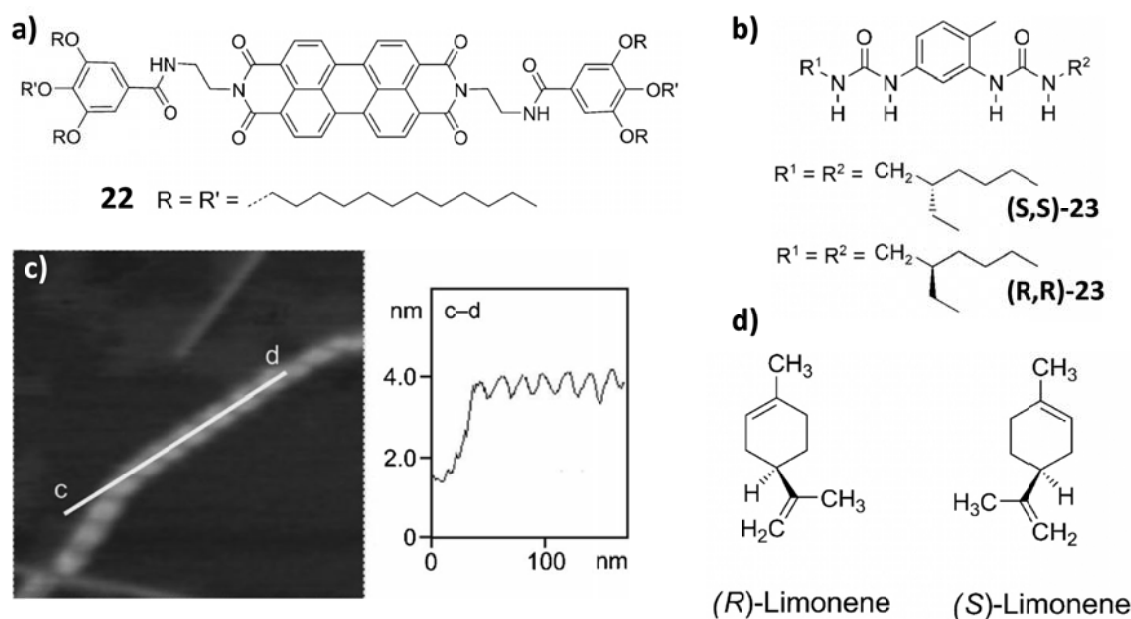
Figure 1.11. *a) Helical assembly of achiral PBI derivative (**22**) in presence of chiral solvent (S)-limonene showing right-handed helical nanofibers (c) as seen in AFM along with its cross-section analysis. b) Chemical structure of enantiomeric bisurea derivative (**23**), which demonstrates ICD in presence of chiral solvent limonene as shown in d) (Reproduced with permission from ref. 33, 34).*

Enantiomeric solvent induced chirality transfer could also be achieved on solid surfaces. To demonstrate such phenomenon at the interface of chiral liquid and surface of highly oriented pyrolytic graphite (HOPG), OPV molecules functionalized with diamino triazine moiety (**24**) was chosen. These were shown to assemble into hydrogen bonded rosette like motif.[35] Interestingly, the deposition of (**24**) from enantiomeric pure solvents resulted in similar rosettes but with a clear bias for either clockwise or anticlockwise rotation in presence of (*S*)- and (*R*)-1-phenyl-octanol solvents respectively (Figure 1.12 b). Hydrogen bonding between solvent and **24** was found to be crucial in inducing surface homochirality. Through a series of STM imaging performed over the time scale of assembly, mechanistic insights into the growth of these aggregates and the emergence of chirality on the surface were obtained. Similar

OPV molecules appended with ureidotriazine and diaminotriazine unit show ICD, which self-assembled in presence of optically active citronellol molecules as solvent.[36] Detailed spectroscopic studies in chiral solvents indicated the formation of chiral solvent sheath, which bias the nucleation process leading to homochiral assembly.
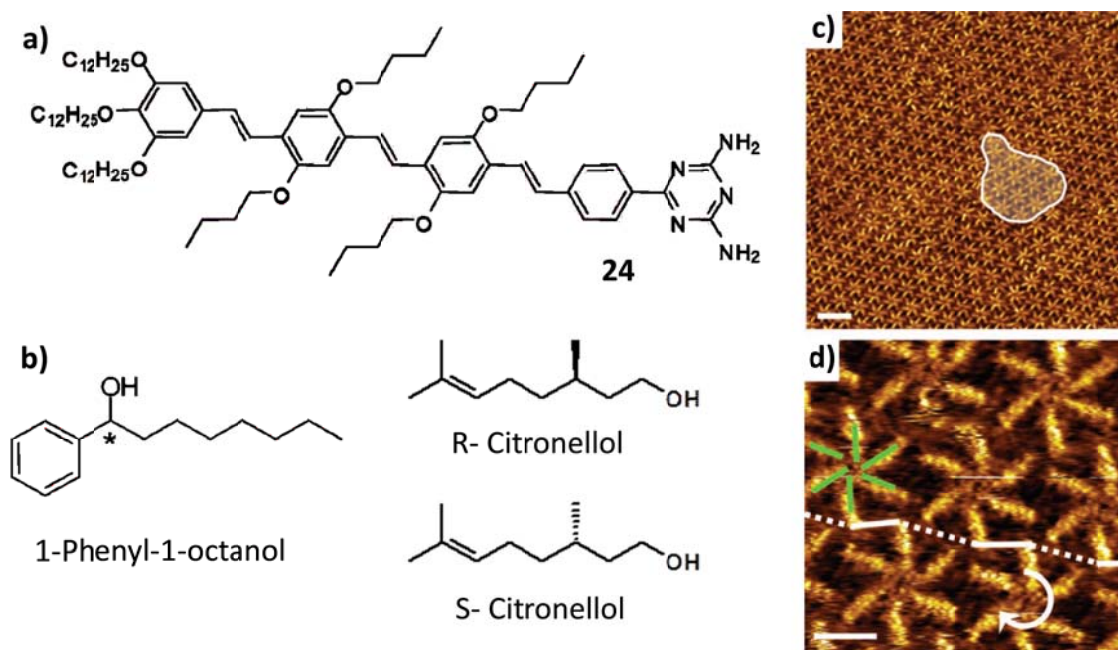
Figure 1.12. a) Chemical structure of achiral OPV-4 (24) which form helical rosette like structure in presence of chiral solvents shown below. STM images of self-assembled 24 monolayer at c) R- and d) S-1-octanol-HOPG interface showing preference for opposite handedness (Reproduced with permission from ref. 35).

1.2.3 DNA Templated Assembly

DNA and related polynucleotides have emerged as unique structural motifs for controlled assembly of a wide variety of molecules with functional properties. They have been utilized for the construction of multichromophoric assembly both by covalent and non-covalent functionalization of DNA with high monodispersity.[37] Yet another feature of these scaffold is their chiral nature, which can be utilized for the induction of supramolecular helicity into the assembly of achiral chromophores. Forces like electrostatic interaction, hydrogen bonding etc. have been utilized for the binding of guest molecules to DNA through sugar-phosphate backbone, groove intercalation, intercalation between base pairs or via complementary hydrogen binding.[38]

Armitage *et al.* have extensively studied the assembly of cyanine dyes on DNA duplex. Binding of cyanine dye (**25**) to [Poly(dA-dT)]$_2$ i.e. double helical DNA results in spontaneous assembly of **25** in a helical fashion (Figure 1.13a).[39] Detailed investigations suggested the

formation of a face to face dimer, which bind onto the minor groove of oligonucleotide duplex in a cooperative manner, where the groove distortion created by binding of one dimer assist in interaction of subsequent dimer. Moreover, organization of achiral dye (**25**) onto the homochiral right-handed DNA duplex induces a strong CD signal. Interestingly, binding to AT-5 duplex, which can hold only one dimer, show a weak positive monosignated signal, whereas AT-10 duplex with two pairs of assembled dimers resulted in a strong bisignated CD signal (Figure 1.13 c, d). Thus a mechanistic insight into the helical organization and its correlation with CD signal is provided. They confirm that a face to face coupling of transition dipole in a dimer can lead to a positive cotton effect. However, binding of second dimer within the minor groove provides additional end to end transition dipoles coupling leading to a bisignated CD signature (Figure 1.13 d).
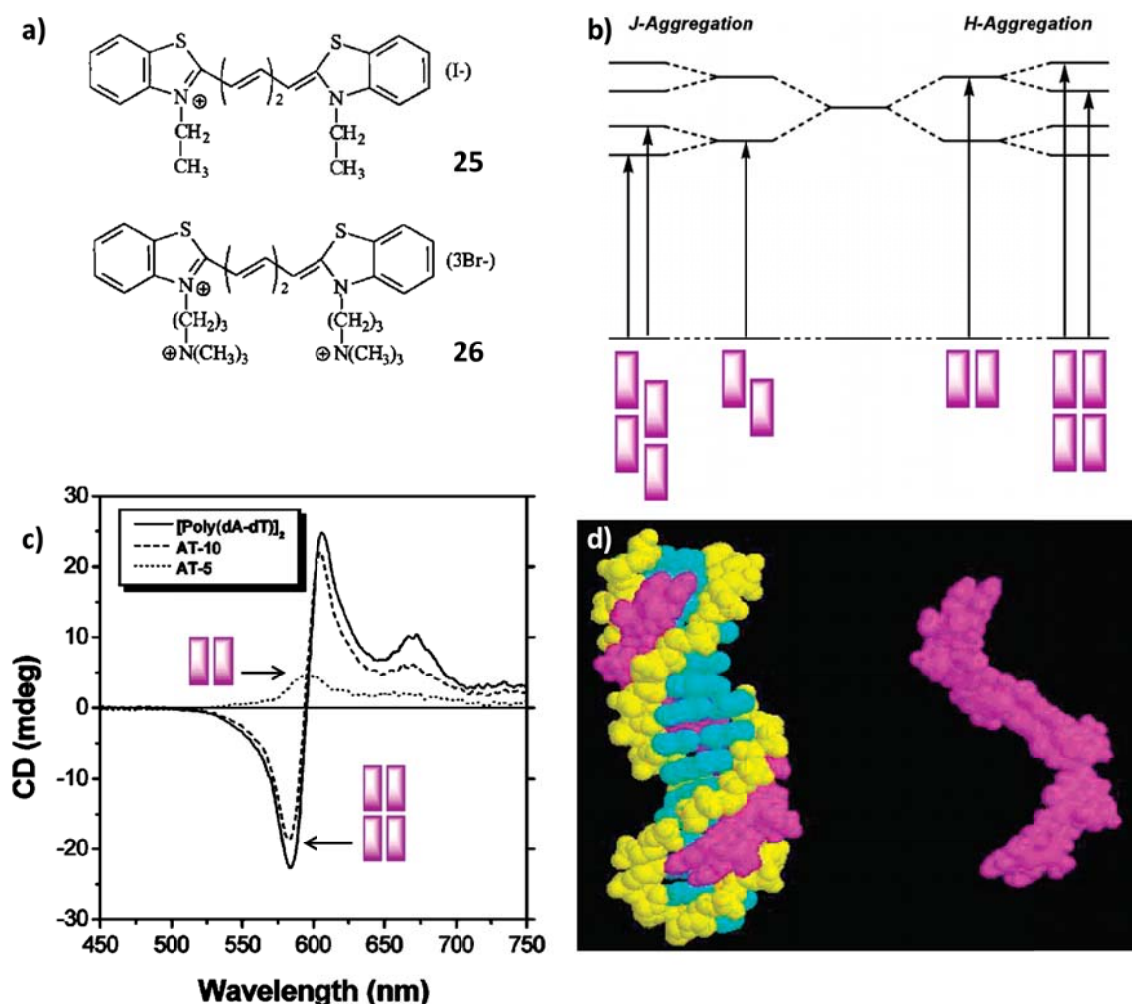
Figure 1.13. *a) Molecular structure of monocationic (**25**) and tricationic (**26**) cyanine dyes and b) energy level splitting pattern in H- and J-aggregates based on coupling of transition dipoles. c) Variation in CD signal of **25** upon interaction with AT based DNA duplex of different length, d) molecular model showing aggregation of 3 pairs of **25** aligned end to end in the minor groove of DNA (Reproduced with permission from ref. 39a).*

Detailed study with similar class of dye molecules like tricationic cyanine dye (**26**) confirm that in general, these molecules can bind to the minor groove of DNA templates.[40] Interestingly, they spontaneously assembly into H- and J-aggregates, with successful ICD in both the states. The formation of these two types of assembly could be controlled by external factors like temperature, ionic strength and DNA template length, dye concentrations etc. Thus, cyanine dye can form DNA templated helical organization with tailor made assemblies.
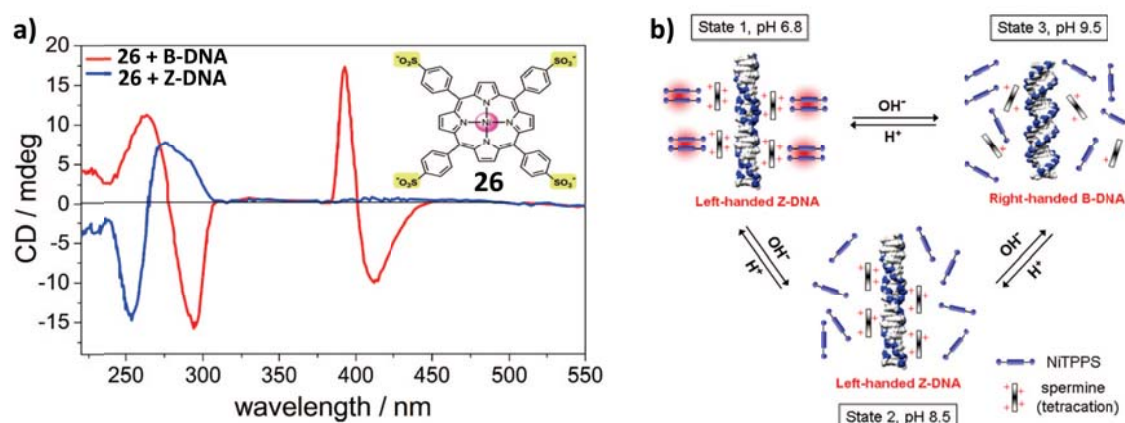
Figure 1.14. *a) CD spectra of porphyrin **26** upon interaction with poly(dG-dC)₂ i.e. (deoxyguanylic acid–deoxycytidylic acid)₂ DNA in left-handed Z and right-handed B conformation in presence of spermine. b) Schematic representation of pH dependent modulation of **26**-DNA-spermine ternary complex (Reproduced with permission from ref. 43).*

Organization of achiral cationic porphyrin into helical domains could be constructed in presence of polynucleotides as well as polypeptides.[41] Purrello *et al.* have utilized it as a chiroptical probe to discriminate B- and Z- DNA in presence of zinc porphyrin. Detailed study revealed two different modes of dye binding to left and right helical form of DNA, leading to differential CD signal.[42] They have also employed tetra anionic porphyrin (**26**) to sense the two helical forms of DNA.[43] These molecules selectively interacts with the spermine stabilized left-handed Z- DNA, whereas the right-handed B-form do not bind due to electrostatic repulsion between the negatively charged DNA and (**26**). Poly(dG-dC)₂ in right-handed B-form do not show any ICD in the soret band (~ 400nm) of porphyrin, whereas the left-handed Z-DNA show strong excitonically coupled negative bisignated CD signal upon interaction with **26** (Figure 1.14a). Interestingly, (**26**)-DNA-spermine ternary complex and the ICD features could be reversibly modulated by varying the pH (Figure 1.14b). This has been proposed to be useful in reversible information storage and logic gates. Very recently, they have also demonstrated that ICD of tricationic corrole derivatives with DNA can be used as a probe for discriminating ss and ds conformation of homochiral polynucleotide.[44]
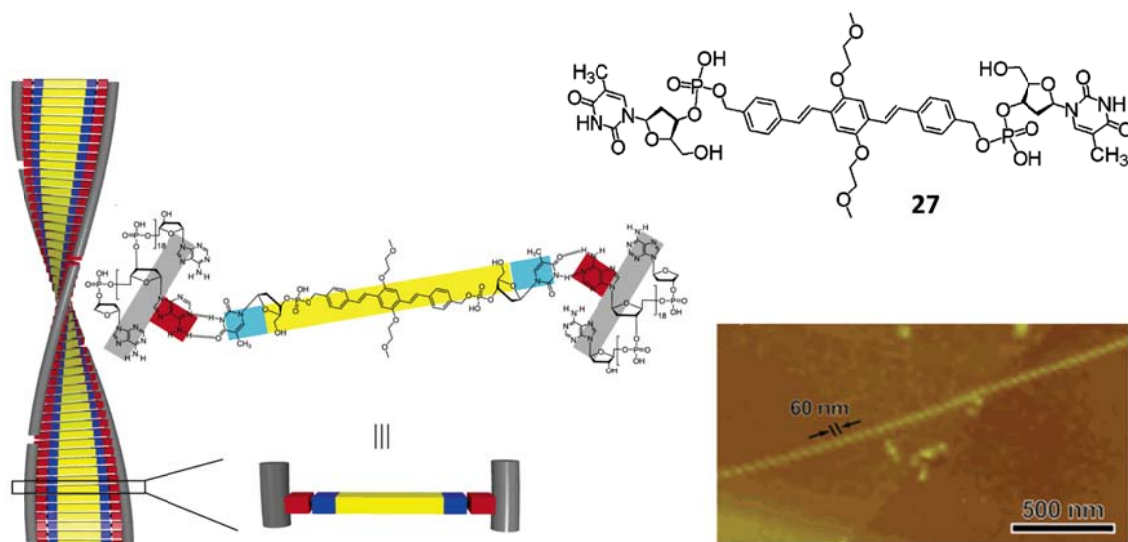
Figure 1.15. *Structure of thymidylic acid functionalized OPV (**27**) and its self-assembly in presence of oligodeoxyadenylic acid as shown in the schematic. Below is the AFM image of binary complex showing helical twist (Reproduced with permission from ref. 45).*

DNA as a scaffold can as well be used to assemble chromophores via complementary hydrogen bonding with the bases. Chromophores functionalized with nucleotide tend to assemble on DNA due to base pairing. For example, OPV functionalized with thymidylic acid (**27**) formed chiral aggregates in presence of dA20 (20 meric oligodeoxyadenylic acid).[45] AFM images clearly demonstrated chirality induction even at the microscopic level, as seen by the formation of right-handed helical nanofibers, in agreement with the CD signal showing positive cotton effect. Moreover, binding of DNA to either one or both sides (chromophore sandwiched between two DNA strands) of the chromophoric assembly could be controlled by changing the ratio of dA20 to (**27**). But the length of these assemblies could not be controlled by the template size and it formed extended stacks as shown in Figure 1.15.
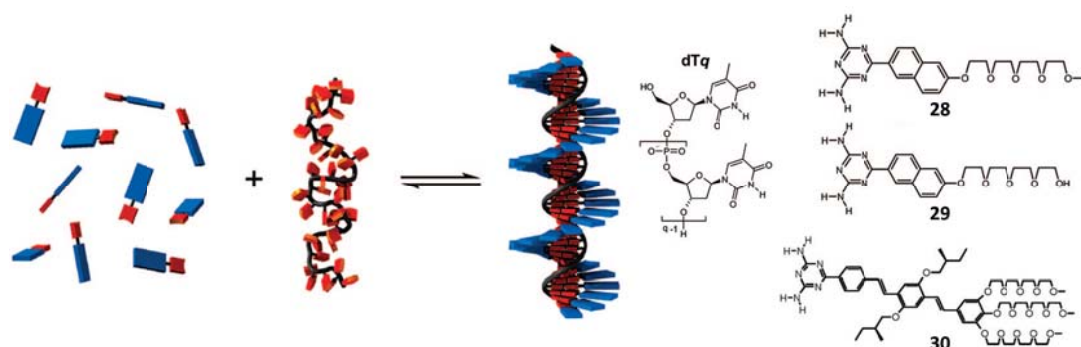
Figure 1.16. *Right: chemical structure of diaminotriazine functionalized naphthalene (**28, 29**) and OPV derivatives (**30**), ssDNA (**dTq**) and left: schematic representation of DNA template helical organization of achiral chromophores (Reproduced with permission from ref. 46, 47).*

In yet another approach, Schenning *et al.* have unsymmetrically functionalized chromophores with hydrogen bonding unit only on one side, leading to 1:1 complex between ssDNA and supramolecular stack of chromophores.[46] Naphthalene (**28**) and OPV (**30**) derivatives were functionalized with diaminotriazine unit, which show efficient ICD upon hydrogen bonding with homochiral oligothymine. Interestingly, ESI-MS (electrospray ionization-mass spectrometry) analysis also confirmed the formation of chromophores decorated DNA scaffold. Further, they synthetically modified **28** by removal of terminal methyl group, thereby exposing the hydroxyl group in the guest molecule (**29**). This eventually helped in suppression of non-templated self-assembly of (**29**) as well as subsequent aggregation DNA-**29** binary complex.[47] Thus, they have successfully demonstrated the construction of helical assemblies with uniform length.

A recent report has shown that 2,6-diaminopurine functionalized naphthalene guest molecules, templated on oligothymine strands show pH switchable handedness of helical assembly in an unprecedented manner.[48] Such DNA template assembly could be dynamically polymerized to construct biomimetic polymers with non-natural bases, wherein the template can be regenerated.[49]

1.3 Supramolecular Chiral Memory
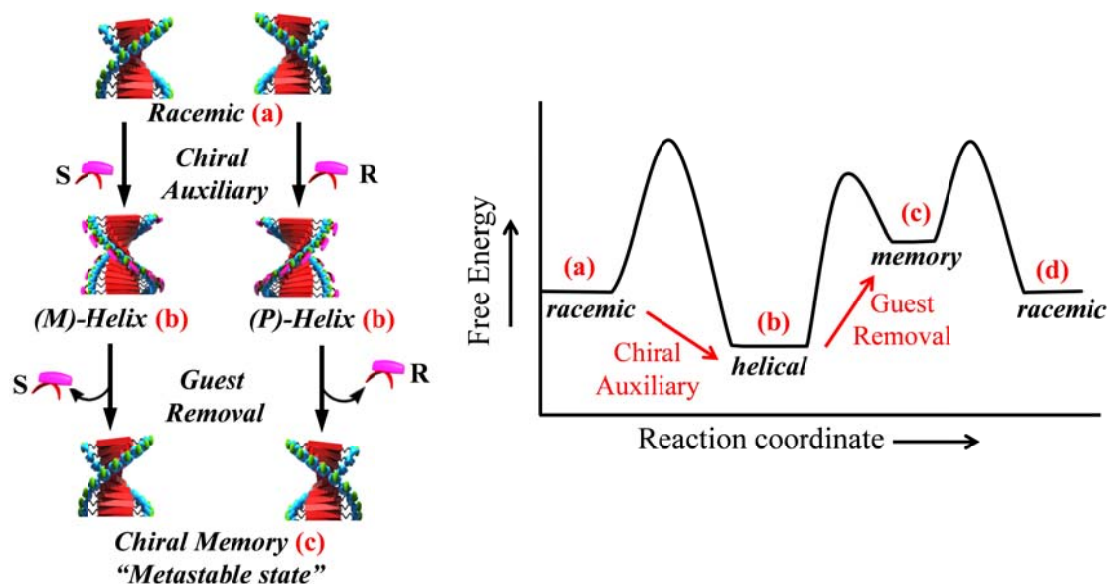
Figure 1.17. *Left: Pictorial representation of step wise assembly process leading to chiral memory and right: the proposed change in free energy at every stage.*

Supramolecular chiral memory is the retention of helical conformation by a self-assembled system, even after removal of chiral information. The guest induced chiral assembly of achiral molecules can preserve its preferred handedness after the detachment of chiral bias,

by entering into a kinetic trap state as against thermodynamically stable racemic form. The course of whole process and the free energy change at every step is shown in Figure 1.17. Thermodynamically stable assembly of achiral molecules is usually in the racemic form (a), which can be biased into a lower energy homochiral organization (b) in presence of an enantiomeric guest molecule (chiral auxiliary). Having acquired the helical preference, removal of these chiral auxiliaries creates a metastable state i.e. chiral memory, by finding a local minimum in the energy landscape (c). Thermodynamically, these assemblies would revert to most stable racemic state (d), whose kinetics would be governed by energy of activation. There are three major prerequisite for construction of metastable assemblies:

a) Helicity induction via chiral auxiliary approach
b) Simple method to remove chiral auxiliary without affecting the helical conformation of self-assembly
c) Stable assemblies with kinetic inertness
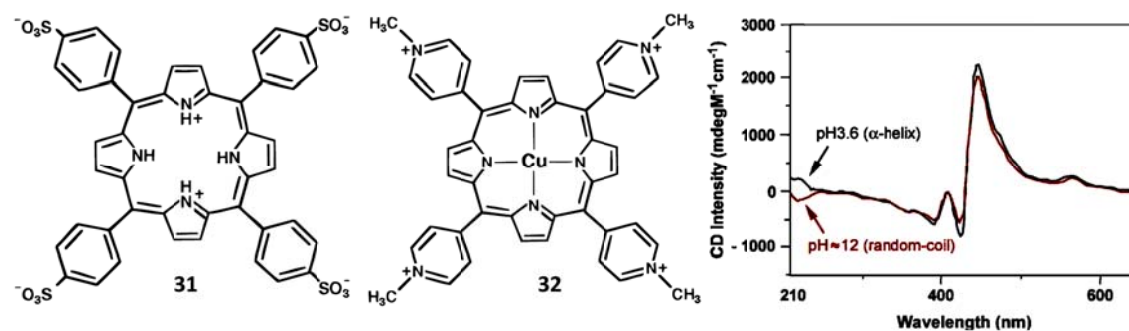
Figure 1.18. *Molecular structure of anionic (**31**) and cationic (**32**) porphyrin and the variation of CD spectra of ternary complex (**31:32**: poly-D-glutamate) at acidic and basic pH leading to chiral memory in porphyrin assembly (Reproduced with permission from ref. 15, 51).*

There are many examples of such metastable helical assemblies in conventional polymers, where the chiral auxiliaries are either removed or substituted by their achiral analogue without affecting the assembly.[4b,3a,b] However, construction of supramolecular analogue requires better design due to highly dynamic nature of these polymers held by non-covalent forces.[50] First ever report of chiral memory in supramolecular assembly was shown in porphyrin aggregates. Purrello *et al.* have previously shown that the chiral polymeric template assisted ICD in assembly of achiral cationic porphyrins.[51] To construct a kinetically inert assembly, they used a heteroassembly of oppositely charged porphyrin **31** and **32**, which form helical ternary complex in presence of homochiral poly-glutamate. Interestingly, addition of excess poly-D-glutamate to a helical assembly of **31-32**-poly-L-glutamate did not show any inversion of CD signal, confirming the kinetic stability of these heteroassemblies, which is

essential for memory. Poly-glutamate is known to undergo a pH dependent conformational transition from chiral α-helix (acidic pH) to achiral random coil (basic pH). However, monitoring the pH dependent CD signal of the helical ternary complex suggest that even after loss of chiral form of template, the porphyrin assembly continues to remain in their kinetically stable helical state (Figure 1.18). This was the unprecedented report where templated chromophores do not follow the chirality of the host. Moreover, these assemblies retain their chiral memory over days and weeks.

While the previous example demonstrates chiral memory, an unambiguous design would require complete removal of chiral component from the solution. Thus, small chiral auxiliary phenylalanine was used for ICD in **33-34** heteroassembly.[52] Homochiral phenlyalanine self-assembles to form non-covalent polymeric template, which induces a helical preference into the porphyrin assembly. Moreover, this supramolecular polymeric template could be easily removed after disassembly by ultrafiltration. The resultant CD signal of the residual aggregate remains unaltered indicating imprinted helical memory. Additionally, imprinted aggregates could also act as a chiral seed resulting in amplification of chirality. Thus, they conclude that the memory based aggregates are inherently chiral, which can self-propagate.
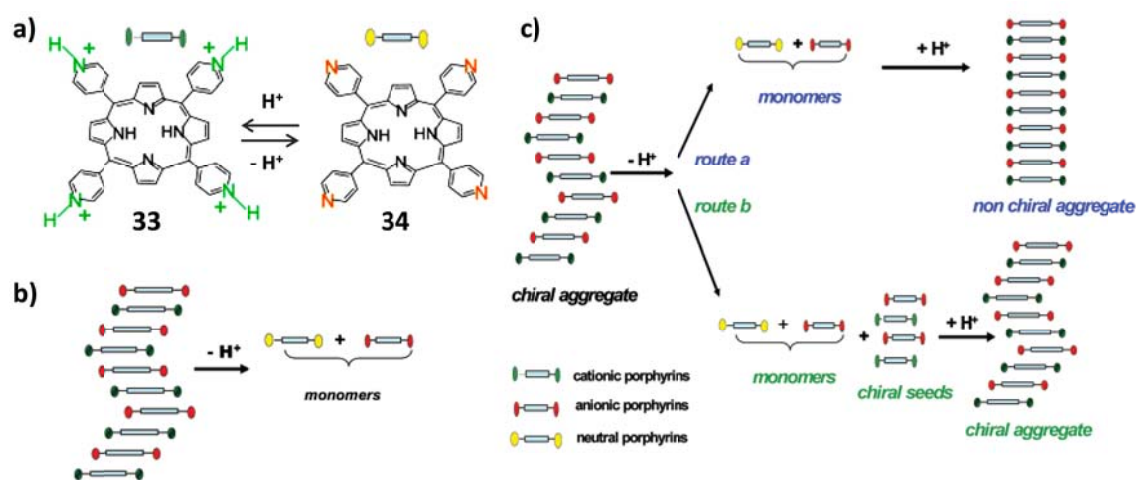
Figure 1.19. *a) pH dependent transition from cationic (**33**) to neutral (**34**) porphyrin, b) schematic representation of aggregate to monomer conversion at basic pH and c) seeding mechanism for self-propagation of chirality by imprinted helical assembly (Reproduced with permission from ref. 53 a, b).*

A simple approach to erase chiral memory in these heteroaggregates is to switch off the electrostatic interactions between the oppositely charged porphyrin (**31-33**).[53] Thus, free pyridine substituted porphyrin was synthesized, which can switch between neutral and cationic

state based on pH (Figure 1.19 a). Co-assembly of **31-33** also show ICD in presence of enantiomeric phenylalanine and imprinted helicity after template removal by ultrafiltration. This imprinted aggregates disintegrate into monomers at high pH because of cationic to neutral transition (Figure 1.19b), resulting in loss of electrostatic attraction. Interestingly, the loss of CD signal at high pH could be completely recovered upon decreasing the pH due to formation of **31-33** heteroaggregation. This could be explained based on the presence of imprinted chiral seeds even at high pH, which self-propagate in acidic medium. This unprecedented report of "erase and write" cycle could be repeated multiple times, thus confirming the versatility of the design (Figure 1.19c). pH dependent reversible memory was also demonstrated with anionic porphyrin complexed with ruthenium tris(phenanthroline) based on the chiral seeding mechanism.[54]
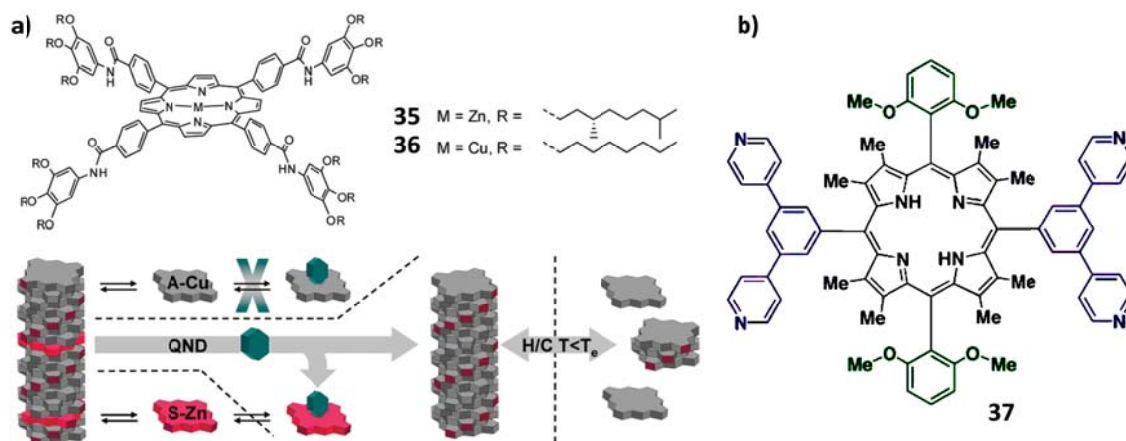
Figure 1.20. *a) Molecular structure of chiral zinc porphyrin (**35**), achiral copper porphyrin (**36**) and schematic representation of their helical coassembly, followed by selective depolymerisation in presence of lewis base quinuclidine (**QND**) resulting in helical memory. b) Chemical structure of fully substituted non-planar porphyrin (**37**), which show ICD and chiral memory (Reproduced with permission from ref. 55, 56).*

Meijer and Schenning *et al.* have shown a novel design for chiral memory via chiral amplification in metalloporphyrins. The co-aggregation of chiral and achiral porphyrins show strong chiral amplification, wherein upon selective removal of chiral component from the stacks, the assembly of achiral chromophores retain their helix handedness due to kinetic stability of the state. Chiral Zn-porphyrin (**35**) and achiral Cu-porphyrin (**36**) upon co-assembly show strong chiral amplification via sergeant and soldiers principle, leading to transfer of chirality from **35** to their co-assembly with **36**.[55] Moreover, addition of a lewis base quinuclidine (**QND**), which selectively coordinates to the chiral Zn-porphyrin (**35**), could extract chiral sergeant leaving a stack of achiral soldiers. Detailed investigations revealed that

the ligation occurs mainly with monomers which is in equilibrium with polymer, resulting in their removal from the co-assembly. Interestingly, even after complete removal of sergeant, the stacks continues to retain its helicity, confirming the chiral memory effect. This memory could be partially erased and recovered by heating and cooling respectively. Aida and coworkers have also shown chiral memory effect in fully substituted porphyrin (**37**), which adopt a nonplanar, saddle shaped racemic form.[56] The molecular and supramolecular chirality could be biased upon interaction with Mandelic acid showing amplified chiral transformation, whereas chiral memory was obtained by substitution with acetic acid.
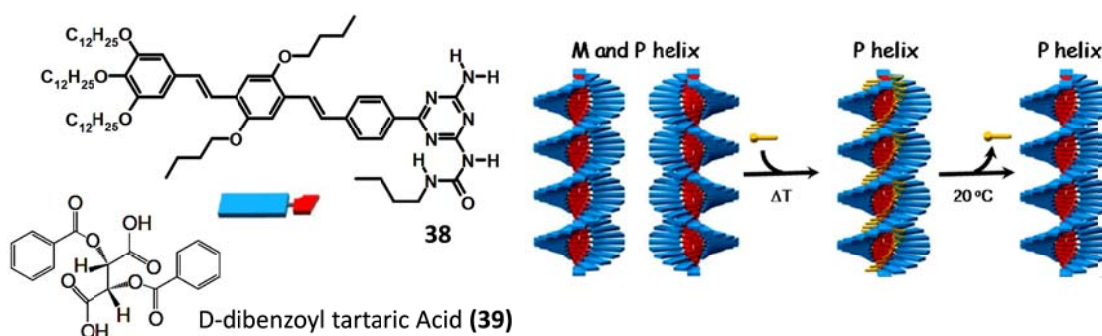
Figure 1.21. *Ureidotriazine functionalized achiral OPV (**38**), its induced helicity with D-tartaric acid (**39**) and schematic representation of chiral memory after removal of tartaric acid (Reproduced with permission from ref. 57, 58).*

OPV is another class of dye molecule whose helical assembly, induction of chirality and chiral memory is well investigated. For example, assembly of achiral OPV functionalized with ureidotriazine unit (**38**) showed strong bisignated CD signal in presence of optically active dibenzoyl tartaric acid (**39**).[57] This chiral bias into the organization of **38** was promoted by orthogonal two point ion pair interaction with **39**. The kinetic stability of these helical assemblies was evident from the retention of CD signal, even after removal of homochiral tartaric acid (**39**) upon extraction with a base (Figure 1.21). These imprinted chiral aggregates were used to understand the mechanism of stereomutation in one dimensional supramolecular polymers. Temperature dependent racemization of stacks followed a 1st order kinetics, indicating a disassembly-assembly mediated process. Interestingly, partial depolymerization at higher temperature followed by polymerization upon cooling completely recovered the preferred helicity. This confirms a nucleation-elongation mechanism, where imprinted chiral state acts as a helical seed for further assembly of achiral **38**. Stabilization of metastable state in OPV have also been employed to probe into off nucleation pathways in supramolecular polymerization process.[58]
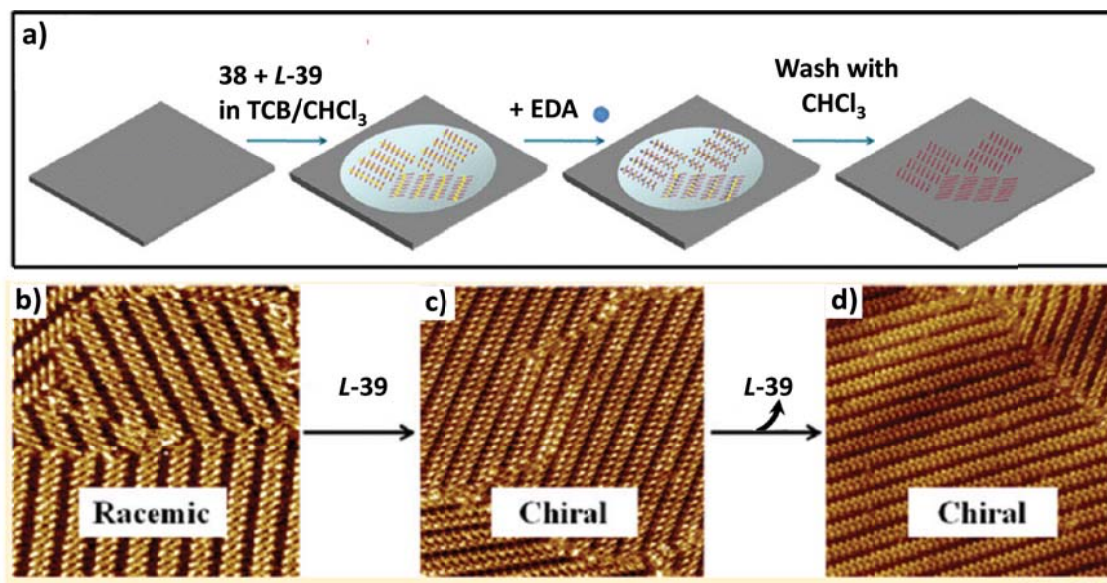
Figure 1.22. *a) Schematic representation of helical memory created at liquid/solid interface. STM images of self-assembled OPV (**38**) monolayer with b) no auxiliary, c) L-**39** and d) after removal of L-**39** from the assembled monolayer resulting in imprinted helicity on surface (Reproduced with permission from ref. 59).*

Interestingly, the chirality induction of **38** with dibenzoyl tartaric acid (**39**) and imprinted helicity could be successfully constructed on surface as well.[59] Achiral monolayer of **38** at liquid/solid interface shows a helical organization on addition of homochiral **39**. About 85% of the assembly demonstrate a helical bias confirming efficient transfer of chirality from the guest to the monolayer. Additionally, removal of chiral auxiliary at the interface, by interaction with a base (ethylenediamine), kinetically traps the organizational chirality at the chloroform−1,2,4-trichlorobenzene/graphite interface (Figure 1.22).

To achieve highly stable memory Aida *et al.* have used an amphiphilic design for the assembly of pyridine appended hexabenzocoronene (HBC) derivative (**40**).[60] Large aromatic core of **40** ensures high kinetic stability to their assemblies. Achiral **40** show strong ICD in presence of (BINAP)/Pt(II), whose handedness could be controlled by the chirality of the auxiliary. Interestingly, morphology of chiral guest appended chromophoric assemblies could be tuned from tubes to helical nanocoils of preferred handedness, just by changing the solvent medium. Moreover, removal of chiral auxiliary did not perturb the ICD signal significantly, confirming the imprinted chirality (Figure 1.23). Remarkably, these helical assemblies of achiral molecules were very stable such that the chiral organization is retained even after heating to 50 °C for 12 hours. Thus, they demonstrate a helical metastable state with high kinetic inertness, which retain their handedness over days to months. This can be attributed to

the large π-surface of HBC derivative, resulting in highly stable assemblies, which is a rational approach towards stable chiral memory.
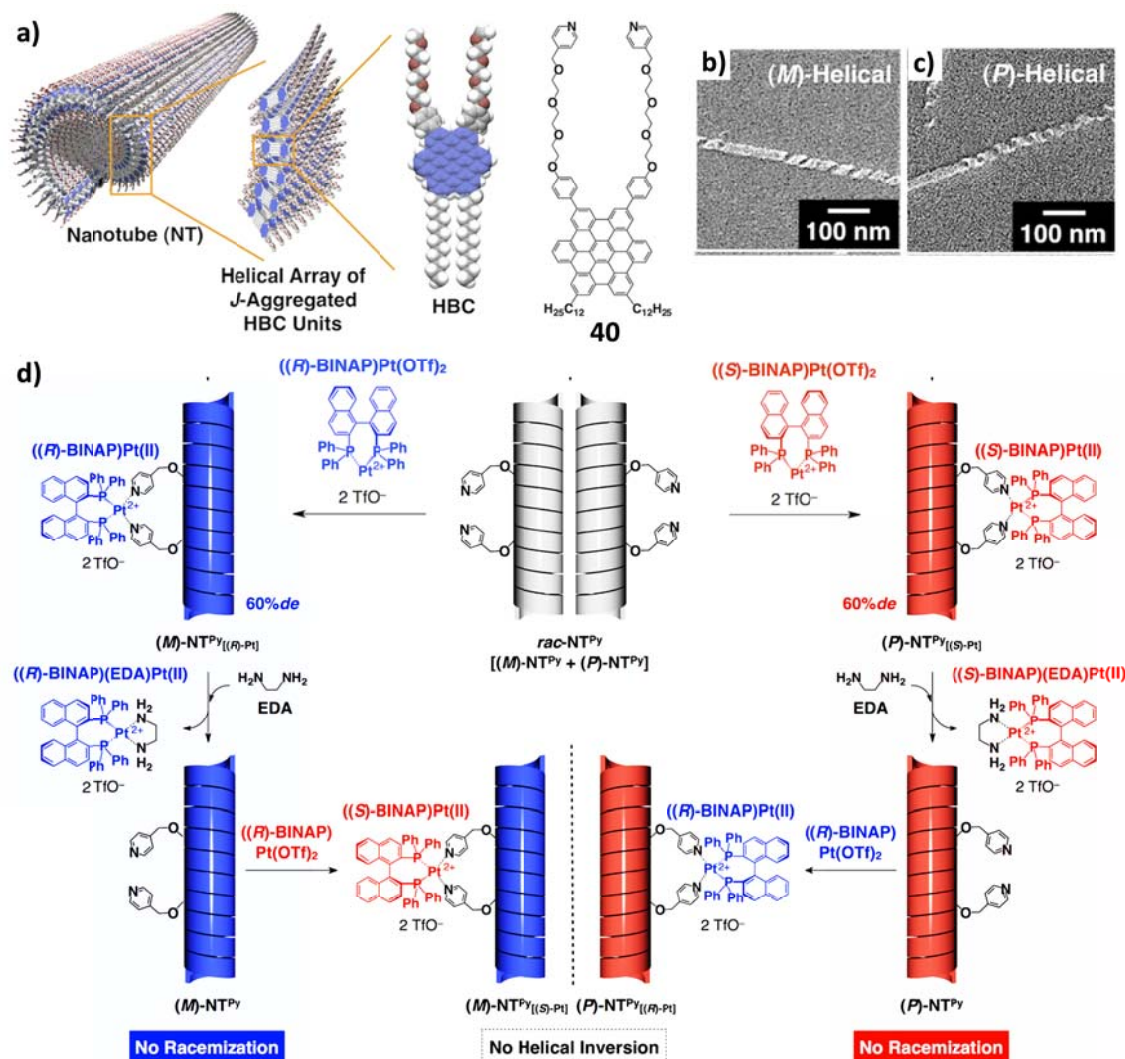
Figure 1.23. *a) Schematic representation of self-assembled amphiphilic HBC into tubular nanostructures and chemical structure of pyridine appended HBC amphiphile (**40**). SEM micrographs of self-assembled **40** in presence of b) R- and c) S-Binap/Pt(II) showing nanocoils of left and right-handedness respectively. d) Schematic illustration of chirality induction and helical memory in tubular nanostructures of **40** (Reproduced with permission from ref. 60).*

1.4 Conclusions and Outlook

This chapter is aimed at highlighting the importance of helical supramolecular polymers as a biomimetic system for chirotechnological applications. It deals with induction of helicity into the assembly of achiral molecules by chiral auxiliary approach. The major emphasis is on the novel design principles that are employed to obtain tailor made properties.

This chapter had two main parts. First one dealt with induction of chirality upon interaction with chiral guest. This was further categorized based on the type of chiral guest utilized. Second part presented a discussion on the synthesis of metastable helical assemblies. With examples from a variety of chromophores, a rational design for the construction of kinetically inert assemblies is presented. In all such cases, the functional aspect of these helix for various application is also outlined.

Recent demonstration of chirotechnological applications from these helical polymers promise a great future in the subject. Moreover, taking advantage of the homochiral nature of most biological stimuli, a biomimetic approach can be useful in understanding various cellular processes, probing biochemical reactions and for biosensing. Another area which remains unexplored is the induction of chirality into the electronic excited state, leading to guest induced circularly polarized luminescence (CPL) and their excited state helical memory. This thesis is directed towards venturing into some of these basic problems and open ways for interesting line of research and applications.

1.5 References and Notes

1. S. Mason, *Chem. Soc. Rev.,* **1988**, *17*, 347.

2. H. Flack, *Acta. Cryst.,* **2009**, *65*, 371.

3. a) E. Yashima and K. Maeda, *Macromolecules,* **2008**, *41*, 3; b) E. Yashima, K. Maeda and T. Nishimura, *Chem. Eur. J.*, **2004**, *10*, 42; c) M. M. Green, N. C. Peterson, T. Sato, A. Teramoto, R. Cook and S. Lifson, *Science*, **1995**, *268*, 1860; d) M. M. Green, J.-Woong Park, T. Sato, A. Teramoto, S. Lifson, R. L. B. Selinger and J. V. Selinger, *Angew. Chem. Int. Ed.*, **1999**, *38*, 3138; e) M. Fujiki, J. R. Koe, K. Terao, T. Sato, A. Teramoto and J. Watanabe, *Polym. J.,* **2003**, *35*, 297.

4. a) A. E. Rowan and R. J. M. Nolte, *Angew. Chem. Int. Ed.*, **1998**, *37*, 63; b) E. Yashima, K. Maeda, H. Iida, Y. Furusho and K. Nagai, *Chem. Rev.*, **2009**, *109*, 6102; c) M. M. Green, K.-S. Cheon, S.-Y. Yang, J.-W. Park, S. Swansburg and W. Liu, *Acc. Chem. Res.*, **2001**, *34*, 672; d) M. Fujiki, J. R. Koe, K. Terao, T. Sato, A. Teramoto and J. Watanabe, *Polym. J.*, **2003**, *35*, 297; e) A. Lohr and F. Würthner, *Isr. J. Chem.*, **2011**, *51*, 1052; f) V. K. Praveen, S. S. Babu, C. Vijayakumar, R. Varghese and A. Ajayaghosh, *Bull. Chem. Soc. Jpn.*, **2008**, *81*, 1196; g) D. K. Smith, *Chem. Soc. Rev.*, **2009**, *38*, 684; h) Y. Wang, J. Xu, Y. Wang and H. Chen, *Chem. Soc. Rev.*, **2013**, *42*, 2930; i) F. J. M. Hoeben, P. Jonkheijm, E. W. Meijer and A. P. H. J. Schenning, *Chem. Rev.*, 2005, **105**, 1491; j) T. F. A. De Greef, M. M. J. Smulders, M. Wolffs, A. P. H. J. Schenning, R. P. Sijbesma and E. W. Meijer, *Chem. Rev.*, **2009**, *109*, 5687.

5. a) M. M. Green, C. Andreola, B. Mufioz and M. P. Reidy, *J. Am. Chem. Soc.,* **1988**, *110*, 4063; b) S. Cantekin, D. W. R. Balkenende, M. M. J. Smulders, A. R. A. Palmans and E. W. Meijer, *Nat. Chem.*, **2011**, *3*, 42.

6. a) E. Yashima, T. Matsushima and Y. Okamoto, *J. Am. Chem. Soc.,* **1995**, *117*, 11596; b) S. Allenmark, *Chirality*, 2**003**, *15*, 409.

7. a) *Circular dichroism: principles and applications,* ed. N. Berova, K. Nakanishi and R. W. Woody, John Wiley & Sons, New York, 2000; b) N. Harada and K. Nakanishi, *Acc. Chem. Res.*, **1972**, *5*, 257; c) M. Simonyi, Z. Bikádi, F. Zsila and J. Deli, *Chirality*, **2003**, 680.

8. a) N. Berova, *Chirality*, **1997**, *9*, 395; b) N. Berova, G. Pescitelli, A. G. Petrovic and G. Proni, *Chem. Commun.*, **2009**, 5958.

9. a) E. Yashima, T. Nimura, T. Matsushima and Y. Okamoto, *J. Am. Chem. Soc.*, **1996**, *118*, 9800; b) H. H. Jo, C.-Y. Lin and E. V. Anslyn, *Acc. Chem. Res.*, **2014**, DOI: 10.1021/ar500147x; c) F. Riobe, A. P. H. J. Schenning and D. B. Amabilino, *Org. Biomol. Chem.*, **2012**, *10*, 9152.

10. E. Yashima, K. Maeda, H. Iida, Y. Furusho and K. Nagai, *Chem. Rev.*, **2009**, *109*, 6102.

11. K. Shimomura, T. Ikai, S. Kanoh, E. Yashima and K. Maeda, *Nat. Chem.,* **2014**, *6*, 429.

12. a) C. Zhao, Q.-F. Sun, W. M. Hart-Cooper, A. G. DiPasquale, F. D. Toste, R. G. Bergman and K. N. Raymond, *J. Am. Chem. Soc.*, **2013**, *135*, 18802; b) L. J. Prins, J. Huskens, F. de Jong, P. Timmerman and D. N. Reinhoudt, *Nature*, **1999**, *398*, 498; c) M. Ziegler, A. V. Davis, D. W. Johnson, and K. N. Raymond, *Angew. Chem. Int. Ed.,* **2003**, *42*, 665; d) M. A. Mateos-Timoneda, M. Crego-Calama and D. N. Reinhoudt, *Chem. Soc. Rev.*, **2004**, *33*, 363.

13. R. Lauceri, T. Campagna, A. Contino and R. Purrello, *Angew. Chem., Int. Ed. Engl.* **1996**, *35*, 215.

14. R. Purrello, L. Monsu' Scolaro, E. Bellacchio, S. Gurrieri and A. Romeo, *Inorg. Chem.,* **1998**, *37*, 3647.

15. E. Bellacchio, R. Lauceri, S. Gurrieri, L. M. Scolaro, A. Romeo and R. Purrello, *J. Am. Chem. Soc.,* **1998**, *120*, 12353.

16. W.-S. Li, D.-L. Jiang, Y. Suna and T. Aida, *J. Am. Chem. Soc.,* **2005**, *127*, 7700.

17. S.-i. Tamaru, S.-y. Uchino, M. Takeuchi, M. Ikeda, T. Hatano and S. Shinkai, *Tetrahedron Lett.,* **2002**, *43*, 3751.

18. T. Ma, C. Li and G. Shi, *Langmuir,* **2008**, *24*, 43.

19. Y. Huang, Y. Yan, B. M. Smarsly, Z. Wei and C. F. J. Faul, *J. Mater. Chem.,* **2009**, *19*, 2356.

20. D. Franke, M. Vos, M. Antonietti, N. A. J. M. Sommerdijk and C. F. J. Faul, *Chem. Mater.,* **2006**, *18*, 1839.

21. M.-a. Morikawa, M. Yoshihara, T. Endo and N. Kimizuka, *J. Am. Chem. Soc.,* **2005**, *127*, 1358.

22. M.-a. Morikawa and N. Kimizuka, *Chem. Commun.,* **2012**, *48*, 11106.

23. J. Xiao, J. Xu, S. Cui, H. Liu, S. Wang and Y. Li, *Org. Lett.,* **2008**, *10*, 645.

24. K. P. Nandre, S. V. Bhosale, K. V. S. Rama Krishna, A. Gupta and S. V. Bhosale, *Chem. Commun.,* **2013**, *49*, 5444.

25. A. A. Sobczuk, Y. Tsuchiya, T. Shiraki, S.-i. Tamaru and S. Shinkai, *Chem. Eur. J.,* **2012**, *18*, 2832.

26. S. J. George, Ž. Tomović, M. M. J. Smulders, T. F. A. de Greef, P. E. L. G. Leclère, E. W. Meijer and A. P. H. J. Schenning, *Angew. Chem. Int. Ed.,* **2007**, *46*, 8206.

27. F. Riobe, A. P. H. J. Schenning and D. B. Amabilino, *Org. Biomol. Chem.*, **2012**, *10*, 9152.

28. J. C. Y. Ng, J. Liu, H. Su, Y. Hong, H. Li, J. W. Y. Lam, K. S. Wong and B. Z. Tang, *J. Mater. Chem. C,* **2014**, *2*, 78.

29. M. M. Green, C. Khatri and N. C. Peterson, *J. Am. Chem. Soc.,* **1993**, *115*, 4941.

30. C. A. Khatri, Y. Pavlova, M. M. Green and H. Morawetz, *J. Am. Chem. Soc.,* **1997**, *119*, 6991.

31. a) A. R. A. Palmans and E. W. Meijer, *Angew. Chem. Int. Ed.*, **2007**, *46*, 8948; b) A. R. A. Palmans, J. A. J. M. Vekemans, E. E. Havinga and E. W. Meijer, *Angew. Chem. Int. Ed. Engl.*, 1997, **36**, 2648.

32. H. von Berlepsch, S. Kirstein and C. Böttcher, *J. Phy. Chem. B,* **2003**, *107*, 9646.

33. V. Stepanenko, X.-Q. Li, J. Gershberg and F. Würthner, *Chem. Eur. J.,* **2013**, *19*, 4176.

34. B. Isare, M. Linares, L. Zargarian, S. Fermandjian, M. Miura, S. Motohashi, N. Vanthuyne, R. Lazzaroni and L. Bouteiller, *Chem. Eur. J.,* **2010**, *16*, 173.

35. N. Katsonis, H. Xu, R. M. Haak, T. Kudernac, Ž. Tomović, S. George, M. Van der Auweraer, A. P. H. J. Schenning, E. W. Meijer, B. L. Feringa and S. De Feyter, *Angew. Chem. Int. Ed.,* **2008**, *47*, 4997.

36. S. J. George, Z. Tomovic, A. P. H. J. Schenning and E. W. Meijer, *Chem. Commun.*, **2011**, *47*, 3451

37. a) R. Varghese and H.-A. Wagenknecht, *Chem. Commun.,* **2009**, 2615; b) T. Nguyen, A. Brewer and E. Stulz, *Angew. Chem. Int. Ed.,* **2009**, *48*, 1974.

38. A. Ruiz-Carretero, P. G. A. Janssen, A. Kaeser and A. P. H. J. Schenning, *Chem. Commun.,* **2011**, *47*, 4340.

39. a) K. C. Hannah and B. A. Armitage, *Acc. Chem. Res.,* **2004**, *37*, 845; b) J. L. Seifert, R. E. Connor, S. A. Kushon, M. Wang and B. A. Armitage, *J. Am. Chem. Soc.,* **1999**, *121*, 2987.

40. M. Wang, G. L. Silva and B. A. Armitage, *J. Am. Chem. Soc.,* **2000**, *122*, 9977.

41. R. F. Pasternack, A. Giannetto, P. Pagano and E. J. Gibbs, *J. Am. Chem. Soc.,* **1991**, *113*, 7799.

42. M. Balaz, M. De Napoli, A. E. Holmes, A. Mammana, K. Nakanishi, N. Berova and R. Purrello, *Angew. Chem. Int. Ed.,* **2005**, *44*, 4006.

43. A. D'Urso, A. Mammana, M. Balaz, A. E. Holmes, N. Berova, R. Lauceri and R. Purrello, *J. Am. Chem. Soc.,* **2009**, *131*, 2046.

44. A. D'Urso, S. Nardis, G. Pomarico, M. E. Fragalà, R. Paolesse and R. Purrello, *J. Am. Chem. Soc.,* **2013**, *135*, 8632.

45. R. Iwaura, F. J. M. Hoeben, M. Masuda, A. P. H. J. Schenning, E. W. Meijer and T. Shimizu, *J. Am. Chem. Soc.,* **2006**, *128*, 13298.

46. P. G. A. Janssen, J. Vandenbergh, J. L. J. van Dongen, E. W. Meijer and A. P. H. J. Schenning, *J. Am. Chem. Soc.,* **2007**, *129*, 6078.

47. P. G. A. Janssen, S. Jabbari-Farouji, M. Surin, X. Vila, J. C. Gielen, T. F. A. de Greef, M. R. J. Vos, P. H. H. Bomans, N. A. J. M. Sommerdijk, P. C. M. Christianen, P. Leclère, R. Lazzaroni, P. van der Schoot, E. W. Meijer and A. P. H. J. Schenning, *J. Am. Chem. Soc.,* **2009**, *131*, 1222.

48. P. G. A. Janssen, A. Ruiz-Carretero, D. González-Rodríguez, E. W. Meijer and A. P. H. J. Schenning, *Angew. Chem. Int. Ed.,* **2009**, *48*, 8103.

49. J. Lin, M. Surin, D. Beljonne, X. Lou, J. L. J. van Dongen and A. P. H. J. Schenning, *Chem. Sci.,* **2012**, *3*, 2732.

50. F. Biedermann and W. M. Nau, *Angew. Chem. Int. Ed.,* **2014**, DOI: 10.1002/anie.201400718.

51. R. Lauceri and R. Purrello, *Supramol. Chem.,* **2005**, *17*, 61.

52. R. Lauceri, A. Raudino, L. M. Scolaro, N. Micali and R. Purrello, *J. Am. Chem. Soc.,* **2002**, *124*, 894.

53. a) A. Mammana, A. D'Urso, R. Lauceri and R. Purrello, *J. Am. Chem. Soc.,* **2007**, *129*, 8062; b) L. Rosaria, A. D'Urso, A. Mammana and R. Purrello, *Chirality,* **2008**, *20*, 411.

54. R. Randazzo, A. Mammana, A. D'Urso, R. Lauceri and R. Purrello, *Angew. Chem. Int. Ed.,* **2008**, *47*, 9879.

55. F. Helmich, C. C. Lee, A. P. H. J. Schenning and E. W. Meijer, *J. Am. Chem. Soc.,* **2010**, *132*, 16753.

56. K. Toyofuku, M. A. Alam, A. Tsuda, N. Fujita, S. Sakamoto, K. Yamaguchi and T. Aida, *Angew. Chem. Int. Ed.,* **2007**, *46*, 6476.

57. S. J. George, R. de Bruijn, Ž. Tomović, B. Van Averbeke, D. Beljonne, R. Lazzaroni, A. P. H. J. Schenning and E. W. Meijer, *J. Am. Chem. Soc.,* **2012**, *134*, 17789.

58. P. A. Korevaar, S. J. George, A. J. Markvoort, M. M. J. Smulders, P. A. J. Hilbers, A. P. H. J. Schenning, T. F. A. De Greef and E. W. Meijer, *Nature,* **2012**, *481*, 492.

59. I. De Cat, Z. Guo, S. J. George, E. W. Meijer, A. P. H. J. Schenning and S. De Feyter, *J. Am. Chem. Soc.,* **2012**, *134*, 3171.

60. W. Zhang, W. Jin, T. Fukushima, N. Ishii and T. Aida, *J. Am. Chem. Soc.,* **2012**, *135*, 114.

CHAPTER-2

Molecular Recognition Driven Helical Assembly with

Tunable Handedness

Chapter-2

Molecular Recognition Driven Helical Assembly with Tunable Handedness

Abstract

Helical assemblies like DNA, proteins etc. are very much central to the efficient functioning of biological systems. In this regard, design of biomimetic helical systems can be useful in understanding the mechanism of such assembly process. Moreover, complete control over their handedness is desirable for various enantioselective chirotechnological applications. Here we present rylene diimide derived (bola)amphiphiles functionalized with dipicolylethylenediamine (DPA) motif which show molecular recognition induced self-assembly. Binding to chiral adenosine phosphates leads to helical organization in otherwise achiral chromophores, through chiral guest (auxiliary) induced helicity. Moreover, their handedness could be controlled just by appropriate choice of chiral auxiliaries (adenosine phosphates).

The design of DPA functionalization could be generalized in both 1,4,5,8-naphthalenetetracarboxylic diimide (NDI) as well as 3,4,9,10-perylenetetracarboxylic diimide (PBI), both of which show adenosine phosphate induced assembly with tunable chirality. Competitive replacement of chiral guest through multivalent interactions shows dynamic helix reversal of these assemblies. Thus, we present an unprecedented stepwise switching of helicity from racemic to M-helix to P-helix before converting them to racemic stacks again.
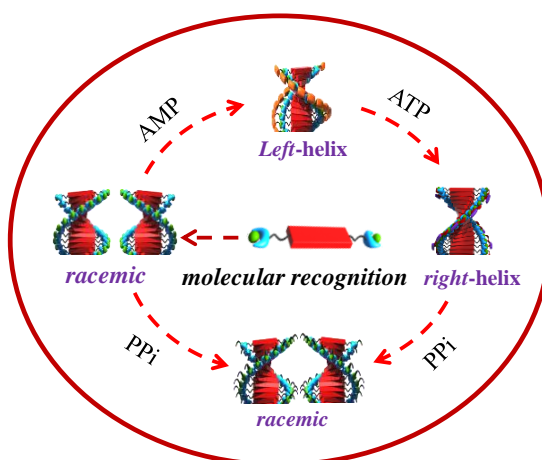
2.1 Introduction

Dynamic helical polymers and supramolecular one-dimensional (1-D) assemblies with tunable handedness, by the specific molecular recognition of chiral guests (auxiliaries), have attracted immense attention as model systems to understand the concepts of chiral amplification.[1,2] Such systems are useful as a biomimetic design for understanding the mechanism of assembly in biological helical polymers like DNA, proteins. Moreover, the molecular recognition properties along with the dynamic nature of these helical systems would be very attractive for the design of stimuli responsive and chirotechnological materials. Although, the supramolecular helical stacks constructed from the assembly of chiral monomers have been well investigated,[2] the molecular recognition driven 1-D assembly of achiral monomers and the resultant induction of chirality from the guests to the achiral/racemic assemblies is seldom reported. In this respect, chiral induction,[3] (preferential) chiral solvation[4] and chiral memory,[5] well known concepts in their macromolecular counterparts, have been recently demonstrated in 1-D supramolecular systems using the principles of host-guest chemistry. However, detailed mechanistic insights and the design of guest responsive, dynamic helical 1-D assemblies remains challenging.

One major advantage of chiral guest induced helical organization of achiral molecules over the traditional helical assembly of chiral monomers is their easy tunability of handedness. Using different enantiomeric form of chiral auxiliaries, the handedness of the host assembly can be easily reversed.[6] This avoids the synthetic challenge involved in making the two chiral forms of monomers, which is necessary in conventional helical (supramoleular) polymers. Moreover, due to the dynamic nature of these non-covalent macromolecules, they can be envisaged to switch their handedness in response to the external stimuli. Control over helix handedness is very crucial for many enantioselective applications, which has been achieved through response to external stimuli like pH, temperature, solvent composition.[7] But a rational design to this effect in having complete control over their handedness is not yet reported.

In this chapter, we describe the adenosine phosphates induced one-dimensional (1-D) self-assembly and the resultant supramolecular chirality of naphthalenediimide (**NDPA-Amph, NDPA**) and perylenebisimide (**PDPA**) based (bola)amphiphiles. Detailed spectroscopic probing provided mechanistic insights into the dynamic molecular recognition, chiral induction process and stability of the assemblies. The binding of multivalent chiral phosphates resulted in high supramolecular chiral order, as evident from the excitonic, bisignated circular dichroism signals, in the resulting NDI and PBI assemblies.[8] Although self-assembly of NDI derivatives have been extensively studied,[8] this is their first report of guest induced chiral self-assembly. These molecules show phosphate selective preferential helicity, i.e. AMP/ADP binding induced

left-handed assembly (*M*-helix), whereas interaction with ATP resulted in right-handed *P*-helix. Detailed molecular mechanics/molecular dynamics (MM/MD) simulations were performed to understand the origin of such unusual guest dependent handedness. Comparison of potential energy profile confirmed the role of van der Waal and hydrogen bonding interactions being responsible for stabilization of one form over the other.

We further present the dynamic reversal of the helical handedness of NDI and PBI stacks through competitive replacement of bound AMP/ADP by ATP. This simple method for dynamic switching of handedness was utilized to bring in a stepwise change in helicity from racemic to *M*-helix to *P*-helix before converting them to racemic stacks again, with an unprecedented control.

2.2 Design Strategy
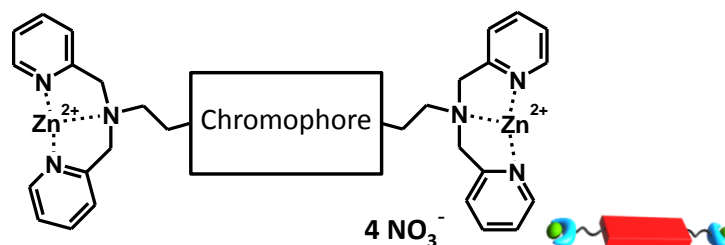
Scheme 2.1. *Pictorial representation of DPA functionalized chromophores.*

The molecular recognition driven 1-D helical self-assembly of chromophores often employed non-directional electrostatic interactions for guest binding.[9] However, we envisioned that chromophore functionalization with specific guest binding groups would give a better control over the resulting self-assembly.[10] On the other hand, use of biologically benign guest molecules, such as adenosine phosphates, would not only facilitate an efficient self-assembly through additional hydrophobic and π-π interactions between the base units, but also act as a chiral handle for imparting chirality to the resulting assemblies. Extensive studies on molecular phosphate sensors suggest that dipicolylethylenediamine-Zinc complex (Zn-DPA) motif can specifically bind to various adenosine phosphates with high association constants (Scheme 2.1).[11] Moreover, functionalization with the chromophores would provide a spectroscopic readout to various transformations. Hence we have designed NDI and PBI based amphiphiles substituted with Zn-DPA motifs (Scheme 2.2), in order to promote guest induced self-assembly and chiral induction through specific binding interactions. **NDPA** and **PDPA** were synthesized following the literature procedure[11] whereas **NDPA-Amph** was synthesized by a statistical reaction of 1,4,5,8-naphthalenetetracarboxylic dianhydride with dodecylamine and N,N-Bis(2-pyridylmethyl)ethane-1,2-diamine followed by zinc metallation (Scheme 2.3). All compounds were characterized by ^{1}H / ^{13}C NMR, HRMS (See Section 2.9 for details).
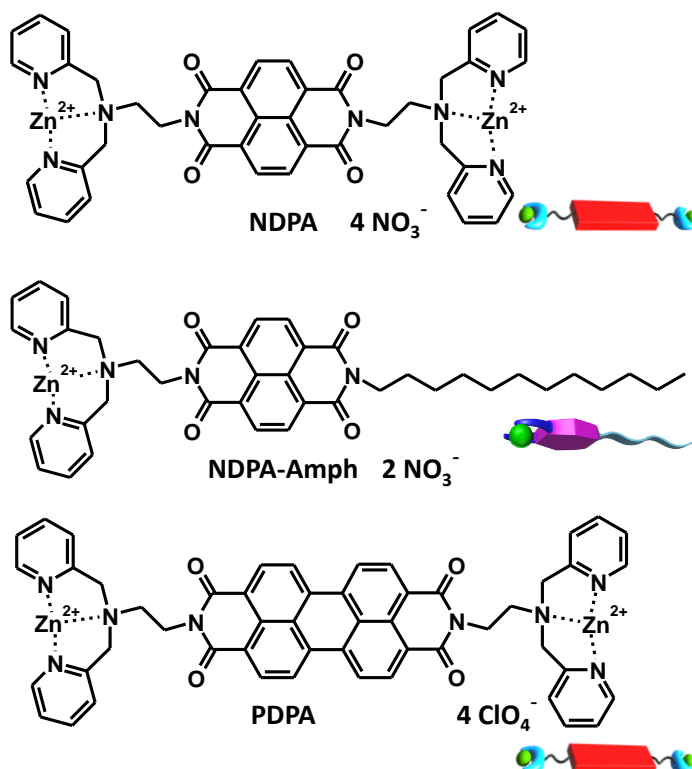
Scheme 2.2. *Molecular structures of **NDPA, NDPA-Amph** and **PDPA**.*

2.3 Guest Induced Helical Self-Assembly of NDPA
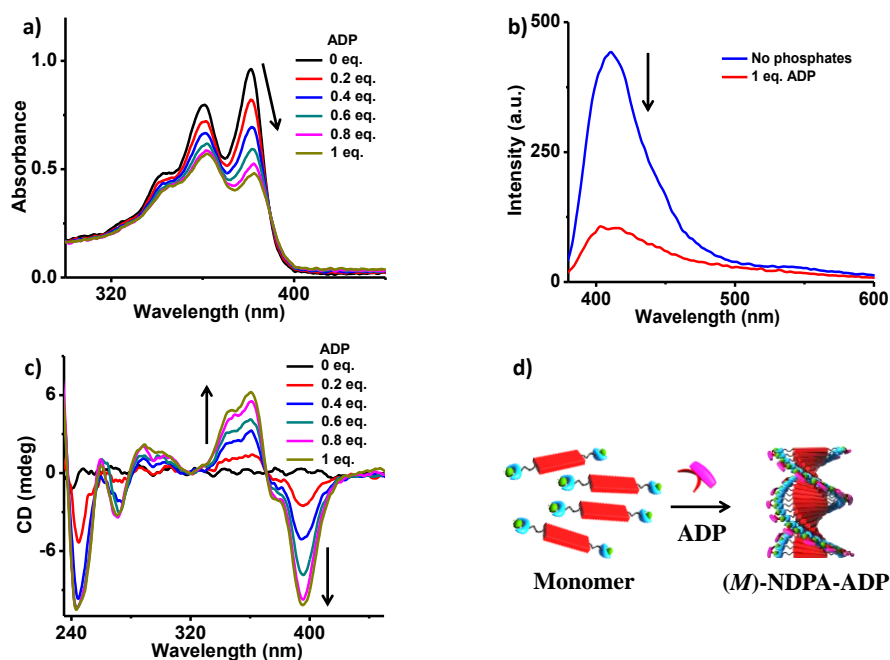
Figure 2.1. *Changes in a) absorption, b) emission and c) CD spectra of **NDPA** upon titration with ADP. d) Schematic representation of ADP binding induced left-handed helical assembly of **NDPA** (c = 5 x 10^{-5} M, 10 mM aq. HEPES buffer).*

The UV/vis absorption studies of **NDPA** (5 x 10^{-5} M, 10 mM aq. HEPES buffer) showed characteristic features of molecularly dissolved NDI chromophores such as sharp absorption bands (λ_{max} = 381 and 361 nm). However, titration of **NDPA** with increasing molar ratios of ADP (0-2 eq.), resulted in broadening of absorption spectra, along with reversal of relative intensity of vibronic bands at 361 nm and 381 nm and decrease in fluorescence intensity characteristic of NDI chromophoric self-assembly (Figure 2.1 a, b).[12] Corresponding Circular Dichroism (CD) spectra showed the gradual evolution of strong Cotton effects, through an isodichroic point at the zero-crossing (370 nm), indicating that ADP binding induces a preferred helical handedness to the resulting assemblies of achiral NDIs (Figure 2.1c). Binding of ADP resulted in negative bisignated CD spectrum, with negative and positive maxima at 395 and 360 nm respectively, characteristic of excitonically coupled chromophores, arranged in left-handed organization.[13] This system presents one among the best excitonically coupled NDI chromophoric assembly known in literature,[8] as they often showed weak bisignated CD signals either due to their low self-association or lack of aromatic interactions in the self-assembly.
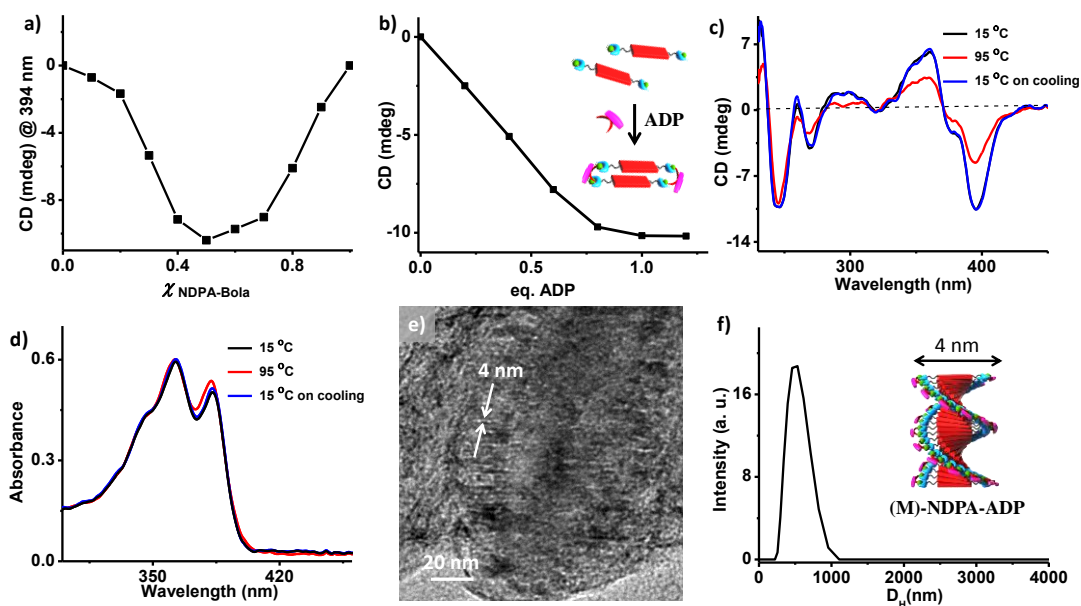
Figure 2.2. *a) Job plot and b) plot of CD intensity (394 nm) of **NDPA** upon titration with ADP (c = 5 x 10^{-5} M, 10 mM aq. HEPES). Temperature dependent c) CD and d) absorption spectra of **NDPA** upon addition of 1 eq. ADP. e) TEM micrographs of **NDPA**-ADP (1 eq.) solution on copper grid (samples were post stained with 1 wt % aq. uranylacetate solution before measurements) and f) shows corresponding dynamic light scattering data (c = 5 x 10^{-5} M, 10 mM aq. HEPES buffer). Inset in f) shows the schematic of resulting helix (M)-**NDPA**-ADP.*

The titration curve obtained by monitoring the CD intensity at 395 nm showed saturation at 1 eq. of ADP, suggesting a 1:1 stoichiometry in the co-assembly (Figure 2.2b).

This is further evident from the Job plot, where the CD intensity probed at 395 nm showed maxima at 0.5 mole fraction of NDI (Figure 2.2a). This suggests that the divalent ADP molecules bind to two Zn-DPA moieties of adjacent NDIs in the assembly, thereby clipping the chromophores together (see Chapter 4.1 for details of phosphate induced clipping), in line with the literature (inset, Figure 2.2b).[11]

To probe into the strength of these ADP binding induced assemblies, temperature dependent CD and absorption spectra were recorded. CD signal at 95 °C shows decrease in intensity but do not disappear completely, whereas absorption spectra show a slight blue shift (1 nm) in band maxima (Figure 2.2 c, d). These data clearly confirm high thermal stability of these helical assemblies, and the decrease in CD signal could be due to weakening of ADP binding (and not their detachment). Furthermore, slow cooling of the various **NDPA**-ADP co-assemblies from 95 °C to 15 °C, did not show any significant change in the intensity of CD signal, indicating that room temperature binding of the chiral guest to NDI indeed leads to the most stable assemblies. TEM micrographs show the formation of 1-D short nanofibers of 4 nm width, which match closely with the dimension of **NDPA** with ADP bound on both side (Figure 2.2e). Formation of self-assembled nanostructures in solution was also confirmed with DLS measurements, which show an average hydrodynamic radius of 500 nm (Figure 2.2f).
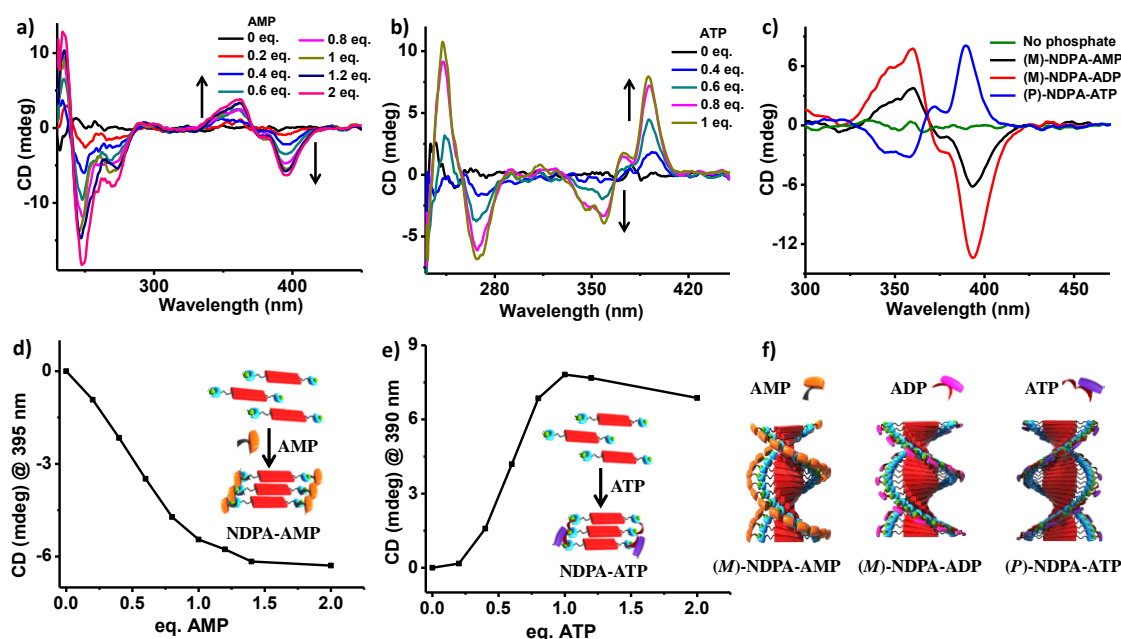
Figure 2.3. *Evolution of CD signals upon binding of a) AMP and b) ATP to **NDPA**. d) and f) show corresponding plot of CD intensity maxima with varying eq. of AMP and ATP respectively, (c = 5 x 10⁻⁵ M, 10 mM aq. HEPES buffer). c) Comparative CD spectra of **NDPA** upon binding to various adenosine phosphates and f) the schematic illustration of corresponding helical assemblies obtained.*

NDPA showed similar assembly behaviour on titration with monovalent AMP with negative bisignated CD signal (Figure 2.3 a, d). However, binding of ATP induces opposite handedness to NDI assemblies as evident from the positive bisignated CD signal, with positive and negative maxima at 390 and 359 nm, respectively (Figure 2.3 b, c, e). The mirror image cotton effects of **NDPA** assemblies obtained with the AMP/ADP when compared with ATP clearly suggests the induction of chirality with opposite handedness (explanation to the opposite handedness is provided using MD simulations in Section 2.5). CD signal upon titration with ATP also shows an initial lag phase, indicating cooperative induction of helicity (Figure 2.3e).

2.4 Helicity Induction in NDPA-Amph Assembly
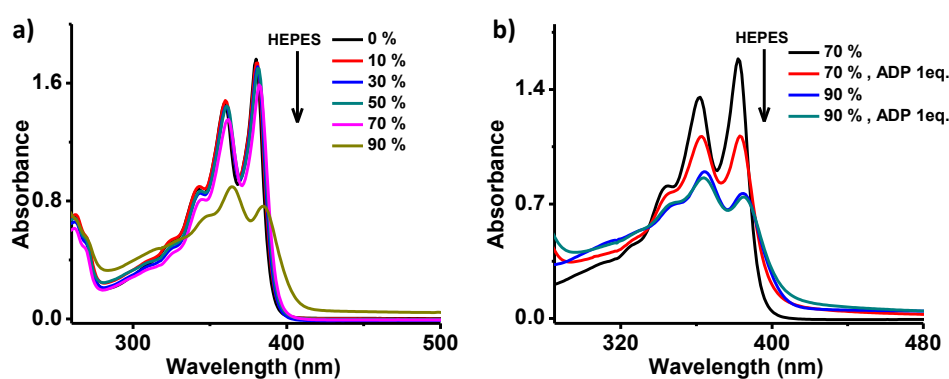
Figure 2.4. *Absorption changes of* ***NDPA-Amph*** *upon a) increasing the percentage of aq. HEPES buffer in THF and b) binding of molar eq. of ADP at varying solvent compositions (c =* *7 x 10^{-5} M).*

In order to understand the role of guest-induced chiral assembly, we further studied the effect of phosphate binding on **NDPA-Amph** derivative, in its monomeric as well as in the assembled states. The amphiphilic nature of the **NDPA-Amph** ensures that they can be self-assembled in THF/water mixture, even in the absence of guest binding. Solvent dependent absorption studies (c = 7 x 10^{-5} M) showed that upto 70% aq. HEPES buffer in THF, it exist in the monomeric state (Figure 2.4a). However in 90% aq. HEPES buffer, the molecule self-assembles, as evident from the broadening of absorption bands with reversal of relative intensity ratio of the absorption maxima at 359 nm and 379 nm.

NDPA-Amph in monomeric and aggregated state showed very different behaviour on binding to phosphates. Monomeric **NDPA-amph** (70% aq. HEPES in THF), self-assembles in a similar way as that of **NDPA** with various phosphates (Figure 2.5a).[14] For example, co-assembly with ADP resulted in negative bisignated CD signal with positive and negative maxima at 357 and 391 nm, respectively (Figure 2.5b). Similarly, helicity induction was observed on binding to AMP and ATP giving negative and positive bisignated CD signals,

respectively (*vide infra*). Remarkably, when ADP was added to the pre-assembled NDI amphiphiles (90% aq. HEPES/THF), chiral induction was not observed, neither at room temperature nor upon cooling the mixture from higher temperatures (Figure 2.6a). As the amphiphilic chromophoric assemblies are known to be less dynamic,[15] it is evident that at higher composition of water, the pre-assembled **NDPA-Amph** molecules are not dynamic enough to reorganize into helical stacks upon guest binding (Figure 2.6b). Hence it can be concluded that, in the present system, guest induced molecular organization is crucial for the induction of supramolecular chirality. This was further supported by the ADP binding induced changes in absorption spectra at these solvent compositions. At 70% aq. HEPES buffer, ADP binding induces further aggregation, whereas at 90% aq. HEPES buffer no change in the spectra was observed (Figure 2.4b).
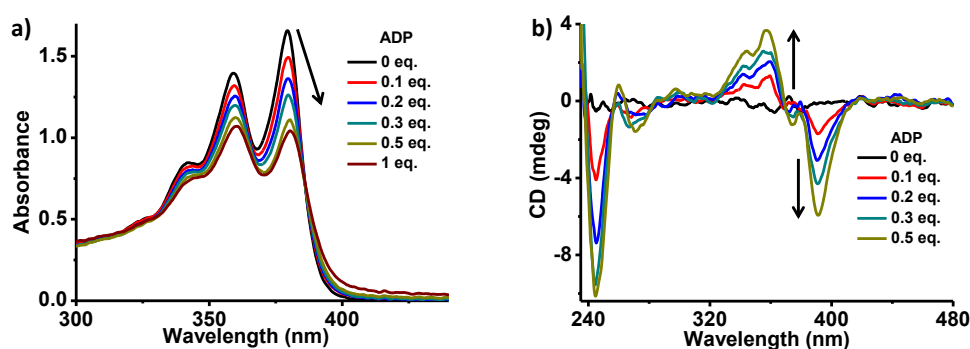
Figure 2.5. *Variation in a) absorption, b) CD spectra of **NDPA-Amph** upon ADP titration, 70% aq. HEPES buffer in THF, c = 7 x 10^{-5} M.*
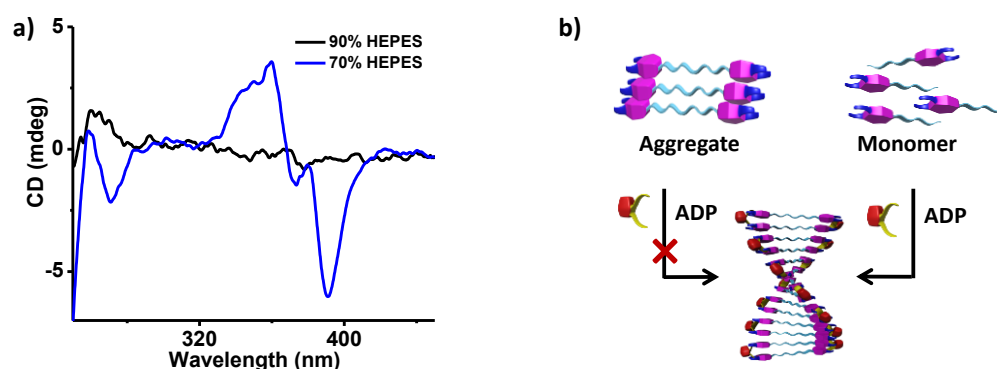
Figure 2.6. *a) CD signal of 0.5 eq. ADP bound **NDPA-Amph** in various solvent compositions and the conclusions drawn on chirality induction process are depicted schematically in b), (c = 7 x 10^{-5} M).*

Transmission Electron Microscopy (TEM) imaging of **NDPA-Amph** (70% water in THF, 7 x 10^{-5} M) assemblies with 0.5 equiv. of ADP, stained with uranyl acetate showed the formation of 1-D nanofibers with a uniform diameter of 8 nm (Figure 2.7). Based on the energy

minimized molecular dimensions of ADP bound **NDPA-Amph** (~ 4 nm), we confirm that the fibers are formed by the π-stacking and solvophobic interactions of the NDI bilayers with non-interdigitated alkyl chains as the hydrophobic interior (inset, Figure 2.7b).
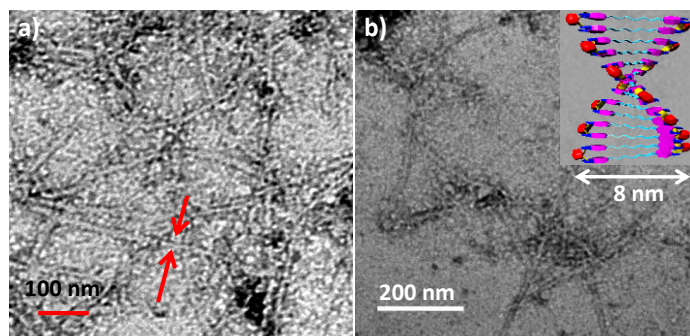
Figure 2.7. *a) and b) TEM images of a 7 x 10^{-5} M solution of **NDPA-Amph**/0.5 eq. ADP (70% water in THF). Inset of b shows schematic of the molecular organization leading to helical stack.*

2.4.1 Competitive Guest Binding
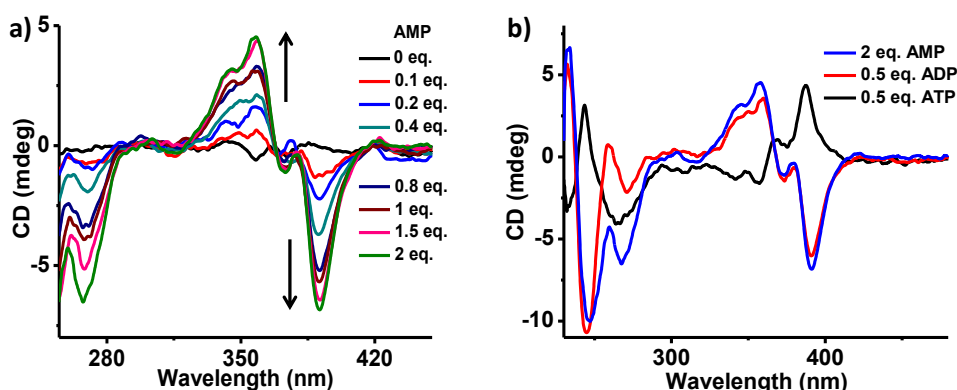
Figure 2.8. *a) Evolution of CD signal with increasing eq. of AMP addition to **NDPA-Amph** and b) mirror image CD spectra of **NDI-Amph** upon binding with various adenosine phosphates, indicating left-handed assembly with AMP/ADP and right-handed with ATP (c = 7 x 10^{-5} M, 70% aq. HEPES buffer in THF).*

Another advantage of these multivalent guests is their strength of interactions, which can be easily modulated based on the number of available binding sites. Thus, ATP with three phosphate groups should have higher association with Zn-DPA when compared to AMP/ADP, which is a mono/divalent phosphate. Thus, we envisaged that based on the strength of binding, ATP should be able to competitively replace the bound AMP or ADP from the NDI stack. Moreover, we observe the induction of opposite chirality in NDI assemblies by different adenosine phosphates, i.e. AMP and ADP showing negative bisignated signal, whereas ATP shows positive bisignated spectra (Figure 2.8). This motivated us to attempt the dynamic helix

reversal through competitive binding of multivalent guests. When a solution of **NDPA-Amph** (c = 7 x 10^{-5} M, 70% aq. HEPES in THF) with 0.5 eq. ADP was titrated with increasing amounts of ATP, a gradual reversal of helicity was observed without any indications of chiral amplification. Interestingly, addition of 0.5 eq. ATP to **NDPA-Amph**/ADP assemblies resulted in a positive bisignated CD signal, which exactly matches with that of **NDPA-Amph**/ATP stacks alone (Figure 2.9). This clearly suggests the competitive replacement of ADP by ATP from the assemblies, as expected and an instantaneous reversal of its helical handedness (the kinetics of these transformations were in < 5 sec and thus could not be probed).[16] We believe that the dynamic helix reversal proceeds through an intra-stack mechanism, as the other reversal pathway, through equilibrium between monomers and the assemblies is unlikely due to high stability of the assemblies.
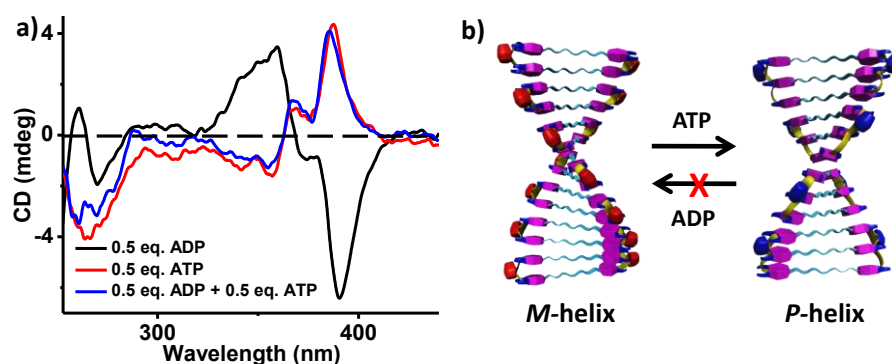
Figure 2.9. *a) CD spectra and b) the schematic of the dynamic helix reversal of **NDPA-Amph**/ADP assembly upon competitive guest binding experiments with ATP (c = 7 x 10^{-5} M, 70% aq. HEPES buffer in THF).*

2.5 Molecular Dynamics Simulation Study*

To understand the origin of opposite handedness in **NDPA** assembly on AMP and ADP binding on one hand, and ATP binding on the other hand, detailed molecular mechanics/molecular dynamics (MM/MD) simulations were performed on stacks of **NDPA** molecules linked to either AMP, ADP or ATP, in right-handed and left-handed structures.

With AMP, the comparison of potential energy profiles on 20 ns MD runs show that the left-handed *M*-helices, i.e. (*M*)-**NDPA**-AMP, are 1.5 to 2.4 kcal/mol.molecule more stable than their right-handed *P*-helices, (*P*)-**NDPA**-AMP. The main contribution of such energy differences between two helices originates from non-bonding (mostly van der Waals) interactions. The global minima and local ordering was better in the left-handed helix compared to its right-handed analogue, as suggested by a smaller average distance between successive

NDPA (4.0 Å versus 4.4 Å), more π-π contacts per molecule (~ 18 versus 15), smaller deviations in average distances and rotational strengths between successive **NDPA**, and stacking defects in *P*-helix compared to *M*-helix (Figure 2.10c, shaded region). This is attributed to the orientation of the ribose moieties, which is related to their chirality. In the *M*-helix, the ribose moieties are close to the **NDPA** cores whereas in the *P*-helix, they are oriented at the periphery of the stack. With this proximity in the *M*-Helix, the hydroxyl groups of the ribose moieties form hydrogen bonding with the oxygen atoms of **NDPA**. These interactions can take place between molecules *n* and *n*+2 or *n*+3, thus contributing to long-range ordering of the assembly. Up to two such hydrogen-bonds per molecule occur in the *M*-helix; they are three times less numerous in the *P*-helix. The simulated CD spectrum of (*M*)-**NDPA**-AMP (Figure 2.10b) shows a negative bisignated signal with zero crossing around 380 nm, and positive and negative maxima located at 367 nm and 395 nm, respectively, in good agreement with experimental spectra (Figure 2.10a).
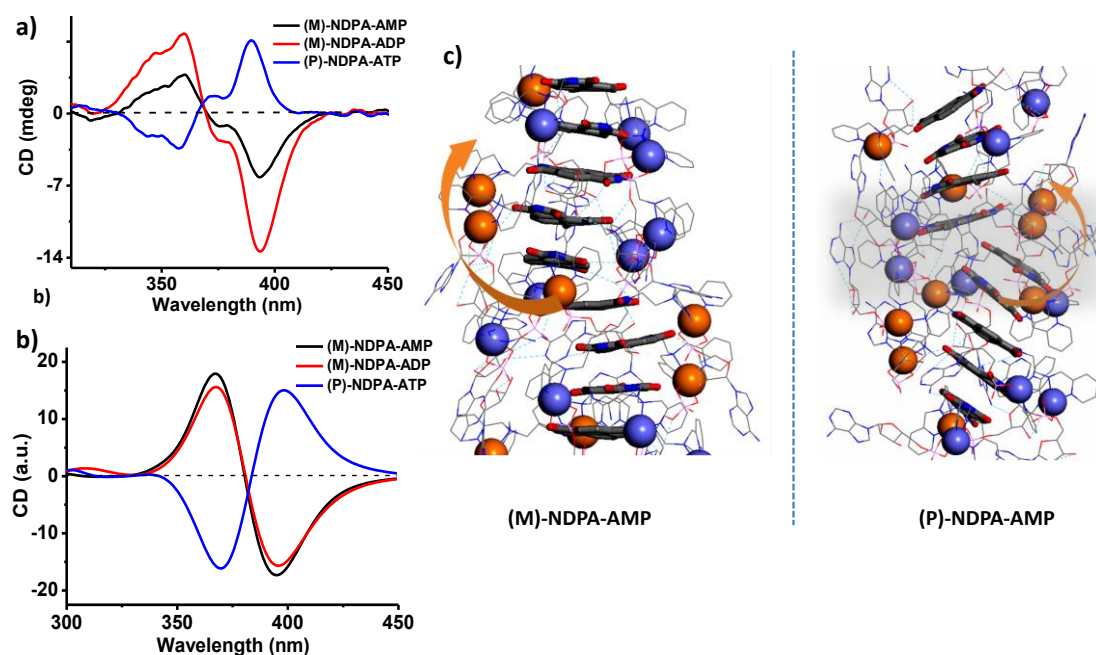
Figure 2.10. *a) Experimental CD spectra of **NDPA** upon binding to various adenosine phosphates. Opposite bisignated Cotton effects of **NDPA** with various adenosine phosphates indicates their reverse helical handedness (c = 5 x 10^{-5} M, aq. HEPES). b) Average trace of simulated CD spectra on several simulated conformations extracted from MD runs. c) Inner structure of left-handed (M)-**NDPA**-AMP and right-handed (P)-**NDPA**-AMP assemblies, obtained at the end of MD. The shaded region highlights the stacking defects of P-helix. The Zn atoms are depicted in balls, with different colors depending on which side of the **NDPA** they are located, to show the chirality of the assembly. **NDPA** are depicted in thick sticks and H-bonds are shown in dashed light blue lines. The arrows guide the eye to show the chirality, the arrow pointing towards the back of the view.*

With ADP, similar observations to AMP were made, both in terms of energy and morphology. The *M* helices are slightly more stable than *P* helices (by 0.5 kcal/mol.molecule). The rotation angle between successive **NDPA**-ADP is around 58° ± 10°, similar to what is found for **NDPA**-AMP (57° ± 11°), i.e. ~around 6.3 **NDPA**/turn for both systems. The stacking distance of **NDPA** is slightly reduced from 4.0 Å to 3.8 Å, from AMP to ADP, likely due to the extra constraint imposed by ADP on adjacent molecules, which form dimers. The simulated CD spectrum for *M*-**NDPA**-ADP (Figure 2.10b) shows a negative bisignated signal with zero crossing around 380 nm, similar to that with AMP.
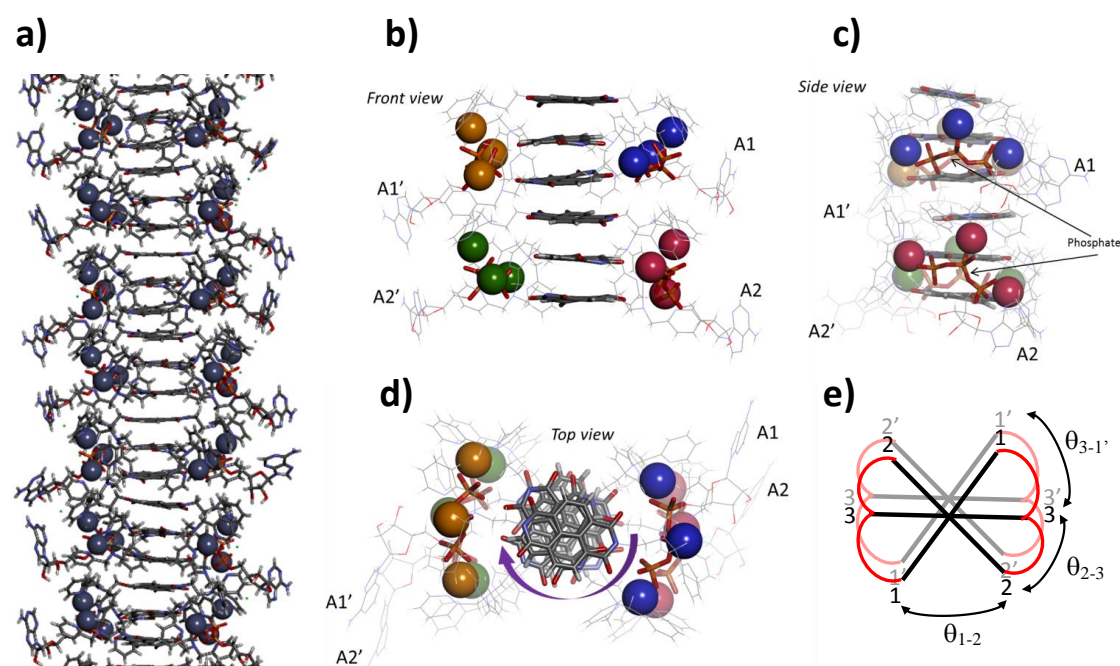
Figure 2.11. *Inner structure of right-handed (P)-**NDPA**-ATP assemblies, obtained at the end of MD. The Zn atoms are depicted in balls. a) a portion of the assembly ; b) and c) lateral views of two trimers (extracted in the middle of the assembly), with the Zn atoms depicted in different colors depending on which side of the **NDPA** they are located. **NDPA** are depicted in thick sticks, and A stands for adenine. d) Top view, with an arrow to guide the eye to show the chirality; e) schematic representation of a top view of two stacked trimers, showing ATP forming a "1-3-2" motif in red, and the angles between successive naphthalenediimide along the stack.*

ATP offers more binding possibilities than AMP or ADP, thus the number of probable structures of assemblies is more. However, two families of assemblies emerged from the simulations, depending on the binding motif: "1-2-3" or "1-3-2". This numbering refers to as both the stacking order and binding motif. The molecules are numbered along the stacking direction: "X-Y-Z" motif means that the **NDPA** molecules form trimers, where molecule X is linked to molecule Y, and molecule Y is linked to molecule Z (Figure 2.11 for the 1-3-2 motif).

The most stable structures are obtained for assemblies with "1-3-2" binding motif. The striking characteristic of these assemblies is that the organization of the adenosine phosphate complexes is not helical. While the naphthalenediimide cores do form an helical assembly (pitch of 6 naphthalenediimides per turn), the Zn-triphosphate complexes form two columns on both sides of the central helix (Figure 2.11 a, b, d). As the pitch of the naphthalenediimide helix is similar for all the adenosine phosphate (6 molecules with ATP, versus ~6.3 with AMP/ADP), as well as the average rotation angle between neighbouring molecules (60° versus 57-58°, respectively), the peculiar arrangement of the complexes is to be explained by symmetry. With AMP, the angle between the adenosine phosphate complexes is the same as the angle between the naphthalenediimides, and thus the complexes also form an helix. With **NDPA**-ATP, because each complex with ATP involves three naphthalenediimides, the angle between the complexes (trimers) is three times the angle between the naphthalenediimides, i.e. about 180°. As a result, the pitch of the assembly of adenosine phosphate complexes is of only two complexes, effectively corresponding to six **NDPA** molecules, the trimers being translational images from each other along the stacking direction. We then investigated in more details a representative "1-3-2" right-handed assembly. Although the average angle between naphthalenediimides is of 60°, a more detailed analysis reveals that there are three population distributions: the angle between molecules 1 and 2, θ_{1-2} is 81° ± 4°. Similarly, θ_{2-3} is 44° ± 4° and $\theta_{3-1'} = 54° ± 4°$, 1' refering to a molecule belonging to a neighbouring trimer (Figure 2.11). The first two angles deviate from the angle found in the **NDPA**-AMP arrangement (~57°) mainly due to the constraints imposed by ATP. The third one, however, measured between molecules belonging to adjacent trimers, i.e. molecules more free to rotate with respect to each other, is not much affected. This result indicates weak steric hindrance between trimers, which are able to stack while conserving the natural angle between single **NDPA** molecules. The sum of the three angles is 179°, corresponding well to the symmetry condition necessary for having adenosine phosphate complexes forming columns instead of helices.

Experimentally, for **NDPA**-ATP, *P*-helices are more stable than the *M*-helices, which is opposite to the situation with AMP and ADP. As the organization within the naphthalenediimide stacks are rather similar in the three systems, the change of helicity has to be found in the adenosine phosphate complexes. Their organization is indeed very different in AMP or ADP systems on the one side and ATP systems on the other side. With AMP and ADP, the adenosine moieties are able to be close enough to the naphthalenediimide cores to form H-bonds, principally via the hydroxyl groups. These interactions, however, no longer exist in the ATP systems as the adenosine moieties are pointing away (Figure 2.10c and Figure 2.11). The simulated CD spectra using the right-handed "1-3-2" **NDPA**-ATP assembly shows a bisignated signal with zero crossing at 383 nm, and positive and negative maxima located at 398 nm and

370 nm, respectively (Figure 2.10b). The comparison of simulated CD spectra based on average traces of MD snapshots on the (*M*)-**NDPA**-AMP and (*P*)-**NDPA**-ATP show almost mirror-image bisignated signals, in fair agreement with the experimental spectra (Figure 2.10a).

2.6 Guest Induced Chirality in PDPA Assembly
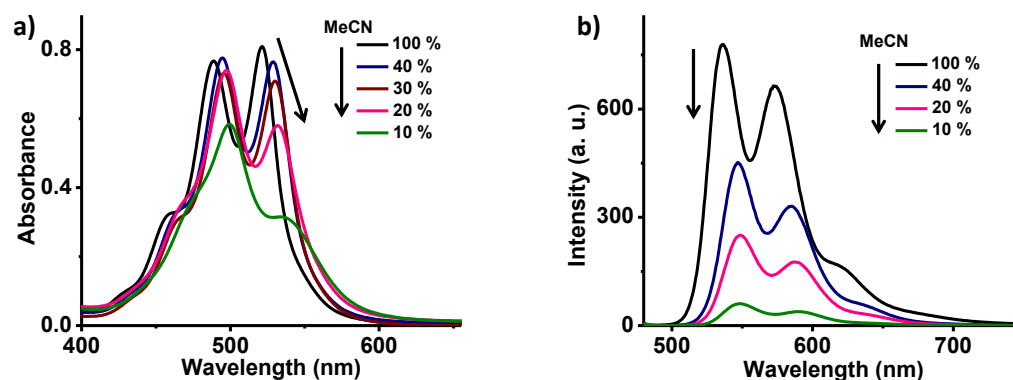
Figure 2.12. *Solvent dependent a) absorption and b) emission spectra (λ_{ex}=470 nm) of **PDPA** with varying percentages of MeCN in aq. HEPES buffer (c = 2 x 10^{-5} M).*

Having established the role of Zn-DPA towards phosphate recognition driven dynamic helical assembly with tunable handedness in NDI derivatives (**NDPA** and **NDPA-Amph**), we envisaged a broader scope of this design in controlling the supramolecular chiral organization of a variety of chromophores. Thus, perylenebisimide (PBI) functionalized with Zn-DPA complex (**PDPA**) was synthesised as a higher rylenediimide analogue of NDI. This compound was completely soluble in MeCN due to the presence of hydrophilic Zn^{2+} group and self-assembled in aq. HEPES buffer, due to hydrophobic and aromatic-aromatic interactions. UV/Vis absorption spectrum of **PDPA** in MeCN (c = 2 x 10^{-5} M) shows sharp vibronic features, characteristic of monomeric PBI chromophores.[2b,c] On increasing percentage of aq. HEPES buffer in MeCN, broadening of absorption band along with change of relative absorbance peak ratio were observed, confirming interchromophoric interactions leading to aggregation (Figure 2.12). Fluorescence spectra show quenching of monomeric emission upon increasing composition of aq. HEPES buffer, a clear proof of H-type (**H1**) cofacial assembly in PBI (detailed self-assembly investigation of **PDPA** will be discussed in Chapter 5).

Self-assembled **PDPA** stacks (90% aq. HEPES buffer in MeCN, c = 2 x 10^{-5} M) were constructed to study adenosine phosphate induced assembly and chirality induction. Binding of adenosine monophosphates (AMP) to **PDPA** stacks i.e. **PDPA**-AMP (90% aq. HEPES in MeCN, 2 x 10^{-5} M) led to complete quenching of monomeric emission band at 549 nm and 590 nm along with redshift of the absorption band indicating further ordering of stacks in **H1** state (Figure 2.13 a, b). Interestingly, the circular dichroism (CD) signal show a negative bisignated

cotton effect with negative and positive maxima at 557 nm, 496 nm respectively (Figure 2.13c), as expected of an excitonically coupled *M*-helix type chiral organization of PBI derivatives i.e. (*M*)-**PDPA**-AMP. Thus, binding of homochiral AMP to **PDPA** stacks results in guest induced chirality into their assembly. Moreover, such a strong induced CD signal also reflects the efficient phosphate recognition by **PDPA** stacks, in agreement with our design. Although, helicity induction upon phosphate binding to the aggregated state of **PDPA** is in contrast to the previous observations in **NDPA-Amph** (Section 2.4, Figure 2.6a), it could be due to further ordering of **PDPA** assembly upon interaction with phosphates as seen from the spectroscopic signatures in Figure 2.13.
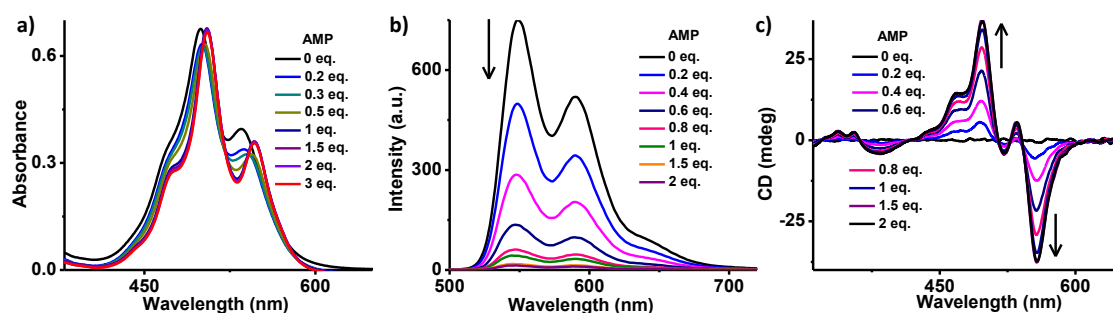
Figure 2.13. *Variation in the a) absorption spectra, b) emission spectra (λ_{ex} = 470 nm) and c) CD signal of **PDPA** upon titration with adenosine monophosphate (AMP) (90% aq. HEPES in MeCN, c = 2 x 10^{-5} M).*

Similar to the observations in **NDPA,** addition of adenosine triphosphate (ATP) to **PDPA** stacks i.e. **PDPA**-ATP (90% aq. HEPES in MeCN, 2 x 10^{-5} M) induced a positive bisignated CD signal i.e. positive at 518 nm followed by negative at 480 nm (Figure 2.14a). This is a clear signature of *P*-helix type organization i.e. (*P*)-**PDPA**-ATP, which is reverse in handedness compared to left-handed helical assembly obtained on AMP binding i.e. (*M*)-**PDPA**-AMP, as described in Figure 2.13. Thus, we clearly establish the general approach of Zn-DPA functionalized chromophores for induction of opposite helicity based on the type of chiral phosphate.

Interestingly, the induction of *P*-helix by ATP binding to **PDPA** stacks could be uniquely characterized by its spectroscopic signatures. For e.g., absorption spectra show a red shift of the band maxima from 499 nm to 514 nm and 535 nm to 564 nm upon interaction with ATP. Fluorescence spectra show gradual decrease of monomeric emission along with evolution of a new red shifted band at 665 nm in **PDPA**-ATP. Excitation spectra collected at the 665 nm emission showed a blue shifted band compared to monomeric absorption, confirming the formation of a new **H2-**type fluorescent aggregate (Figure 2.14d). Thus, we see that the **PDPA**-

ATP leads to supramolecular reorganization where the resultant aggregates are very different from that of **PDPA**-AMP as seen from the opposite CD signal, new emission band and the red shifted absorption.[17]
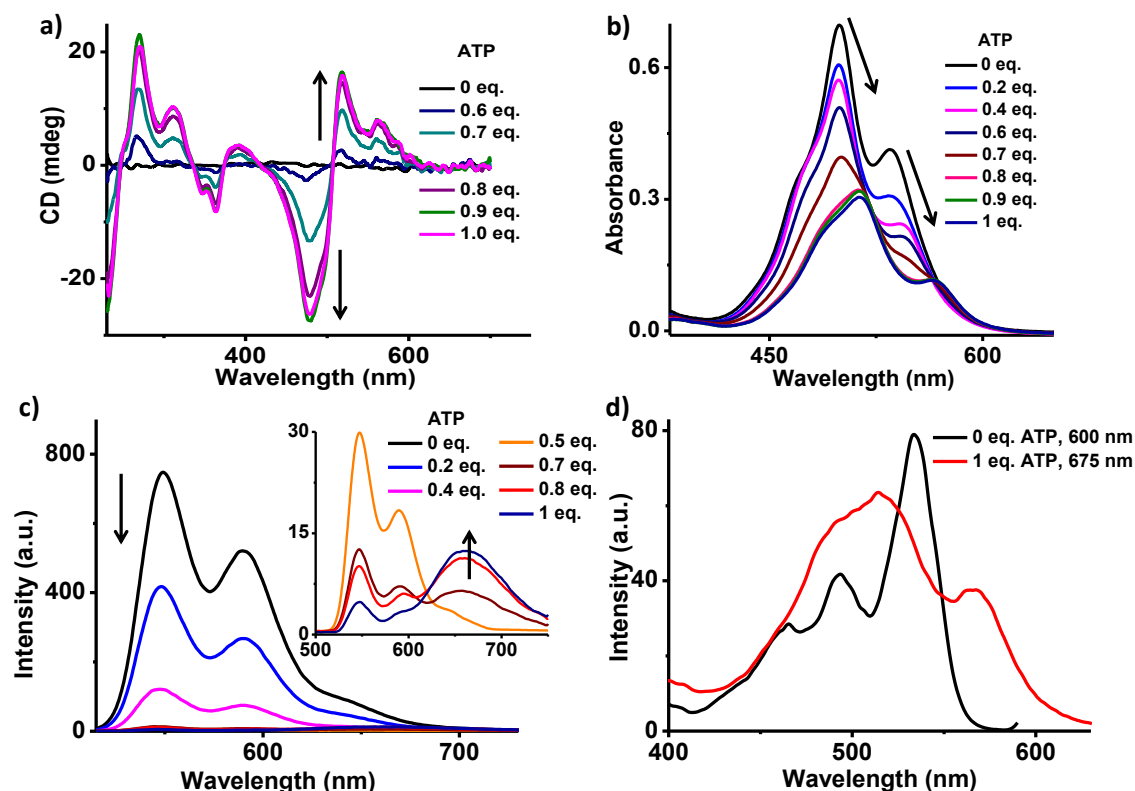
Figure 2.14. *Variation in the a) CD signal, b) absorption spectra and c) emission spectra ($\lambda_{ex} = 470$ nm) of **PDPA** upon titration with ATP, whereas d) shows the difference in the excitation spectra collected with and without ATP (90% aq. HEPES in MeCN, $c = 2 \times 10^{-5}$ M).*

2.7 Dynamic Helix Reversal

Having shown the induction of opposite helicity in **PDPA** stacks bound with either AMP or ATP, we envisaged that based on the strength of binding, ATP should be able to competitively replace the bound AMP from the stack leading to inversion of helix from (*M*)-**PDPA**-AMP to (*P*)-**PDPA**-ATP. Towards this goal, ATP was added in a stepwise manner to a solution of (*M*)-**PDPA**-AMP, while monitoring the CD spectra. We notice that the CD spectra inverts gradually from a negative bisignated signal to a positive bisignated signal, passing through an isodichroic point at zero crossing of 418 nm (Figure 2.15b). The final signal obtained after AMP replacement by ATP was same in intensity as compared to the **PDPA**-ATP, confirming complete substitution.
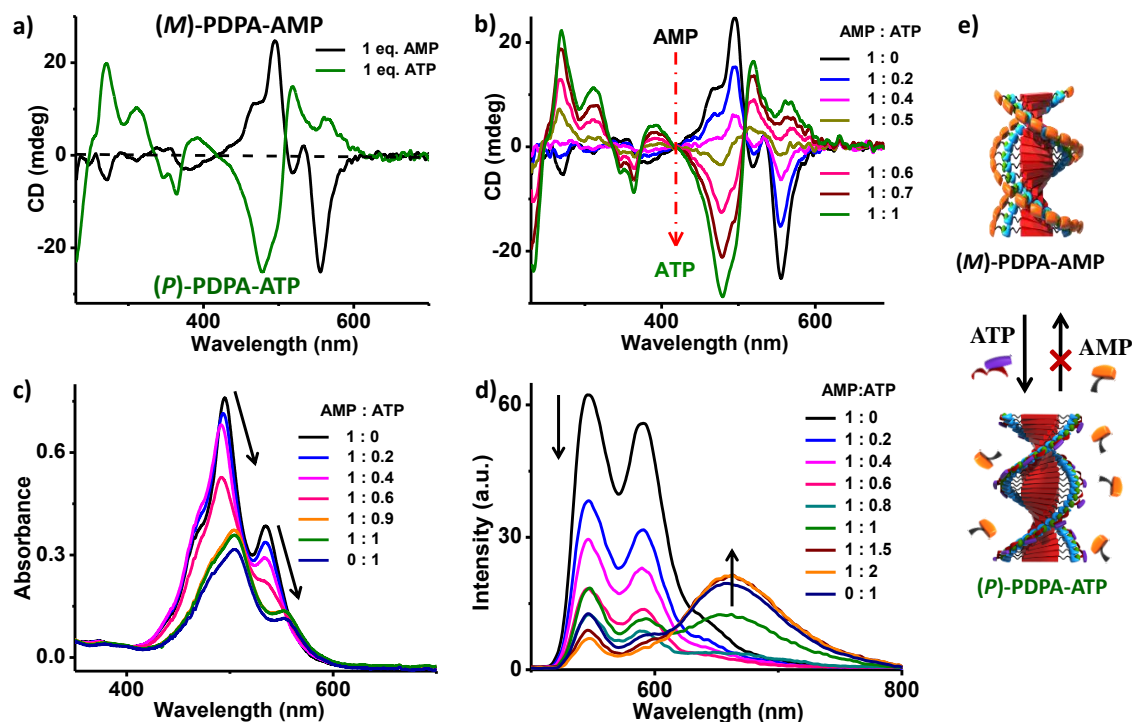
Figure 2.15. *a) CD spectra of (M)-**PDPA**-AMP and (P)-**PDPA**-ATP showing their mirror image relation. Variation in b) CD signal, c) absorption spectra and d) emission spectra upon addition of ATP to (M)-**PDPA**-AMP solution (90% aq. HEPES in MeCN, c = 2 x 10^{-5} M). e) Schematic representation of dynamic helix reversal through competitive replacement of AMP by ATP.*

Further confirmation of **PDPA**-ATP formation also comes from the absorption and emission changes. Addition of ATP to **PDPA**-AMP led to a bathochromic shift in absorption maxima, whereas emission spectra show evolution of a new emission band at higher wavelength (665 nm) along with further quenching of monomeric emission (Figure 2.15 c, d). The final spectra after AMP replacement closely resembled the **PDPA**-ATP signal, clearly proving quantitative replacement. Moreover, these changes were almost instantaneous, where the addition of an aliquot of ATP to (*M*)-**PDPA**-AMP led to sudden jump in the CD signal (*vide infra*). Such an observation also confirms the highly dynamic nature of these helical assemblies.

Results thus far have shown a very simple approach for the dynamic reversal of supramolecular helicity. Such a rational approach to switching of helicity in a step wise manner can also be employed in gaining a complete control over their helical states i.e. racemic form or either of the left of right-handed enantiomeric helix. In this regard, we utilized an inorganic phosphate, PPi [(P$_2$O$_7$)$^{4-}$] which is a divalent phosphate, but is known to show very strong interactions with Zn-DPA due to high charge density. Being achiral in nature, we speculated

that it can be used for conversion of homochiral stacks to racemic form.
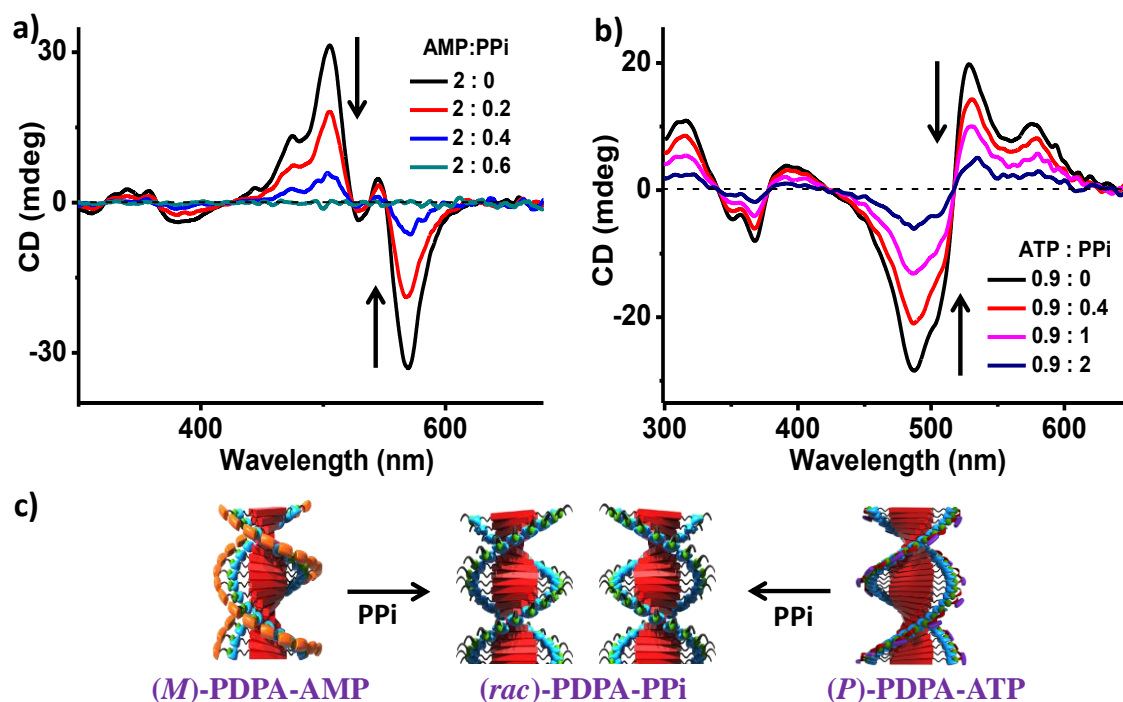
Figure 2.16. *Variation in CD signal upon addition of achiral PPi to a) (M)-**PDPA**-AMP and b) (P)-**PDPA**-ATP (90% aq. HEPES in MeCN, c = 2 x 10^{-5} M). Schematic in c) shows the transition from helical to racemic assembly by competitive replacement of AMP and ATP by PPi.*

When increasing amount of PPi was added to (*M*)-**PDPA**-AMP, we notice that the negative bisignated CD signal gradually decreases, with complete loss upon addition of 0.6 eq. of PPi (Figure 2.16a). Such an observation can be attributed to competitive removal of AMP by achiral PPi, thereby converting **PDPA**-AMP to **PDPA**-PPi stacks. As PPi do not have a chiral centre, their binding to **PDPA** stacks can only create racemic helices,[18] leading to conversion from (*M*)-**PDPA**-AMP to (*rac*)-**PDPA**-PPi. Similar experiments were also performed by addition of PPi to **PDPA**-ATP. As expected, we notice a continuous decrease in positive bisignated CD signal (Figure 2.16b). This again confirms the transformation from (*P*)-**PDPA**-ATP to (*rac*)-**PDPA**-PPi. We observe that the amount of PPi required to replace ATP is much higher compared to the case with AMP removal. This can be easily justified due to stronger association of ATP to **PDPA** stacks in comparison to the AMP. With these experiments, we have shown that apart from switching of helicity from a left-handed to right-handed assembly, we can dynamically convert them into their racemic form, providing next level of control over their helical states.
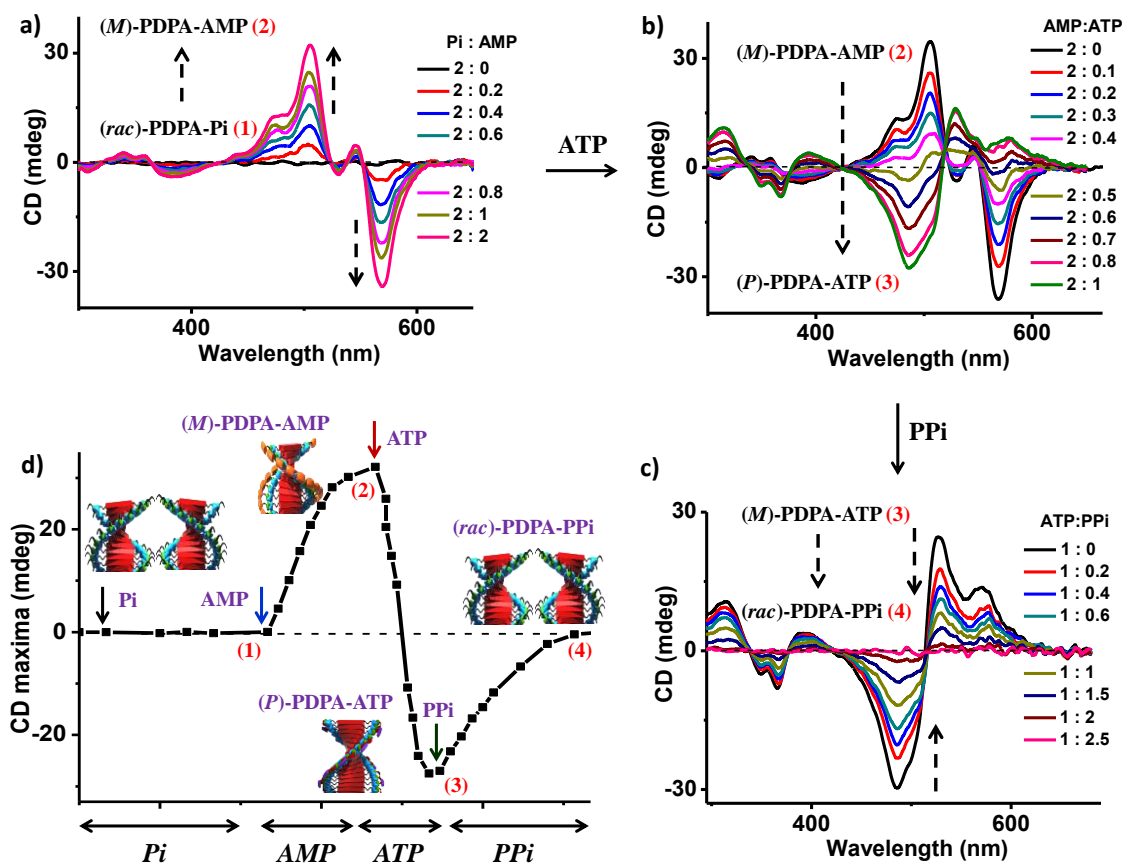
Figure 2.17. *Variation in CD signal upon sequential addition of a) AMP to (rac)-**PDPA**-Pi followed by b) ATP and subsequently c) PPi (90% aq. HEPES in MeCN, c = 2 x 10⁻⁵ M). d) shows the plot of CD maxima near 500 nm upon tandem addition of various phosphates, whereas the schematic represents the respective processes.*

With this unique system, we have shown control over various single step transitions like inversion of helicity, racemic to homochiral and vice-versa. The next challenge in this regard was to perform them in a sequential manner in one pot. This can be achieved by tandem addition of different phosphates, in order to complete one helix cycle from racemic to left followed by right-handed helix before converting them back to racemic again. Thus, we started with a solution of **PDPA** prebound with inorganic Pi [$(PO_4)^{3-}$], an achiral guest which provides a racemic assembly (*rac*)-**PDPA**-Pi. To this solution AMP was added continuously, which can replace Pi, thereby converting them into a homochiral left-handed assembly (Figure 2.17a). This could be easily monitored by the evolution of negative bisignated CD signal, confirming the formation of (*M*)-**PDPA**-AMP. Subsequently, this solution was subjected to increasing amounts of ATP. As expected, we see a reversal of CD signal from negative to positive bisignated CD signal passing through an isodichroic point with zero crossing at 423 nm (Figure 2.17b). This clearly indicates transition between two states, i.e. from left-handed (*M*)-**PDPA**-AMP to right-handed (*P*)-**PDPA**-ATP. Next step in this sequential process was the addition of

achiral PPi to the above obtained (*P*)-**PDPA**-ATP solution. CD spectra shows continuous decrease in signal intensity, which finally resulted in CD silent state at higher eq. of PPi (Figure 2.17c). This evidently confirm the transformation from ATP bound right-handed helix to (*rac*)-**PDPA**-PPi. A better picture of the whole process could be obtained by the plot of maximum CD intensity (~ 495 nm) against sequential addition of various phosphates. Thus, CD silent feature of (*rac*)-**PDPA**-Pi, show increase in signal upon AMP addition, followed by its reversal in presence of ATP, before further decrease to zero CD signal in presence of PPi (Figure 2.17d). Thus, we have shown a sequential change of helical states from racemic to left-handed, followed by right-handed before converting them back to racemic **PDPA** stacks (Figure 2.17d), covering one complete helix cycle.
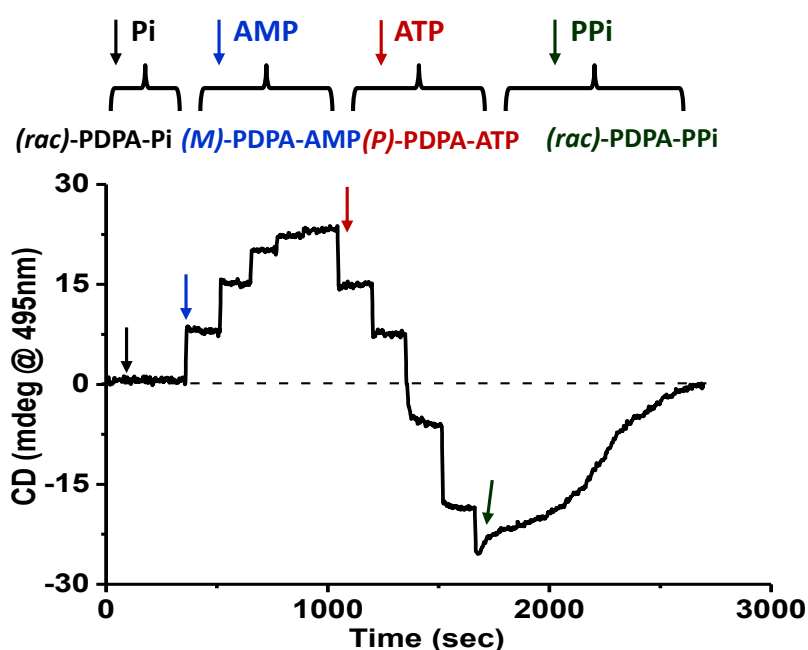
Figure 2.18. *Plot of CD signal with time showing sharp jumps in CD intensity monitored at 495 nm, upon sequential addition of Pi (black arrow) followed by AMP (blue arrow), ATP (blue arrow) and finally PPi (green arrow) confirming very fast response to change of binding phosphates (90% aq. HEPES in MeCN, c = 2 x 10^{-5} M).*

To prove the highly dynamic nature of these assemblies leading to fast switchability of the helical states, time dependent variation in CD intensity was monitored upon tandem addition of various phosphates. Addition of AMP to (*rac*)-**PDPA**-Pi show sharp jump in the CD signal with each aliquot of AMP (Figure 2.18). This steep rise in signal with a step wise change upon AMP binding indicates instantaneous transition from racemic state to (*M*)-**PDPA**-AMP. Similar observation was also made on ATP addition to the above solution leading to dynamic helix reversal. However, upon addition of PPi to ATP, we notice that these changes are not instantaneous but has a finite kinetics. This could be due to strong association of ATP to

PDPA stacks, such that PPi takes a finite amount of time to replace them, leading to (*rac*)-**PDPA**-PPi.[19]
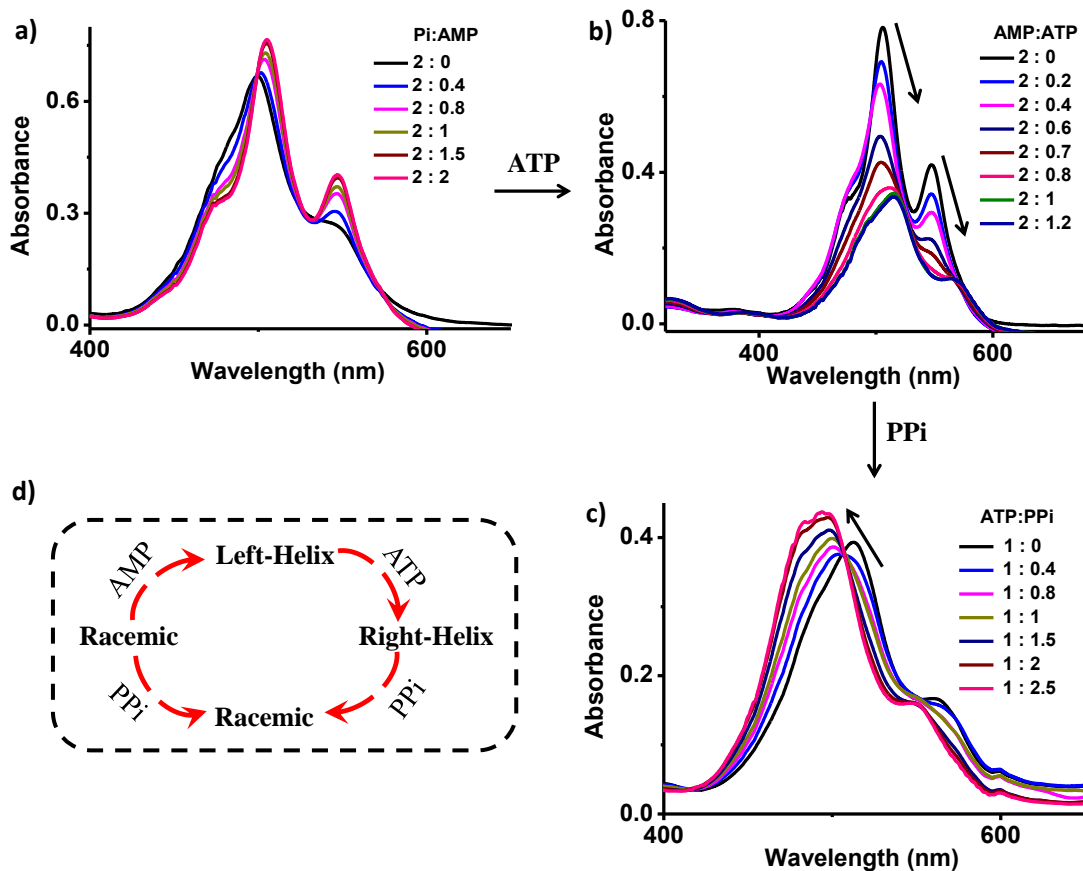
Figure 2.19. *Variation in absorption spectra upon sequential addition of a) AMP to (rac)-**PDPA**-Pi followed by b) ATP and subsequently c) PPi (90% aq. HEPES in MeCN, c = 2 x 10^{-5} M). d) is a pictorial representation of transformation over one complete helix cycle.*

Further confirmation of these phosphate replacements comes from the plot of change in absorption spectra at various stage of helix transitions. In the first step of Pi replacement by AMP, we notice a red shift in the absorption spectra due to stronger aggregation behaviour of **PDPA**-AMP (Figure 2.19a). Upon further addition of ATP, a significant red shift in the absorption maxima was observed, which has been shown to be characteristic of **PDPA**-ATP (Figure 2.14b, Figure 2.19b). Interestingly, addition of PPi to the above solution led to a blue shift in the absorption spectra as expected after removal of ATP from **PDPA** stacks, leading to the formation of **PDPA**-PPi. Thus, both optical and chiroptical readout unambiguously confirm to the step wise dynamic replacement of phosphates leading to one complete helix cycle from racemic to left-handed helix followed by right-handed helix before converting them back to racemic as shown in Figure 2.19d.

2.8 Conclusions

In summary, we have showed a novel supramolecular design, based on dipicolylethylenediamine functionality, for the adenosine phosphate recognition driven one-dimensional helical assembly of achiral chromophores. These stacks show preferential helix formation based on the nature of bound adenosine phosphate. Binding of AMP/ADP resulted in left-handed helical assembly, whereas ATP induced right-handed organization. Detailed molecular dynamic (MD) simulations have clearly indicated the crucial role of van der Waals' forces and hydrogen bonding interactions in stabilizing the preferred handedness. The broader scope of this approach was established by demonstrating it in both NDI and PBI derivatives. We have also shown a novel strategy for the dynamic helical reversal of supramolecular assemblies, based on competitive replacement of the guest molecules due to multivalent interactions. This strategy was effectively utilized in establishing a complete control over the helical states of assembly by completing one helix cycle. This rational design for unprecedented control over the helix handedness along with its dynamic and versatile stimuli response holds great promise as material for enantioselective and other chirotechological applications.

2.9 Experimental Section

General Methods:

Transmission Electron Microscopy (TEM): TEM measurements were performed on a JEOL, JEM 3010 operated at 300 kV. Samples were prepared by placing a drop of the solution on carbon coated copper grids followed by drying at room temperature. The images were recorded with an operating voltage 300 kV. In order to get a better contrast sample was stained with uranyl acetate (1 wt % in water) before the measurements. For TEM, water was used instead of aq. HEPES solution to avoid masking of nanostructures due to HEPES deposition upon drying.

Optical Measurements: Electronic absorption spectra were recorded on a Perkin Elmer Lambda 900 UV-Vis-NIR Spectrometer and emission spectra were recorded on Perkin Elmer LS 55 Luminescence Spectrometer. UV-Vis and emission spectra were recorded in 10 mm path length cuvettes. Circular Dichroism measurements were performed on a Jasco J-815 spectrometer where the sensitivity, time constant and scan rate were chosen appropriately. Corresponding temperature dependent measurements were performed with a CDF – 426S/15 Peltier-type temperature controller with a temperature range of 263-383 K and adjustable temperature slope.

NMR Measurements: NMR spectra were obtained with a Bruker AVANCE 400 (400 MHz) Fourier transform NMR spectrometer with chemical shifts reported in parts per million (ppm) with respect to residual solvent peak.

Dynamic light scattering (DLS) Experiments: The measurements were carried out using a NanoZS (Malvern UK) employing a 532 nm laser at a back scattering angle of 173°. The samples were measured in a 10 mm glass cuvette.

Sample Preparation: All samples for spectroscopic measurements in NDI derivatives were prepared by injecting the stock solution of **NDPA-Amph** or **NDPA** into required volume of solvent (aq. HEPES buffer and THF, wherever applicable). For **PDPA**, all samples for spectroscopic measurements were prepared by injecting the stock solution of **PDPA** (solvent MeCN) into required volume of solvent (aq. HEPES buffer in MeCN, wherever applicable). Required amount of phosphates were injected into these solutions and were mixed by manual shaking before measurements.

Phosphates stock solutions were prepared in 10^{-2} M concentration by dissolving the required amount of compound in HEPES buffer solution.

Materials: N,N-Bis(2-pyridylmethyl)ethane-1,2-diamine was synthesized based on reported procedure.[11] All other chemicals were purchased from the commercial sources and were used as such. Spectroscopic grade solvents were used for all optical measurements.

Legends in graphs represent molar eq. with respect to **NDI or PBI**.

Molecular Modelling Simulations (methodology):

Stacks of **NDPA** linked to either AMP, ADP, or ATP were modeled with the Materials Studio 6.0 modeling package (Accelrys), by molecular mechanics (MM) and molecular dynamics (MD) methods using an adapted version of Dreiding as a force field.[20] To maintain full complexation in **NDPA** during MD, a bond between the sp^3 nitrogen atom and the zinc atom had to be built. The Dreiding force field was accordingly adapted, increasing the (N_3-Zn) equilibrium distance from 2.022 Å to 2.585 Å, and replacing the *-Zn-* angle bending term by new angle bending terms, Cl-Zn-Cl, Cl-Zn-N_R, O_3-Zn-O_3, O_3-Zn-N_R, and N_R-Zn-N_R, with the same constants as those for *-Zn-*. These adaptations and the validation of the new force field were based on a **NDPA** structure optimized from DFT calculations at the B3LYP/6-31G* level, using the LANL2DZ effective core potential and associated basis set to describe the zinc ion.

For ATP-based systems, due to a number of binding possibilities with different orders of binding, i.e. "1-2-3" or "1-3-2", isolated trimers were built and optimized, before stacking them into supramolecular assemblies of 33 molecules (11 trimers). For AMP- and ADP-based systems, supramolecular assemblies of 32 molecules were directly built. The initial distance between **NDPA** planes in the stacks is about 3.8 Å and the angle between the molecular axis of neighbouring molecules is set to a value typically between 30° and 60° to avoid steric crowding of the side groups. These assemblies were optimized by MM, and submitted to a 100 ps relaxation Molecular Dynamics with the **NDPA** cores frozen, to relax most of the steric constraints in the periphery of the assembly, while avoiding disorganizing the stack. Then, a production MD is performed without any constraint during 20 ns.

The MM energy minimizations were performed with a conjugate gradient algorithm and a convergence criterion of 0.001 kcal/mol.Å. The long-range interaction cutoff distance was set to 14 Å with a spline width of 3 Å. The charges on the atoms were assigned from the PCFF force field,[21] and tested as previously reported on other types of structures.[22] The MD simulations were performed in the canonical (N,V,T) ensemble. The Nosé thermal bath coupling[23] was used to maintain the temperature at 300 K, with a coupling constant of 0.05. The Verlet velocity algorithm was used to integrate the equations of motion with a 1 fs time step.

The calculation of the excitonic CD spectra involves two steps. First, the lowest 30 excited states of the 32 **NDPA** molecules extracted from the MD trajectories above are computed at the Intermediate Neglect of Differential Overlap/Singles-Configuration Interaction (INDO/SCI) level (using an active space of 30 occupied and 30 empty molecular orbitals). Then, an excitonic Hamiltonian encompassing a total of 32x30 basis functions (30 localized excitations per molecule) is built on the basis of INDO/SCI[24] excitation energies and exciton couplings. The latter are calculated as Coulomb interactions between transition densities, thus going beyond the usual point dipole model.[25] Diagonalization of this Hamiltonian yields a set of 960 exciton states α with energies $\hbar\omega_\alpha$ and wavefunctions $|\psi_\alpha>$, for which the oscillator strength f_α and the rotational strength R_α are computed as:[26]

$$f_\alpha = \sum_{i,n} \frac{\left|\left\langle \psi_\alpha \left| \hat{\underline{\mu}}_{i,n} \right| G \right\rangle\right|^2}{\left|\underline{\mu}_{i,n}\right|^2},$$

$$R_{\alpha} = \frac{\eta \omega_{\alpha}}{c} \sum_{i,n} \sum_{j,n'} \frac{\langle \psi_{\alpha} | \hat{\underline{\mu}}_{i,n} | G \rangle \times \langle G | \hat{\underline{\mu}}_{j,n'} | \psi_{\alpha} \rangle \cdot (\underline{r}_n - \underline{r}_{n'})}{|\underline{\mu}_{i,n}| \, |\underline{\mu}_{j,n'}|} \; ,$$

where c is the speed of light, $\mu_{i,n}$ the transition dipole moment from the ground state /g> to the excited state |i> of molecule n along the stack, $\hat{\underline{\mu}}_{i,n} = \underline{\mu}_{i,n} (|i,n\rangle\langle g| + h.c.)$ the corresponding dipole operator, /G> the ground state of the helical stack (product state of all /g>), and $|\psi_{\alpha}\rangle = \sum_{i,n} c_{i,n}^{\alpha} |i,n\rangle$ the exciton state wavefunctions expanded in terms of the $c_{i,n}^{\alpha}$ eigenvectors. The absorption/CD response at input frequency ω is calculated on the basis of the oscillator/rotational strengths as:

$$Abn(\omega) = <\sum_{\alpha} f_{\alpha} \, G(\omega - \omega_{\alpha})> \, ,$$

$$CD(\omega) = <\sum_{\alpha} R_{\alpha} \, G(\omega - \omega_{\alpha})> \, ,$$

where $G(\omega-\omega_{\alpha})$ is a Gaussian function centered around ω_{α} with variance $\sigma = 0.1$ eV. The brackets denote a configurational average over the positional and energetic disorder as explored during the MD simulations. Here, a total of 8 supramolecular helical structures, each consisting of 32 (for **NDPA**-AMP/ADP assemblies) or 33 (for **NDPA**-ATP assemblies) molecules, were used. This approach was found to yield CD spectra that are stable with respect to configurational averaging.

<u>**Synthesis:**</u>

NDPA and **PDPA** were synthesized and characterized according to the literature procedure.[11]

Synthesis of **NDPA-Amph** was peformed according to Scheme 2.3. Procedures are given below.

Synthesis of 1: 1,4,5,8-Naphthalenetetracarboxylic dianhydride (1 g, 3.73 mmol) was added to N,N-Bis(2-pyridylmethyl)ethane-1,2-diamine (1.08 g, 4.47 mmol) and dodecylamine (0.82 g, 4.47 mmol) in 20 ml DMF and the reaction mixture was stirred at 120 °C overnight. DMF was evaporated under vacuum and residue was extracted with chloroform and water. Organic layer was dried over anhydrous Na_2SO_4, and solvent was evaporated. Compound was purified by column chromatography to give 110 mg of desired product **1** (Yield = 5%). Low yield was mainly due to a) statistical three possible products, b) presence of basic pyridine group in the compound which tend to stick to silica gel during column chromatography. ^{1}H NMR (400MHz,

CDCl$_3$) : δ 8.77 (d, 2H, J = 7.6 Hz), 8.67 (d, 2H, J = 7.6 Hz), 8.36 (m, 2H), 7.30 (m, 4H), 7.00 (m, 2H), 4.40 (t, 2H, J = 6.2 Hz), 4.20 (m, 2H), 3.90(s, 4H), 2.95 (t, 2H, J = 6.2 Hz), 1.25 (m, 20H), 0.87 (t, 3H, J =7 Hz); ^{13}C NMR δ_C (100 MHz, CDCl$_3$): 163.00, 162.76, 159.55, 149.05, 136.24, 131.07, 130.99, 126.84, 126.79, 126.76, 123.00, 121.98, 60.42, 51.42, 41.20, 38.63, 32.05, 29.78, 29.76, 29.73, 29.67, 29.48, 29.25, 27.25, 22.82, 14.25; MS (ESI): m/z calcd for C$_{40}$H$_{45}$N$_5$O$_4$: 659.84 [M$^+$], found: 659.0.
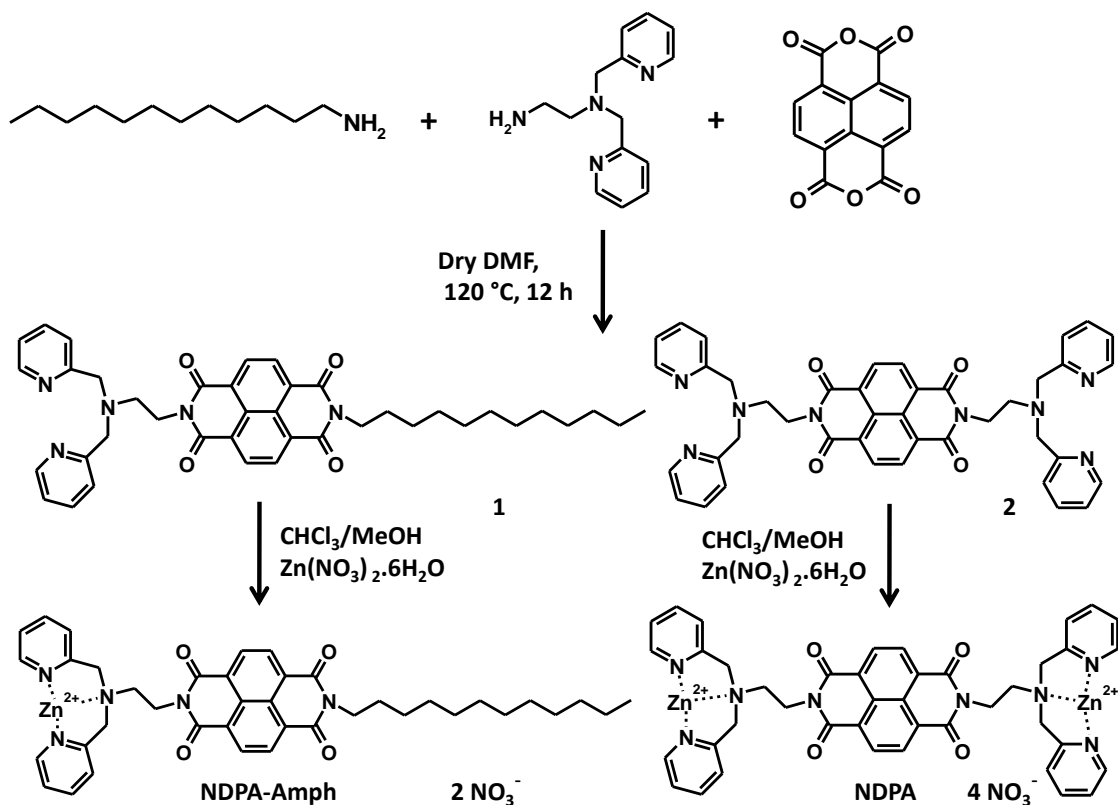
Scheme 2.3. *Synthetic scheme for **NDPA-Amph** and **NDPA** based amphiphiles.*

Synthesis of NDPA-Amph

50 mg (0.07 mmol) of **1** was taken in CHCl$_3$ (3 ml) and was added drop wise to a solution of Zn(NO$_3$)$_2$.6H$_2$O (42 mg, 0.1 mmol) in methanol (1 ml). The reaction mixture was then stirred for 30 minutes at room temperature and then the solvent was evaporated. The residue obtained was dissolved in CHCl$_3$ and filtered to remove the unreacted Zn(NO$_3$)$_2$.6H$_2$O. Filtrate was concentrated under reduced pressure to get 50 mg of the desired product **NDPA-Amph** as white solid (Yield = 78.5%). ^{1}H NMR (400MHz, CDCl$_3$) : δ 8.82 (d, 2H, J = 4.9 Hz), 8.70 (d, 2H, J = 7.6 Hz), 8.62 (d, 2H, J = 7.6 Hz), 8.04 (dt, 2H, J = 7.7, 1.6 Hz), 7.58 (m, 4H), 4.70 (m, 2H, J = 15 Hz), 4.50 (m, 2H), 4.40 (m, 2H), 4.16 (t, 2H, J = 7.6 Hz), 2.82 (t, 2H, J = 7.6 Hz), 1.24-1.72 (m, 20H), 0.86 (t, 3H, J = 6.8 Hz); ^{13}C NMR δ_C (100 MHz, CDCl$_3$): 162.70, 162.66, 153.9, 149.07, 140.95, 131.31, 130.99, 127.23, 126.74, 126.72, 125.95, 125.59, 124.43, 56.42,

47.68, 41.22, 33.52, 32.04, 29.75, 29.74, 29.71, 29.64, 29.46, 29.43, 28.18, 27.21, 22.81, 14.24; HRMS (ESI): m/z: calcd for M-Zn(NO$_3$)$_2$ i.e. C$_{40}$H$_{45}$N$_5$O$_4$: 659.8134, found : 660.3562.

2.10 References and Notes

1. a) E. Yashima, K. Maeda and Y. Okamoto, *Nature,* **1999**, *399*, 449; K. Maeda and E. Yashima, *Top. Curr. Chem.*, **2006**, *265*, 47; b) E. Yashima and K. Maeda, *Macromolecules*, **2008**, *41*, 3; M. M. Green, K.-S. Cheon, S.-Y. Yang, J.-W. Park, S. Swansburg and W. Liu, *Acc. Chem. Res.*, **2001**, *34*, 672; c) M. Fujiki, J. R. Koe, K. Terao, T. Sato, A. Teramoto and J. Watanabe, *Polym. J.*, **2003**, *35*, 297.

2. a) A. R. A. Palmans and E. W. Meijer, *Angew. Chem. Int. Ed.*, **2007**, *46*, 8948; b) A. Lohr and F. Würthner, *Isr. J. Chem.,* **2011**, *51***,** 1052; c) A. Lohr and F. Würthner, *Angew. Chem. Int. Ed.*, **2008**, *47*, 1232; d) S. J. George, A. Ajayaghosh, P. Jonkheijm, A. P. H. J. Schenning and E. W. Meijer, *Angew. Chem. Int. Ed.*, **2004**, *43*, 3422; in *Chirality at the Nanoscale*, ed. D. B. Amabilino, Wiley-Vch Verlag GmbH & Co. KGaA, Weinheim, 1st edn., **2009**; e) M. A. Mateos-Timoneda, M. Crego-Calama, and D. N. Reinhoudt, *Chem. Soc. Rev.,* **2004**, *33,* 363.

3. a) H. Fenniri, B.-L. Deng, and A. E. Ribbe, *J. Am. Chem. Soc.* **2002**, *124*, 11064; b) S. J. George, Ž. Tomović, M. M. J. Smulders, T. F. A. de Greef, P. E. L. G. Leclère, E. W. Meijer and A. P. H. J. Schenning, *Angew. Chem. Int. Ed.,* **2007**, *46*, 8206; c) J. Xiao, J. Xu, S. Cui, H. Liu, S. Wang and Y. Li, *Org. Lett.,* **2008**, *10*, 645; d) A. A. Sobczuk, Y. Tsuchiya, T. Shiraki, S.-ichi Tamaru and S. Shinkai, *Chem. Eur. J.,* **2012**, *18*, 2832; e) K. Toyofuku, Md. A. Alam, A. Tsuda, N. Fujita, S. Sakamoto, K. Yamaguchi and T. Aida, *Angew. Chem. Int. Ed.,* **2007**, *46,* 6476.

4. a) A. R. A. Palmans, J. A. J. M. Vekemans, E. E. Havinga and E. W. Meijer, *Angew. Chem. Int. Ed. Engl.*, **1997**, *36*, 2648; b) S. J. George, Ž. Tomović, A. P. H. J. Schenning and E. W. Meijer, *Chem. Commun.,* **2011**, *47*, 3451; c) B. Isare, M. Linares, L. Zargarian, S. Fermandjian, M. Miura, S. Motohashi, N. Vanthuyne, R. Lazzaroni and L. Bouteiller, *Chem. Eur. J.*, **2010**, *16*, 173; d) N. Katsonis, H. Xu, R. M. Haak, T. Kudernac, Ž. Tomović, S. J. George, M. Van der Auweraer, A. P. H. J. Schenning, E. W. Meijer, B. L. Feringa and S. D. Feyter, *Angew. Chem. Int. Ed.*, **2008**, *47*, 4997; e) S. Ghosh, X-Q. Li, V. Stepanenko and F. Würthner, *Chem. Eur. J.*, **2008**, *14*, 11343.

5. a) P. A. Korevaar, S. J. George, A. J. Markvoort, M. M. J. Smulders, P. A. J. Hilbers, A. P. H. J. Schenning, T. F. A. de Greef and E. W. Meijer, *Nature,* **2012**, *481*, 492; b) I. D. Cat, Z. Guo, S. J. George, E. W. Meijer, A. P. H. J. Schenning and S. D. Feyter, *J. Am. Chem. Soc.,* **2012***, 134,* 3171; c) A. Mammana, A. D'Urso, R. Lauceri and R. Purrello, *J. Am. Chem. Soc.*, **2007**, *129*, 8062.

6. K. Shimomura, T. Ikai, S. Kanoh, E. Yashima and K. Maeda, *Nat. Chem.,* **2014**, *6*, 429.

7. a) N. Ousaka, Y. Takeyama and E. Yashima, *Chem. Sci.*, **2012**, *3*, 466; b) P. G. A. Janssen, A. Ruiz-Carretero, D. González-Rodríguez, E. W. Meijer and A. P. H. J. Schenning, *Angew. Chem. Int. Ed.*, **2009**, *48*, 8103, c) M. Fujiki, *J. Am. Chem. Soc.,* **2000,** *122***,** 3336; d) H. Nakako, R. Nomura and T. Masuda, *Macromolecules*, **2001**, *34*, 1496; e) M. M. Bournan and E. W Meijer, *Adv. Mater.*, **1995**, *7*, 385; f) E. Ohta, H. Sato, S. Ando, A. Kosaka, T. Fukushima, D. Hashizume, M. Yamasaki, K. Hasegawa, A. Muraoka, H. Ushiyama, K. Yamashita and T. Aida, *Nat. Chem.*, **2011**, *3*, 68.

8. a) S. V. Bhosale, S. V. Bhosale and S. K. Bhargava, *Org. Biomol. Chem.,* **2012**, *10*, 6455; b) H. Shao and J. R. Parquette, *Chem. Commun.,* **2010**, *46***,** 4285; c) H. Shao, J. Seifert, N. C. Romano, M. Gao, J. J. Helmus, C. P. Jaroniec, D. A. Modarelli and J. R. Parquette, *Angew. Chem. Int. Ed.*, **2010**, *49*, 7688; d) G. D. Pantoş, P. Pengo and J. K. M. Sanders, *Angew. Chem. Int. Ed.*, **2007**, *46*, 194; e) M. R. Molla, A. Das and S. Ghosh, *Chem. Commun.,* **2011**, *47*, 8934.

9. a) M.-A. Morikawa, M. Yoshihara, T. Endo and N. Kimizuka, *J. Am. Chem. Soc.,* **2005**, *127*, 1358; b) I. O. Hirata, M. Takeuchi and S. Shinkai, *J. Am. Chem. Soc.,* **2006**, *128,* 16008; c) T. Ma, C. Li and G. Shi, *Langmuir,* **2008**, *24*, 43.

10. S. Yagai, S. Mahesh, Y. Kikkawa, K. Unoike, T. Karatsu, A. Kitamura and A. Ajayaghosh, *Angew. Chem. Int. Ed.,* **2008**, *47*, 4691.

11. a) H. N. Lee, Z. Xu, S. K. Kim, K. M. K. Swamy, Y. Kim, S.-J. Kim and J. Yoon, *J. Am. Chem. Soc.,* **2007**, *129*, 3828; b) X. Chen, M. J. Jou and J. Yoon, *Org. Lett.*, **2009**, *11*, 2181; c) S. K. Kim, D. H. Lee, J.-I. Hong and J. Yoon, *Acc. Chem. Res.,* **2009**, *42*, 23; d) T. Sakamoto, A. Ojida and I. Hamachi, *Chem. Commun.*, **2009**, 141.

12. S. V. Bhosale, C. H. Jani, S. J. Langford, *Chem. Soc. Rev.,* **2008**, *37*, 331.

13. J. Gawroński, M. Brzostowska, K. Kacprzak, H. Kołbon and P. Skowronek, *Chirality*, **2000**, *12*, 263.

14. Addition of higher eq.s of phosphates resulted in higher order aggregation, due to cross-linking, resulting in the decrease of CD intensity.

15. a) F. J. M. Hoeben, I. O. Shklyarevskiy, M. J. Pouderoijen, H. Engelkamp, A. P. H. J. Schenning, P. C. M. Christianen, J. C. Maan and E. W. Meijer, *Angew. Chem. Int. Ed.,* **2006**, *45*, 1232; b) M. Kumar and S. J. George, *Chem. Eur. J.,* **2011**, *17*, 11102, c) K. V. Rao and S. J. George, *Org. Lett.,* **2010**, *12*, 2656.

16. Absence of chiral induction in pre-assembled **NDI-Amph** assemblies is probably due to different energy minima (achiral stack) or solvent composition compared to helical co-assembled counterparts with ADP.

17. Although **PDPA**-AMP and **PDPA**-ATP show negative and positive bisignated CD signal respectively, they are not a mirror image pair. They form opposite helical assembly, but are not enantiomers, as evident from their absorption and emission features (Figure 2.23).

18. Although we describe **PDPA**-PPi to be racemic assemblies, an achiral state cannot be ruled out.

19. Such behaviour can also be due to chiral memory in the system, but as the system is highly dynamic, we can rule out such effects.

20. S. L. Mayo, B. D. Olafson and W. A. Goddard, *J. Phys. Chem.,* **1990**, *94*, 8897.

21. a) H. Sun, *J. Comput. Chem.,* **1994**, *15*, 752 ; b) H. Sun, *Macromolecules,* **1995**, *28*, 701.

22. P. Brocorens, M. Linares, C. Guyard-Duhayon, R. Guillot, B. Andrioletti, D. Suhr, B. Isare, R. Lazzaroni and L. Bouteiller, *J. Phys. Chem. B*, **2013**, *117*, 5379.

23. S. A. Nosé, *Mol. Phys.,* **1984**, *52*, 255.

24. J. Ridley and M. Zerner, *Theor. Chim. Acta,* **1973**, *32*, 111.

25. D. Beljonne, J. Cornil, R. Silbey, P. Millié and J. L. Brédas, *J. Chem. Phys.,* **2000**, *112*, 4749.

26. F. C. Spano, S. C. J. Meskers, E. Hennebicq and D. Beljonne, *J. Am. Chem. Soc.,* **2007**, *129*, 7044.

CHAPTER-3

Dynamic Helical Supramolecular Polymer with Stimuli Responsive Handedness: In situ probing of Enzymatic ATP Hydrolysis

Chapter-3

Dynamic Helical Supramolecular Polymer with Stimuli Responsive Handedness: In situ probing of Enzymatic ATP Hydrolysis

Abstract

Design of artificial systems which can respond to fluctuations in concentration of adenosine phosphates are essential in understanding the energy economy of biological systems. Helical assemblies of chromophores, which dynamically respond to such changes, can provide real-time chiroptical readout of various chemical transformations. Towards this concept, we present a supramolecular helix of achiral chromophores, which shows chiral adenosine phosphate responsive tunable handedness along with dynamic reversal of helicity. This system, composing of naphthalenediimide chromophores with phosphate recognition unit, shows opposite handedness on binding with ATP compared to ADP/AMP. Such differential signalling along with stimuli dependent fast stereomutations has been capitalized to probe the reaction kinetics of enzymatic ATP hydrolysis. Detailed chiroptical analysis provide mechanistic insights into the enzymatic hydrolysis and various intermediate steps. Thus a unique "all-in-one" dynamic helical assembly to monitor the real time reaction processes via its stimuli-responsive chiroptical signalling is conceptualized.
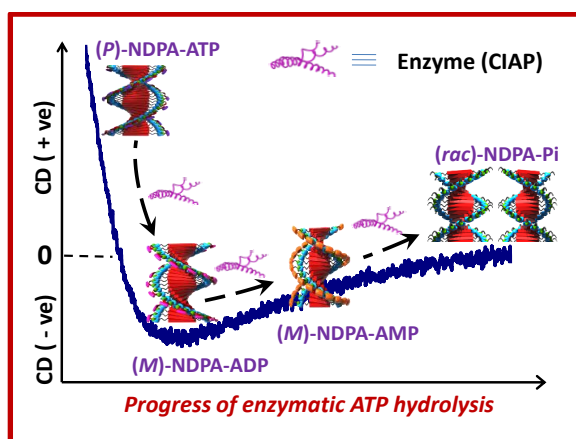
Manuscript based on this work is under submission.

3.1 Introduction

Helically organized polymeric[1] and supramolecular[2] assemblies have been the subject of considerable interest as biomimetic systems to understand and appreciate asymmetric preferences like homochirality in nature. Typical designs of helical assemblies consist of optically active monomers, which bias the handedness during the (supramolecular) polymerization process.[3] In this respect, helicity induction in racemic/achiral assemblies, constructed from "achiral" monomers, through non-covalent interactions with the chiral guest molecules is an alternative, synthetic strategy. Various types of forces like hydrogen bonding,[4] acid-base/electrostatic interactions,[5] preferential chiral solvation etc.[6] have been employed for this purpose. Such a strategy also allows easy tunability of handedness just by changing the chirality of the guest molecules, thereby avoiding many synthetic challenges.

The host-guest design for helical assemblies provides new opportunities to investigate mechanistic details of supramolecular chirality along with many practical chirotechnological applications. For example, this design has been used for the asymmetric synthesis of metastable homochiral systems (chiral memory) from kinetically stable assemblies, by the post-synthetic removal of chiral guest molecules (auxiliaries).[7] In particular, this approach has helped to understand the mechanistic pathways of racemisation and various off-nucleation processes of supramolecular polymers.[8] Recently, Yashima *et al* have utilized the memory of helical polymers for the construction of chiral stationary phase for chromatographic separation of enantiomers.[7g] Interestingly, the order of eluting enantiomers could be easily controlled by dynamically switching the chirality of the stationary phase upon interactions with the guest of opposite chirality. On the other hand, dynamic helical assemblies, with stimuli responsive chiroptical and conformational responses have been utilized as enantioselective sensors and actuators.[9] These properties find applications in determining the absolute chirality of drug molecules/natural products, enantiomeric purity of samples etc. Another advantage, which can be envisaged of dynamic helical assembly, is their real-time chiroptical readout in response to various processes and stimuli influencing the assembly.[10] Due of the non-covalent nature of these interactions, they are expected to show fast response to such changes. Here we show a novel concept of using a stimuli-responsive, dynamic helical assembly for the real time probing of an enzymatic reaction.

Adenosine phosphates are biologically relevant chiral molecules which define the energy economy of most living systems.[11] They exist in various forms like ATP, ADP, AMP and their interconversion phenomena is directly related to various processes occurring in the living cell. Many assays used for monitoring these adenosine phosphates are either specific to

one of these phosphates or they follow aliquot method instead of monitoring *in situ*.[12] Although, molecular recognition based fluorescence probing has been reported to monitor their real-time dynamics, they usually monitor the disappearance kinetics of one of these forms.[10, 13] However, probing various forms of these phosphates demand better design of systems. In order to probe the interconversion of adenosine phosphates (AMP/ADP/ATP), specific signalling is required which can distinguish various phosphates. Hence, dynamic helical system which can differentially respond to these chiral phosphates provide a viable alternative.
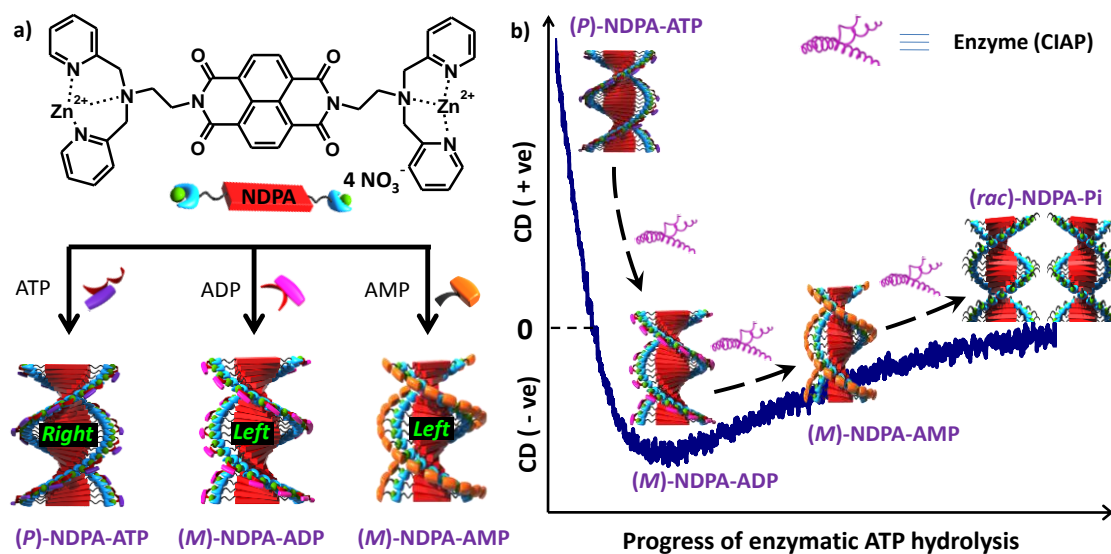
Scheme 3.1. *Enzyme responsive helical handedness of **NDPA**-ATP / ADP / AMP / Pi supramolecular polymer: a) Molecular structure of **NDPA** along with the pictorial representation of adenosine phosphates induced helical supramolecular organization with preferred handedness. b) Schematic illustration of the dynamic helix reversals upon enzyme (CIAP) action on the **NDPA** bound ATP molecules and their respective chiroptical readout as probe to monitor real-time reaction kinetics.*

In this work, we present a supramolecular helical assembly that responds to various adenosine phosphates with a differential chiroptical signalling. This system was constructed by the self-assembly of naphthalenediimide chromophores, end functionalized with zinc coordinated dipicolylethylenediamine receptor motifs (**NDPA**).[14] These chromophores show induction of opposite handedness on binding to AMP and ADP when compared to ATP (Scheme 3.1a, Figure 3.1b).[15] Very fast response to the change of binding guests as well as lack of any chiral amplification makes the chosen **NDPA** assembly most suited to study the real-time *in situ* conversion kinetics of adenosine phosphates from one form to another. This was further proven conceptually by the enzymatic hydrolysis of ATP. The utilization of

supramolecular handedness as a probe, not only to monitor enzymatic ATP decay but also to follow its course of stepwise conversion to ADP, AMP and finally to phosphates is unprecedented and provides useful insight into the hydrolytic pathway (Scheme 3.1). Moreover, this also provides an "all in one" method to study the individual hydrolysis kinetics of all forms of adenosine phosphates. Additionally, this strategy provides a unique way to control the stereomutation rates of helical assemblies by changing the concentrations of external stimuli (in the present case an enzyme).

3.2 Results and Discussion

In the previous chapter, we described the one-dimensional (1-D) supramolecular polymerization of **NDPA** in water by the molecular recognition of various adenosine phosphates (Chapter 2, Section 2.2).[15] The absorption spectrum of **NDPA** alone (5 x 10^{-5} M) in aqueous HEPES buffer (10 mM HEPES solution in water) shows sharp absorption bands (λ_{max} = 381 nm and 361 nm), characteristic of NDI chromophores devoid of intermolecular interactions and are indicative of monomeric nature of these chromophores (Figure 3.1a). Binding of anionic adenosine phosphates to cationic **NDPA** resulted in the stacking of NDI chromophores via synergistic hydrophobic and π-π interactions, characterized by the broadening of absorption band, along with the intensity reversal of vibronic bands at 360 nm and 380 nm. Chiroptical probing of these co-assembled stacks with circular dichroism (CD) spectroscopy showed strong bisignated Cotton effects and are indicative of a helical bias in the supramolecular organization of achiral NDIs induced by homochiral adenosine phosphates. The mode of binding probed through CD Job plot and titrations showed that AMP, ADP and ATP bind through one, two and three point of attachment respectively (Chapter 2, Section 2.2).[15] Also, comparative absorption spectra show that the interchromophoric interactions can be modulated depending upon the bound guest. ATP shows the strongest interactions followed by ADP and weakest by AMP, as evident from their change in intensity ratio (I_{0-0}/I_{0-1}) of two lower energy vibrational transitions in the absorption spectra (Figure 3.1a). Interestingly, AMP and ADP imparted *M*-helicity to the **NDPA** stacks, as evident from the negative bisignated CD signal (negative and positive maxima at 395 and 360 nm, respectively), whereas ATP induced *P*-helicity with positive bisignated CD signal (positive and negative maxima at 390 and 359 nm, respectively) (Figure 3.1b), as discussed in the previous chapter (Section 2.3).
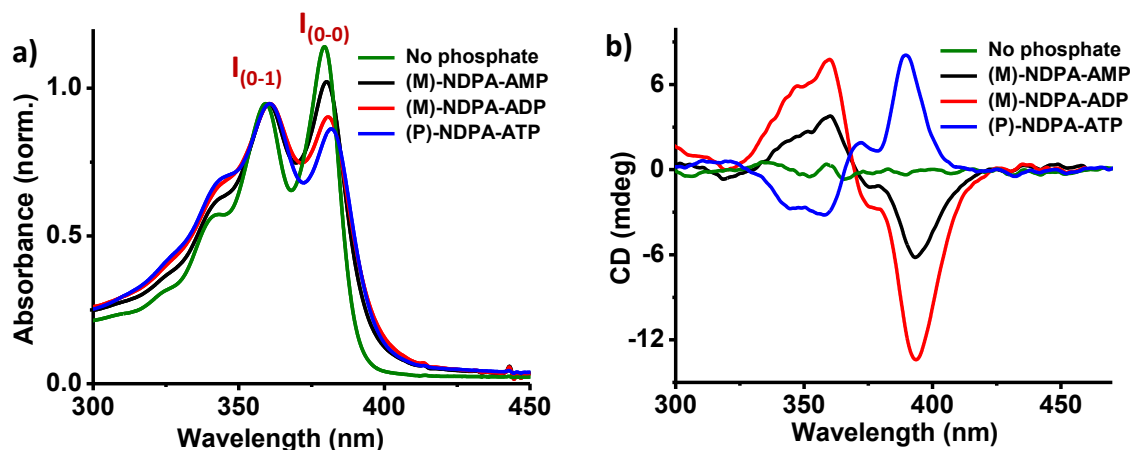
Figure 3.1. *Adenosine phosphates induced helical assembly of **NDPA**: a) Absorption spectra (normalized at 360 nm) and b) CD spectra of **NDPA** assemblies with 1 eq. of various bound adenosine phosphates. Normalized absorption spectra shows that binding of ATP or ADP leads to strong interchromophoric interactions among **NDPA**, AMP binding leads to weaker aggregates as evident from the ratio of absorbance at 0-0 and 0-1 transitions i.e. $I_{(0-0)}/I_{(0-1)}$ value for AMP = 1.07, ADP = 0.95, ATP = 0.91. All samples were measured at 5 x 10^{-5} M solution of **NDPA** in aq. HEPES buffer.*

The multivalent nature of certain chiral phosphate auxiliaries (ATP / ADP) offers an efficient strategy to modulate the handedness of **NDPA** stacks through competitive replacement of phosphates, provided that the assembly is dynamic. Addition of 1 eq. of ATP to a solution of AMP or ADP bound helical assembly, *(M)*-**NDPA**-AMP or *(M)*-**NDPA**-ADP, (c = 5 x 10^{-5} M in aq. HEPES buffer with 1 eq. of AMP or ADP), resulted in an inversion of CD signal (Chapter 2). This indicates the formation of *(P)*-**NDPA**-ATP stacks, by the competitive replacement of AMP or ADP by ATP, thereby reversal of helical handedness. We envisaged that the unique differential signalling of Cotton effect via stereomutation in the **NDPA** helix upon binding to different nucleotides could be explored to probe their conversion from ATP to ADP or AMP and *vice versa*. However, in order to probe the interconversion kinetics of the bound phosphate molecules, the helical assembly must meet few requirements i.e. 1) The stereomutation process in response to variation in phosphate concentration should not be the rate-determining step. In other words a rapid, dynamic helix reversal of the stacks is essential and 2) there should not be any chiral amplification so that the absolute CD intensity of the assembly, at any given point of time, directly signals the concentration of bound phosphates.

3.2.1 Dynamic Helix Reversal
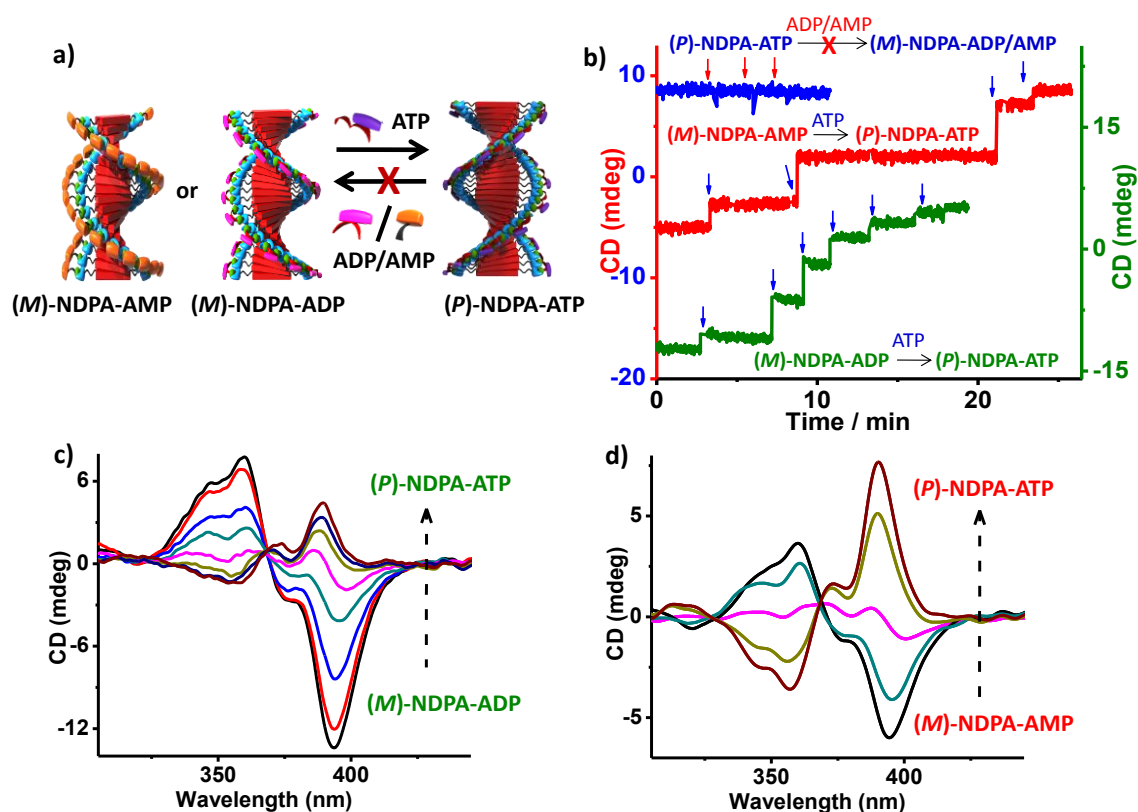
Figure 3.2. *Dynamic Helix Reversal: a) Pictorial representation of helicity reversal in **NDPA** assembly via competitive binding of multivalent adenosine phosphates. b)-d) Stepwise dynamic helix reversal experiments performed by sequential addition of ATP to (M)-**NDPA**-AMP and (M)-**NDPA**-ADP assemblies (5 x 10^{-5} M **NDPA** in aq. HEPES with 1 eq. of respective phosphates). b) Green and red traces show the sharp jumps in CD signal intensity of (M)-**NDPA**-ADP and (M)-**NDPA**-AMP, respectively, monitored at 394 nm, upon sequential addition of ATP, represented by the blue arrows. These sharp rise in CD intensities are characteristic of fast helicity reversal and the formation of (P)-**NDPA**-ATP stacks, which is further evident from the corresponding CD spectral changes shown in c and d. Horizontal nature of red trace (t = 10 → 20 min) suggests that prolonged waiting time does not affect the intensity. Blue trace in b) shows the CD intensity of (P)-**NDPA**-ATP upon sequential addition of AMP at time intervals as indicated by the red arrows. The retention of handedness suggests the inability of AMP/ADP to replace the pre-bound ATP molecules.*

The dynamic nature of the helix reversal in **NDPA** assemblies was investigated using competitive guest binding. Thus, CD intensity of *(M)*-**NDPA**-AMP and *(M)*-**NDPA**-ADP stacks (5 x 10^{-5} M in aq. HEPES) upon addition of small amounts of ATP at regular intervals were monitored at 390 nm, as a function of time. Interestingly, both AMP and ADP bound stacks displayed sharp jumps in CD intensity with each successive addition of ATP (Figure

3.2b, red and green traces). For *(M)*-**NDPA**-ADP stacks, the signal reversal occurs through multiple stepwise rise of intensity with each subsequent addition of ATP. Furthermore, the reversal of negative bisignated CD signal to positive bisignated signal is characteristic of stereomutation and indicates the formation of *(P)*-**NDPA**-ATP stacks, by the competitive replacement of ADP with ATP (Figure 3.2c). Similar behaviour was observed for *(M)*-**NDPA**-AMP assemblies, where again quantum rise in the signal was observed (Figure 3.2b red trace and 3.2d) with each subsequent addition of ATP. Such instantaneous changes in Cotton effects provide strong evidence for fast switching of helicity in these dynamic supramolecular polymers.
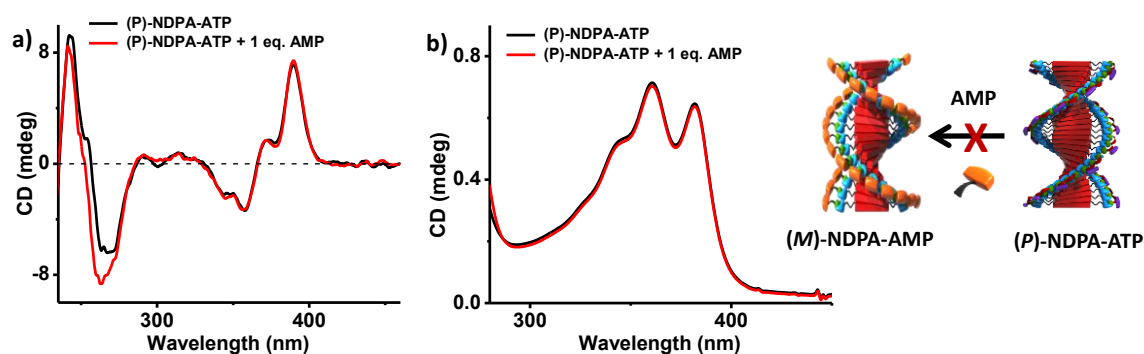
Figure 3.3. *Competitive binding between AMP and ATP: a) CD and b) absorption spectra of (P)-**NDPA**-ATP (5 x 10⁻⁵ M) with different eq. of AMP. Lack of any significant change in the signal confirms inability of AMP to replace ATP competitively. Schematic on the right side depicts the same process.*
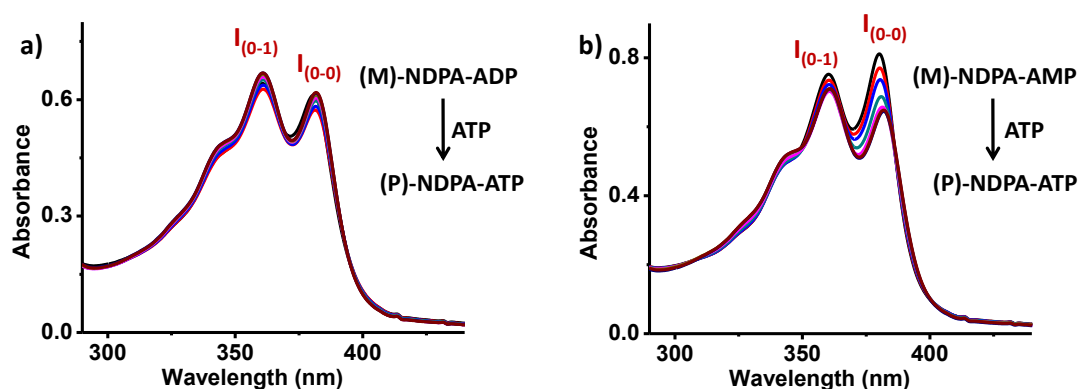
Figure 3.4. *ATP based competitive replacement: Changes in the absorption spectra of a) (M)-**NDPA**-ADP and b) (M)-**NDPA**-AMP on competitive replacement with multivalent ATP (5 x 10⁻⁵ M in aq. HEPES buffer).*

However, upon addition of AMP/ADP to ATP bound helical stack, *(P)*-**NDPA**-ATP, did not show any changes in the CD intensity, as the multivalent ATP cannot be competitively

replaced by AMP or ADP (blue trace Figure 3.2b, Figure 3.3). At this stage, we note that the two processes, i.e. replacement of (i) AMP by ATP and (ii) ADP by ATP show similar CD signal changes and thus cannot be differentiated chiroptically. However, these transformations could be easily probed via the changes in their absorption spectra, as the strength of intermolecular interactions varies with different phosphates. A closer look at the absorption spectra shows that removal of ADP by ATP in Figure 3.4a do not show any significant change in absorption spectra. But a clear decrease in the absorbance along with 2 nm red shift of absorption peak at 380 nm was observed when AMP was substituted by ATP as seen in Figure 3.4b. This high band intensity at 380 nm, characteristic of weak NDI aggregates, are expected from AMP with one coordinating site, which lack the ability to clip chromophores for better stabilization. Whereas ADP and ATP with two and three point of attachments can clip to stabilize the chromophoric aggregates, thus justifying the observed variation in absorption spectra (Figure 3.1a).

3.2.2 Chiral Amplification
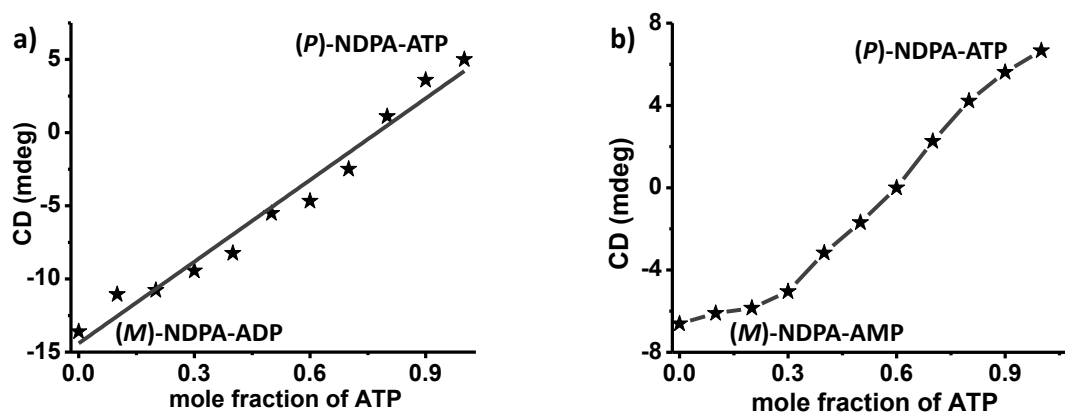
Figure 3.5. *'Majority rules' like experiment performed using a mixture of a) ADP-ATP and b) AMP-ATP. The linear relationship (grey line) of the CD intensity rules out any chiral amplification in the stacks. The total concentration of phosphates was chosen in such a way that all the binding sites are occupied and CD intensity was monitored at the CD maxima of 390 nm (positive) and 394 nm (negative). Zero CD intensity do not appear at 0.5 mole fraction of ATP due to non-racemic nature of the (M)-**NDPA**-AMP and (P)-**NDPA**-ATP helices, which is also reflected in their unequal maximum CD intensity (Figure 3.1b).*

In order to evaluate the chiral amplification, "Majority Rules" like experiments performed with mixture of adenosine phosphates, AMP/ATP or ADP/ATP. Adenosine phosphates were taken in appropriate eq. such that all the DPA sites are bound to phosphates. Plot of resultant CD intensity against the mole fraction of guest molecules show a linear relation (Figure 3.5), demonstrating the absence of chiral amplification effects in phosphate

bound **NDPA** stacks. Thus, the present dynamic chiral assembly is endowed with two unique properties, i.e. fast helical response to replacement of binding phosphates and lack of any chiral amplification, enabling the system with an unprecedented ability to probe real time hydrolysis kinetics of adenosine phosphates.

3.3 Enzymatic ATP Hydrolysis
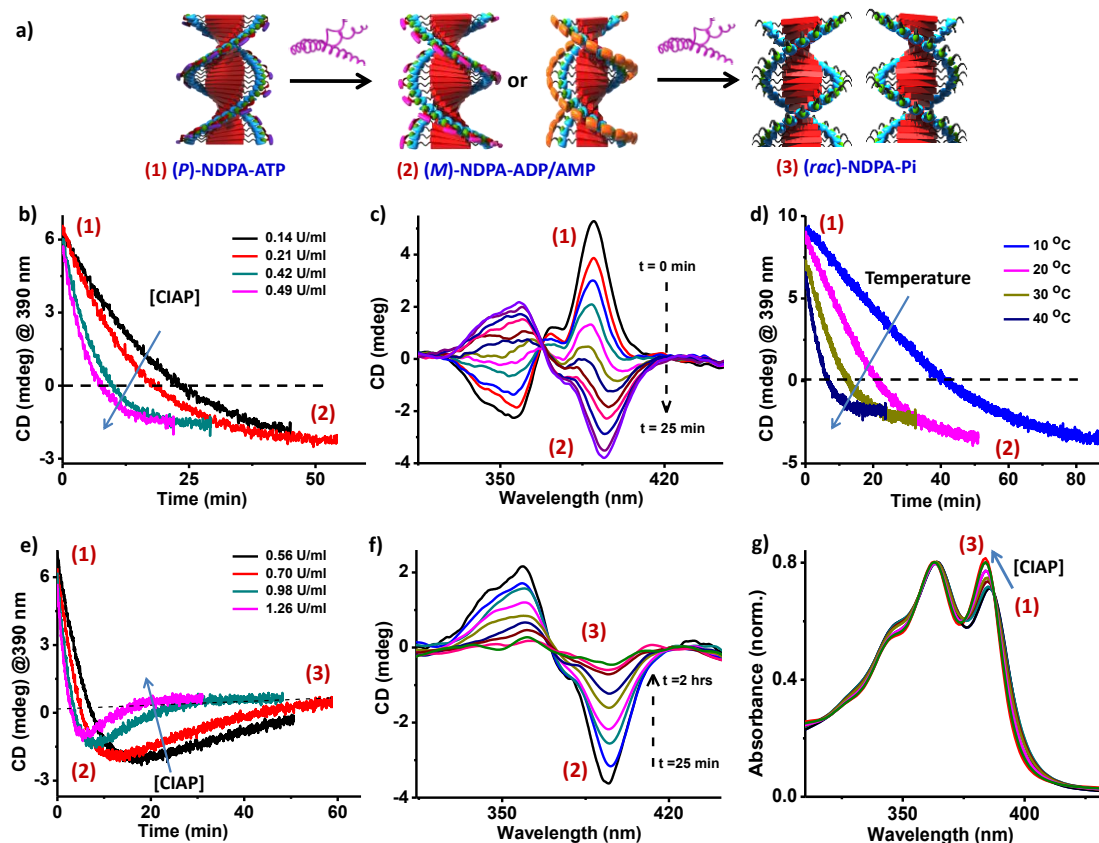
Figure 3.6. *Stepwise enzymatic ATP hydrolysis and subsequent dynamic helix reversals: CD kinetic analyses of CIAP triggered stereomutation processes of (P)-**NDPA**-ATP (c = 5 x 10^{-5} M) self-assembly. a) Schematic illustration of enzymatic action on (P)-**NDPA**-ATP supramolecular helix (State 1), which first undergoes helix inversion to form (M)-**NDPA**-ADP/AMP stacks (State 2) followed by racemisation to form Pi stabilized racemic assemblies, (rac)-**NDPA**-Pi (State 3). b-d) show the spectral changes during the transformation from (1)→(2) and e-g) describes transition from (2)→(3). b) and e) show time dependent changes in the CD intensity at 390 nm, with increasing concentration of CIAP at 35 °C. Time dependent CD spectral changes, upon addition of 0.84 U/ml of CIAP at 20 °C are shown in c) (1)→(2) and f) (2)→(3), whereas g) shows corresponding absorption changes (normalized) from (1)→(3). d) Time dependent changes in the CD intensity (390 nm) of (P)-**NDPA**-ATP with 0.28 U/ml of CIAP at varying temperature.[16] In b) kinetics was not probed for prolonged time to see transition from 2→3.*

Next, we probed the dynamic helicity changes of the **NDPA** stacks, upon *in situ* hydrolysis of the bound chiral phosphate molecules. Since enzymatic cleavage is one of the simplest known methods of phosphate hydrolysis inside the living cells, Calf Intestinal Alkaline Phosphatase (CIAP) was the chosen enzyme, which is known to dissociate all three forms of adenosine phosphates to adenosine and phosphates.[17] Thus, CIAP (0.21 U/ml) was added to *(P)*-**NDPA**-ATP helical stacks and CD signal was monitored at 390 nm as a function of time. Interestingly, the CD signal gradually decreases with time, indicating the decrease in ATP concentration on enzymatic hydrolysis with CIAP. Remarkably, the net CD intensity reverses from positive to negative, where the final signal resembles that of either ADP or AMP bound **NDPA** assemblies (Figure 3.6b, 1→2). The formation of *(M)*-**NDPA**-ADP/AMP stacks is further obvious from the time dependent CD spectra of *(P)*-**NDPA**-ATP assembly with CIAP (0.84 U/ml) monitored at 20 °C, which showed a gradual inversion of positive to negative bisignated signal passing through an isodichroic point at 368 nm, suggesting complete reversal of helicity (Figure 3.6c). This inversion of CD signals with time, clearly indicates the dynamic reversal of helical handedness of **NDPA** stacks as a result of conversion of ATP to ADP/AMP through enzymatic hydrolysis.

T (k)	k_{ATP} (min^{-1})
283.15	0.0287
293.15	0.0586
303.15	0.1104
313.15	0.2274
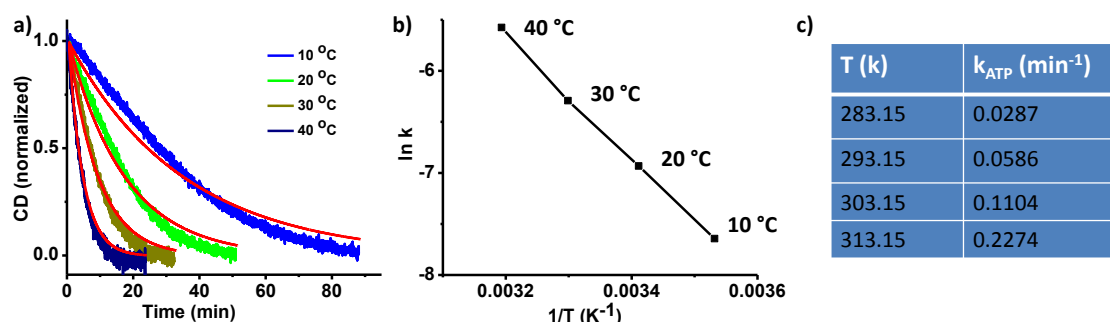
Figure 3.7. Kinetic analysis of the (1)→(2) stereomutation process of (P)-NDPA-ATP assembly: a) Time dependent CD intensity at 390 nm monitored at different temperature (c = 5 x 10^{-5} M, 1 eq. ATP, with 0.28 U / ml CIAP) and corresponding fits (solid lines) using 1st order kinetic model and b) the resultant Arrhenius plot. Table in c) shows the increase in rate constant with temperature, which almost doubles with every 10 K rise. These data corresponds to the Figure 3.6d. All CD signals were normalized between zero and one for ease of fitting into kinetic model.

Furthermore, kinetics of this process was probed with varying concentration of enzyme, which exhibited faster helix-reversals on increasing concentration of enzyme (Figure 3.6b). This unambiguously proves that the rate of helix-reversal directly reflects the progress of enzymatic hydrolysis reaction. From a supramolecular perspective, this enzymatic hydrolysis also provides an unprecedented strategy to modulate the stereomutation kinetics of dynamic,

helical supramolecular polymers. Rate of stereomutation could also be controlled by temperature variation as seen in Figure 3.6d. Time dependent CD intensity of *(P)*-**NDPA**-ATP stacks with 0.28 U/ml of CIAP indicated faster helicity reversal at higher temperatures following a first order kinetics (Figure 3.7c). We notice that the final CD signal obtained after stereomutation (1→2) in Figure 3.6d decreases upon increasing temperature. To understand this process we studied the temperature dependent CD intensity changes in absence of enzyme. It is evident that as the temperature increases, the CD signal vanishes along with blue shift in absorption spectra (382 nm to 380 nm, Figure 3.8 a, b). Upon cooling, the signal red shifts again to 382 nm along with recovery of CD signal. The vibronic features of the absorption spectra at high temperature do not resemble that of a monomeric **NDPA**. These observations indicate that the decrease in CD signal with increasing temperature at both (**1**) and (**2**) state of *(P)*-**NDPA-**ATP (Figure 3.6d) is due to weaker ATP binding at elevated temperatures (and not their detachment as monomeric absorption features were not observed in Figure 3.8b).
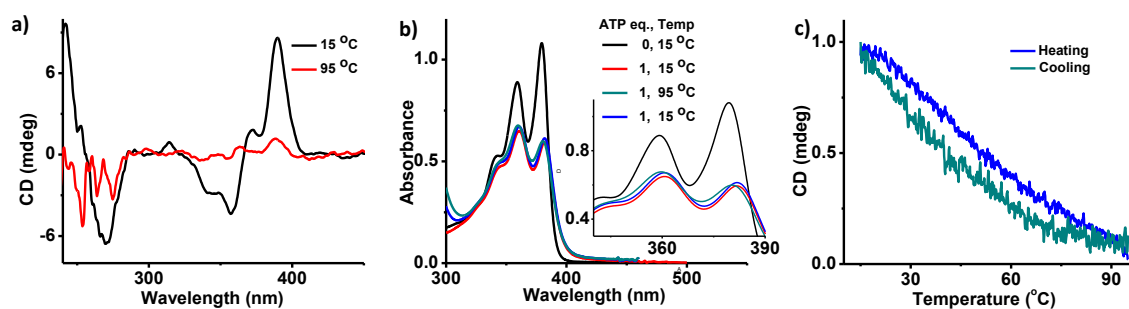
Figure 3.8. *Temperature dependent helical assembly without enzyme: Temperature dependent changes in a) CD and b) absorption spectra of (P)-**NDPA**-ATP assembly upon heating and cooling (5 x 10^{-5} M in aq. HEPES buffer). c) Temperature dependent variation in CD intensity at 390 nm during one complete cycle of heating and cooling. These measurements were performed in absence of enzyme.*

At higher enzyme concentrations ($\geq$ 0.56 U / ml), *(P)*-**NDPA**-ATP showed an interesting phenomenon that apart from the inversion of CD signal in the initial stages, the CD intensity goes to zero at later times and saturates (Figure 3.6e, 1→2→3). This clearly suggests two-step process, where ATP is first converted to ADP/AMP leading to reversal of helicity followed by further hydrolysis to adenosine and achiral phosphates, thereby loss of chiral information. Increasing CIAP concentration revealed faster kinetics for both these processes, characteristic of enzyme controlled reaction pathways. The transition from 2→3 was not probed in Figure 3.6b, as it would take a very long time due to slow kinetics at lower enzyme concentrations.

The disappearance of CD signal at **3** suggests either disassembly of the **NDPA** stacks in the absence of any bound adenosine phosphates or the formation of racemic stacks stabilized by achiral phosphate $Pi[(PO_4)^{3-}]$ produced on hydrolysis. Absorption spectra obtained after complete hydrolysis is significantly different from that of **NDPA** alone without phosphates, indicating that it is not monomeric. We observe that after stereomutation, the absorption maxima show 2 nm blue shift (386 nm to 384 nm) along with change in the ratio of band intensity indicating weakening of aggregates (Figure 3.6g). Moreover, addition of CIAP to **NDPA** do not show any change in the absorption as well as CD signal (Figure 3.9), confirming that the CIAP do not have any specific interactions with **NDPA**. However, titration with Pi i.e. $(PO_4)^{3-}$ show strong interaction with **NDPA** leading to NDI aggregation, as seen from the changes in vibronic features of the absorption spectra (Figure 3.10a). As expected, upon complete hydrolysis of ATP by CIAP, 3 eq. of Pi would be released, which can bind to the **NDPA** resulting in racemic assembly due to achiral nature of Pi. The absorption spectrum after complete stereomutation resemble that of Pi bound **NDPA,** thereby ruling out the possibility of **NDPA** deaggregation (Figure 3.10b). Hence, in the absence of any interactions from CIAP, the final state corresponds to Pi bound racemic assemblies i.e. (*rac*)-**NDPA**-Pi. Such two-step transitions were not evident at low enzyme concentrations (Figure 3.6b) as the 2→3 process would take very long time to complete under those conditions. Results thus far have demonstrated that the dynamic helix reversal of the present system can be successfully utilized to probe the enzyme controlled hydrolysis of ATP and provide useful insights into its stepwise course of action.
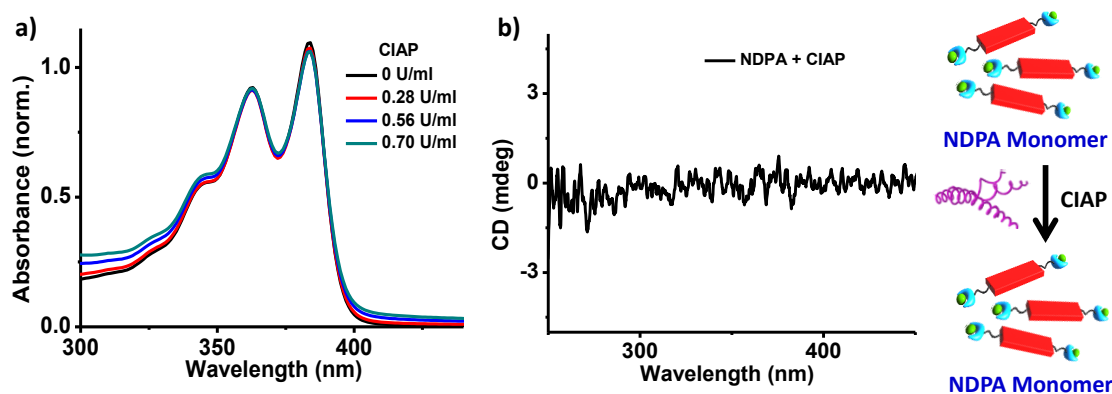
Figure 3.9. *Enzyme interaction with **NDPA**. a) Absorption and b) CD spectral variations on addition of CIAP to **NDPA**. All measurements were done with 5 x 10^{-5} M solution in aq. HEPES buffer. Schematic on right side depicts the influence of CIAP on state of **NDPA** assembly.*
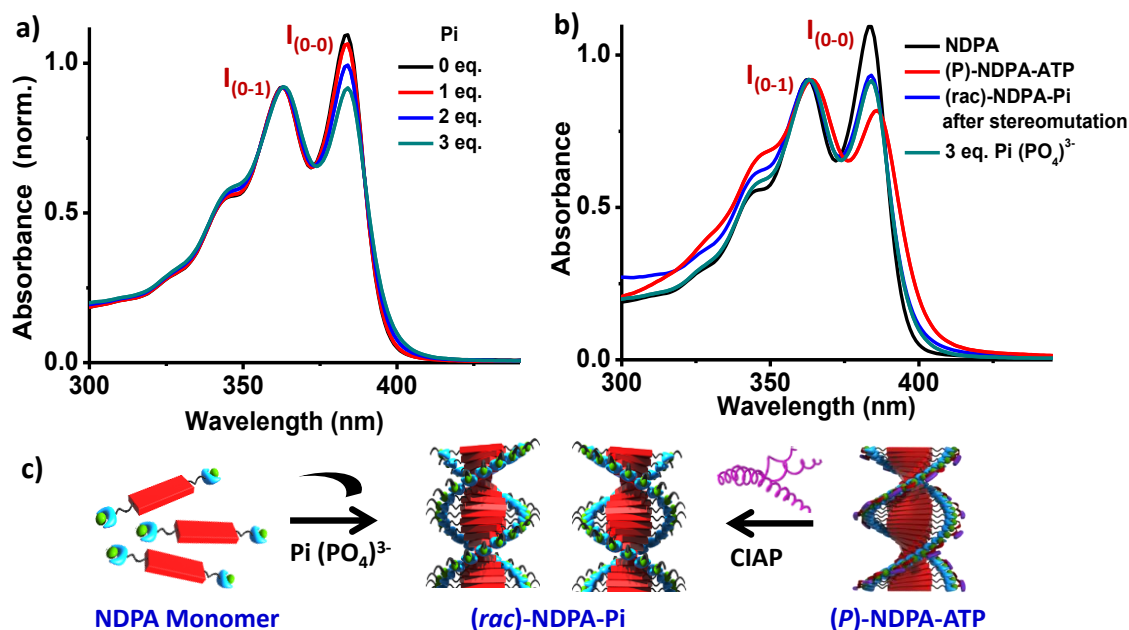
Figure 3.10. *Pi binding of **NDPA**: a) Absorption spectra of **NDPA** upon binding with Pi i.e. $(PO_4)^{3-}$. Changes in the ratio of band intensity suggest significant interchromophoric interactions in **NDPA** on binding to Pi. b) Changes in the absorption spectra upon enzymatic hydrolysis of ATP with CIAP and its comparison with Pi bound **NDPA**. Schematic in c) depicts the respective processes. All experiments were at 5 x 10^{-5} M **NDPA** in aq. HEPES buffer.*

3.4 Enzymatic ADP/AMP Hydrolysis

To gain further insights into various intermediate steps involved in the ATP hydrolysis, similar enzymatic hydrolysis reactions with pure *(M)*-**NDPA**-ADP and *(M)*-**NDPA**-AMP assemblies were also performed. As expected, the time dependent CD signals monitored at 394 nm (35 °C) gradually goes to zero, suggesting the direct formation of *(rac)*-**NDPA**-Pi assemblies (Figure 3.11). Absorption spectra obtained after complete hydrolysis were distinct from that of **NDPA** alone without phosphates, as seen from their $I_{(0-0)}/I_{(0-1)}$ value indicating that it is not monomeric (Figure 3.12 a, b). In addition, the spectra after stereomutation matches well with the Pi bound **NDPA** stacks confirming that **NDPA** is indeed aggregated due to Pi binding.
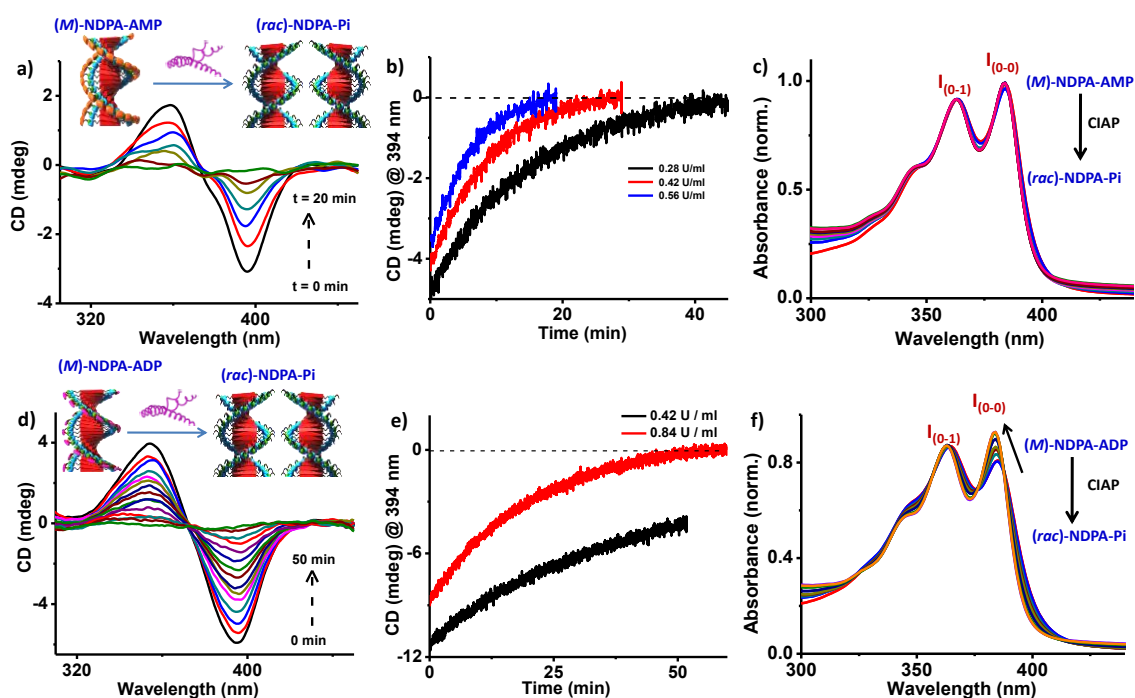
Figure 3.11. *Kinetic analysis of **NDPA** bound AMP and ADP hydrolysis: Time dependent CD spectra showing the racemization process of a) (M)-**NDPA**-AMP (c = 5 x 10^{-5} M) with CIAP (0.42 U/ml), d) (M)-**NDPA**-ADP (c = 5 x 10^{-5} M) with CIAP (0.84 U/ml) at 35 °C. Schematic shows the pictorial representation of the enzymatic AMP/ADP hydrolysis. b) and e) show the corresponding CD intensity monitored at 394 nm probing the racemisation process of (M)-**NDPA**-AMP and (M)-**NDPA**-ADP respectively, with varying concentrations of CIAP at 35 °C. c) and f) show changes in absorption spectra corresponding to hydrolysis of AMP/ADP prebound to **NDPA** with CIAP (0.70 U/ml, 35 °C).*

The plot of AMP and ADP hydrolysis were fitted into 1st order reaction kinetics model (Figure 3.12 d, e). These plots revealed a faster racemisation rate for the *(M)*-**NDPA**-AMP than that of *(M)*-**NDPA**-ADP. For example, at 35 °C and with 0.42 U/ml of CIAP, the racemisation rate constant of *(M)*-**NDPA**-AMP (k_{amp}= 0.129 min^{-1}), was six times higher than that of *(M)*-**NDPA**-ADP (k_{adp}= 0.021 min^{-1}), suggesting faster hydrolysis of AMP than ADP (Figure 3.12f). Such differences in the rate of hydrolysis is also evident from the comparative plot of time dependent CD intensity decay in *(M)*-**NDPA**-AMP and *(M)*-**NDPA**-ADP with 0.84 U/ml of CIAP at 35 °C (Figure 3.13b). Experiments conducted at various concentrations of enzyme show a linear increase in rate constant upon addition of higher amounts of enzyme (Figure 3.13a). This confirms that the decay profile is indeed governed by enzymatic hydrolysis of adenosine phosphates.
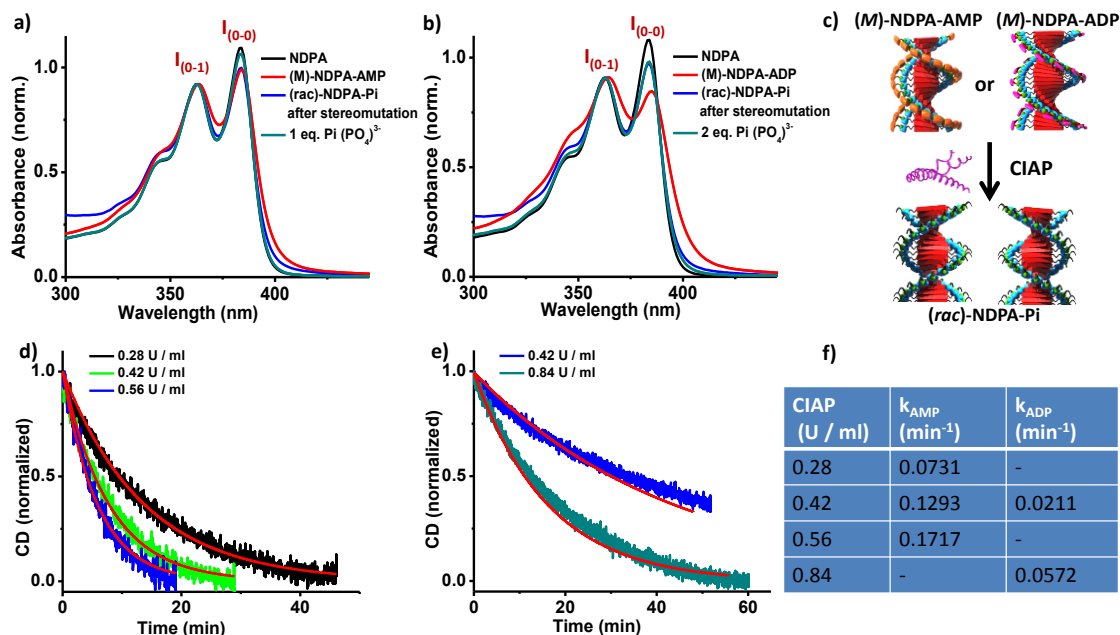
Figure 3.12. *Changes in the absorption spectra upon enzymatic hydrolysis of a) (M)-**NDPA**-AMP and b) (M)-**NDPA**-ADP with CIAP (0.7 U/ml, 35 °C) and its comparison with completely racemized state (rac)-**NDPA**-Pi obtained by action of CIAP as well as the Pi bound **NDPA**. Time dependent CD signal change with varying CIAP concentration to d) (M)-**NDPA**-AMP, e) (M)-**NDPA**-ADP at 35 °C and their respective 1st order kinetic fit (solid red line). d) Correspond to kinetic decay data of Figures 3.11b and b) for Figures 3.11e. f) Table shows the comparative rate constant of bound AMP and ADP hydrolysis at various CIAP concentrations. All CD signals were normalized between zero and one for ease of fitting into kinetic model. The empty data points in f) is due to their extreme kinetics of the processes like hydrolysis of bound AMP at high CIAP concentration will be too fast to probe reliably .*
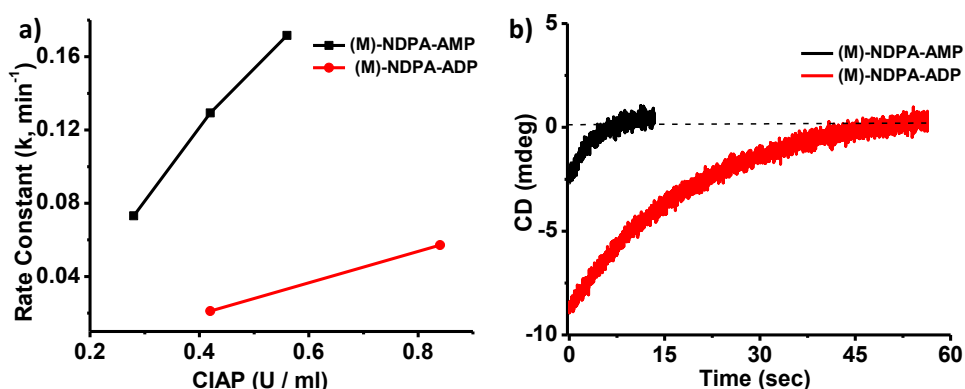
Figure 3.13. *a) Plot of hydrolysis rate constants of **NDPA** bound AMP and ADP (k_{amp} and k_{adp}) against varying concentration of CIAP at 35 °C as per Figure 3.12f. We see that at a given CIAP concentration, k_{amp} is higher than k_{adp} confirming that ADP hydrolysis is much slower than AMP. b) Time dependent variation in CD signal of (M)-**NDPA**-AMP and (M)-**NDPA**-ADP (c=5 x 10^{-5} M) with CIAP (0.84 U/ml) at 35 °C monitored at 390 nm.*

Revisiting the conversion from (1)→(2) (Figure 3.6e), as hydrolysis of ADP is much slower than that of AMP, the negative signal at (2), which is obtained after stereomutation, must be governed mainly by the presence of *(M)*-**NDPA**-ADP assemblies. Careful analysis of the absorption spectral changes show that the transformation from 1→2 (when the CD signal reverses in Fig. 3.6c) do not show any change in absorption spectra (Figure 3.14a). This was expected from the ATP → ADP transition, which do not affect the absorption spectra (Figure 3.4a). Whereas, the later process from 2→3 (when the CD signal goes to zero in Figure 3.6f), we notice changes in the vibronic features of **NDPA** absorbance ($I_{(0-0)}/I_{(0-1)}$ value, Figure 3.14b) as expected of the transition from ADP → AMP → Pi (Figure 3.4b). Above results clearly indicate that (1)→(2) transformation is governed by ATP→ADP, whereas (2)→(3) is ADP→AMP→Pi. The single isodichroic point in the time-dependent CD spectra during stereomutation and their first order kinetics (Figure 3.6 c, d) further supported that the process is majorly governed by the conversion between two distinct assemblies, *(P)*-**NDPA**-ATP and *(M)*-**NDPA**-ADP.
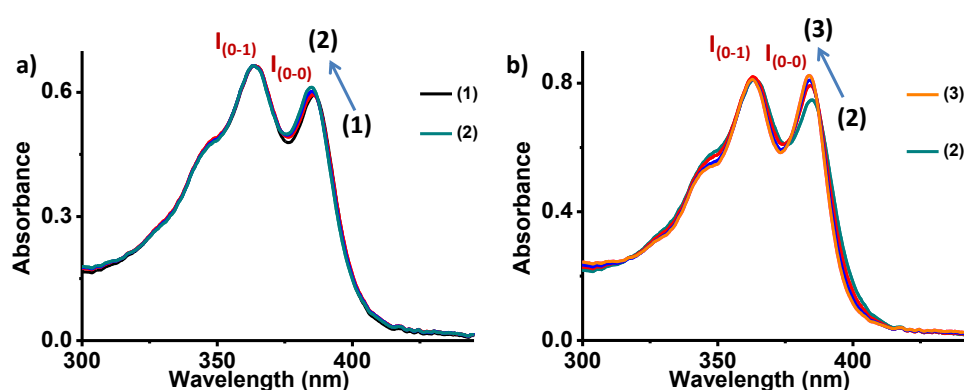
Figure 3.14. *Absorption changes in (P)-**NDPA**-ATP during stepwise hydrolysis of ATP: Variation in absorption spectra of (P)-**NDPA**-ATP solution upon stepwise hydrolysis of ATP during a) 1→2 and b) 2→3. These absorption changes correspond to Figure 3.6 c, f (c = 5 x 10^{-5} M, 35 °C with CIAP (0.7 U/ml)).*

Results thus far have shown that dynamic helix reversals in the **NDPA** supramolecular helical system can be used to probe the mechanistic pathways of enzymatic ATP hydrolysis and possible pathway is via ATP to ADP to AMP before converting to adenosine and phosphates. Furthermore, ^{31}P NMR measurements and phosphate (Pi) assay experiments corroborated the conclusions drawn from CD kinetic analysis. Time dependent NMR changes upon enzymatic ATP hydrolysis shows that the peak at -23.1 ppm (characteristic of ATP, marked with red star) vanishes soon after addition of CIAP, whereas the other two peaks at -11.2 ppm, -10.2 ppm (characteristic of ADP, marked with blue triangle) remain intact initially (Figure 3.15). This indicates a fast conversion from ATP to ADP. On further passage of time, ADP peak also

vanishes to give only AMP signal followed by conversion to Pi and adenosine. Thus we notice that enzymatic ATP hydrolysis without **NDPA** also follows the same pathway (ATP→ADP→ AMP) and confirms our finding by circular dichroism in presence of **NDPA**. Time dependent variation in concentration of Pi [$(PO_4)^{3-}$] was also monitored upon action of enzyme on *(M)*-**NDPA**-AMP and *(M)*-**NDPA**-ADP. Probing the concentration of Pi released upon hydrolysis can give an indirect measure of the rate of hydrolysis. This was performed using a well known Pi assay (Chen's method).[12b] We see that ADP hydrolysis is indeed much slower when compared with AMP (Figure 3.16a), in line with the conclusions drawn previously by monitoring CD signal (Figure 3.13). Both measurements were done with CIAP (0.84 U/ml) and **NDPA** (c = 5 x 10^{-5} M) at 35 °C. Unlike the helix reversal measurements for kinetic analysis, Chen's assay is not an *in situ* measurement due to highly acidic conditions required for metal complex formation, so aliquots at regular intervals were analyzed. In addition, this method can only probe the net Pi released and cannot distinguish the stepwise hydrolysis of ATP via ADP/AMP to Pi.
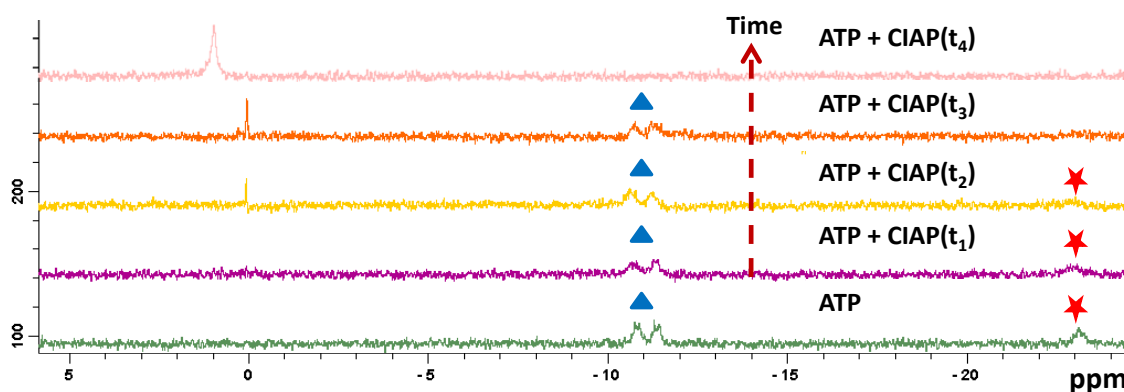
Figure 3.15 . *^{31}P NMR signature of enzymatic process. Time dependent changes in the ^{31}P NMR spectra of ATP in presence of CIAP and its comparison with ATP without CIAP indicating stepwise enzymatic hydrolysis of ATP.*

To understand if enzyme selectively hydrolyses the unbound or bound phosphates, CD kinetic measurements of *(P)*-**NDPA-ATP** in presence of other phosphates (one eq. of ATP followed by addition of 1 eq. of either AMP or ADP) were performed. As expected, due to competitive binding, ATP should be bound to **NDPA** to form *(P)*-**NDPA**-ATP stacks, whereas AMP or ADP must be free in solution. Absence of initial lag phase and gradual decrease in signal from time t=0 suggests that CIAP has no preferential action to unbound phosphates compared to bound ones (Figure 3.16b). If enzymatic action were to be preferential to unbound phosphates, we should have obtained constant CD signal initially till all unbound phosphates are consumed and only then signal should have started to decrease.
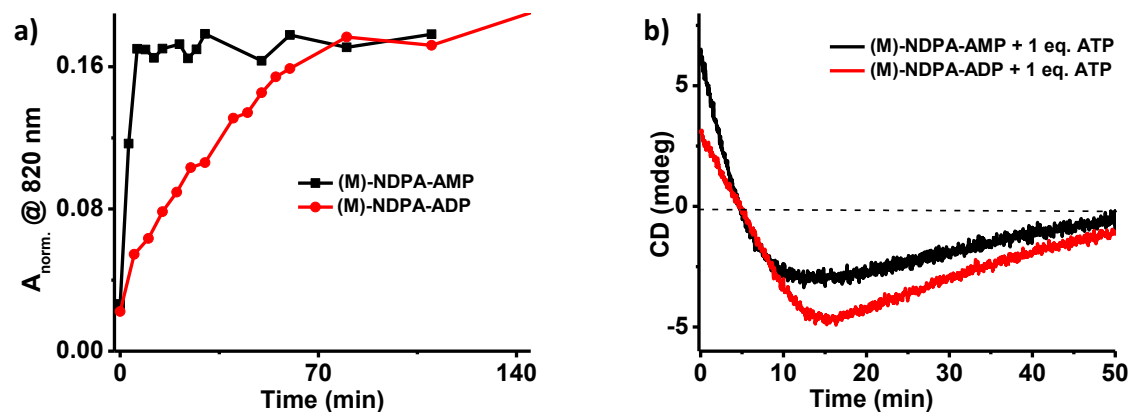
Figure 3.16. *a) Inorganic method for Pi estimation: Pi assay results using Chen's method to determine the amount of Pi released on enzymatic hydrolysis. The graph shows comparative hydrolysis kinetics of **NDPA** bound AMP and ADP clearly confirming that AMP hydrolysis is much faster compared to ADP. b) Mechanistic insight on enzymatic action: Time dependent variation in CD signal of 5 x 10⁻⁵ M **NDPA** (aq. HEPES buffer) on competitive replacement of AMP and ADP by 1 eq. of ATP (CIAP = 0.70 U/ml) at 35 °C monitored at 390 nm.*

3.5 Conclusions

To conclude, we have presented a unique dynamic, helical assembly which shows adenosine phosphate binding induced supramolecular chirality with tunable handedness. MD simulations suggest weak van der Waals forces being responsible for preferential helicity with various phosphates. Furthermore, we show a fast and dynamic switching of helicity through competitive replacement of AMP/ADP by multivalent ATP guest molecules. This stimuli-responsive helical system with instantaneous reversal of handedness has been utilized for *in situ* monitoring the kinetics of enzymatic hydrolysis of adenosine phosphates. Detailed kinetic analyses provided insights into various aspects of this hydrolysis process like number of steps involved in the course of reaction and the rate limiting step of the reaction. A clear understanding of the kinetics involved in various processes makes the present system unique for probing phosphates interconversion kinetics. In addition, this system presents an interesting example, where the rate of stereomutation can be modulated by an external stimulus such as enzyme. Such a dynamic system, with positively charged surface and responsiveness to biological energy currency can be used for probing *in vivo* hydrolysis and their concentration fluctuation inside the living cells.

3.6 Experimental Section

<u>**General Methods**</u>:

Optical Measurements: Electronic absorption spectra were recorded on a Perkin Elmer Lambda 900 UV-Vis-NIR Spectrometer and emission spectra were recorded on Perkin Elmer Ls 55 Luminescence Spectrometer. UV-Vis spectra were recorded in 10 mm path length cuvettes. Circular Dichroism measurements were performed on a Jasco J-815 spectrometer where the sensitivity, time constant and scan rate were chosen appropriately. Corresponding temperature dependent measurements were performed with a CDF – 426S/15 Peltier-type temperature controller with a temperature range of 263-383 K and adjustable temperature slope.

NMR Measurements: NMR spectra were obtained with a Bruker AVANCE 400 (400 MHz w.r.t. ^{1}H nuclei) Fourier transform NMR spectrometer with chemical shifts reported in parts per million (ppm).

Sample Preparation: All samples for spectroscopic measurements were prepared by injecting the 5 x 10 $^{-5}$ M stock solution of **NDPA** into required volume of aq. HEPES buffer. Required amount of phosphates were injected into it and the solution was mixed by manual stirring before measurements. Commercially available CIAP was 2.8 units per mg and stock solution of CIAP was prepared by dissolving 1 mg of CIAP in 80 μl of aq. HEPES buffer. Each enzyme kinetics measurement were performed by adding appropriate amount of CIAP stock solution into the phosphate bound helical stacks at a given temperature and all measurements were initiated immediately. Stepwise dynamic helix reversal measurements in Figure 2a were performed by injecting aliquots of corresponding phosphates at regular interval to phosphate prebound helical stack.

"*(P)*-**NDPA**-ATP" term used in main text refers to 5 x 10^{-5}M solution of **NDPA** (in 10 mM aq. HEPES buffer) with 1 eq. of ATP. Similarly for ADP, AMP and Pi [$(PO_4)^{3-}$] bound helical stacks were denoted as "*(M)*-**NDPA**-ADP", "*(M)*-**NDPA**-AMP" and "*(rac)*-**NDPA**-Pi" respectively.

All CIAP based hydrolysis kinetics of AMP/ADP/ATP were studied with 1 eq. of respective adenosine phosphates for the ease of comparison.

Phosphate's assay by Chen's method: Chen's reagent was prepared by adding 1:1:1:2 solution of 10% ascorbic acid (w/v), 2.5% ammonium molybdate (w/v), 6N H_2SO_4 and water respectively. A 5 x 10^{-5} M solution of **NDPA** prebound with the appropriate phosphates were treated with suitable amount of CIAP at 35 °C. At regular time interval 250 μl aliquot of the above solution was added to 1 ml of Chen's reagent with proper mixing. All such solutions

were incubated for 30 minutes at 35 °C and then absorbance was recorded at 820 nm. This absorbance corresponds to the reduced form of phosphomolybdate complex (formed by Pi released during hydrolysis reaction).

Materials: CIAP (2.8 units/mg) was purchased from Sisco Research Laboratory Pvt. Ltd. India. All other chemicals were purchased from the commercial sources and were used as such. Spectroscopic grade solvents were used for all optical measurements.

Synthesis: NDPA was synthesized following the reported procedure and was characterized accordingly.[14]

3.7 References and Notes

1. a) M. M. Green, K.-S. Cheon, S.-Y. Yang, J.-W. Park, S. Swansburg and W. Liu, *Acc. Chem. Res.,* **2001**, *34*, 672; b) E. Yashima, K. Maeda, H. Iida, Y. Furusho and K. Nagai, *Chem. Rev.,* **2009**, *109*, 6102; c) M. Fujiki, J. R. Koe, K. Terao, T. Sato, A. Teramoto and J. Watanabe, *Polym. J.,* **2003**, *35*, 297.

2. a) A. R. A. Palmans and E. W. Meijer, *Angew. Chem. Int. Ed.,* **2007**, *46*, 8948; b) A. Lohr and F. Würthner, *Isr. J. Chem.,* **2011**, *51*, 1052; c) A. E. Rowan and R. J. M. Nolte, *Angew. Chem. Int. Ed.,* **1998**, *37*, 63; d) Y. Ruff, T. Moyer, C. J. Newcomb, B. Demeler and S. I. Stupp, *J. Am. Chem. Soc.,* **2013**, *135*, 6211; e) J. J. L. M. Cornelissen, J. J. J. M. Donners, R. de Gelder, W. S. Graswinckel, G. A. Metselaar, A. E. Rowan, N. A. J. M. Sommerdijk and R. J. M. Nolte, *Science,* **2001**, *293*, 676.

3. a) S. Cantekin, D. W. R. Balkenende, M. M. J. Smulders, A. R. A. Palmans and E. W. Meijer, *Nat. Chem.,* **2011**, *3*, 42; b) N. Ousaka, Y. Takeyama, H. Iida and E. Yashima, *Nat. Chem.,* **2011**, *3*, 856; c) K. Toyofuku, M. A. Alam, A. Tsuda, N. Fujita, S. Sakamoto, K. Yamaguchi and T. Aida, *Angew. Chem. Int. Ed.,* **2007**, *119*, 6596; d) Z. Huang, S.-K. Kang, M. Banno, T. Yamaguchi, D. Lee, C. Seok, E. Yashima and M. Lee, *Science,* **2012**, *337*, 1521; e) F. Würthner, C. Bauer, V. Stepanenko and S. Yagai, *Adv. Mater.,* **2008**, *20*, 1695; f) A. Gopal, M. Hifsudheen, S. Furumi, M. Takeuchi and A. Ajayaghosh, *Angew. Chem. Int. Ed.,* **2012**, *51*, 10505; g) A. Lohr and F. Würthner, *Angew. Chem. Int. Ed.,* **2008**, *47*, 1232; h) Y. Haketa, Y. Bando, K. Takaishi, M. Uchiyama, A. Muranaka, M. Naito, H. Shibaguchi, T. Kawai and H. Maeda, *Angew. Chem. Int. Ed.,* **2012**, *51*, 7967; i) F. Aparicio, B. Nieto-Ortega, F. Nájera, F. J. Ramírez, J. T. López Navarrete, J. Casado and L. Sánchez, *Angew. Chem. Int. Ed.,* **2014**, *53*, 1373; j) G. P. Spada, S. Lena, S. Masiero, S. Pieraccini, M. Surin and P. Samorì, *Adv. Mater.,* **2008**, *20*, 2433; k) V. K. Praveen, S. S. Babu, C. Vijayakumar, R. Varghese and A. Ajayaghosh, *Bull. Chem. Soc.*

Jpn., **2008**, *81*, 1196; l) J. J. L. M. Cornelissen, M. Fischer, N. A. J. M. Sommerdijk and R. J. M. Nolte, *Science,* **1998**, *280*, 1427.

4. a) H. Fenniri, B.-L. Deng and A. E. Ribbe, *J. Am. Chem. Soc.,* **2002**, *124*, 11064; b) P. G. A. Janssen, A. Ruiz-Carretero, D. González-Rodríguez, E. W. Meijer and A. P. H. J. Schenning, *Angew. Chem. Int. Ed.,* **2009**, *48*, 8103.

5. a) S. J. George, Ž. Tomović, M. M. J. Smulders, T. F. A. de Greef, P. E. L. G. Leclère, E. W. Meijer and A. P. H. J. Schenning, *Angew. Chem. Int. Ed.,* **2007**, *46*, 8206; b) J. C. Y. Ng, J. Liu, H. Su, Y. Hong, H. Li, J. W. Y. Lam, K. S. Wong and B. Z. Tang, *J. Mater. Chem. C,* **2014**, *2*, 78; c) J. Xiao, J. Xu, S. Cui, H. Liu, S. Wang and Y. Li, *Org. Lett.,* **2008**, *10*, 645.

6. a) S. J. George, Z. Tomovic, A. P. H. J. Schenning and E. W. Meijer, *Chem. Commun.,* **2011**, *47*, 3451; b) A. R. A. Palmans, J. A. J. M. Vekemans, E. E. Havinga and E. W. Meijer, *Angew. Chem. Int. Ed. Engl.,* **1997**, *36*, 2648; c) N. Katsonis, H. Xu, R. M. Haak, T. Kudernac, Ž. Tomović, S. George, M. Van der Auweraer, A. P. H. J. Schenning, E. W. Meijer, B. L. Feringa and S. De Feyter, *Angew. Chem. Int. Ed.,* **2008**, *47*, 4997; d) V. Stepanenko, X.-Q. Li, J. Gershberg and F. Würthner, *Chem. Eur. J.,* **2013**, *19*, 4176.

7. a) E. Yashima, K. Maeda and Y. Okamoto, *Nature,* **1999**, *399*, 449; b) A. Mammana, A. D'Urso, R. Lauceri and R. Purrello, *J. Am. Chem. Soc.,* **2007**, *129*, 8062; c) S. J. George, R. de Bruijn, Ž. Tomović, B. Van Averbeke, D. Beljonne, R. Lazzaroni, A. P. H. J. Schenning and E. W. Meijer, *J. Am. Chem. Soc.,* **2012**, *134*, 17789; d) W. Zhang, W. Jin, T. Fukushima, N. Ishii and T. Aida, *J. Am. Chem. Soc.,* **2012**, *135*, 114; e) L. J. Prins, J. Huskens, F. de Jong, P. Timmerman and D. N. Reinhoudt, *Nature,* **1999**, *398*, 498; f) R. Lauceri, A. Raudino, L. M. Scolaro, N. Micali and R. Purrello, *J. Am. Chem. Soc.,* **2002**, *124*, 894; g) K. Shimomura, T. Ikai, S. Kanoh, E. Yashima and K. Maeda, *Nat. Chem.,* **2014**, *6*, 429.

8. a) P. A. Korevaar, S. J. George, A. J. Markvoort, M. M. J. Smulders, P. A. J. Hilbers, A. P. H. J. Schenning, T. F. A. De Greef and E. W. Meijer, *Nature,* **2012**, *481*, 492; b) P. A. Korevaar, T. F. A. de Greef and E. W. Meijer, *Chem. Mater.,* **2013,** *26*, 576.

9. a) T. Ikeda, O. Hirata, M. Takeuchi and S. Shinkai, *J. Am. Chem. Soc.,* **2006**, *128*, 16008; b) F. Riobe, A. P. H. J. Schenning and D. B. Amabilino, *Org. Biomol. Chem.,* **2012**, *10*, 9152; c) E. Yashima, T. Matsushima and Y. Okamoto, *J. Am. Chem. Soc.,* **1995**, *117*, 11596; d) J. Wang and B. L. Feringa, *Science,* **2011**, *331*, 1429; e) T. Kudernac, N. Ruangsupapichat, M. Parschau, B. Macia, N. Katsonis, S. R. Harutyunyan, K.-H. Ernst and B. L. Feringa, *Nature,* **2011**, *479*, 208; f) E. Ohta, H. Sato, S. Ando, A. Kosaka, T. Fukushima, D. Hashizume, M. Yamasaki, K. Hasegawa, A. Muraoka, H. Ushiyama, K. Yamashita and T. Aida, *Nat. Chem.,* **2011**, *3*, 68.

10. a) G. Das, P. Talukdar and S. Matile, *Science* **2002**, *298*, 1600; b) Y. Liu and K. S. Schanze, *Anal. Chem.,* **2008**, *81*, 231.

11. S. Biswas, K. Kinbara, T. Niwa, H. Taguchi, N. Ishii, S. Watanabe, K. Miyata, K. Kataoka and T. Aida, *Nat. Chem.,* **2013**, *5*, 613.

12. a) P. E. Stanley, *J. Biolumin. Chemilumin.* **1989**, *4*, 375; b) P. S. Chen, T. Y. Toribara and H. Warner, *Anal. Chem.,* **1956**, *28*, 1756.

13. M. Zhao, M. Wang, H. Liu, D. Liu, G. Zhang, D. Zhang and D. Zhu, *Langmuir,* **2008**, *25*, 676.

14. H. N. Lee, Z. Xu, S. K. Kim, K. M. K. Swamy, Y. Kim, S.-J. Kim and J. Yoon, *J. Am. Chem. Soc.,* **2007**, *129*, 3828.

15. M. Kumar, N. Jonnalagadda and S. J. George, *Chem. Commun.,* **2012**, *48*, 10948.

16. All experiments were done with one eq. of adenosine phosphates for better kinetics comparison.

17. a) A. Willia, *Chem. Commun.*, **1996**, 676; b) C. Wang, Q. Chen, Z. Wang and X. Zhang, *Angew. Chem. Int. Ed.*, **2010**, *49*, 8612.

CHAPTER-4

Self-assembly of Coronene Bisimide Bolaamphiphile

Chapter-4.1   *Dynamic Multivalent Scaffold for Phosphate Recognition by Self-assembly of Coronene bisimide Based Bolaamphiphile*

Chapter-4.2   *Molecular Chaperone Stabilized Metastable Helical Assemblies of Achiral Coronene bisimide Derivative*

Chapter-4.1

Dynamic Multivalent Scaffold for Phosphate Recognition by Self-assembly of Coronene bisimide Based Bolaamphiphile

Abstract

Multivalent interaction, a ubiquitous phenomenon in most biological systems, is key to highly selective and sensitive analyte recognition. In this chapter, we demonstrate a biomimetic supramolecular approach for the construction of functional multivalent scaffold. Coronene bisimide (CBI) functionalized with dipicolylethylenediamine (DPA) based molecular recognition unit, self-assemble to form a cationic supramolecular polymer. These polyvalent aggregates show adenosine phosphate recognition based turn on fluorescence, as compared to their monomeric analogue displaying less efficient turn off emission response. Insights into the self-assembly process and mode of phosphate interaction were provided through detailed spectroscopic, microscopic and mass spectrometry analysis. Highly dynamic nature of these scaffolds was established through competitive binding of multivalent guest. Finally, in vivo studies revealed the presence of these aggregated chromophores inside living cells, with their potential in probing phosphate rich regions.
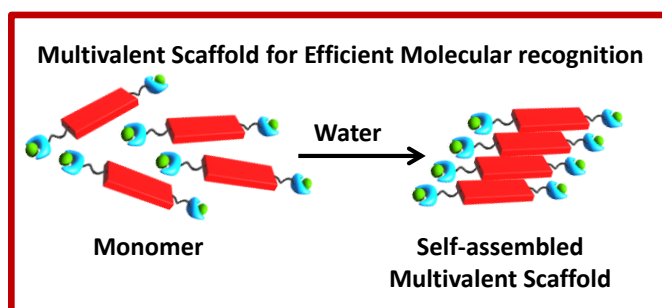
Manuscript based on this work is under preparation.

4.1.1 Introduction

Functional π-conjugated systems with molecular recognition unit have been well-studied as efficient molecular chemosensors with highly sensitive optical signalling.[1] However, most biological systems utilize an evolved approach of multivalent interactions between receptor and analyte molecules, for specific and efficient stimuli response.[2] Hence integration of these molecular receptors into self-assembled multivalent scaffolds with multiple binding sites has been recently employed as a synthetic mimic of multi-functional biomacromolecules for efficient molecular recognition.[3] These artificial systems often exhibit cooperative analyte binding leading to enhanced signalling.[4] Another desirable property from such multivalent systems is their signal amplification. This concept was successfully demonstrated in conjugated polymers, where exciton generated over large number of chromophores can be channelled into the trap state created upon analyte recognition.[5] Such a strategy has also been utilized in chromophoric self-assembled networks for highly sensitive detection of analytes.[6] Among multivalent scaffolds, supramolecular systems finds preference compared to their macromolecular analogues due to their highly dynamic nature and analyte responsive adaptable molecular organization. Recently, supramolecular polymerization of discotic molecules decorated with molecular recognition unit were investigated for the construction of polyvalent scaffold towards bacterial detection and biomolecules/cell clustering.[7] However, a biomimetic design of multivalent self-assembled systems for molecular recognition driven enhanced response to biological stimuli remains challenging.

In this chapter, we present a dynamic multivalent scaffold constructed via supramolecular polymerization of a novel coronene bisimide (CBI) derivative (**ZnCPA**) end functionalized with dipicolylethylenediamine–zinc complex (Zn-DPA). Zn-DPA is known for its specific binding to various phosphates and has been demonstrated in various molecular and supramolecular phosphate sensors.[8] This cationic scaffold shows efficient binding to adenosine phosphate, a biologically relevant stimulus, with clear binding preferences based on multivalent interactions with the analytes. The strength of phosphate binding and their ability to clip chromophores together was established through detailed spectroscopic and mass spectrometric analysis. Interestingly, polyvalent **ZnCPA** scaffold show 'turn on' fluorescence response to phosphate recognition with better sensitivity in contrast to its molecular analogue, which results in turn-off emission. Moreover, interaction with ATP led to chiral guest induced helical organization into otherwise achiral **ZnCPA** assembly. We also show the highly dynamic nature of this self-assembled scaffold and its efficient cellular uptake for potential *in vivo* phosphate sensing inside live cells.

4.1.2 Multivalent Scaffold Synthesis
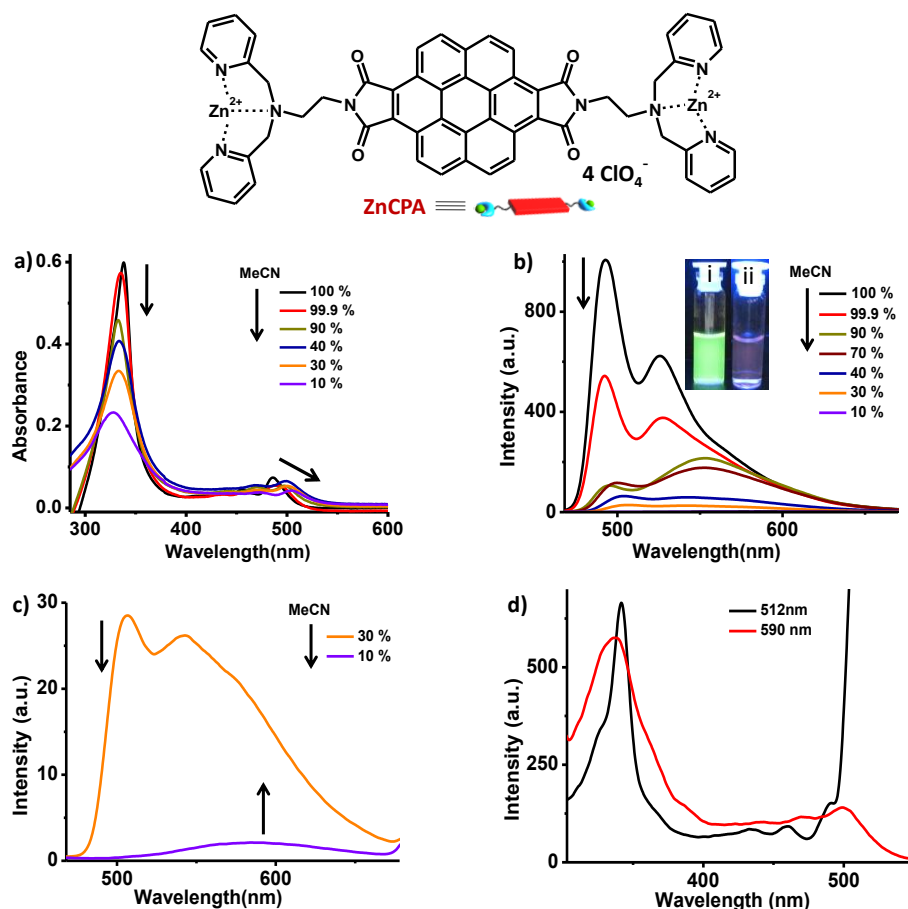
*Figure 4.1.1. Molecular structure of **ZnCPA** bolaamphiphile and its schematic representation. Variation in a) absorption spectra, b) Emission spectra (λ_{ex} = 350 nm) of **ZnCPA** with varying percentage of MeCN in aq. HEPES buffer, c) is the zoomed in portion of b) at lower percentage of MeCN showing the evolution of aggregate band (c = 1 x 10^{-5} M). Inset b: fluorescence color change corresponding to i) 100% MeCN solution, ii) 10% MeCN in aq. HEPES buffer under 365 nm UV illumination. c) Excitation spectra of **ZnCPA** collected at monomer band (512 nm) and aggregate band (590 nm) (30% MeCN in aq. HEPES buffer, c = 1 x 10^{-5} M).*

ZnCPA was synthesized by the condensation reaction of 3,4,9,10-coronene tetracarboxylic dianhydride[9] with N,N-bis(2-pyridylmethyl)ethane-1,2-diamine followed by zinc metallation (Figure 4.1.1). From their molecular design, Zn-DPA group provides the phosphate specific recognition unit,[8] whereas the CBI based aromatic core would assist in self-assembly leading to supramolecular multivalent scaffold for their application in enhanced signalling. This bolaamphiphilic molecule is completely soluble in solvents like MeCN/DMF and self-assembles in presence of water due to hydrophobic and aromatic-aromatic interactions. Absorption spectra of **ZnCPA** (1 x 10^{-5} M) show broadening of bands along with red shift (486 nm to 504 nm) upon increasing percentages of aq. HEPES in MeCN (Figure 4.1.1a). The

emission spectra show quenching of monomeric emission at 493 nm and 525 nm along with appearance of a new red shifted band at 584 nm at higher percentage of aq. HEPES (Figure 4.1.1 b, c). These spectroscopic features clearly indicate J-type molecular organization of CBI chromophores in the self-assembled scaffold,[10] which was further supported by excitation spectra collected at 512 nm and 590 nm (Figure 4.1.1d). Red shift in the excitation spectra at 590 nm compared to 512 nm indicates their origin from aggregated and monomeric species respectively.
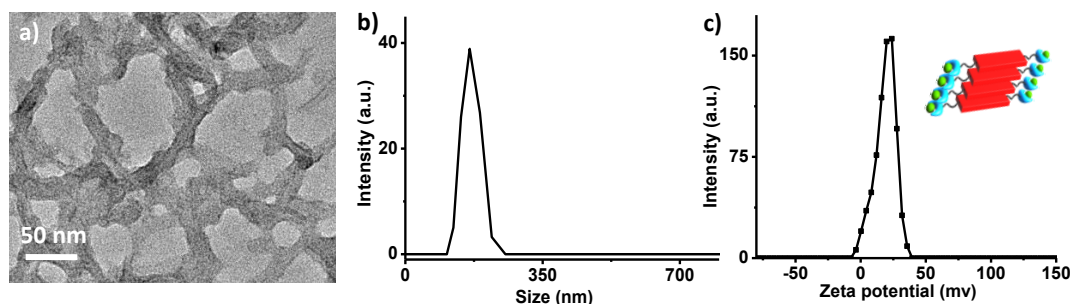
Figure 4.1.2. *a) TEM image (20% MeCN in water, 5 x 10^{-5} M), b) DLS and c) zeta potential measurement (90% aq. HEPES in MeCN, 5 x 10^{-5} M) of self-assembled **ZnCPA** scaffold. Inset c) schematic depiction of the cationic multivalent scaffold formed by self-assembly.*

The self-assembled scaffolds were constructed in MeCN–aq. HEPES buffer solvent mixture. TEM micrographs of **ZnCPA** scaffold show the formation of nanotapes of ~12nm width (Figure 4.1.2a). Dynamic light scattering data show hydrodynamic size distribution of 100-250 nm, confirming the formation of nanostructures in solution (Figure 4.1.2b). Zeta potential measurements further suggest the presence of cationic Zn-DPA groups on the surface of these nanostructures, in agreement with the bolaamphiphilic design and thus providing a supramolecular analogue of well studied cationic polymers for molecular recognition (Figure 4.1.2c).
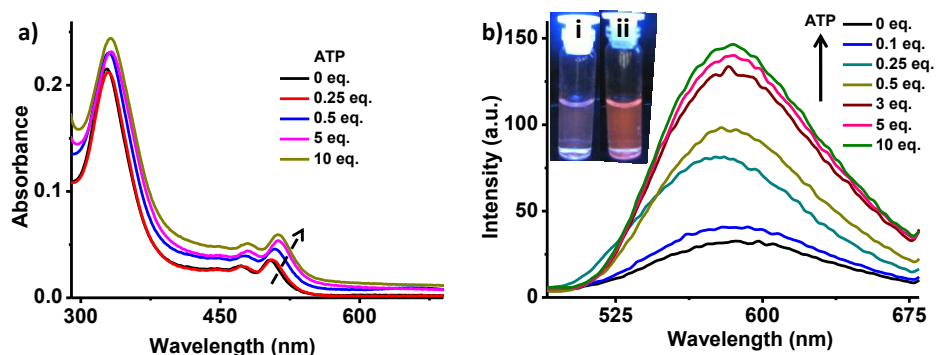
Figure 4.1.3. *Variation in a) absorption and b) emission spectra of **ZnCPA** scaffold upon ATP titration (90% aq. HEPES in MeCN, c = 1 x 10^{-5} M). Inset b): Photographs showing the emission changes with i) no ATP and ii) 1 eq. ATP under 365 nm UV illumination.*

Self-assembled **ZnCPA** scaffolds were further used for adenosine phosphate based anion responsive studies. Binding of ATP to **ZnCPA** scaffold (1 x 10^{-5} M, 90% aq. HEPES in MeCN) showed a bathochromic shift in absorption spectra from 503 nm to 513 nm along with increase in scattering at higher wavelengths, indicating strengthening of aggregation upon ATP binding (Figure 4.1.3a). ATP binding to the scaffold is further evident from the enhancement of emission intensity (Figure 4.1.3b) due to the prevention of photoelectron transfer (PET) upon phosphate binding.[11]   A plot of emission enhancement ratio (I/I_o) show nearly 4 times fluorescence increase upon binding with ATP (Figure 4.1.4a). Similarly, binding of ADP, AMP and PPi [$(P_2O_7)^{4-}$] also showed enhanced emission (Figure 4.1.4, Figure 4.1.5). Comparison among various adenosine phosphates show that ATP and ADP binding leads to saturation of emission at lower eq. of phosphates, whereas AMP takes more than 5 eq. for the same (Figure 4.1.4a). These suggest highly efficient binding of multivalent guests like ADP / ATP with multiple binding sites, whereas a weak binding for AMP with single binding site. Moreover, we notice that AMP binding to **ZnCPA** scaffold could reach highest enhancement ratio (I/I_o) of 8.9, whereas ADP and ATP show only 4 times rise.
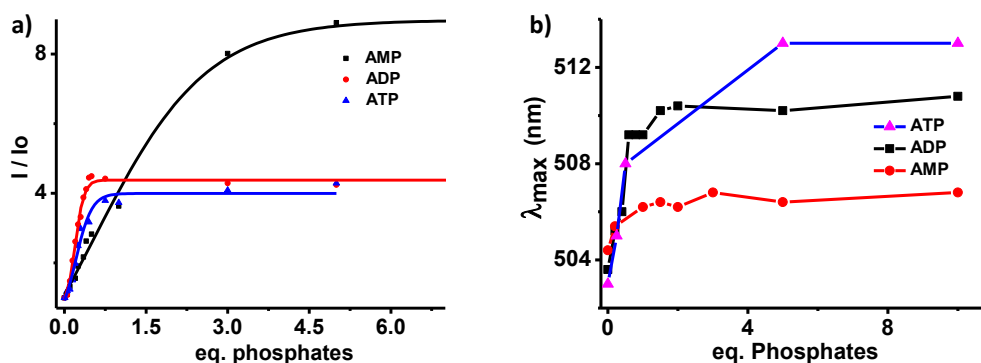
Figure 4.1.4. Plot of a) fluorescence enhancement ratio (I/I_o) and b) shifts in the absorption maxima of **ZnCPA** scaffold as a function of increasing eq. of various adenosine phosphates (90% aq. HEPES buffer in MeCN, c = 1 x 10^{-5} M, λ_{ex} = 350 nm).

To explain these observations, we need to consider two competing forces, i.e. phosphate binding induced a) enhanced emission by preventing PET and b) aggregation induced quenching of emission. Multidentate guests like ATP and ADP can clip to these multivalent **ZnCPA** scaffold strongly through three and two point of attachment respectively, leading to efficient stacking of chromophores.[8] However, AMP with single binding site exhibits weakest association, which cannot facilitate clipping of chromophores (*vide infra*). Extent of shift in absorption maxima at around 503 nm (λ_{max}) does reflects the strength of aggregation. Thus, a plot of red shift in absorption maxima upon binding of ATP to **ZnCPA** scaffold show largest red shift (10 nm) and decreases to 7 nm with ADP, whereas AMP shows barely 2 nm shift, implying weakest association (Figure 4.1.4b). This is expected as ATP with 3 point of

binding is expected to have strongest association through multivalent interactions followed by ADP and least for AMP, which interacts with only one binding site. Thus, due to inefficient interactions, higher AMP eq. are required to saturate all binding site leading to fluorescence saturation, whereas the weaker interchromophoric interactions of **ZnCPA** scaffold prevents fluorescence quenching caused by aggregation leading to such a signalling behaviour.
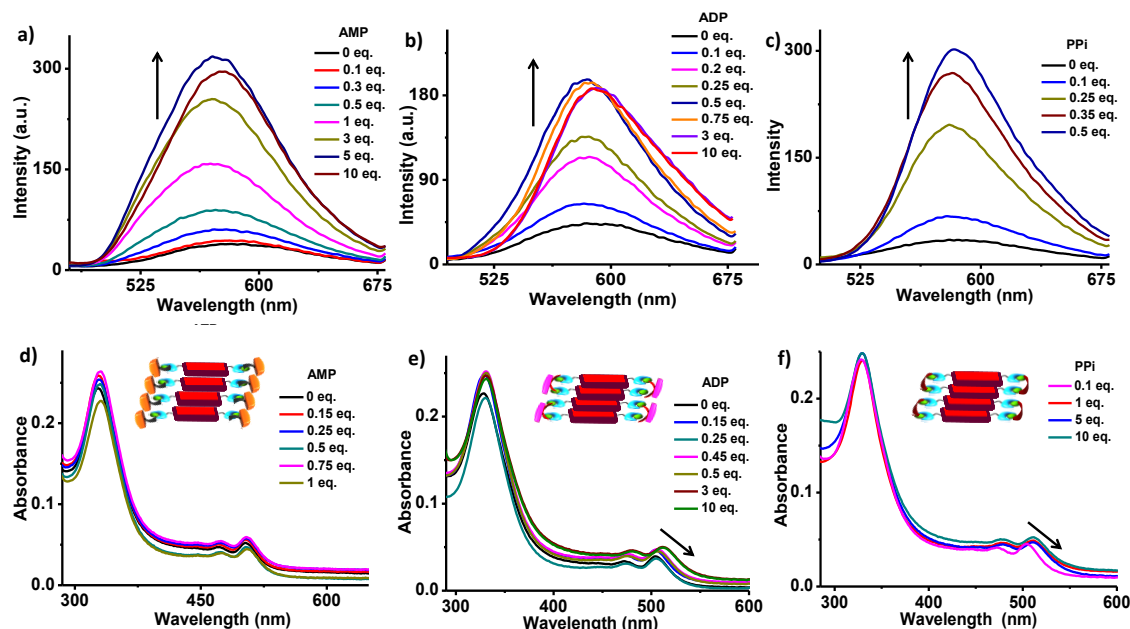
Figure 4.1.5. *Changes in emission spectra of **ZnCPA** scaffold upon increasing eq. of a) AMP, b) ADP and c) PPi. Corresponding absorption spectral changes upon varying eq. of d) AMP e) ADP and f) PPi are shown (90% aq. HEPES buffer in MeCN, c = 1 x 10^{-5} M). Inset shows the schematic illustration of the difference in binding modes of various phosphates.*

4.1.3 Supramolecular Clipping of Chromophores
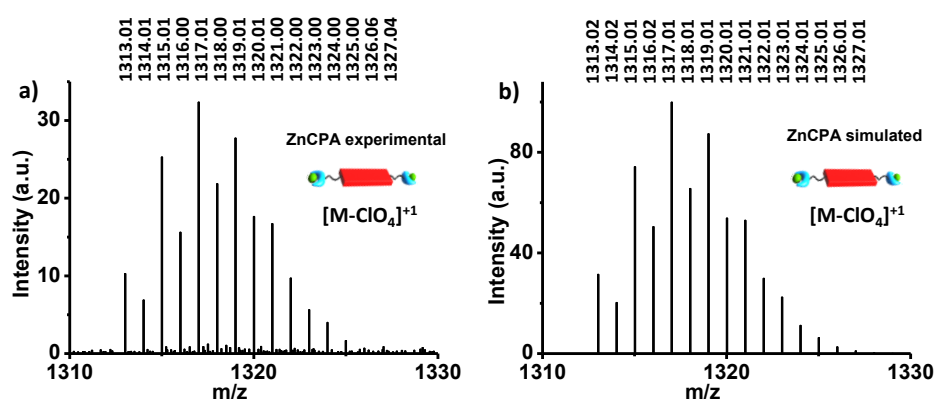
Figure 4.1.6. *a) High resolution ESI-MS spectra of **ZnCPA** whereas b) is the simulated isotopic pattern of the same. The experimental results in a) is in close agreement with the expected pattern shown in b). Schematic represent the corresponding species.*
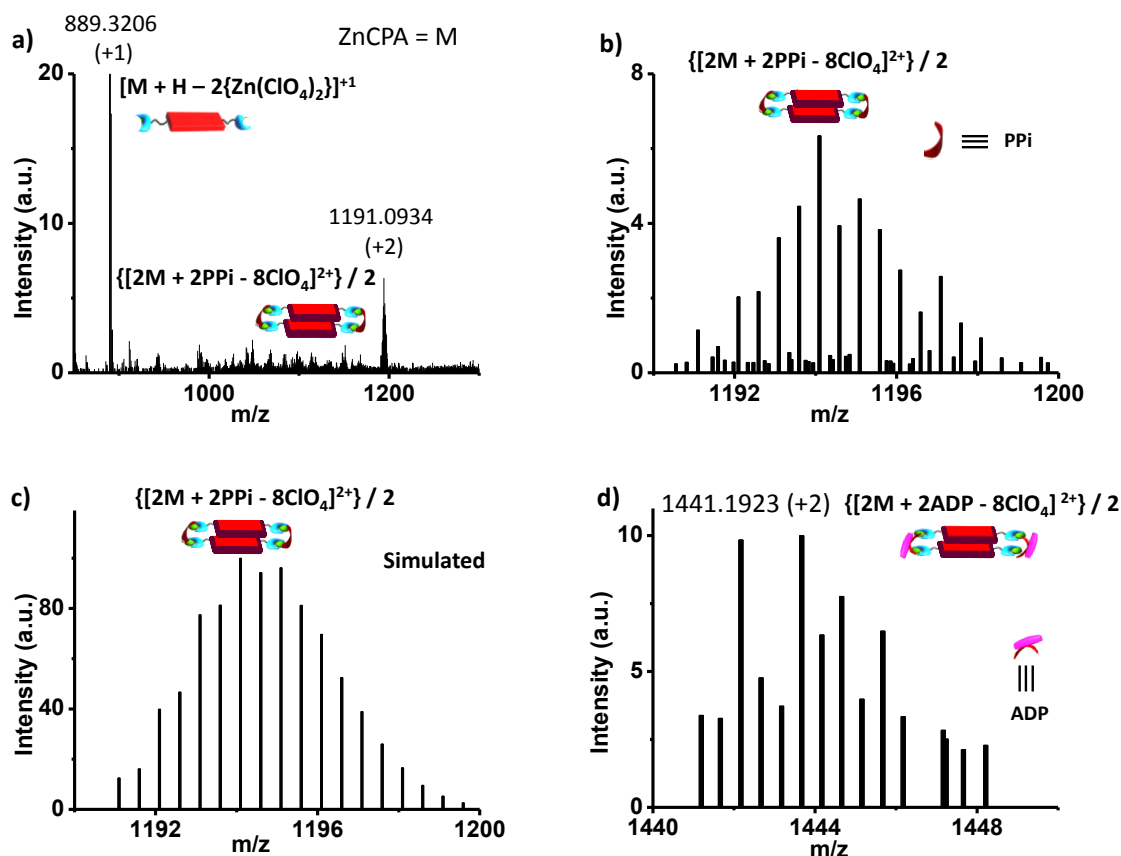
Figure 4.1.7. *a) High resolution ESI-MS spectra of **ZnCPA** with 1 eq. PPi showing both singly and doubly charged species, whereas b) is the zoomed in portion of a) showing the isotopic pattern of doubly charged species. c) is the simulated isotopic pattern of the expected PPi clipped species, which is in close agreement with the experimental data in b). d) High resolution ESI-MS spectra of **ZnCPA** with 1 eq. ADP showing isotopic pattern of doubly charged species. The m/z = 1441.1923 (+2) corresponds to [2**ZnCPA** + 2ADP - 8ClO$_4$]$^{+2}$/2 whereas the expected value is m/z = 1441.1888 (+2). Schematic in the inset represent the corresponding clipped product.*

To further probe into the clipping mode of phosphate binding, high resolution electrospray ionization mass spectrometry (HR-ESI-MS) was performed in positive ion mode. **ZnCPA** alone shows a singly charged species at m/z = 1313.01, which corresponds to [**ZnCPA**-ClO$_4$]$^{+1}$ ion (Figure 4.1.6). Upon addition of stoichiometric amount of PPi, 1313.01 peak vanishes with the emergence of a new doubly charged species at m/z = 1191.09 (Figure 4.1.7 a, b). This exactly matches the expected m/z value of [2**ZnCPA** + 2PPi – 8ClO$_4$]$^{+2}$ confirming the formation of PPi clipped **ZnCPA** dimer. Moreover, the obtained isotopic pattern fairly matches with the simulated data (Figure 4.1.7 b, c). Similar results were also obtained upon clipping with ADP, thereby suggesting highly stable complexation under ESI-MS conditions (Figure 4.1.7d). On the other hand, dimer masses could not be obtained upon

binding to monovalent guests like AMP, due to their inability to clip the chromophores. Moreover, higher order aggregates could not be observed most likely due to their instability under mass spectrometer conditions.
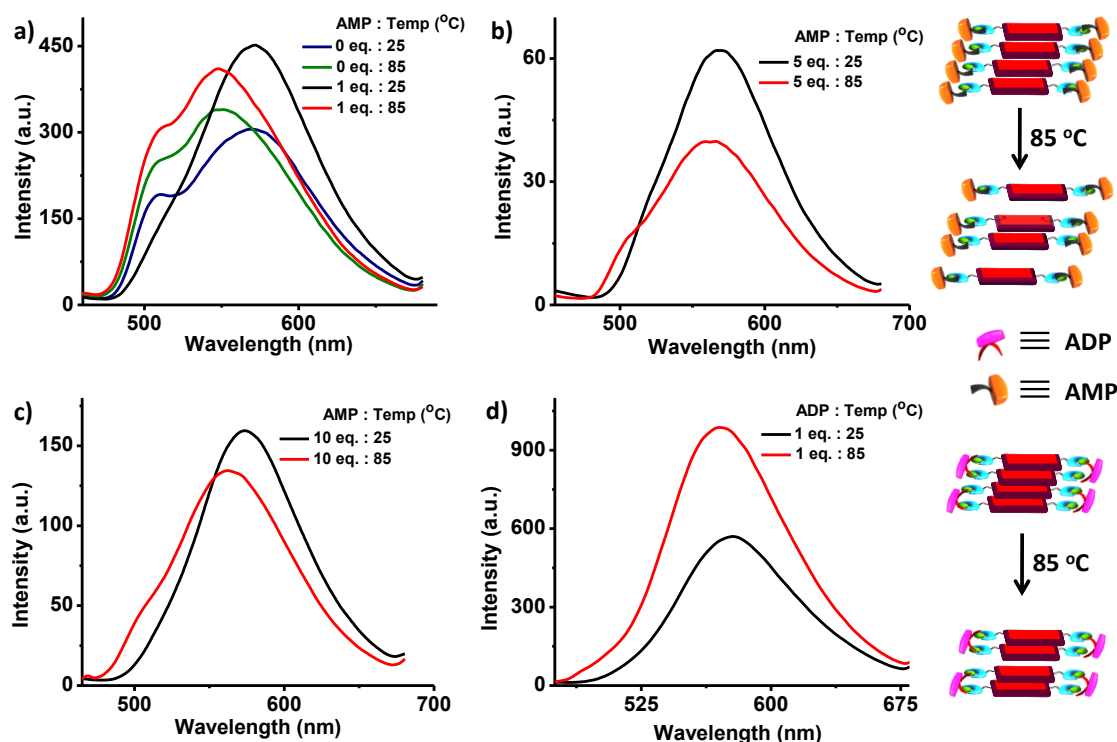
Figure 4.1.8. *Temperature dependent emission spectra of **ZnCPA** scaffold with a) 1 eq., b) 5 eq., c) 10 eq. AMP and d) 1 eq. ADP (30% MeCN in aq. HEPES buffer, c = 1 x 10^{-5} M, λ_{ex} = 350 nm). On the right side is the corresponding schematic demonstrating the phenomenon.*

Further proof for the phosphate clipping in solution state comes from the temperature dependent spectroscopic changes. Emission spectra of **ZnCPA** were recorded in a partially aggregated state i.e. at 30% MeCN in aq. HEPES buffer (c = 1 x 10^{-5} M, λ_{ex} = 350 nm), which showed peaks at 510 nm and 570 nm, corresponding to monomeric and aggregated species respectively (Figure 4.1.8a). On binding to AMP and ADP, the monomer band vanishes with enhancement in aggregate emission at 570 nm, indicating guest binding induced aggregation. When both the solutions were heated to 85 °C, the **ZnCPA**-AMP solution show a blue shift in the aggregate emission band (570 nm to 550 nm) along with the emergence of monomeric emission at 510 nm. This is a clear proof of weakening of aggregate leading to emergence of monomer emission. To rule out the possibility of AMP cleaving out of scaffold at higher temperature, one can see that the luminescence intensity of **ZnCPA**-AMP solution is higher than the one without AMP at 85 °C (Figure 4.1.8a). This suggest that even if partial deaggregation has occurred, AMP is still bound to the monomeric state leading to enhanced emission by preventing PET. Experiments were also done with higher eq. of AMP (5 eq., 10

eq.) so as to make sure all **ZnCPA** sites are occupied (Figure 4.1.8 b, c). In all cases, we indeed see the monomeric features at higher temperatures, in line with the above explanation.
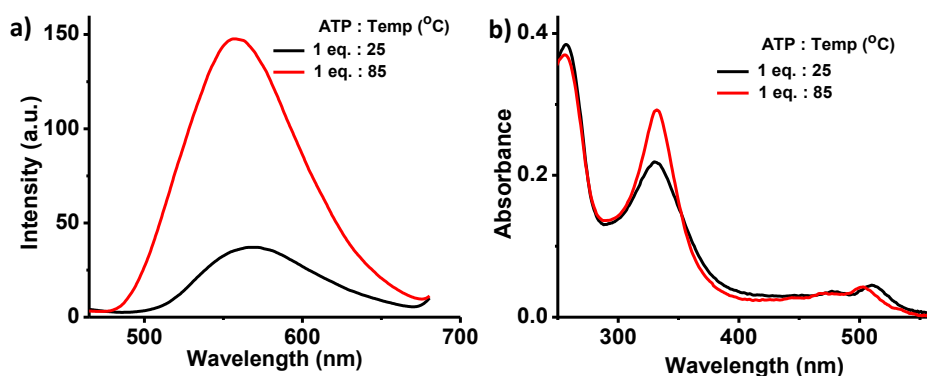
Figure 4.1.9. *Temperature dependent variation in a) emission spectra, b) absorption spectra of* ***ZnCPA*** *with 1 eq. of ATP (30% MeCN in aq. HEPES, c = 1 x 10^{-5} M, λ_{ex} = 350 nm).*

Interestingly, heating the **ZnCPA**-ADP solution also showed blue shift in aggregate emission band (578 nm to 570 nm) with 1.8 times enhancement in aggregate fluorescence, in agreement with weakening of the self-assembled scaffold through decreased π-π interactions, thus decreasing aggregation induced quenching. But, unlike the AMP case, there was no evolution of monomer emission, where on heating even if π-π interaction is affected, phosphate binding continues to clip the chromophores together (Figure 4.1.8d). Here again ADP remains bound to **ZnCPA** even at 85 °C, as evident from the fact that monomeric emission band do not come up. **ZnCPA**-ATP also behaved in a fashion similar to **ZnCPA**-ADP, which falls in line with our hypothesis (Figure 4.1.9). Even the absorption spectra at 85 °C show blue shift in peak maxima from 510 nm to 503 nm, confirming the lower strength of interchromophoric interactions. Thus, we confirm multivalent phosphate induced clipping of **ZnCPA** molecules, which keeps them together even at higher temperature.

To gain insight into the molecular organization of these phosphate bound **ZnCPA** scaffold, TEM analysis was done. The tape like nanostructure of **ZnCPA** scaffolds show transformation into 1-D nanofibers upon interaction with ATP. Three or four of these fibers tend to bundle up where the width of individual fibers were ~5 nm, which closely matches the molecular dimension of **ZnCPA** with ATP attached on both sides (Figure 4.1.10a). Due to highly fluorescent nature of these aggregates, they could also be visualized through confocal fluorescent microscopy as shown in Figure 4.1.10b. We observe highly fluorescent yellow emissive fibrillar morphology and the emission spectra taken at these nanostructures which match well with the solution state measurements (Figure 4.1.10c).
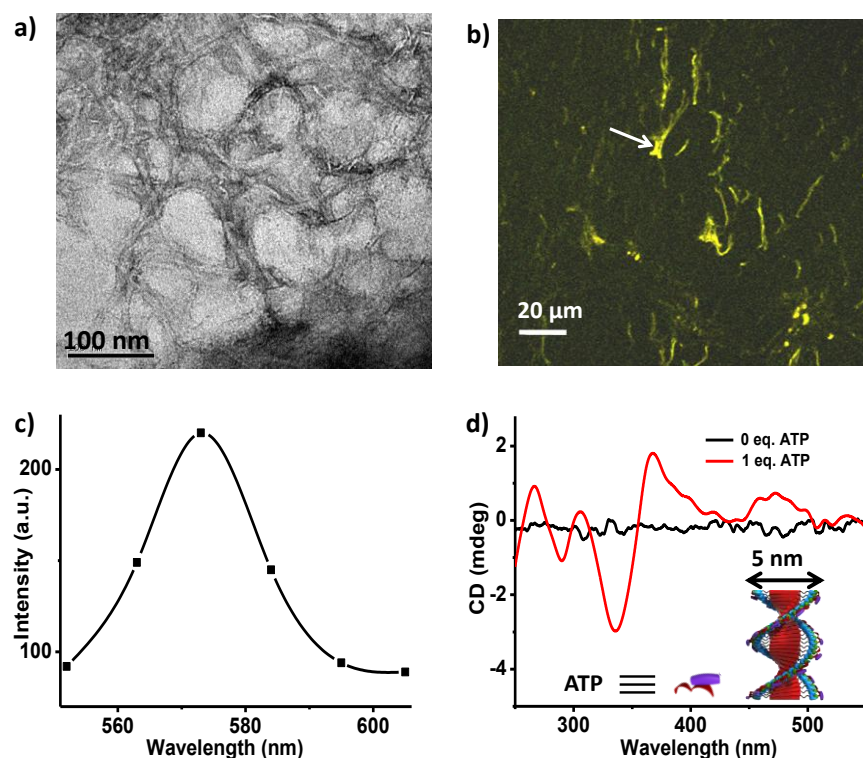
Figure 4.1.10. *a) TEM micrograph of 1-D nanofibers of **ZnCPA**-ATP (0.66 eq. ATP, 5 x 10⁻⁵ M solution, 80% water in MeCN). b) Confocal image of **ZnCPA**-ADP scaffold (1 eq. ADP, 5 x 10⁻⁵ M, 30% MeCN in aq. HEPES), white arrow indicates the spot where fluorescence spectrum was recorded which is shown in c). d) CD signal of **ZnCPA**-ATP assembly (2 x 10⁻⁵ M, 70% aq. HEPES in MeCN). Schematic in inset d) depicts the molecular organization leading to P-helical assembly.*

Interestingly, these adenosine phosphate attached scaffolds showed preferred helical handedness, suggesting the expression of supramolecular chirality due to the chiral nature of bound phosphates. This is evident from their chiroptical properties investigated through circular dichroism (CD) spectroscopy. **ZnCPA** scaffold with no chiral centres was CD silent indicating absence of preferred helicity into their supramolecular ordering. However, interaction with ATP resulted in a positive bisignated CD signal with their positive and negative maxima at 367 nm and 336 nm respectively, with zero crossing at 355 nm (Figure 4.1.10d). This once again demonstrates the efficient interaction of adenosine phosphates to the **ZnCPA** scaffold, resulting in excitonic coupling of chromophores. Further details on the chirality induction process will be discussed in the following chapter (Chapter 4.2).

4.1.4 Self-assembled Scaffold Based Recognition

To establish the role of self-assembly for enhanced phosphate recognition, guest induced emission changes were recorded at various degree of aggregation. Extent of

aggregation could be easily controlled by changing the solvent from 100% MeCN (monomeric state) to increasing composition of aq. HEPES buffer, leading to better aggregation. Binding of ADP to **ZnCPA** monomers (99.9% MeCN) shows nearly 50% decrease in the monomer emission (493 nm, Figure 4.1.11a). In a partially aggregated state (70% MeCN in aq. HEPES buffer), ADP binding greatly diminishes monomer band and a red shifted aggregate band appears at 545 nm. These data supports the fact that phosphate binding decreases emission due to enhanced aggregation, as aggregation quenches the emission of the chromophores. However, in a completely aggregated state (10% MeCN in aq. HEPES buffer), we see significant enhancement (> 4 times) in emission on binding with 1 eq. of ADP (Figure 4.1.11 b). Thus, we confirm the crucial role of self-assembled **ZnCPA** scaffold in efficient response to guest binding. Moreover, aggregated state show fluorescence turn on behavior, which is more desirable compared to monomeric species exhibiting fluorescence quenching on phosphate binding.
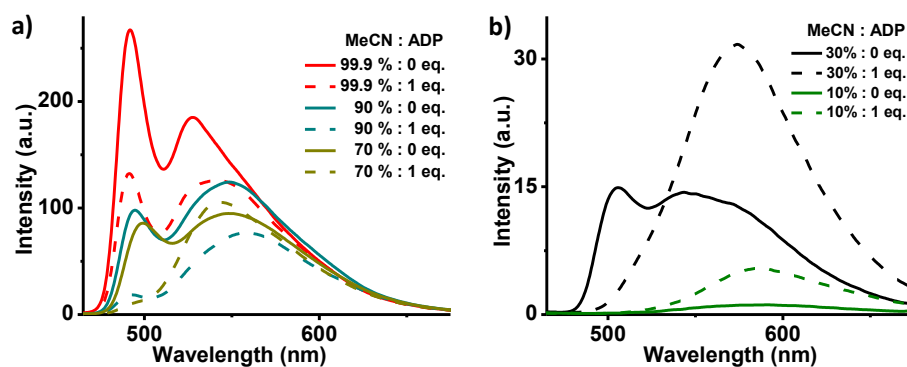
Figure 4.1.11. *Emission changes obtained on binding of one eq. of ADP to* ***ZnCPA*** *at a) 99.9% to 70%, b) 30% to 10% MeCN in aq. HEPES buffer (c=1 x 10^{-5} M, λ_{ex}=350 nm).*

Another interesting property which can be envisaged from these self-assembled scaffolds is its dynamic nature. This could be confirmed by competitive replacement study. Addition of ADP to highly emissive solution of **ZnCPA**-AMP (10eq.), shows quenching of fluorescence along with red shift of band maxima (573 nm to 585 nm) almost instantaneously (Figure 4.1.12). The resultant emission spectra closely resemble the **ZnCPA**-ADP state, confirming dynamic exchange of bound guest molecules. Similar observations were also made with AMP replacement by ATP (Figure 4.1.12). Thus, we confirm the highly dynamic as well as multivalent nature of these self-assembled scaffolds, which allows preferencial binding of ATP/ADP over AMP.
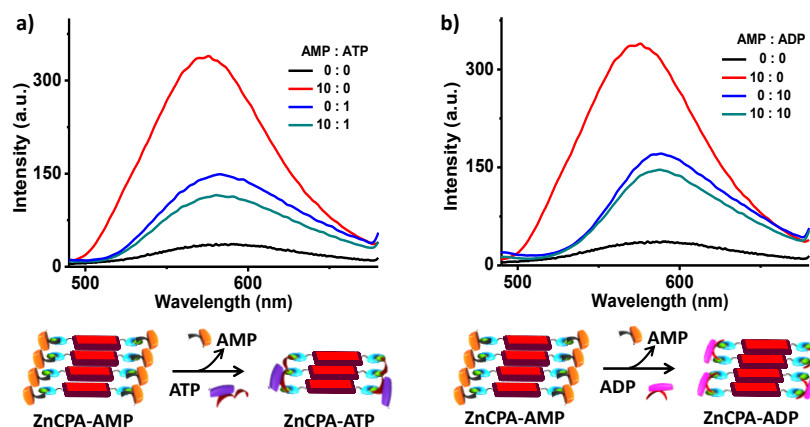
Figure 4.1.12. *Variation in Fluorescence spectra upon competitive binding of a) ATP over AMP and b) ADP over AMP to **ZnCPA** scaffold (10% MeCN in aq. HEPES buffer, c = 1 x 10^{-5} M, λ_{ex} = 350 nm). Below is the schematic representing the competitive binding process.*

Having proven the role of supramolecular self-assembled scaffold in enhanced signalling of adenosine phosphate and its dynamic multivalent preferences, *in vivo* studies were performed to prove their potential for practical applications. U-87 HeLa cells were incubated with **ZnCPA** scaffold for 24 hrs [50 μM **ZnCPA**, 2% DMSO in aq. DMEM (Dulbecco's Modified Eagle's Medium)]. Confocal fluorescence microscopic imaging shows emission in two distinct wavelength range i.e. green and yellow (Figure 4.1.13). The green emission is expected to be coming from the monomeric **ZnCPA** species as seen in Figure 4.1.1b. The origin of yellow emission can be traced back to aggregation of **ZnCPA**, thus confirming the presence of aggregates inside cell as well. Also the high intensity yellow emission could also be due to binding of various phosphates inside the cell. As proven before, due to multivalent interactions with ATP and its high concentration inside cells, the yellow emission might originate from ATP binding. Thus the present system can be useful in tracking the ATP rich regions in cells as well as their concentration fluctuation, which can be investigated in future.
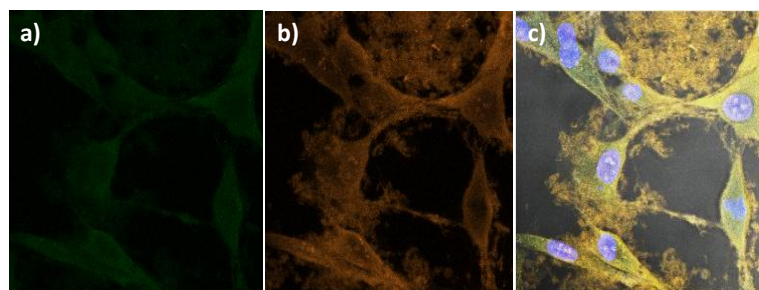
Figure 4.1.13. *Confocal images of U-87 HeLa cells stained with **ZnCPA** scaffold (50 μM **ZnCPA**, 2% DMSO in aq. DMEM) collected at a) green emission and b) yellow emission, whereas c) shows the merged image of both emission.*

4.1.5 Conclusions

In conclusion, we have shown a novel design for the construction of dynamic multivalent scaffold by self-assembly of dipicolylethylenediamine substituted coronene bisimide. These functional supramolecular polymers respond to biological stimuli like adenosine phosphate with turn on of aggregate emission. Detailed optical, microscopic and mass spectrometry measurements proved the clipping mode of phosphate binding leading to formation of fluorescent nanofibers. Phosphate recognition based turn on fluorescence was utilized to prove the crucial role of self-assembly and multivalent interactions in efficient signalling. These dynamic polycationic scaffolds with cellular uptake holds great potential for *in vivo* and *in vitro* phosphate recognition.

4.1.6 Experimental Section

<u>**General Methods:**</u>

Transmission Electron Microscopy (TEM): TEM measurements were performed on a JEOL, JEM 3010 operated at 300 kV. Samples were prepared by placing a drop of the solution on carbon coated copper grids followed by drying at room temperature. The images were recorded with an operating voltage 300 kV. For better contrast sample was stained with uranyl acetate (1 wt % in water) before the measurements.

Optical Measurements: Electronic absorption spectra were recorded on a Perkin Elmer Lambda 900 UV-Vis-NIR Spectrometer and emission spectra were recorded on Perkin Elmer Ls 55 Luminescence Spectrometer. UV-Vis and emission spectra were recorded in 10 mm path length cuvette. Circular Dichroism measurements were performed on a Jasco J-815 spectrometer where the sensitivity, time constant and scan rate were chosen appropriately.

NMR Measurements: NMR spectra were obtained with a Bruker AVANCE 400 (400 MHz) Fourier transform NMR spectrometer with chemical shifts reported in parts per million (ppm) with respect to TMS.

Confocal Microscopy Imaging: Confocal Fluorescence Microscopy imaging was done at room temperature using a Zeiss LSM 510 META laser scanning confocal microscope with a laser excitation of $\lambda_{ex} = 488$ nm.

High-Resolution Mass-Spectrometry (HR-MS): HRMS measurements were performed with Agilent Technologies Q-TOF-LCMS system, 6538 instrument. Measurements were done in ESI mode (positive mode).

Materials: All chemicals / solvents were purchased from the commercial sources and were used as such. Spectroscopic grade solvents were used for all optical measurements.

Synthesis of **ZnCPA** was peformed according to Scheme 4.1.1. Procedures are given below.
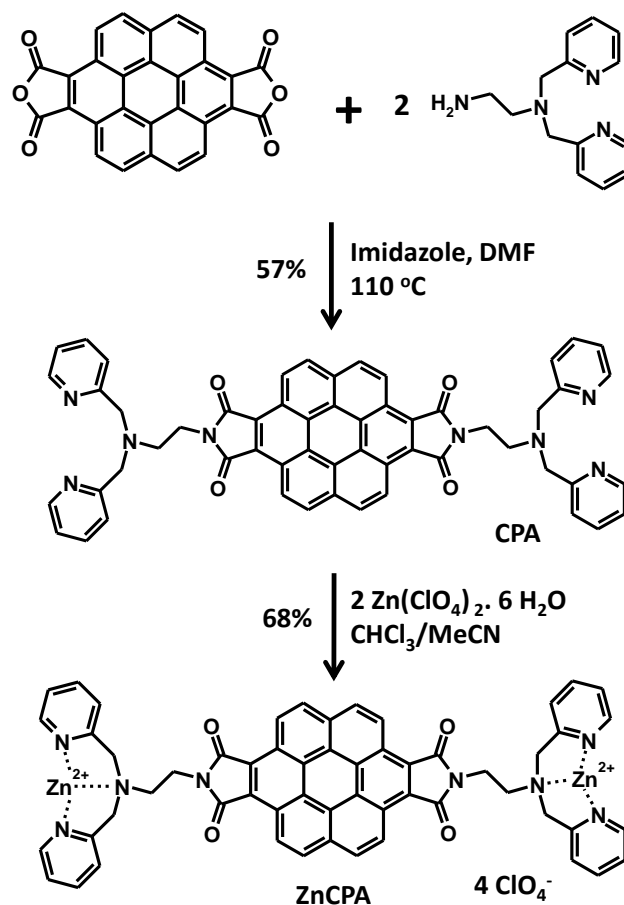
Scheme 4.1.1. *Chemical pathway for the synthesis of **CPA** and **ZnCPA** along with their schematic representation.*

Synthesis of CPA:

182 mg (0.41 mmoles) of 3,4,9,10-coronene tetracarboxylic dianhydride and 250 mg (1.03 mmoles) of N,N-Bis(2-pyridylmethyl)ethane-1,2-diamine were heated with 300 mg of imidazole at 110 °C along with stirring. The pasty mixture stopped stirring in 30 min. and 5 ml of DMF was added to continue stirring the mixture overnight at 110 °C. The reaction mixture turned its colour from brownish red to bright yellow to dark yellow. Reaction mixture was cooled to room temperature and water was added for precipitation. Yellow solid was filtered and washed with water followed by MeOH (excess) to remove imidazole and DMF. Compound was dissolved in CHCl$_3$ and filtered to remove insoluble impurities. The obtained solid was dried under vacuum overnight at 80 °C. Product weighed 206 mg i.e. 57% yield. ^{1}H NMR δ_H

(400 MHz; CDCl$_3$): 9.57 (d, J=8Hz, 4H, ArH), 8.65 (d, J=8Hz, 4H, ArH), 8.38 (d, J=4Hz, 4H, ArH), 7.35 (d, J=8Hz, 4H, ArH), 7.13 (m, 4H, ArH), 6.87 (m, 4H, ArH), 4.20 (t, J=6Hz, 4H, NCH$_2$), 3.98 (s, 8H, ArCH$_2$), 3.14 (t, J=6Hz, 4H, NCH$_2$CH$_2$): ^{13}C NMR δ_C (100 MHz, CDCl$_3$): 169.5, 159.5, 149.0, 136.3, 124.0, 123.2, 122.4, 121.9, 128.7, 60.4 (all ^{13}C peaks could not be resolved due to weak signal as a result of interchromophoric interactions). HRMS (ESI): m/z: calcd for C$_{56}$H$_{41}$N$_8$O$_4$: 889.3215 [M+H]$^+$, found : 889.3206.

Synthesis of ZnCPA:

50 mg of CPA was dissolved in 25 ml of CHCl$_3$. To the stirring solution of CPA, 1ml solution 42 mg of Zn(ClO$_4$)$_2$.6H$_2$0 in MeCN was added and the whole solution was stirred for 2 hrs. A red color precipitate was obtained which was filtered and washed with CHCl$_3$. The red solid was dissolved in minimum amount of MeCN and it was precipitated from CHCl$_3$. The solid was filtered and dried in vacuum at 80 °C. 63 mg of compound was obtained (yield= 68%). ^{1}H NMR δ_H (400 MHz; CD$_3$CN): 9.55 (br, 2H), 8.74 (br, 8H), 8.12 (br, 4H), 7.68 (br, 8H), 4.61 (d, J=16Hz, 4H), 4.29 (d, J=16Hz, 4H), 4.14 (br, 4H), 3.28 (br, 4H). ^{1}H NMR peaks were much broader for the coronene signals when compared to those of pyridine of DPA due to strong aggregation tendency at high concentration. ^{13}C NMR could not be measured successfully for the same reason. HRMS (ESI): m/z: calcd for C$_{56}$H$_{40}$N$_8$O$_{20}$Cl$_3$Zn$_2$: 1313.0205 [M-ClO$_4$]$^+$, found: 1313.0108.

4.1.7 References and Notes

1. a) A. Ikeda and S. Shinkai, *Chem. Rev.*, **1997**, *97*, 1713; F. Zeng and S. C. Zimmerman, *Chem. Rev.*, **1997**, *97*, 1681; b) X. Zhang, J. Yin and J. Yoon, *Chem. Rev.*, **2014**, *114*, 4918; c) A. E. Hargrove, S. Nieto, T. Zhang, J. L. Sessler and E. V. Anslyn, *Chem. Rev.*, **2011**, *111*, 6603; d) A. Ajayaghosh, *Acc. Chem. Res.*, **2005**, *38*, 449; E. Arunkumar, A. Ajayaghosh and J. Daub, *J. Am. Chem. Soc.*, **2005**, *127*, 3156; e) D. Ramaiah, P. P. Neelakandan, A. K. Nair and R. R. Avirah, *Chem. Soc. Rev.*, **2010**, *39*, 4158.

2. a) M. Mammen, S.-K. Choi and G. M. Whitesides, *Angew. Chem. Int. Ed.*, **1998**, *37*, 2754; b) W. J. Lees, A. Spaltenstein, J. E. Kingery-Wood and G. M. Whitesides, *J. Med. Chem.*, **1994**, *37*, 3419.

3. a) M.-a. Morikawa, M. Yoshihara, T. Endo and N. Kimizuka, *J. Am. Chem. Soc.*, **2005**, *127*, 1358; b) J. Liu, M.-a. Morikawa and N. Kimizuka, *J. Am. Chem. Soc.*, **2011**, *133*, 17370; c) A. C. Rodrigo, A. Barnard, J. Cooper and D. K. Smith, *Angew. Chem. Int. Ed.*, **2011**, *50*, 4675; d) K.-R. Wang, H.-W. An, L. Wu, J.-C. Zhang and X.-L. Li, *Chem. Commun.*, **2012**, *48*, 5644; e) K. M. Kim, D. J. Oh and K. H. Ahn, *Chem. Asian J.*, **2011**, *6*, 122; f) I. van Baal, H. Malda, S. A. Synowsky, J. L. J. van Dongen, T. M. Hackeng, M.

Merkx and E. W. Meijer, *Angew. Chem. Int. Ed.*, **2005**, *44*, 5052; g) M. A. C. Broeren, J. L. J. van Dongen, M. Pittelkow, J. B. Christensen, M. H. P. van Genderen and E. W. Meijer, *Angew. Chem. Int. Ed.*, **2004**, *43*, 3557; h) J. Geng, F. Biedermann, J. M. Zayed, F. Tian and O. A. Scherman, *Macromolecules*, **2011**, *44*, 4276.

4. a) M. Takeuchi, M. Ikeda, A. Sugasaki and S. Shinkai, *Acc. Chem. Res.*, **2001**, *34*, 865; b) S. Shinkai, M. Ikeda, A. Sugasaki and M. Takeuchi, *Acc. Chem. Res.*, **2001**, *34*, 494.

5. a) T. L. Andrew and T. M. Swager, *J. Polym. Sci., Part B: Polym. Phys.*, **2011**, *49*, 476; b) Q. Zhou and T. M. Swager, *J. Am. Chem. Soc.*, **1995**, *117*, 12593; c) S. W. Thomas, G. D. Joly and T. M. Swager, *Chem. Rev.*, **2007**, *107*, 1339; d) D. T. McQuade, A. E. Pullen and T. M. Swager, *Chem. Rev.*, **2000**, *100*, 2537.

6. a) C. Giansante, A. L. Olive, C. Schäfer, G. Raffy and A. Del Guerzo, *Anal. Bioanal. Chem.*, **2010**, *396*, 125; b) K. K. Kartha, S. S. Babu, S. Srinivasan and A. Ajayaghosh, *J. Am. Chem. Soc.*, **2012**, *134*, 4834; c) S. Srinivasan, P. A. Babu, S. Mahesh and A. Ajayaghosh, *J. Am. Chem. Soc.*, **2009**, *131*, 15122.

7. a) M. K. Müller and L. Brunsveld, *Angew. Chem. Int. Ed.*, **2009**, *48*, 2921; b) D. A. Uhlenheuer, K. Petkau and L. Brunsveld, *Chem. Soc. Rev.*, **2010**, *39*, 2817; c) K. Petkau-Milroy, D. A. Uhlenheuer, A. J. H. Spiering, J. A. J. M. Vekemans and L. Brunsveld, *Chem. Sci.*, **2013**, *4*, 2886.

8. a) H. N. Lee, Z. Xu, S. K. Kim, K. M. K. Swamy, Y. Kim, S.-J. Kim and J. Yoon, *J. Am. Chem. Soc.*, **2007**, *129*, 3828; b) X. Chen, M. J. Jou and J. Yoon, *Org. Lett.*, **2009**, *11*, 2181; c) S. K. Kim, D. H. Lee, J.-I. Hong and J. Yoon, *Acc. Chem. Res.*, **200**8, *42*, 23; d) T. Sakamoto, A. Ojida and I. Hamachi, *Chem. Commun.*, **2009**, *141*; e) T. Noguchi, T. Shiraki, A. Dawn, Y. Tsuchiya, L. T. N. Lien, T. Yamamoto and S. Shinkai, *Chem. Commun.*, **2012**, *48*, 8090; f) M. Kumar, N. Jonnalagadda and S. J. George, *Chem. Commun.*, **2012**, *48*, 10948; g) M. Kumar, O. A. Ushie and S. J. George, *Chem. Eur. J.*, **2014**, *20*, 5141; h) M. Kumar and S. J. George, *Chem. Sci.*, 2014, DOI: 10.1039/C4SC00813H; i) A. Ojida, I. Takashima, T. Kohira, H. Nonaka and I. Hamachi, *J. Am. Chem. Soc.*, **2008**, *130*, 12095.

9. S. Alibert-Fouet, I. Seguy, J.-F. Bobo, P. Destruel and H. Bock, *Chem. Eur. J.*, **2007**, *13*, 1746.

10. a) K. V. Rao and S. J. George, *Org. Lett.*, **2010**, *12*, 2656; b) C. Kulkarni, R. Munirathinam and S. J. George, *Chem. Eur. J.*, **2013**, *19*, 11270.

11. The lone pair of nitrogen coordinating with –OH of phosphate further prevent PET, thereby enhancement in emission.

Chapter-4.2

Molecular Chaperone Stabilized Metastable Helical Assemblies of Achiral Coronenebisimide Derivative

Abstract

Phosphate recognition driven non-covalent synthesis of helical supramolecular polymers by self-assembly of achiral coronenebisimide functionalized with dipicolylethylenediamine unit is presented. Adenosine diphosphate (ADP) induced a left-handed helical assembly whose handedness could be retained even after removal of chiral auxiliary. Use of an enzyme enabled the removal of ADP and subsequent stabilization of helical conformation in a metastable state (helical memory). A molecular chaperone approach was employed for the stabilization of imprinted helicity in an otherwise highly dynamic assembly. Detailed kinetic analysis provides insight into the stereomutation process. Moreover, the stability of the the metastable state could be easily controlled by changing the solvent composition. Thus, we illustrate a unique biomimetic approach for the construction and stabilization of chiral metastable state.

Imprinted Chirality   **Stereomutation**

(M)-ZnCPA-ADP   **Chaperone**   *(M)*-ZnCPA-CIAP   **Time**   *(rac)*-ZnCPA-CIAP
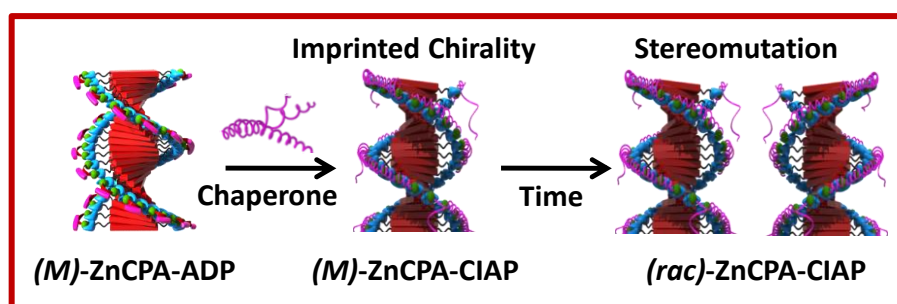
Manuscript based on this work is under preparation.

4.2.1 Introduction

Asymmetric organization of chromophores, by transfer of molecular chirality into supramolecular level has provided new insights into understanding and applications of non-covalent helical assemblies.[1,2] In this regard, induction of chirality into assembly of achiral molecules, upon interaction with chiral guest via non-covalent forces like hydrogen bonding,[3] chiral solvation,[4] acid-base/electrostatic interactions[5] etc. has been considered as an intelligent design. These stimuli responsive dynamic helical assemblies have been utilized for various chiroptical applications like enantioselective sensors, real-time monitoring of chemical reaction etc.[6] Another application of such chiral auxiliary approach is for the construction of helical metastable state, by removal of chiral guest molecules while preserving the helical organization in a so called "chiral memory". Such systems have been greatly utilized for understanding the stereomutation kinetics of helical polymer and probing into various pathway complexities in supramolecular polymers.[7] These phenomena, well understood in polymeric materials, finds greater challenge in supramolecular systems due to kinetic instability of these non-covalent homochiral architectures.[8] The challenge today is to design a non-invasive means of removing chiral information and stabilization of helical organization in their metastable state. These have been mainly achieved by substituting the chiral guests with their achiral analogue to stabilize the kinetic state.[9] In this context, use of biological macromolecules as a molecular chaperone, for stabilization of helical organization, provides an elegant design for imprinted helical memory in dynamic systems.

Molecular chaperones are a group of proteins which assist in assembly/disassembly of biological macromolecules via non-covalent interactions.[10] They are very essential in stabilizing the non-native and active conformation of biopolymers, which is central to their activity. For e.g. heat shock protein based chaperone stabilizes and protects the conformation of active protein from cellular stress and other stimuli like temperature. In this chapter, we report a biomimetic design of helical metastable state in dynamic assembly, by use of an enzyme as a molecular chaperone for its dual action, i.e. a) removal of chiral auxiliary and b) stabilization of homochiral metastable state. Coronene bisimide (CBI) functionalized with dipicolylethylenediamine motif (**ZnCPA**) self-assembles in water (aq. HEPES buffer), whereas binding to adenosine diphosphate (ADP) induces helical organization into their one dimensional (1-D) nanostructures. Spectroscopic and microscopic studies provided mechanistic insight into the unprecedented guest induced helicity in achiral CBI. Addition of enzyme (CIAP) competitively bind to the stacks by replacing ADP, thereby stabilizing kinetically trapped helical memory. Also, from a supramolecular perspective, we show that the stability of metastable state could be controlled just by varying solvent medium.
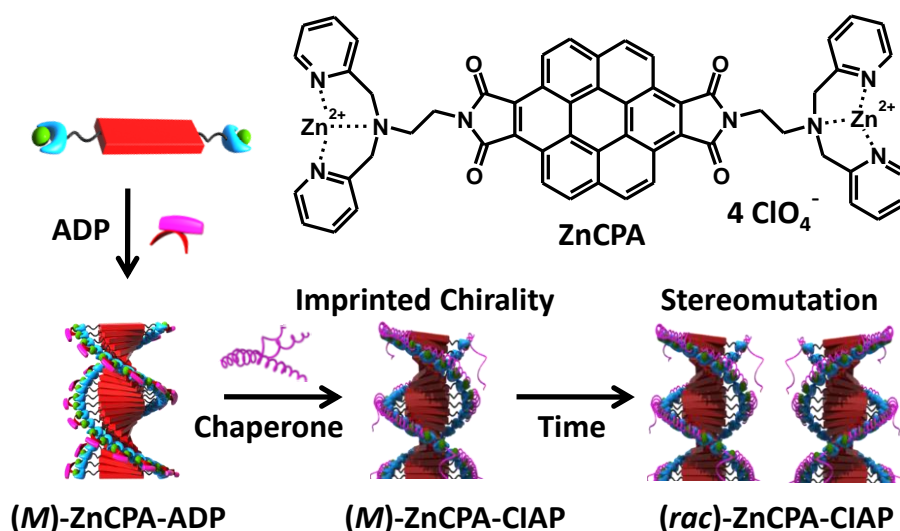
Scheme 4.2.1. *Chemical structure of **ZnCPA** and the schematic representation of molecular chaperone design for imprinted helical memory.*

As per the molecular design, our studies in Chapter-2 have successfully demonstrated DPA functionalized diimides for specific guest recognition induced tunable chirality.[11] Substituting with a larger aromatic core like coronene was envisaged to bring more strength and kinetic stability to these supramolecular assemblies due to enhanced π- π and hydrophobic interactions. Reports on removal of chiral guests often require either substitution with their achiral/racemic analogue or their reaction with other chemicals,[12] which can hamper the soft nanostructures. We present the use of bio macromolecule as a chaperone, to bring about removal of chiral guests like ADP along with stabilization of helical nanostructures, through competitive binding at physiological conditions. Through detailed investigation,-formation of a kinetic trap state and the existence of local minima in the energy landscape is well illustrated.

4.2.2 Induced Circular Dichroism

The target molecule **ZnCPA** was synthesized as described in previous chapter (Section 4.1.6). This bolaamphiphilic molecule was completely soluble in non aqueous polar solvents like MeCN, DMF and self-assembled in water through hydrophobic and aromatic-aromatic interactions. Therefore, all spectroscopic studies were performed in appropriate composition of MeCN – aq. HEPES buffer (10 mM solution in water). On increasing percentage of aq. HEPES in MeCN, continuous broadening and red shift of band in absorption spectra along with quenching of monomer emission band and the appearance of a weakly emissive red shifted band was observed as shown before in Chapter 4.1 (Figure 4.1.1). These are characteristic features of J-type aggregate formation in coronene diimide derivatives.[13]
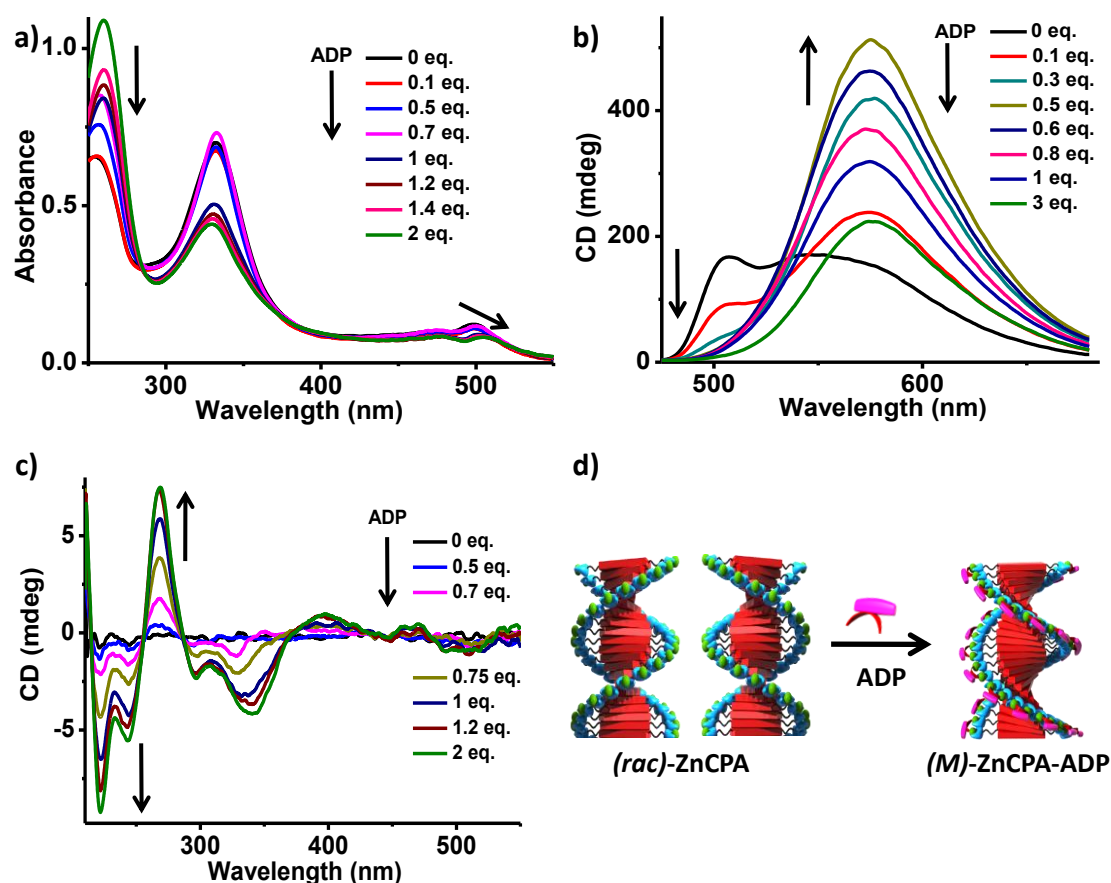
Figure 4.2.1. *Changes in a) absorption spectra, b) emission intensity (λ_{ex}=350 nm) and c) CD signal of **ZnCPA** upon addition of increasing eq. of ADP (30% MeCN in aq. HEPES buffer, c = 2 x 10^{-5} M). Schematic in d) shows ADP binding induced helical organization into assembly of **ZnCPA**.*

Binding of homochiral guest like ADP to **ZnCPA** stacks results in broadening of absorption bands along with their red shift from 409 nm to 505 nm, indicating guest induced improved ordering (Figure 4.2.1a). Simultaneously, fluorescence spectra shows quenching of monomeric emission at 506 nm along with 3.5 times enhancement of aggregate band at 575 nm (Figure 4.2.1b). As discussed in previous chapter (Section 4.1.2), such a turn on of emission intensity has been attributed to prevention of photo electron transfer (PET) upon interaction of DPA substituted chromophores with adenosine phosphate.[14] Moreover, ADP binding induced a left-handed helical assembly (*M*)-**ZnCPA**-ADP, as evident from the negative bisignated CD signal, negative at 343 nm and positive at 268 nm, with a zero crossing at 286 nm (Figure 4.2.1c, 30% MeCN in aq. HEPES, c = 2 x 10^{-5} M). Bisignation at the red shifted π-π* transition (500 nm region) was also clearly visible at higher concentration (c = 4 x 10^{-5} M), indeed confirming the efficient binding of ADP leading to chirality transfer into assembly of achiral **ZnCPA** (Figure 4.2.2a).

Interestingly, plot of CD intensity on titration with ADP showed CD silent till 0.5 eq. of ADP, beyond which the signal increased gradually saturating at 1 eq. of ADP (Figure 4.2.2b). Such a non-linear response suggest a highly cooperative induction of helicity, whereas saturation at 1 eq. ADP once again proves clipping mode of binding. Absorption and emission changes were compared to understand if conformational variation has any role in such an unusual cooperative signaling. Simultaneous monitoring of absorption features reveal that till 0.5 eq. ADP, there are no significant changes in spectra, beyond which the S_0-S_2 electronic transition band (330 nm) begins to broaden and S_0-S_1 transition band (502 nm) red shifts to 506 nm (Figure 4.2.3a and its inset). Similar observations were made at 90% HEPES in MeCN wherein the evolution of CD signal was accompanied by the absorption red shift (504 nm to 510 nm) (Figure 4.2.3b and its inset). A comparative plot of CD intensity and absorption maxima (π-π* transition at 500 nm region) against ADP eq. show that at both the compositions i.e. 70% and 90% aq. HEPES in MeCN, the changes in CD signal closely follow the absorption signal (Figure 4.2.3 a, b). Since such absorption changes indicate variation in supramolecular ordering, we propose that ADP binding induced conformational reorganization of stacks is responsible for such cooperative chirogenesis.[15]
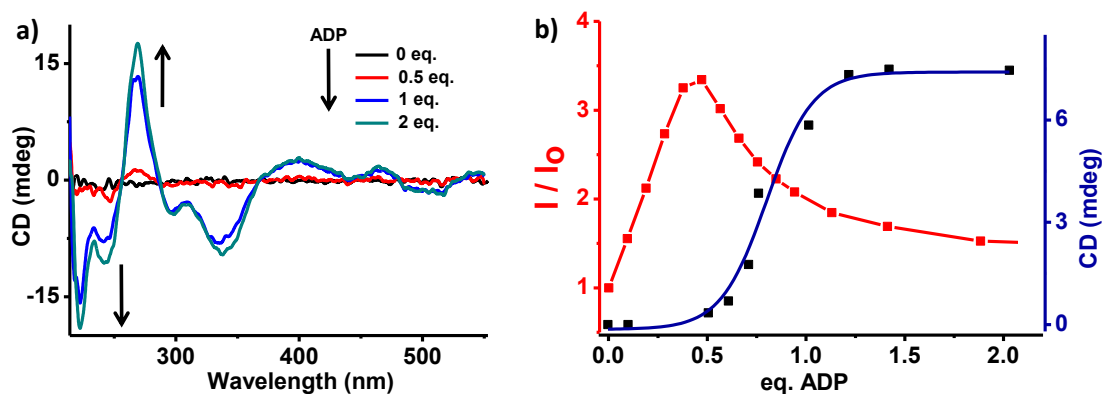
Figure 4.2.2. *a) Induction of CD signal in **ZnCPA** at higher concentration (30% MeCN in aq. HEPES buffer, c = 4 x 10^{-5} M), showing bisignation of π-π* transition (500 nm region). b) Data points showing the changes in fluorescence intensity (red trace, 585 nm) and CD signal (blue trace, 268.5 nm) against eq. of ADP (30% MeCN in aq. HEPES buffer, c = 2 x 10^{-5} M).*

To further probe into such unusual behavior, fluorescence measurements were performed with increasing molar eq. of ADP. Simultaneously monitoring CD signal (268.5 nm) and luminescence intensity (585 nm) against varying eq. of ADP at 70% HEPES in MeCN shows a clear two stage transition (Figure 4.2.2b). Till 0.5 eq. ADP, we see that emission intensity reaches its maxima, indicating that even at lower eq. of phosphates, they bind to **ZnCPA**. Moreover, when emission reaches a maximum, CD signal is still silent. Further, CD

signal continues to rise till 1 eq. ADP, whereas fluorescence signal begin to decrease.[16] As explained before, when the CD signal sets in, we observe stronger aggregation as seen from the bathochromic absorption shifts (Figure 4.2.3). Thus decrease in emission could be due to ADP binding induced aggregation leading to quenching of fluorescence.
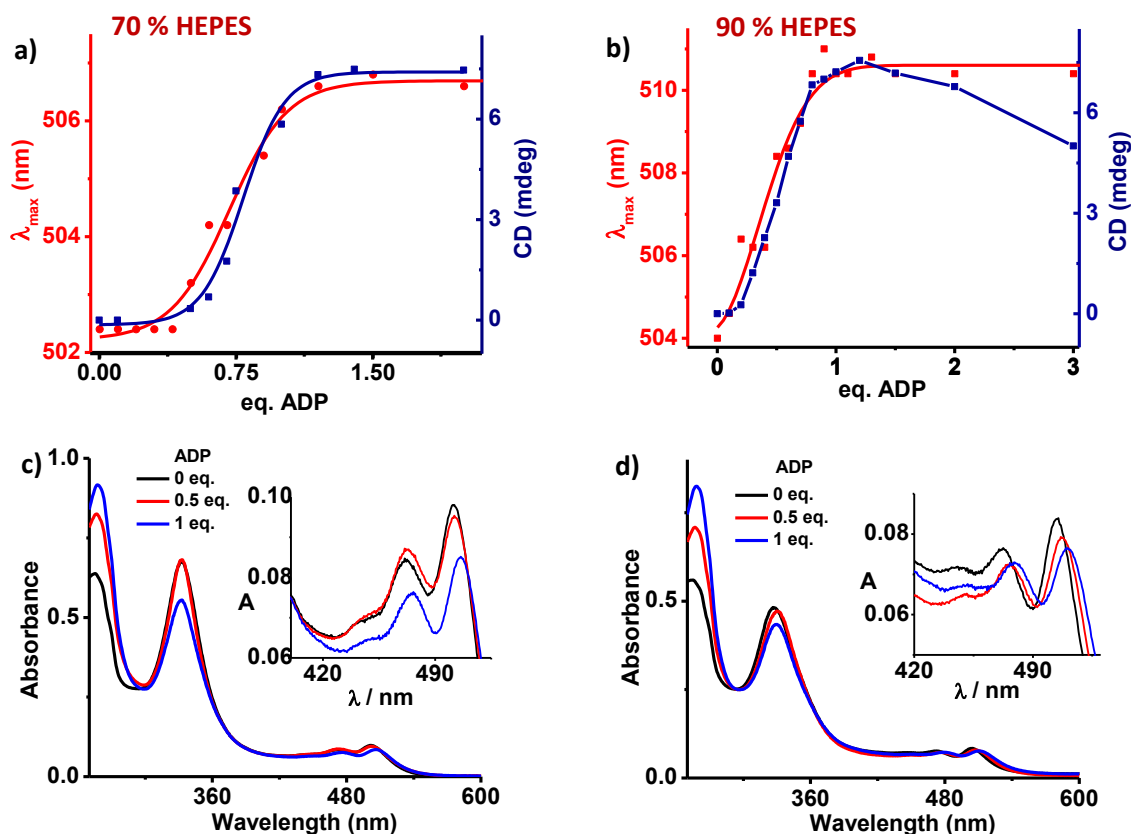
Figure 4.2.3. *Simultaneous probing the variation in CD signal (268.5nm) and shift in absorption peak against eq. of ADP at a) 70% aq. HEPES, b) 90% aq. HEPES in MeCN, 2 x 10^{-5} M; c) and d) show respective absorption spectral changes on binding to varying eq. of ADP. Inset in c) and d) are the zoomed in portions highlighting respective absorption changes.*

Microscopic studies were performed to gain insight into the molecular reorganization and two stage transitions. Transmission Electron Microscopy imaging at 0.5 eq. ADP shows the formation of well-defined one dimensional individual fibers with width ~ 3.5-4.5 nm (Figure 4.2.4a) matching the molecular dimension of **ZnCPA** attached to ADP on one sides and growth axis being the π-π stacking direction. These high aspect ratio individual fibers bundles together on increasing from 0.5 eq. to 1 eq. ADP, wherein all the binding sites are occupied. Widths of these nanofibers were ~ 4.6 nm (Figure 4.2.4 b, c white arrow) which matches the molecular dimension of chromophores with both sides phosphates bound as shown in the schematic. The bundling of nanofibers can be due to increased lipophilic character upon ADP binding, which decreases the interstack electrostatic repulsion when all the binding sites are occupied.
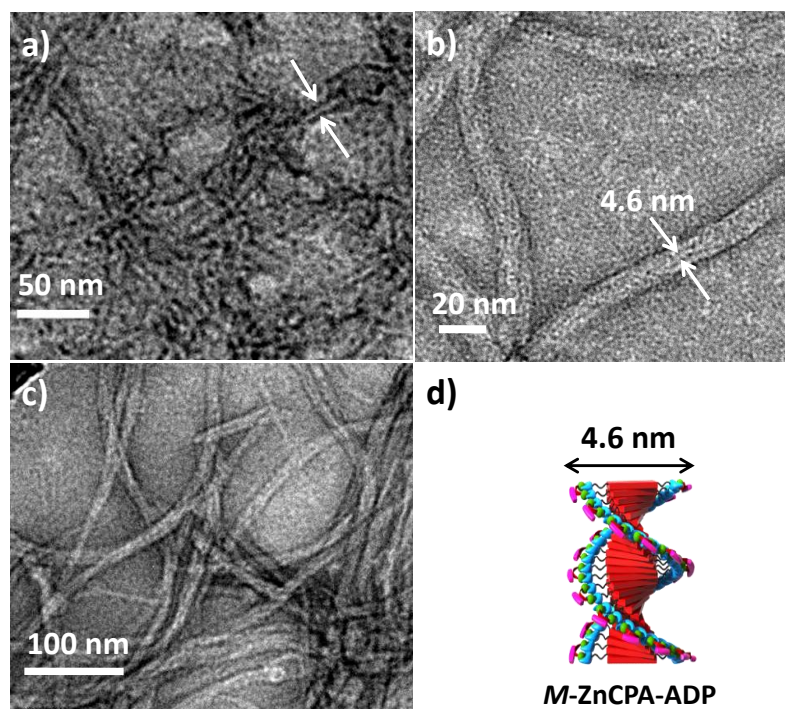
Figure 4.2.4. *TEM images of **ZnCPA** with a) 0.5 eq. ADP and b), c) 1 eq. ADP (70% water in MeCN, 5 x 10⁻⁵ M solution). Samples were post stained with uranylacetate (1 wt % in water) before measurements. Schematic in d) represent the probable supramolecular organization.*

4.2.3 Chaperone Stabilized Imprinted Helicity

Having understood the chiral auxiliary (ADP) induced helicity into the assembly of achiral **ZnCPA**, we investigated the stability of these stacks to retain its handedness even after removal of chiral information, i.e. ADP. First, we introduced an inorganic polycationic scaffold, aminoclay (details in Section 4.2.7), in an attempt where ADP which are bound to **ZnCPA** stacks, can preferentially interact with multivalent positively charged aminoclay, thereby removing them from the **ZnCPA** stacks. However, addition of aminoclay to (*M*)-**ZnCPA**-ADP led to instantaneous loss of CD signal (Figure 4.2.5a). Absorption spectra also show a blue shift of band (493 nm to 496.5 nm) which indicates the removal of ADP from the stacks, thereby weakening of aggregates. Thus, we confirm that the stacks are so dynamic that the removal of phosphate cannot stabilize the preferred helical organization. So, in a more appropriate approach, we could substitute bound ADP with its achiral analogue PPi $[(P_2O_7)^{4-}]$ through competitive binding of multivalent guest, which could then retaining its helical organization. To the contrary, we found that increasing amount of PPi also lead to complete loss of CD signal (Figure 4.2.5 c). The lost helicity reiterates the low stability and highly dynamic nature of these chiral assemblies. Thus, retention of helicity in absence of chiral guests

mandates the stabilization of these stacks with an external agent leading to a kinetically trapped chiral memory state. Therefore, we chose an enzyme, calf-intestinal alkaline phosphatase (CIAP) for its dual action i.e. 1) hydrolysis of phosphoanhydride bonds of ADP, resulting in phosphate and neutral adenosine[17] and 2) its negatively charged surface (*vide infra*) which is aptly suited to stabilize the positively charged assembly of **ZnCPA** through electrostatic interactions.
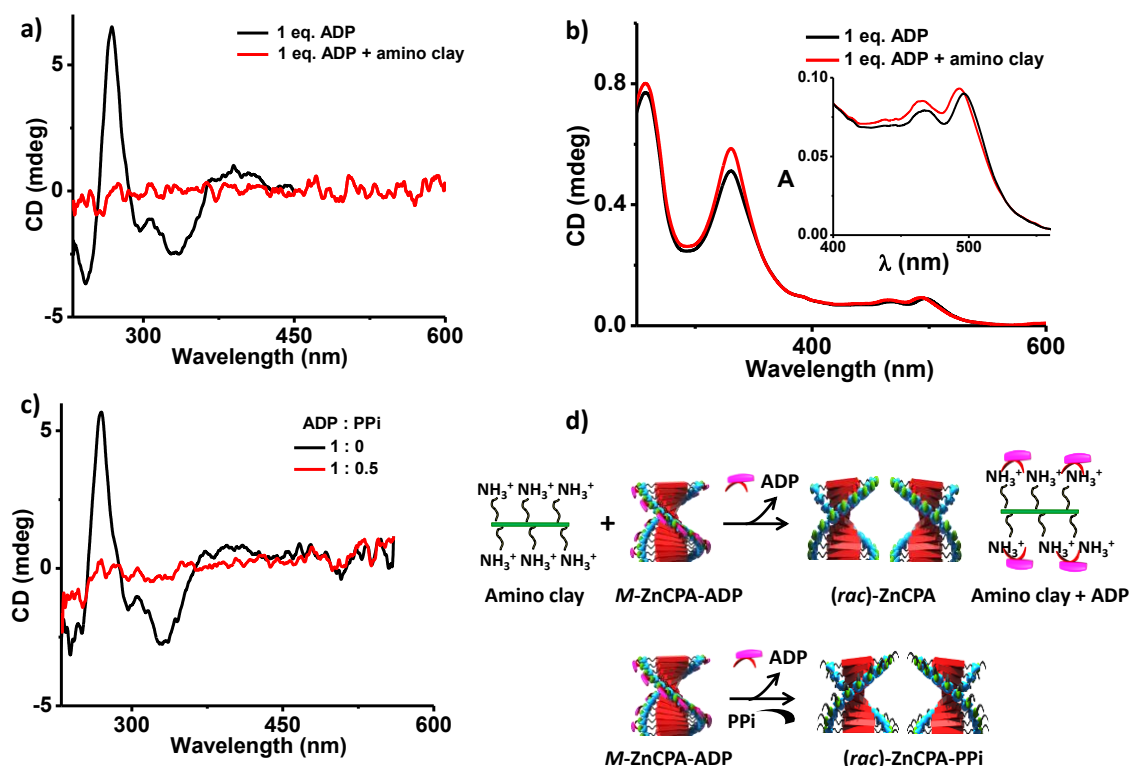
Figure 4.2.5. *Variation in CD signal of (M)-***ZnCPA***-ADP upon addition of a) inorganic polycationic scaffold i.e. aminoclay, c) PPi for competitive replacement of bound ADP. b) shows change in absorption spectra corresponding to a) (70% aq. HEPES in MeCN, 2 x 10⁻⁵ M). d) Schematic representation of the processes shown in a) and c).*

Zeta potential measurement for CIAP confirmed negatively charged surface (-16.8 mV) whereas **ZnCPA** with cationic Zn^{2+} on either side of molecule was shown to be positively charged (+18.7 mV) (Figure 4.2.6a). Upon mixing the two solutions, i.e. **ZnCPA** and CIAP, the surface shows charge neutralization, indicating binding of CIAP to **ZnCPA** stacks through multivalent electrostatic interactions (90% aq. HEPES buffer in MeCN, c = 2 x 10⁻⁵ M). Thus, we envisaged that CIAP can be used to remove the bound ADP and stabilize the chiral memory state.
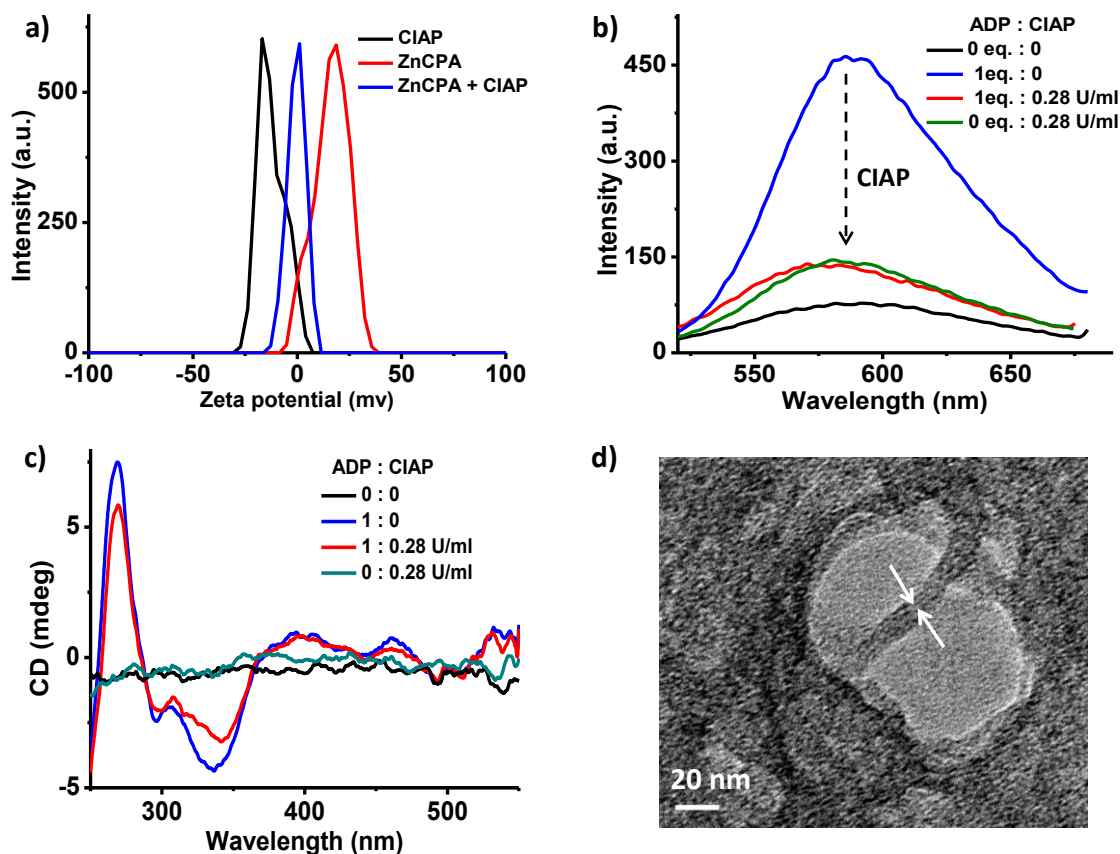
Figure 4.2.6. *a) Zeta potential measured for **ZnCPA** stacks, CIAP and their mixture. Variation in b) fluorescence and c) CD spectra upon addition of CIAP (0.28 U/ml) to (M)-**ZnCPA**-ADP (1 eq.) (90% aq. HEPES in MeCN, 2 x 10⁻⁵ M). d) TEM micrograph of self-assembled **ZnCPA**-ADP (1 eq.) upon addition of CIAP (0.28 U/ml) (90% water in MeCN, 2 x 10⁻⁵ M). For better contrast in TEM samples were post stained with uranylacetate (1 wt % in water) before measurements.*

Role of CIAP in construction and stabilization of chiral memory state was investigated spectroscopically. Since binding of ADP has been shown to enhance the emission intensity, this could be used as a useful tool to probe the removal of chiral auxiliary. Thus, an aq. HEPES solution of CIAP was added to (*M*)-**ZnCPA**-ADP (90% aq. HEPES in MeCN with 1 eq. ADP, 2 x 10⁻⁵ M) and emission spectra were obtained immediately. We see that fluorescence signal quenches completely to resemble the state without any ADP, indicating that all ADP have been replaced from the stack (Figure 4.2.6b). Slight enhancement in emission compared to unbound **ZnCPA** is due to CIAP binding to stacks, as we notice slight increase in emission upon addition of CIAP to free **ZnCPA** stacks (Figure 4.2.6b). This also supports the previous conclusion of interaction between **ZnCPA** and CIAP, as evident from zeta potential measurements. Having proven the very fast removal of bound ADP upon interaction with

CIAP, we looked at the corresponding CD signal changes. Interestingly, there was no significant change in the CD signal after CIAP addition at 20 °C (Figure 4.2.6c).[18] That is to say, we have shown complete removal of chiral auxiliary without disrupting the helical organization in a dynamic system. Further proof of retaining self-assembled nanostructure comes from the TEM analysis of (*M*)-**ZnCPA**-ADP upon addition of CIAP. We observe that the well defined 1-dimensional fibrillar morphology of ADP bound stacks is retained even after removal of ADP (Figure 4.2.6d). This once again confirms the role of CIAP in providing conformational stability to dynamic assembly. These experiments clearly indicate the stabilization of chiral metastable state into a local minima in energy landscape leading to chiral memory (imprinted chirality), where the strength of memory would be governed by the parameters like temperature and interchromophoric interactions (*vide infra*).

4.2.4 Role of Enzyme

Results thus far have proven that addition of CIAP leads to removal of bound ADP from the **ZnCPA** stacks and subsequent binding of CIAP to the stacks. However, to investigate into the fate of ADP in presence of enzyme, detailed spectroscopic investigations were performed. For e.g., to probe the enzymatic hydrolysis of ADP in presence of CIAP, ^{31}P NMR of ADP was recorded in pure D_2O and in 10% CD_3CN in D_2O (Figure 4.2.7a). It is to be noted that since all the ADP binding studies were performed in MeCN - aq. HEPES composition, NMR measurements were also done in same solvent mixture. In pure aq. HEPES Solution, we notice that the signal corresponding to ADP at -11 ppm vanishes with time in presence of CIAP (**2**), indicating complete hydrolysis of ADP in presence of enzyme. However, when the same experiments were repeated in presence of 10% CD_3CN in D_2O, ADP persists without hydrolysis (4), implying enzyme inactivity. Thus we conclude that CIAP shows enzymatic action only in 100% aqueous medium (aq. HEPES buffer), whereas in presence of even 10% MeCN in aq. HEPES, which is essential for **ZnCPA** based study, it loses its activity, probably due to loss of enzyme's active conformation in organic solvents.[19] Having confirmed that the enzyme do not hydrolyze the ADP, but we have already shown its completely removal from the stacks in presence of CIAP (Figure 4.2.6b), suggest that the negatively charged CIAP is competitively replacing the bound ADP and in the process stabilizing the helical organization as shown in schematic (Figure 4.2.7b). This is analogous to "molecular chaperones", which provide stability to the functional conformation of macromolecules.[20] In our case, the CIAP based protein molecules are utilized for stabilizing the chiral memory based kinetic state via non-covalent forces. Detailed experimental evidences described below confirmed the hypothesis of bound ADP replacement by CIAP and its interactions with the stacks along with loss of enzymatic activity.
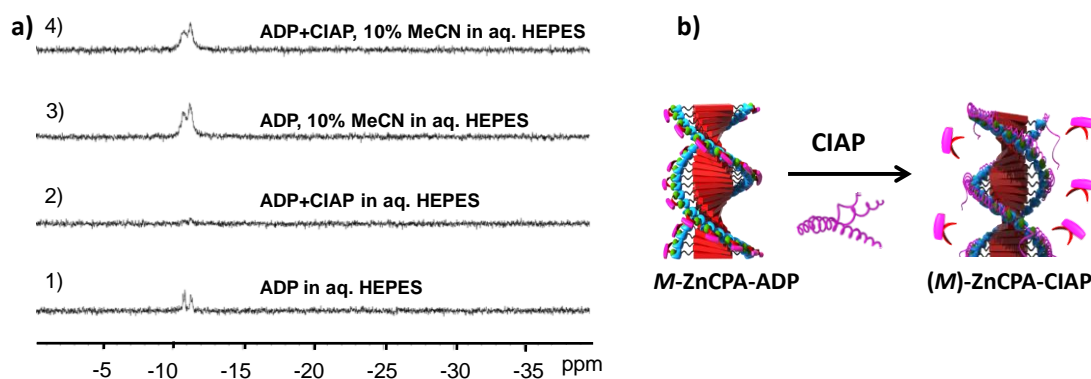
Figure 4.2.7. *^{31}P NMR of ADP recorded in D_2O (1 and 2) and in 10% CD_3CN in D_2O (3 and 4) to probe the enzymatic cleavage of ADP with CIAP. All CIAP based measurements (2 and 4) were performed after 12 hrs of CIAP addition to a 2×10^{-3} M solution of ADP. Schematic in b) represents the action of CIAP in competitive replacement of ADP and stabilization of stacks.*

Emission spectra of (*M*)-**ZnCPA**-ADP were monitored with increasing amount of CIAP added, which show gradual quenching. Interestingly, plot of variation in fluorescence intensity (580 nm) versus time, upon increasing amount of CIAP added at regular interval showed a stepwise sharp decrease in emission with each addition (Figure 4.2.8a). Moreover, the sharp decrease followed by no further change till the next aliquot of CIAP, suggest that the enzyme is no more a catalyst but as a ligand for replacing ADP. For enzyme to be active as a catalyst, we should have observed a fluorescence decay kinetics due to time dependent enzymatic hydrolysis. Secondly, the extent of ADP removal from **ZnCPA** stacks is directly proportional to the net concentration of CIAP added (till a critical concentration when all ADP are removed). This once again rules out the catalytic behaviour, where the concentration of catalyst governs the rate of the reaction and not the percentage conversion. Thus we confirm the loss of enzyme activity in 10% MeCN as well as fast removal of bound ADP from the stacks.
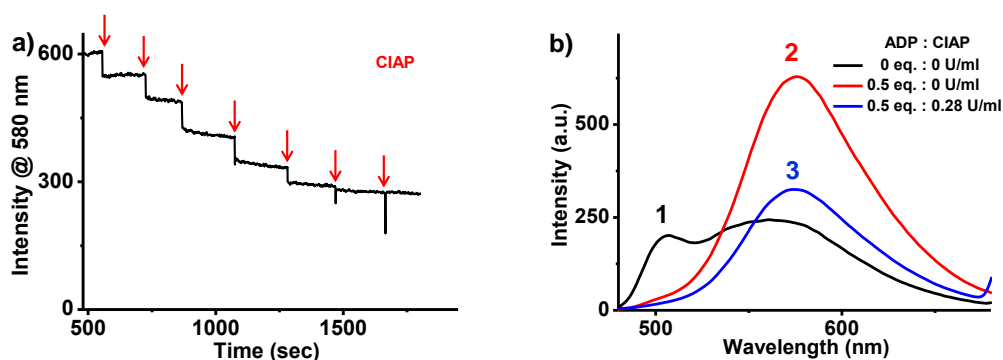
Figure 4.2.8. *a) Time dependent variation in emission intensity of **ZnCPA**-ADP upon sequential addition of CIAP aliquots (90% aq. HEPES in MeCN, 2×10^{-5} M). Red arrow indicate addition of CIAP in aliquots. b) Emission spectra of **ZnCPA** in a partially aggregated state (70% aq. HEPES buffer in MeCN, 2×10^{-5} M) upon binding to ADP followed by CIAP.*

To further elucidate the binding of enzyme to the **ZnCPA** stacks, emission changes upon ADP binding followed by CIAP addition were monitored in a partially aggregated state (70% aq. HEPES buffer in MeCN). In absence of any phosphate, in **1** we observe two bands at 500 nm and 580 nm corresponding to monomer and aggregate emission implying partial aggregation in 70% aq. HEPES buffer (Figure 4.2.8b). Binding of ADP leads to complete aggregation as shown by loss of monomer band and enhanced aggregate emission in **2**. Upon addition of CIAP, we see decrease in aggregate emission intensity indicating removal of ADP in **3**. But as monomer band did not reappear suggest the conformational stabilization by binding of CIAP to the stacks (Figure 4.2.8b). CD spectra of **ZnCPA** stacks in presence of CIAP alone did not show any characteristic signal suggest its role only as a structure stabilizing motif and not as chiral auxiliary for induction of helicity (Figure 4.2.9a). Moreover, when ADP and CIAP were premixed before injecting into the **ZnCPA** stacks (90% aq. HEPES in MeCN), complete loss of CD signal was observed (Figure 4.2.9b). This again reiterates the preferential binding of CIAP over ADP, which cannot induce helicity into the **ZnCPA** stacks. With all the above experiments we have conclusively proven the following: i) Enzyme activity of CIAP is lost in presence of 10% MeCN in aq. HEPES buffer, ii) negatively charged CIAP competitively binds to **ZnCPA** stacks via electrostatic interactions and iii) the removal of ADP upon CIAP addition is very fast (< 5sec).
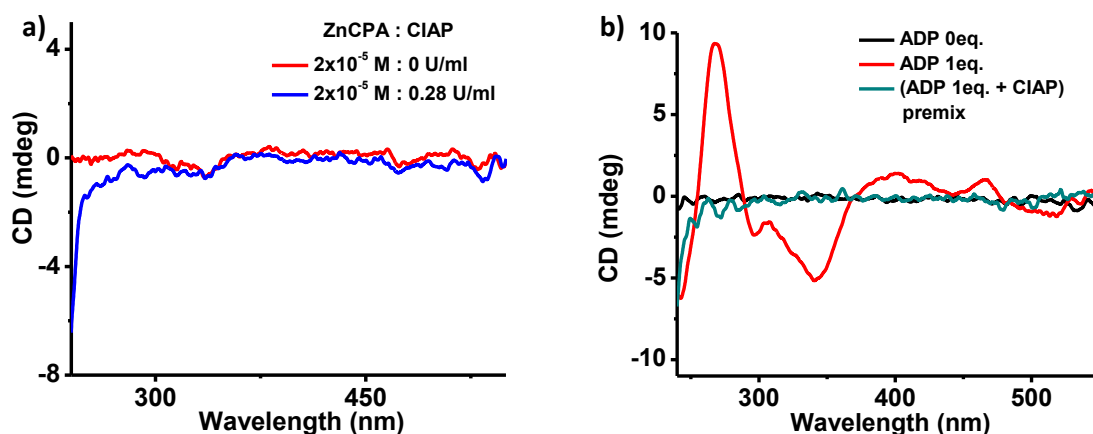
Figure 4.2.9. *Control experiments showing a) CD signal upon addition of CIAP to* **ZnCPA** *stacks without ADP and b) complete loss of CD signal upon premixing of ADP (1 eq.) and CIAP (0.28 U/ml) prior to its interaction with* **ZnCPA** *stacks, confirming that the enzyme preferentially binds to the stacks in comparison to ADP and thus loss of helicity (90% aq. HEPES buffer in MeCN, 2 x 10^{-5} M).*

4.2.5 Kinetics of Stereomutation

Having constructed the imprinted (*M*)-**ZnCPA**-CIAP based metastable state in coronenebisimide assembly, we probed into the stereomutation kinetics i.e. conversion from (*M*)-**ZnCPA**-CIAP to (*rac*)-**ZnCPA**-CIAP. Time dependent variation in CD signal (268.5 nm) at various temperatures show the transition from imprinted helical (*M*)-**ZnCPA**-CIAP to (*rac*)-**ZnCPA**-CIAP. We observe that the rate of racemization increases as we increase the temperature from 25 °C to 30 °C, leading to complete loss of CD signal at varying time scale (Figure 4.2.10a). This clearly proves that the racemization is an activation energy driven process as indicated in the energy level diagram (Figure 4.2.11, c →d). Interestingly, at lower temperatures like 2.5 °C, the kinetics becomes so slow that we do not see any significant loss of CD signal with time, confirming the integrity of helical organization leading to a metastable state. When same experiment was performed without CIAP, we observe complete retention of CD signal even at temperatures like 30 °C (Figure 4.2.10b, black trace). These experiments confirm the retention of imprinted handedness even in the absence of chiral guest (chiral / helical memory).
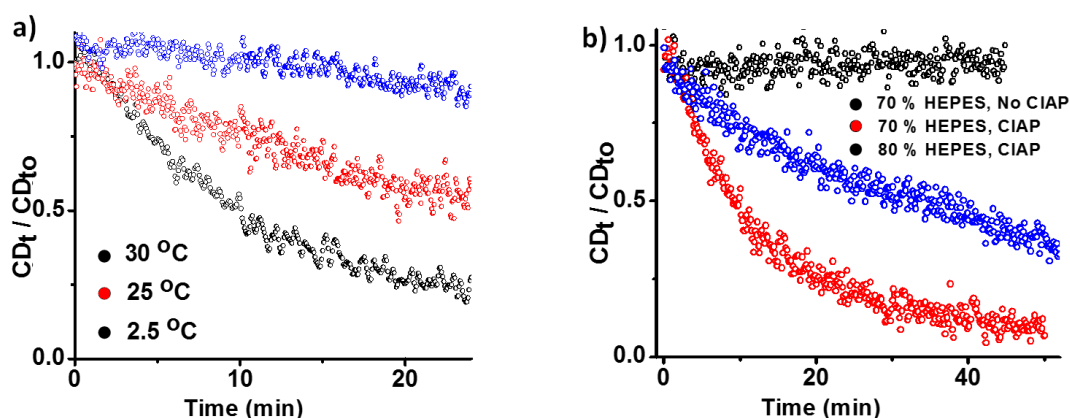
Figure 4.2.10. *Time dependent variation in CD signal intensity of (M)-**ZnCPA**-ADP (1 eq.) monitored at 268.5nm, upon addition of CIAP (0.28 U/ml) at a) varying temperatures (70% aq. HEPES in MeCN) and b) varying solvent composition at 30 °C (c = 2 x 10^{-5} M). CD intensities are normalized for ease of comparison.*

As aq. HEPES induces interchromophoric interaction in **ZnCPA**, we envisaged that the exciton coupling and strength of chiral memory could be improved by increasing composition of aq. HEPES in MeCN. Thus, time dependent CD intensity was monitored as a function of solvent composition. We notice that at 30 °C, as we increase the composition from 70% to 80% aq. HEPES in MeCN, the kinetics of racemization decreases (Figure 4.2.10b, red and blue trace).[21] Looking at the energy level diagram, increasing composition of aq. HEPES buffer

stabilizes the (c) memory state (Figure 4.2.11), consequently higher activation energy is required for stereomutation. Thus, variation in solvent composition provides a unique and simple method to control the strength of helical memory and modulate the stereomutation kinetics.
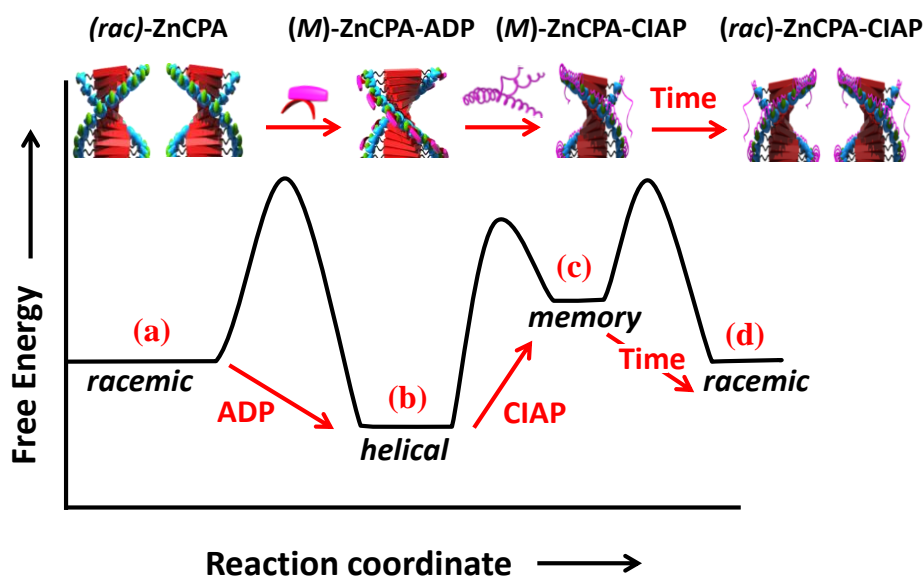
Figure 4.2.11.*Energy level diagram providing a qualitative picture of the probable change in free energy at each stage of chiral memory process along with their schematic representations.*

To gain control over erasing the imprinted helicity, temperature dependent experiments were performed. Monitoring CD signal (268.5 nm) over one heating-cooling cycle for the two helical stacks i.e. (*M*)-**ZnCPA**-ADP and (*M*)-**ZnCPA**-CIAP showed clear differences. The ADP bound helical stacks i.e. (*M*)-**ZnCPA**-ADP showed CD silent features at elevated temperature, whereas complete recovery of signal upon cooling (Figure 4.2.12a). From the previous chapter (Section 4.1.3), we have shown that the clipped phosphates do not detach even at higher temperatures. So the loss of CD signal at higher temperatures could be due to weakening of aggregates leading to poor exciton coupling, resulting in racemization of helical stacks. However, upon cooling it regains the same CD signal as the chiral auxiliary (ADP) is still bound to the stacks. But, in the (*M*)-**ZnCPA**-CIAP imprinted memory state, upon cooling we do not observe any CD signal as the chiral guest (ADP) has been replaced with CIAP and there is no drive to force them into chiral stacks anymore (Figure 4.2.12b). Interestingly, upon partial racemization of helical memory by heating till 30 °C, further cooling continues to retain its segmental helicity and rules out any chiral amplification or nucleation-elongation pathways (Figure 4.2.12c).[22]
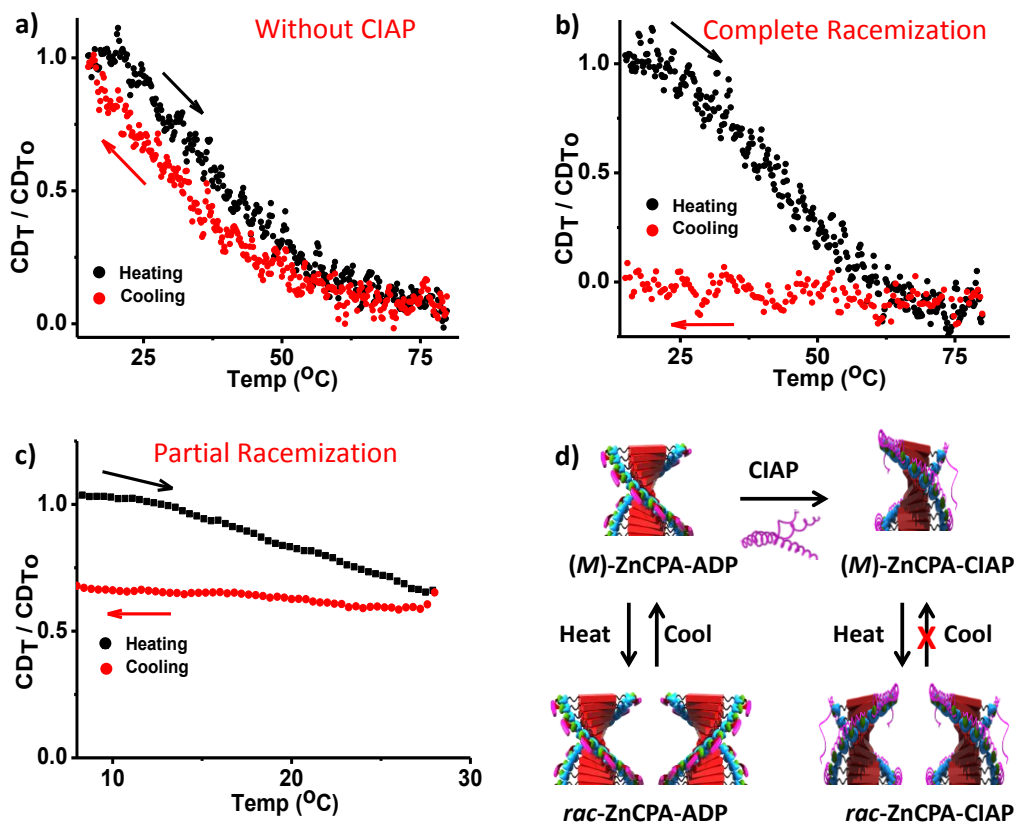
Figure 4.2.12. *Temperature dependent variation in CD intensity upon heating and cooling (M)-ZnCPA-ADP (1eq. ADP) a) without CIAP showing complete recovery,b) with CIAP (0.28 U/ml) showing complete racemization and c) with CIAP(0.28 U/ml) upon heating till 30 °C for partial racemization and subsequent cooling, (monitored at 268.5nm, 70% aq. HEPES buffer in MeCN, 2×10^{-5} M).d) Schematic representation of racemization process in presence of CIAP.*

4.2.6 Conclusions

In conclusion, we have demonstrated DPA functionalized CBI as a supramolecular design principle for ADP binding induced supramolecular helicity. We have successfully created a metastable chiral memory state by removal of chiral auxiliaries in a highly dynamic self-assembly. Use of enzyme as a biomimetic analogue of molecular chaperone was essential for the stabilization of imprinted helical conformation in an otherwise dynamic assembly. Detailed spectroscopic and microscopic investigations confirmed the role of enzyme in removal of bound ADP and stabilization of trapped kinetic state. Finally, we demonstrate a unique method to control the strength of memory, just by changing the solvent medium. With this imprinted memory, we can work towards better kinetically stable systems for second generation helicity transfer and chiral amplification and asymmetric catalysis.

4.2.7 Experimental Section

<u>**General Methods:**</u>

Transmission Electron Microscopy (TEM): TEM measurements were performed on a JEOL, JEM 3010 operated at 300 kV. Samples were prepared by placing a drop of the solution on carbon coated copper grids followed by drying at room temperature. The images were recorded with an operating voltage 300 kV. In order to get a better contrast samples were stained with uranyl acetate (1 wt % in water) before the measurements.

For TEM, water was used instead of aq. HEPES solution to avoid masking of nanostructures due to HEPES deposition upon drying.

Optical Measurements: Electronic absorption spectra were recorded on a Perkin Elmer Lambda 900 UV-Vis-NIR Spectrometer and emission spectra were recorded on Perkin Elmer Ls 55 Luminescence Spectrometer. UV-Vis and emission spectra were recorded in 10 mm path length cuvettes. Fluorescence spectra of solutions were recorded with 350 nm excitation wavelength. Circular Dichroism measurements were performed on a Jasco J-815 spectrometer where the sensitivity, time constant and scan rate were chosen appropriately. Corresponding temperature dependent measurements were performed with a CDF – 426S/15 Peltier-type temperature controller with a temperature range of 263-383 K and adjustable temperature slope.

NMR Measurements: NMR spectra were obtained with a Bruker AVANCE 400 (400 MHz) Fourier transform NMR spectrometer with chemical shifts reported in parts per million (ppm) with respect to TMS.

Sample Preparation: Aq. HEPES buffer used was a 10 mM HEPES solution in water. All samples for spectroscopic measurements were prepared by injecting the stock solution of **ZnCPA** in MeCN into appropriate volume of solvent (aq. HEPES buffer and MeCN). To that required amount of phosphates were injected and the solution was mixed by manual shaking before measurements.

Commercially available CIAP was 2.8 units per mg and stock solution of CIAP was prepared by dissolving 1 mg of CIAP in 80 μl of aq. HEPES buffer. For each measurement, 20 μl of this stock solution was added into 2.5 ml of required solution making the net CIAP concentration to be 0.28 U/ml.

Materials: 3,4,9,10-coronenetetracarboxylic dianhydride,[23] N,N-Bis(2-pyridylmethyl)ethane-1,2-diamine[24] was synthesized based on reported procedure. CIAP was purchased from Sisco Research Laboratory Pvt. Ltd. India. All other chemicals were purchased from the commercial

sources and were used as such. Spectroscopic grade solvents were used for all optical measurements.

Aminoclay: The amino clay used is a layered magnesium organosilicate having the structure analogous to 2:1 trioctahedral smectites with an approximate composition of $R_8Si_8Mg_6O_{16}(OH)_4$, where R is covalently linked aminopropyl substituents. These are highly soluble in water due to covalent functionalization with organo amines.[25] The resultant amino functionalized clays, amino clay are soluble in water via protonation of their amine groups and exfoliate into single layers due to charge repulsion. These exfoliated sheets resemble like multivalent 2D cationic macromolecules and can be used to co-assembled anionically charged molecules.

<u>**Synthesis of ZnCPA**</u>: This was synthesized as described in the previous chapter (Section 4.1.6).

4.2.8 References and Notes

1. a) A. R. A. Palmans and E. W. Meijer, *Angew. Chem. Int. Ed.*, **2007**, *46*, 8948; b) A. E. Rowan and R. J. M. Nolte, *Angew. Chem. Int. Ed.*, **1998**, *37*, 63; c) E. Yashima, K. Maeda, H. Iida, Y. Furusho and K. Nagai, *Chem. Rev.*, **2009**, *109*, 6102; d) M. M. Green, K.-S. Cheon, S.-Y. Yang, J.-W. Park, S. Swansburg and W. Liu, *Acc. Chem. Res.*, **2001**, *34*, 672; e) M. Fujiki, J. R. Koe, K. Terao, T. Sato, A. Teramoto and J. Watanabe, *Polym. J.*, **2003**, *35*, 297; f) A. Lohr and F. Würthner, *Isr. J. Chem.*, **2011**, *51*, 1052; g) V. K. Praveen, S. S. Babu, C. Vijayakumar, R. Varghese and A. Ajayaghosh, *Bull. Chem. Soc. Jpn.*, **2008**, *81*, 1196; h) D. K. Smith, *Chem. Soc. Rev.*, **2009**, *38*, 684; i) Y. Wang, J. Xu, Y. Wang and H. Chen, *Chem. Soc. Rev.*, **2013**, *42*, 2930.

2. a) Z. Huang, S.-K. Kang, M. Banno, T. Yamaguchi, D. Lee, C. Seok, E. Yashima and M. Lee, *Science*, **2012**, *337*, 1521; b) Y. Nakano, A. J. Markvoort, S. Cantekin, I. A. W. Filot, H. M. M. ten Eikelder, E. W. Meijer and A. R. A. Palmans, *J. Am. Chem. Soc.*, **2013**, *135*, 16497; c) M. Banno, T. Yamaguchi, K. Nagai, C. Kaiser, S. Hecht and E. Yashima, *J. Am. Chem. Soc.*, **2012**, *134*, 8718; d) F. García and L. Sánchez, *J. Am. Chem. Soc.*, **2012**, *134*, 734; e) A. Gopal, M. Hifsudheen, S. Furumi, M. Takeuchi and A. Ajayaghosh, *Angew. Chem. Int. Ed.*, **2012**, *51,* 10505; f) K. Toyofuku, M. A. Alam, A. Tsuda, N. Fujita, S. Sakamoto, K. Yamaguchi and T. Aida, *Angew. Chem. Int. Ed.*, **2007**, *119*, 6596; g) J. Kumar, T. Nakashima, H. Tsumatori and T. Kawai, *J. Phys. Chem. Lett.*, 2**014**, *5*, 316; h) Ž. Tomović, J. van Dongen, S. J. George, H. Xu, W. Pisula, P. Leclère, M. M. J. Smulders, S. De Feyter, E. W. Meijer and A. P. H. J. Schenning, *J. Am. Chem. Soc.*, **2007**, *129*,

16190; i) F. Aparicio, B. Nieto-Ortega, F. Nájera, F. J. Ramírez, J. T. López Navarrete, J. Casado and L. Sánchez, *Angew. Chem. Int. Ed.*, **2014**, *53*, 1373; j) A. Ajayaghosh, R. Varghese, S. Mahesh and V. K. Praveen, *Angew. Chem. Int. Ed.*, **2006**, *45*, 7729; k) W. Jin, T. Fukushima, M. Niki, A. Kosaka, N. Ishii and T. Aida, *Proc. Natl. Acad. Sci. U. S. A.*, **2005**, *102*, 10801.

3. a) H. Fenniri, B.-L. Deng and A. E. Ribbe, *J. Am. Chem. Soc.,* **2002**, *124*, 11064; b) P. G. A. Janssen, A. Ruiz-Carretero, D. González-Rodríguez, E. W. Meijer and A. P. H. J. Schenning, *Angew. Chem. Int. Ed.,* **2009**, *48*, 8103.

4. a) S. J. George, Z. Tomovic, A. P. H. J. Schenning and E. W. Meijer, *Chem. Commun.,* **2011**, *47*, 3451; b) A. R. A. Palmans, J. A. J. M. Vekemans, E. E. Havinga and E. W. Meijer, *Angew. Chem., Int. Ed. Engl.,* **1997**, *36*, 2648; c) N. Katsonis, H. Xu, R. M. Haak, T. Kudernac, Ž. Tomović, S. George, M. Van der Auweraer, A. P. H. J. Schenning, E. W. Meijer, B. L. Feringa, S. De Feyter, *Angew. Chem. Int. Ed.,* **2008**, *47*, 4997; d) V. Stepanenko, X.-Q. Li, J. Gershberg, F. Würthner, *Chem. Eur. J.,* **2013**, *19*, 4176.

5. a) S. J. George, Ž. Tomović, M. M. J. Smulders, T. F. A. de Greef, P. E. L. G. Leclère, E. W. Meijer and A. P. H. J. Schenning, *Angew. Chem. Int. Ed.,* **2007**, *46*, 8206; b) J. C. Y. Ng, J. Liu, H. Su, Y. Hong, H. Li, J. W. Y. Lam, K. S. Wong, B. Z. Tang, *J. Mater. Chem. C,* **2014**, *2*, 78; c) J. Xiao, J. Xu, S. Cui, H. Liu, S. Wang, Y. Li, *Org. Lett.,* **2008**, *10*, 645.

6. a) F. Biedermann and W. M. Nau, *Angew. Chem. Int. Ed.*, **2014**, DOI: 10.1002/anie.201400718; b) F. Riobe, A. P. H. J. Schenning and D. B. Amabilino, *Org. Biomol. Chem.,* **2012**, *10*, 9152.

7. a) P. A. Korevaar, S. J. George, A. J. Markvoort, M. M. J. Smulders, P. A. J. Hilbers, A. P. H. J. Schenning, T. F. A. De Greef and E. W. Meijer, *Nature,* **2012**, *481*, 492; b) P. A. Korevaar, T. F. A. de Greef and E. W. Meijer, *Chem. Mater.,* **2013,** *26*, 576; c) S. J. George, R. de Bruijn, Ž. Tomović, B. Van Averbeke, D. Beljonne, R. Lazzaroni, A. P. H. J. Schenning and E. W. Meijer, *J. Am. Chem. Soc.*, **2012**, *134*, 17789.

8. a) I. D. Cat, Z. Guo, S. J. George, E. W. Meijer, A. P. H. J. Schenning and S. D. Feyter, *J. Am. Chem. Soc.,* **2012***, 134,* 3171; b) A. Mammana, A. D'Urso, R. Lauceri and R. Purrello, *J. Am. Chem. Soc.*, **2007**, *129*, 8062; c) W. Zhang, W. Jin, T. Fukushima, N. Ishii, T. Aida, *J. Am. Chem. Soc.,* **2012**, *135*, 114; d) F. Helmich, C. C. Lee, A. P. H. J. Schenning, E. W. Meijer, *J. Am. Chem. Soc.,* **2010**, *132*, 16753.

9. a) E. Yashima, K. Maeda, H. Iida, Y. Furusho and K. Nagai, *Chem. Rev.*, **2009**, *109*, 6102; b) E. Yashima, K. Maeda and Y. Okamoto, *Nature,* **1999,** *399*, 449.

10. a) F. U. Hartl, A. Bracher and M. Hayer-Hart, *Nature*, **2011**, *475*, 324; b) D. S. Schlitzer and B. M. Novak, *J. Am. Chem. Soc.,* **1998**, *120*, 2196.

11. M. Kumar, N. Jonnalagadda and S. J. George, *Chem. Commun.*, **2012**, *48*, 10948.

12. a) E. Yashima, K. Maeda, *Macromolecules,* **2008**, *41*, 3; b) E. Yashima, K. Maeda and T. Nishimura, *Chem. Eur. J.*, **2004**, *10*, 42.

13. a) K. V. Rao and S. J. George, *Org. Lett.*, **2010**, *12*, 2656; b) C. Kulkarni, R. Munirathinam and S. J. George, *Chem. Eur. J.*, **2013**, *19*, 11270.

14. a) S. K. Kim, D. H. Lee, J.-I. Hong and J. Yoon, *Acc. Chem. Res.,* **2009**, *42*, 23; b) T. Sakamoto, A. Ojida and I. Hamachi, *Chem. Commun.*, **2009**, 141.

15. Amount of ADP required to initiate molecular reorganization leading to chiral induction decreases from 0.5 eq. to 0.2 eq. for 70% and 90% aq. HEPES in MeCN respectively. This is due to increase in intermolecular interactions with increasing aq. HEPES composition. Thus lower amount of guest molecules are sufficient to bring about the necessary conformational changes.

16. Decrease in emission beyond 0.5 eq. ADP can be due to higher order aggregation leading to bundling as seen from the TEM analysis.

17. a) A. Willia, *Chem. Commun.*, **1996**, 676; b) C. Wang, Q. Chen, Z. Wang and X. Zhang, *Angew. Chem. Int. Ed.*, **2010**, *49*, 8612.

18. Binding of CIAP to **ZnCPA** didn't show any CD signal.

19. M. Krishnaswamy and U. W. Kenkare, *J. Biol. Chem.*, **1970**, *245,* 3956.

20. F. U. Hartl, A. Bracher and M. Hayer-Hart, *Nature*, **2011**, *475*, 324.

21. Even though 90% HEPES in MeCN is expected to have the slowest kinetics, it couldn't be studied due to its tendency to come out of solution on long standing.

22. S. J. George, R. de Bruijn, Ž. Tomović, B. Van Averbeke, D. Beljonne, R. Lazzaroni, A. P. H. J. Schenning and E. W. Meijer, *J. Am. Chem. Soc.*, **2012**, *134*, 17789;

23. S. Alibert-Fouet, I. Seguy, J.-F. Bobo, P. Destruel and H. Bock, *Chem. Eur. J.*, **2007**, *13*, 1746.

24. a) H. N. Lee, Z. Xu, S. K. Kim, K. M. K. Swamy, Y. Kim, S.-J. Kim and J. Yoon, *J. Am. Chem. Soc.,* **2007**, *129*, 3828; b) X. Chen, M. J. Jou and J. Yoon, *Org. Lett.*, **2009**, *11*, 2181.

25. S. L. Burkett, A. Press and S. Mann, *Chem. Mater.* **1997***, 9*, 1071.

CHAPTER-5

Homotropic and Heterotropic Allosteric Regulation of

Supramolecular Chirality

~ 128 ~

Chapter-5

Homotropic and Heterotropic Allosteric Regulation of Supramolecular Chirality

Abstract

Allosteric regulation, a key biological phenomenon, has been utilized by nature to control various processes. In this chapter, we have demonstrated it for controlling the supramolecular handedness of an artificial self-assembled system. Supramolecular assembly of Perylene bisimide (PBI) functionalized with dipicolylethylenediamine (DPA) binding sites demonstrates bistable chiral on-off state by the non-covalent interaction of adenosine phosphate guest. Both homotropic and heterotropic allosteric control of supramolecular chirality in this otherwise helically dormant assembly could be achieved by the binding of chiral guest (ADP) and achiral phosphate guest (PPi), respectively. Through detailed spectroscopic and morphological investigations, the role of supramolecular reorganization in such an effect has been clearly established. Thus, we present a stimuli responsive helical supramolecular polymer, which show both homotropic and heterotropic allosteric effects with cooperative signalling, hitherto unknown in artificial biomimetic systems.

Allosteric Regulation of Supramolecular Chirality
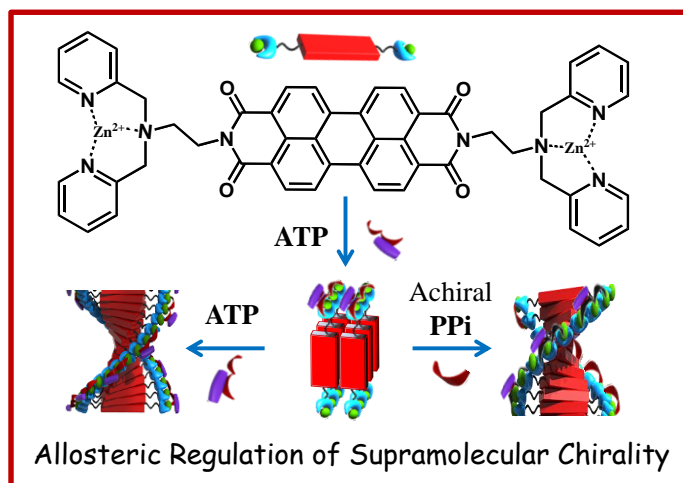
5.1 Introduction

Macromolecular helical assemblies have inspired chemists not only as structural mimics of biomolecules, but also as model systems to understand the chiral amplification in nature.[1] These assemblies are mainly constructed by the presence of a chiral centre in the monomeric unit itself.[2] But, such a design involves greater synthetic challenge, wherein creation of opposite handed assembly requires both the enantiomeric monomer units. In this respect, asymmetric synthesis of helical (supramolecular) polymers obtained via non-covalent binding of chiral guests (auxiliaries) to achiral/racemic assemblies offer a simplistic synthetic design with easily switchable helicity and novel chirotechnological functions.[3] For example, this design has been used to construct metastable helical states[4] (helical memory) from conformationally stable assemblies to study various stereomutation processes and its application in enantiomeric purification. Dynamic assemblies with stimuli responsive handedness have been utilized as chiroptical sensors to determine the absolute chirality of natural products, drug molecules and enantiomeric excess of chiral mixtures.[5] Another important aspect which can be envisaged from such macromolecular systems with multiple binding sites is the allosteric cooperativity, a strategy vastly employed by nature for efficient regulation of a number of biological processes.[6] Biomimetic molecular analogues of allosteric cooperative binding with non-linear response to analyte concentrations have recently gathered much attention. Such systems have been employed for the design of sensors with amplified signalling, wherein a small change in the analyte concentration at the steep transition region is expressed into a large variation in the output signal.[7] Although many molecular complexes have been investigated for such purposes, an allosteric modulation of supramolecular chirality in extended helical assemblies of π-conjugated chromophores still remains underexplored.
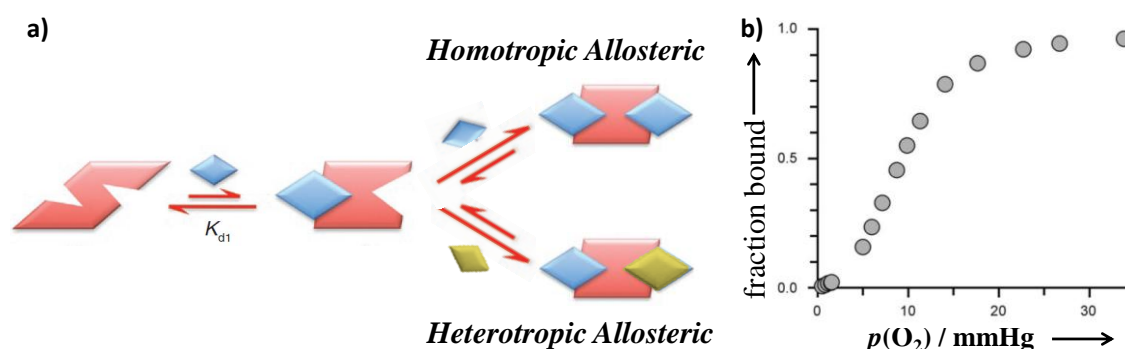
Scheme 5.1. *a) Schematic representation of conformational variation leading to homotropic and heterotropic allosteric effects. b) Shows the cooperative binding of dioxygen to haemoglobin as a well-known example of allosteric effect. Adapted with permission from ref. 6b, copyright 2008, Macmillan Publishers Ltd: Nat. Chem. Biol.; Adapted with permission from ref. 6c, copyright 2009, Wiley-VCH.*

Allosteric communication across multiple binding sites allows the ligation at one site to influence the outcome of subsequent binding at remote place and which is usually achieved due to conformational variation of the receptors upon guest recognition (Scheme 5.1a). The initial ligand binding can either enhance or hinder further binding to the host leading to either positive or negative cooperativity, respectively. Another classification can also be made depending on whether the subsequent binding is by same or different guest, leading to homotropic or heterotropic allosteric regulation, respectively.[7a-b] Nature has extensively utilized this phenomenon for amplified signalling and controlling complex processes like autoregulation. One of the well-known examples is that of oxygen molecules binding to haemoglobin in a positive allosteric manner, as characterized by an initial lag phase followed by a sharp rise in signal intensity (Scheme 5.1b).[6] This has also been assigned to conformational change in metalloporphyrin assembly upon dioxygen binding, leading to such effects. Many proteins undergo nucleotide binding induced allosteric transformation, which are very crucial for their activity.[8] In specific, adenosine triphosphate (ATP) has been well utilized as an effector molecule in various enzymatic processes, both as an inhibitor or activator. For example, glycolysis is mediated by Phosphofructokinase-1 (PFK-1) enzyme, where ATP is involved in both homotropic and heterotropic allosteric processes, leading to its autoregulation.[9] In almost all these cases, multivalent interactions between host and guest is essentially involved.

5.2 Design of Artificial Allosteric System

In this chapter, we report a supramolecular polymeric multivalent scaffold, which exhibits both homotropic and heterotropic allosterism in the expression of chirality, by dynamic conformational changes in response to the binding of various adenosine phosphates. Co-assembled stacks of Perylene bisimide (PBI) and ATP exist in on and off chiral states depending upon the concentration of ATP (Scheme 5.2). Detailed spectroscopic investigations suggested two different molecular assemblies responsible for such "all or nothing" behaviour. This is also reflected in their microscopic characteristics showing a transition from two dimensional (2-D) sheets to one dimensional (1-D) nanofibers in their off and on state respectively. The ATP bound helically dormant off-state could be stimulated to chiral on-state either by further addition of ATP (homotropic) or even by the addition of other ditopic guests like achiral pyrophosphate (PPi, $P_2O_7^{4-}$) or ADP (heterotropic). Through detailed investigations, a mechanistic insight into this unprecedented allosteric induction of chirality in extended assembly of chromophores is provided.

Towards the realization of allosteric regulation of chirality in artificial multivalent systems, we designed a PBI chromophore (**PDPA**), end functionalized with dipicolylethylenediamine-Zinc (**DPA-Zn**) receptor motifs (Scheme 5.2), which is known to

specifically bind to phosphates.[10] Hence, adenosine phosphates have been used as the chiral guests, which can assist in chromophoric assembly and bias the helical handedness of the resultant supramolecular stacks.
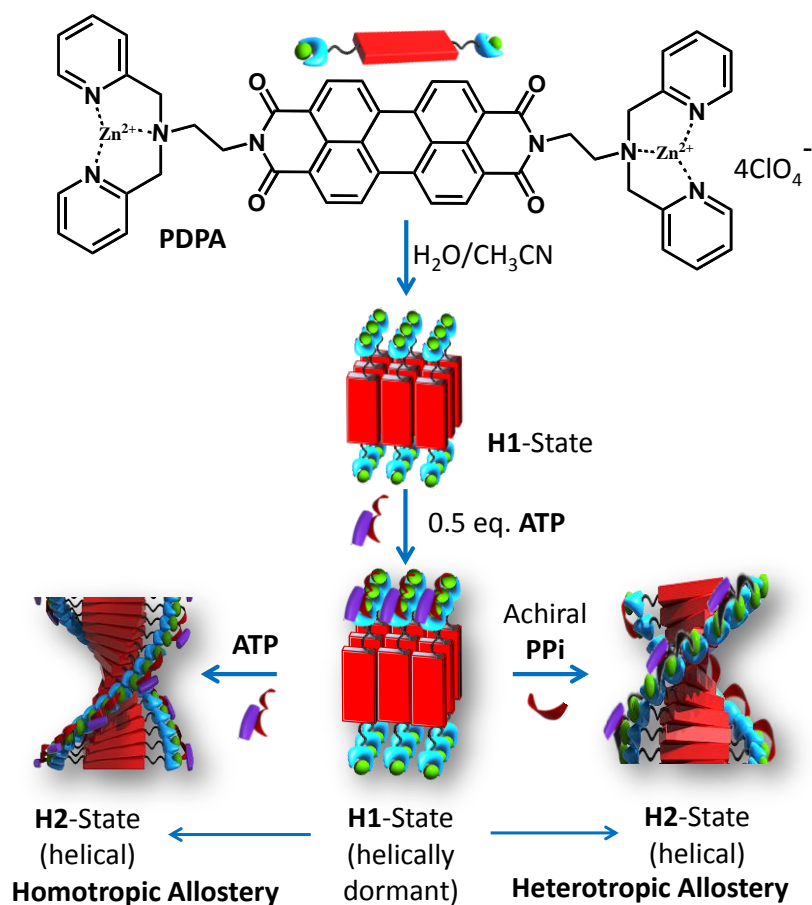
Scheme 5.2. *Chemical structure of **PDPA** and schematic of the guest induced allosteric regulation of supramolecular chirality in **PDPA**-assembly.*

We first constructed self-assembled stacks of **PDPA** in aq. HEPES buffer/CH$_3$CN solvent mixture (9/1 v/v, c = 2 x 10^{-5} M). **PDPA** is molecularly dissolved in CH$_3$CN due to the presence of two polar end groups, whereas water induces interchromophoric association due to hydrophobic and π-π stacking interactions. Spectroscopic investigations show characteristic signatures of a PBI assembly. For e.g. the UV/Vis absorption spectrum of **PDPA** in MeCN showed sharp vibronic features at 460 nm, 488 nm and 521 nm due to S$_0$-S$_1$ electronic transition with the breathing vibration of perylene core polarized along the long molecular axis, characteristic of monomeric PBI chromophores (Figure 5.1a).[11] Upon increasing the percentage of aq. HEPES buffer in MeCN, broadening of absorption spectra and change of relative absorbance peak ratio were observed. Fluorescence signal (λ$_{ex}$ = 470 nm) in Figure 5.1b show sharp bands at 536 nm, 572 nm and 625 nm in MeCN which are typical of monomer emission

in PBI. Upon increasing composition of aq. HEPES, we see a gradual quenching of the monomer emission with no additional band. The excitation spectra collected at 600 nm also revealed its monomeric origin (Figure 5.1c). These spectral features confirm that the **PDPA** chromophores are arranged in a 'H-type' cofacial manner (**H1**-state).[2] Percentage of aggregation was also plotted with varying composition of MeCN in aq. HEPES (Figure 5.1d), which shows that at 10% MeCN in aq. HEPES buffer, ~ 93% of **PDPA** molecules are aggregated.[12] These **H1** assembly formed 2-dimensional nanosheets (Figure 5.1e), as visualized through transmission electron microscopy (TEM).
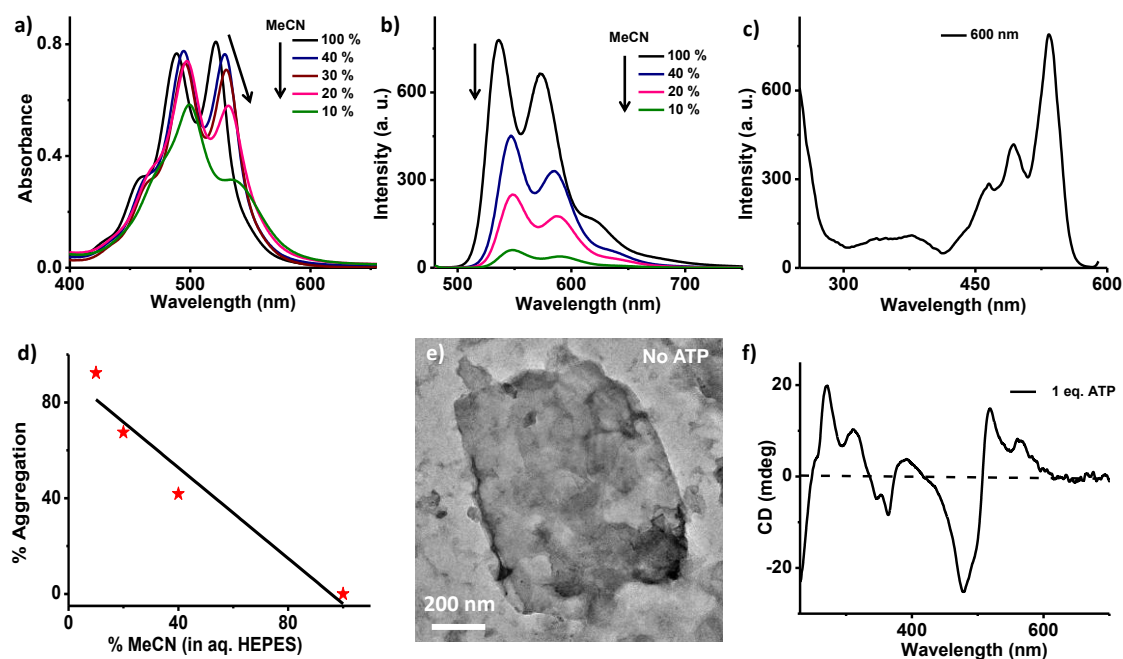
Figure 5.1. *Self-assembly of **PDPA**: Solvent dependent a) absorption and b) emission spectra (λ_{ex}=470 nm) of **PDPA** with varying percentages of MeCN in aq. HEPES buffer (c = 2 x 10^{-5} M). c) Excitation spectra of **PDPA** assembly collected at 600 nm showing monomeric features (10% MeCN in aq. HEPES solution, c = 2 x 10^{-5} M). d) Plot of percentage aggregation at varying composition of MeCN in HEPES.[12] e) TEM micrograph of nanostructure obtained from 2 x 10^{-5} M solution of **PDPA** (10% MeCN in water) without ATP (**PDPA**-stack). f) CD spectrum of **PDPA** with 1 eq. ATP (10% MeCN in aq. HEPES solution, c = 2 x 10^{-5} M).*

When the **H1**-assembly was mixed with one eq. (eq.) of ATP, a positive bisignated CD signal, i.e. positive at 518 nm followed by negative at 480 nm, in the PBI absorption region with a zero-crossing at 507 nm was observed,[2n] characteristic of excitonically coupled right-handed helical organization of PBI chromophores (Figure 5.1f). Such efficient chirality induction to achiral chromophoric assembly further reveals the specific binding of phosphate

guest molecules to the DPA-Zn sites of the receptor stacks, in congruence with the molecular design.

5.3 Supramolecular Reorganization for Allosteric Effect

Interestingly, CD titration experiments in which increasing eq. of ATP was added to the **H1**-stacks show that signal remains silent till 0.5 eq. ATP, beyond which sharp rise in CD signal was observed, which continues to enhance passing through an isodichroic point. Highly cooperative nature of this chiral induction process was further reflected in the plot of CD intensity at 480 nm with eq. of ATP guests, which clearly shows a non-linear sigmoidal curve with a sharp inflection point at 0.5 eq. of ATP (Figure 5.2d).[13]
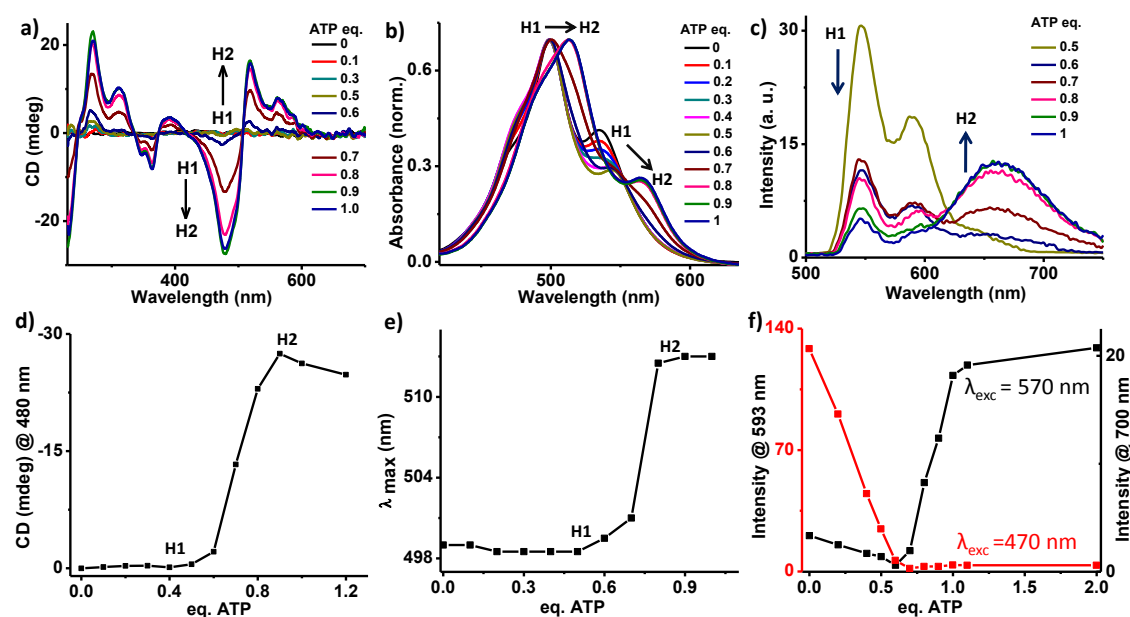
Figure 5.2. *Homotropic allosteric regulation of helicity: Spectroscopic changes characterizing* **H1** *to* **H2** *transition of* **PDPA***-assembly upon ATP binding (legends in a-c show eq. of ATP). Evolution of a) CD signal and d) plot of CD intensity at 480 nm upon ATP titration. b) Shows the normalized absorption changes and corresponding variation in λ_{max} is plotted in e) to show two states of the assemblies on ATP binding. c) Shows decrease in monomeric emission intensity and evolution of new emission band upon ATP addition (λ_{ex}=470 nm), whereas f) shows comparative emission plot at 593 nm and 700 nm upon selective excitation at 470 nm and 570 nm respectively (CH$_3$CN in aq. HEPES, 1:9 v/v, c =2 x 10^{-5} M).*

To gain mechanistic insights into the cooperative process in **PDPA**-assembly, we have performed detailed spectroscopic measurements, which revealed the allosteric mechanism behind the observed "all or nothing" behaviour giving rise to bistable on/off chiral assembly. Monitoring the changes in absorption spectra upon ATP titration, a continuous decrease in

absorbance along with broadening of bands were noticed, without any significant shift in λ_{max} till 0.5 eq. of ATP. However, on further addition of ATP, the peak maxima takes a bathochromic jump from 499 nm to 514 nm and 535 nm to 564 nm which saturates beyond 0.8 eq. of ATP. This two-state change is lucidly visualized in the normalized absorption spectra and the plot of λ_{max} vs eq. of ATP, consistent with the CD spectral changes (Figure 5.2 b, e).

Furthermore, fluorescence intensity monitored upon ATP titration resulted in a gradual decrease in the residual monomeric fluorescence (λ_{ex} = 470 nm) at 593 nm till 0.5 eq. of ATP (Figure 5.2c). Such an observation has already been assigned to H-aggregates of PBI and indicates that initial addition of ATP ensures complete aggregation of **PDPA** monomers to **H1**-assembly. Beyond 0.5 eq. of ATP, as the CD signal begins to appear, a new red-shifted emission peak at 665 nm emerged, which also saturates along with the CD signal. To probe into the genesis of this band, an excitation spectrum was recorded by monitoring the emission at 675 nm, which showed a maximum of 514 nm, which is 20 nm hypsochromically shifted compared to the monomer absorption (Figure 5.3b), indicating a new kind of fluorescent H-type assembly (**H2**-assembly).[14] Probing the emission intensity at 593 nm (monomer) and 700 nm (**H2**-assembly) upon selective excitation at λ_{ex} = 470 nm and 560 nm respectively, revealed that the red shifted emission sets in only after 593 nm band disappears, showing their mutually exclusive nature (Figure 5.2f, 5.3a). The observation of initial lag phase in all the above three measurements (Figure 5.2 d, e, f), could not have been due to phosphate binding selectively to monomers initially, as ~93% of **PDPA** molecules were already aggregated without ATP binding under these conditions (Figure 5.1d).
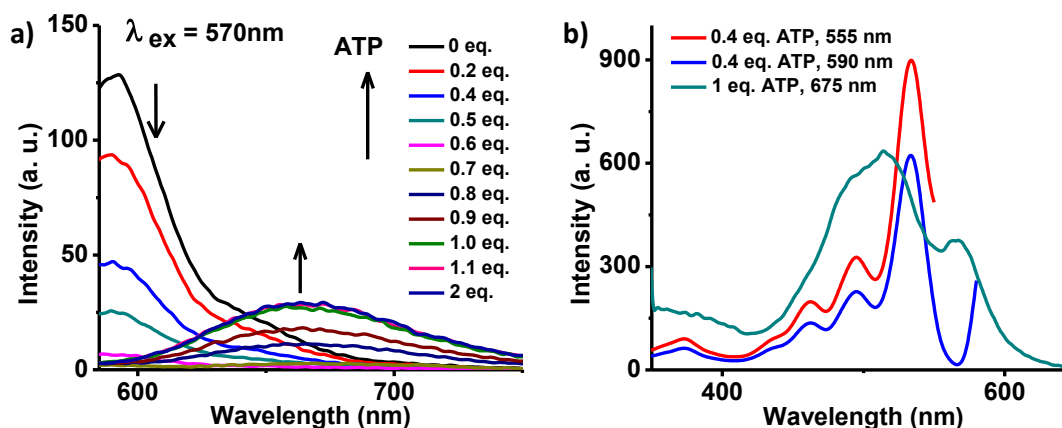
*Figure 5.3. Emission and excitation spectral changes upon **H1** to **H2** transition of **PDPA** assembly, induced by ATP: a) Emission spectra upon selective excitation of aggregate at λ_{ex}= 570 nm. b) Comparative excitation spectra at various states of aggregation i.e. in **H1** and **H2** state collected at various fluorescence bands. All measurements were done in 10% MeCN in aq. HEPES solution, c = 2 x 10^{-5} M **PDPA**.*

All the above spectroscopic signatures clearly indicate a supramolecular reorganization being responsible for allosteric cooperativity. In order to obtain direct evidence of conformational transition, detailed transmission electron microscopy (TEM) imaging on various **PDPA** assemblies were performed. **PDPA** alone self assembles to form two-dimensional (2-D) sheets (Figure 5.1e), where the electron density mapping of exposed edges revealed the thickness of individual layers to be around 3.8 nm, which corresponds to the molecular length of **PDPA**. This suggests that the molecules are arranged in a perpendicular fashion along the thickness of the sheets via π-stacking interactions, with hydrophilic DPA-Zn binding sites exposed outside. Up to 0.4 eq. of ATP binding (**H1**-state), their 2-D morphology remains unperturbed, in agreement with their unaltered spectroscopic signatures, suggesting similar molecular organization to that of unbound stacks (Figure 5.4a). Upon further binding of ATP, which leads to molecular reorganization from **H1**-state to **H2**-state, a morphology transition from 2-D sheets to 1-D nanofibers was observed. TEM images show fiber bundles composed of 2-4 nanofibers with an average width of 5.0 nm, which correlates to the molecular dimension of **PDPA** molecules with ATP bound on both DPA-Zn sides (Figure 5.4 b-d). The length of these fibers is in the range of 300-500 nm, where growth is the direction of π-stacking.
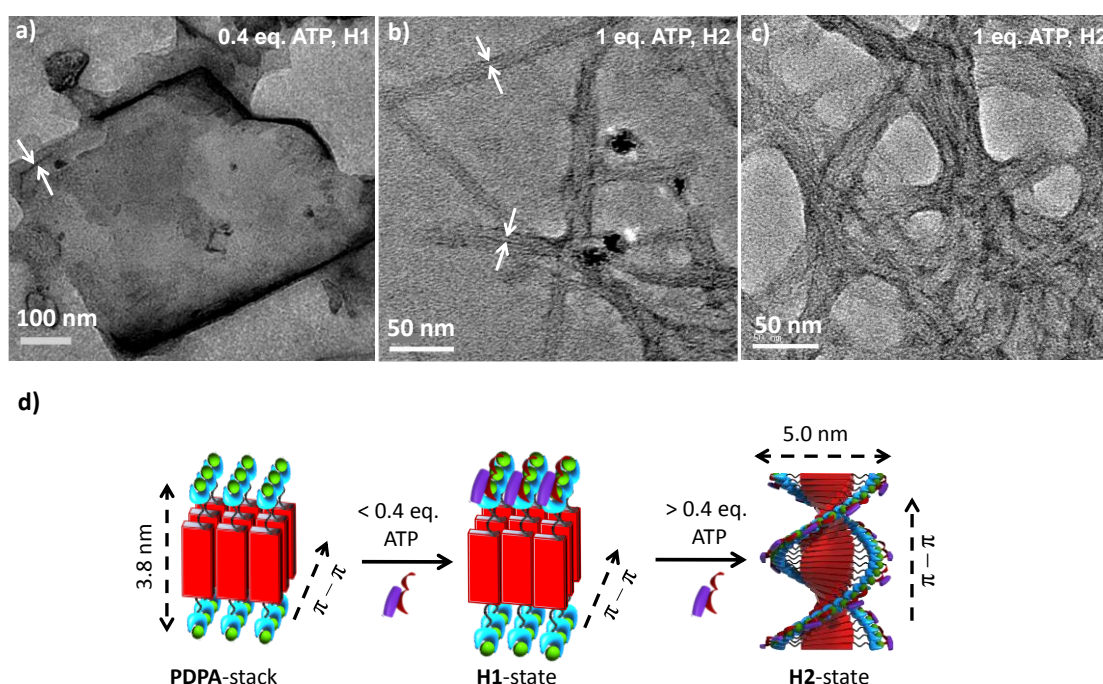

Figure 5.4. *Morphological evidences of **H1** to **H2** transition: TEM images of nanostructures obtained from 2 x 10^{-5} M solution of **PDPA** (10% MeCN in water) with a) 0.4 eq. ATP (**H1**), b) and c) 1 eq. ATP (**H2**). d) Schematic depicting the morphology transition of **PDPA**-assembly upon ATP binding along with the probable molecular organization in each state.*

Thus, the conformational change of **PDPA** assembly from **H1**-state to **H2**-state is pivotal for the cooperative expression of helicity upon guest binding. The **H1**-state can be best described as a prochiral assembly, which remains in a helically dormant state despite the attachment of chiral guests to nearly half of its available binding sites. However, further binding of ATP molecules to the remaining free sites of the assembly activated its helical conformation, thus exemplifying a homotropic allosteric mechanism for the regulation of supramolecular chirality. For the present system, homotropic allostery could be achieved only in presence of ATP and failed with other phosphates like ADP/AMP/PPi.[15]

5.4 Heterotropic Allosteric Regulation of Helicity

We envisage that, any heterotropic binding of multivalent guest molecules to prochiral **H1**-assembly, would also trigger the molecular reorganization to induce supramolecular chirality. Thus, attempts were made to demonstrate heterotropic allosteric regulation of helically dormant **PDPA-**assembly containing partially bound ATP (**H1**-state), using different achiral and chiral phosphate guests. Remarkably, the successive addition of PPi, which is an achiral ditopic phosphate, to the helically dormant **H1**-state obtained with 0.5 eq. of ATP, showed the induction of (*P*)-handed helicity similar to the **H2**-state obtained by ATP alone (Figure 5.5a). Thus, the system is uniquely bestowed with the ability to probe the presence of achiral guest through chiral induction, whereas amplified signalling is achieved through highly cooperative effect.
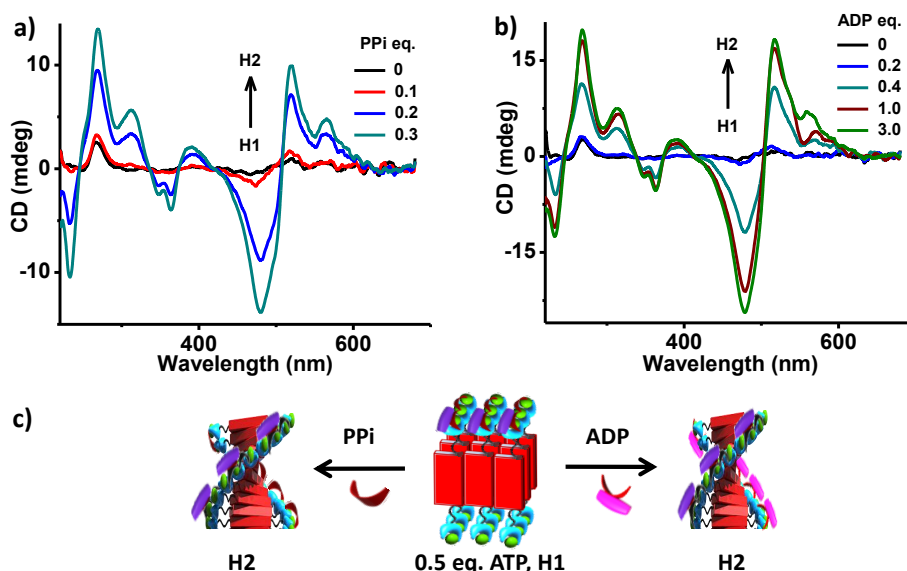
Figure 5.5. *Heterotropic allosteric regulation of supramolecular helicity: Variation in CD signal of **PDPA**-assembly in **H1**-state (0.5 eq. ATP) upon addition of a) achiral PPi and b) ADP (10% MeCN in aq. HEPES solution, c = 2 x 10⁻⁵ M). c) Schematic representation of the two processes.*

Further, we have used ADP, another chiral divalent phosphate, as the heterotropic guest. Individual binding of adenosine diphosphate (ADP) to **PDPA** produced a negative bisignated CD signal, negative at higher wavelength (557 nm) followed by positive at 496 nm, an opposite bisignated spectra when compared to ATP bound stacks (Figure 5.6a). Unlike ATP binding, ADP did not show any allosteric effect indicating a different mode of binding in these cases. Even the emission spectra changes on ADP binding showed just quenching of monomer emission without evolution of any additional band, confirming formation of **H1** aggregates (Figure 5.6b). Interestingly, addition of ADP to the prochiral **H1**-state (0.5 eq. ATP) also activates the helicity to attain the **H2**-state and more importantly with the right-handed (*P*)-helicity as preferred by ATP rather than the heterotropic guest ADP (Figure 5.5b). Thus both PPi and ADP bind to **H1**-state to form helical **H2**-state, hence representing heterotropic allosteric regulation of supramolecular chirality even by the addition of achiral or different chiral guests.
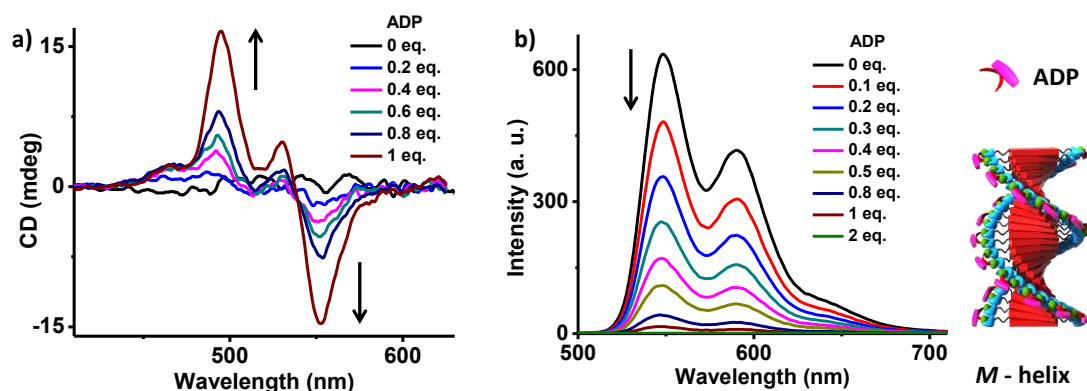
Figure 5.6. *Binding of ADP to **PDPA**-assembly: Variation in a) CD spectra b) emission spectra of **PDPA** upon titration with ADP (10% MeCN in aq. HEPES solution, c = 2 x 10⁻⁵ M). Schematic on the right side is a representation of ADP bound helical stacks which is opposite in handedness w.r.t ATP bound stacks. Legends in the graph represent molar eq. with respect to **PDPA**.*

Heterotropic allosteric transformation of **H1** to **H2** was further confirmed by detailed spectroscopic and microscopic studies. For example, on binding of PPi and ADP to **H1**-state, new emission band at 665 nm was observed, a characteristic feature of **H2**-aggregates (Figure 5.7). Furthermore, addition of 0.25 eq. of PPi to **H1**-state (0.5 eq. ATP) also led to the morphology transition from 2-D sheets to 1-D nanofibers, analogous to ATP addition, thus confirming the **H2**-state (Figure 5.7). Interestingly, binding of monophosphates like Pi or AMP did not show any heterotropic allosteric regulation of supramolecular handedness, indicating that multivalent guest binding is crucial for inducing the conformational change in **PDPA-**

assembly (Figure 5.7 c, f). Thus the present system shows both homotropic and heterotropic allosteric effects with cooperative signalling, hitherto unknown in artificial biomimetic systems.
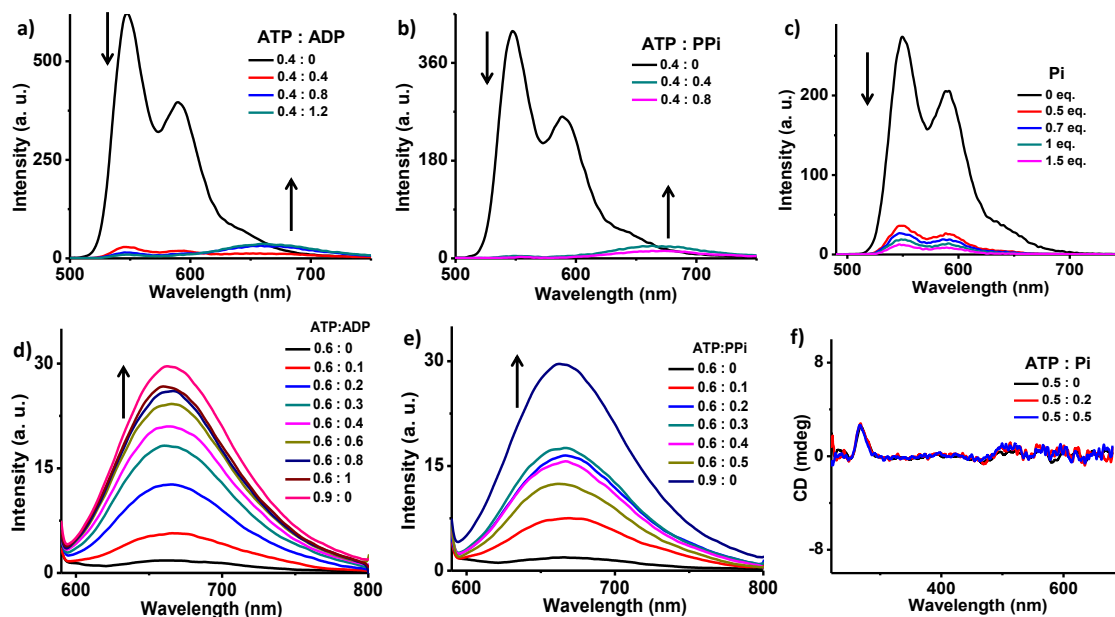
Figure 5.7. *Variation in fluorescence spectra upon binding of a) ADP and b) PPi to the **H1**-state of the **PDPA**-assembly pre-bound with 0.4 eq. of ATP (λ_{ex}= 470nm), suggesting the formation of **H2**-states. This is more clear upon the selective excitation of the assembly at 570 nm, which is shown in d) and e) for ADP and PPi, respectively. These emission signals show heterotropic allosteric effect leading to transition from **H1** to **H2** state with ADP, PPi. It should be noted that, in the ADP case the emission intensity reaches close to that of ATP alone (ATP:ADP = 0.9:0), whereas in PPi case only half the intensity could be achieved. This can be due to the competitive replacement of ATP by PPi as shown in Figure 5.10d. c) Variation in emission spectra of **PDPA**-assembly on titration with Pi. f) Shows changes in the CD signal on addition of Pi to **H1**-state (0.5 eq. ATP), (10% MeCN in aq. HEPES solution, c = 2 x 10^{-5} M).*

Detailed heterotropic allosteric experiments of prochiral **H1**-states containing varying fraction of ATP bound sites (0.1-0.5 eq.), with PPi or ADP guests, shed some light on the mechanism of allosteric regulation assisted chiral manifestation. Figures 5.9 and 5.10 show the results of PPi and ADP titration, respectively, with different **H1**-states, obtained by varying eq. of pre-bound ATP molecules onto the **H1**-state. It is important to note that, with the increase in pre-bound ATP (or decrease in free binding sites on **H1**-assembly), both ADP and PPi induces higher CD signal, and the maximum allosteric induction of helicity was observed, when the **H1**-assembly is pre-bound with around 0.5 eq. of ATP molecules. This is further evident from the plot of ascending eq. of pre-bound ATP versus the maximum CD intensity attained, which show a positive slope with PPi and ADP (Figure 5.10c). As expected, binding of

monophosphate like Pi does not show induction of chirality, which reiterates the significance of multivalent guests to induce the allosteric regulation (Figure 5.7f).[16] These observations suggest that chromophores which are bound by ATP at least on one side, can only contribute to the helicity upon conversion to **H2**-state by binding with heterotropic guests like ADP and PPi. It is further evident that the handedness of **H2**-helical assembly with bound ATP and achiral PPi guest is governed by the bound chiral ATP molecules.
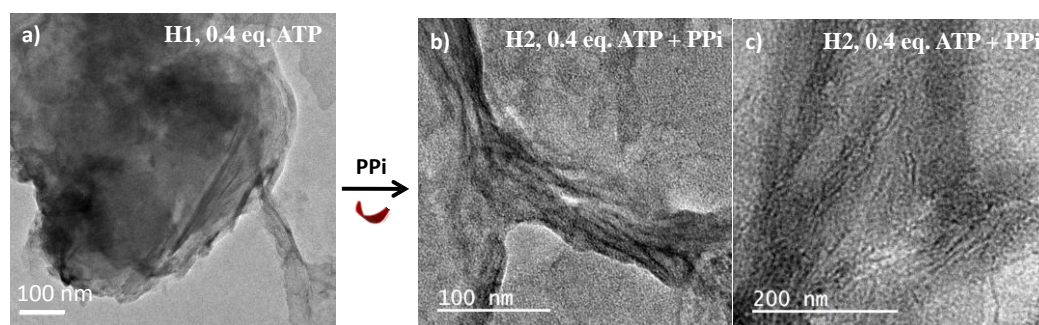
*Figure 5.8. TEM images showing **H1** to **H2** transition upon PPi addition to ATP bound **H1** state. a) 2-D sheets of **H1**-state with 0.4 eq. ATP and b), c) nanofibers obtained upon addition of PPi to **H1**-state (0.25 eq. PPi + 0.5 eq. ATP), through heterotropic allosteric regulation (10% MeCN in water, c = 2 x 10^{-5} M).*

Similarly, in the case of ATP-ADP bound stacks, ATP again controls the handedness (Figure 5.9 d-f), despite the fact that chiral ADP has a preference for opposite helicity (Figure 5.6).[17] It is clear that at lower eq. of ATP, many **PDPA** molecules would be free from ATP at both binding sites, and thus they cannot express heterotropic allosteric effects. This is further evident from the fact that, at very low eq. of ATP like 0.1 eq. ATP, we observe that initial addition of ADP shows signal corresponding to ADP bound stacks which is opposite in direction to the **H2**-state (Figure 5.9f). Further, ADP addition leads to manifestation of **H2**-state, thereby co-existence of two bisignated signals i.e. one from only ADP bound portion and other from ATP bound **H2**-state. Due to non-enantiomeric nature of these ATP and ADP bound stacks which are not exactly mirror images, their co-existence in a given solution could be easily visualized in CD signal. Such observations confirm the fact that parts of the stacks which are free from ATP do not undergo allosteric regulation and they behave independently. This also hints towards absence of any significant chiral amplification in these stacks. In addition, any contribution of chiral amplification in the allosteric regulation of chirality was ruled out by performing Sergeant and Soldiers like experiments with mixture of guest molecules in the **H2**-state of the assembly (Figure 5.11).
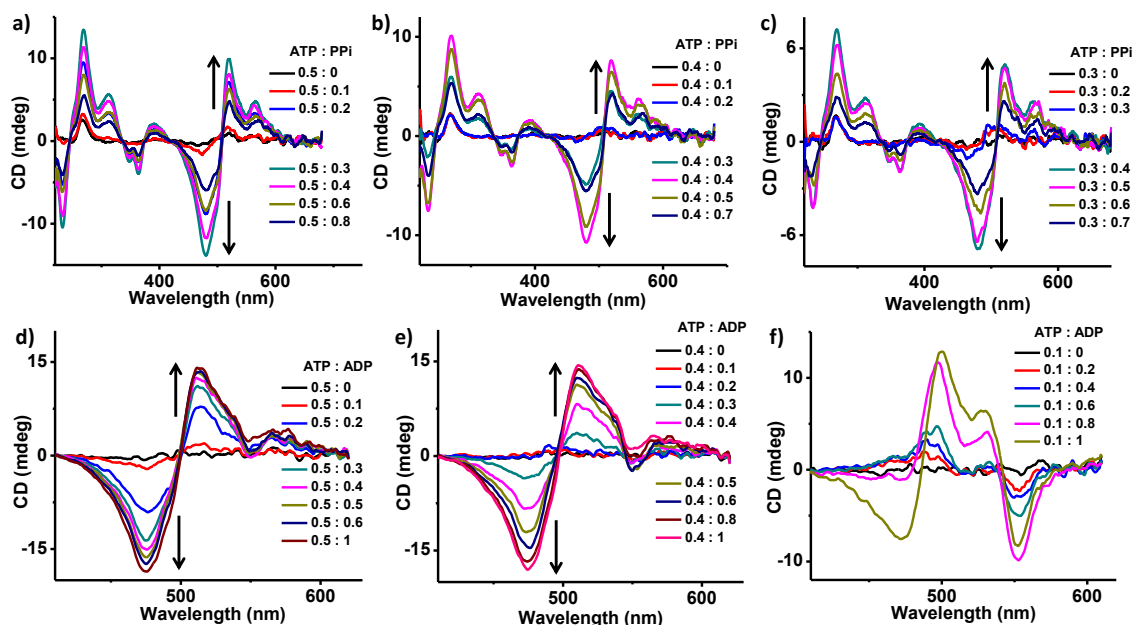
Figure 5.9. *Evolution of CD signal upon addition of increasing eq. of PPi to **PDPA**-assembly pre-bound with a) 0.5 eq., b) 0.4 eq., c) 0.3 eq. of ATP. Higher amounts of PPi begin to decrease the CD intensity due to competitive replacement of ATP by PPi as seen in Figure 5.10e. Similar CD spectra plotted upon addition of increasing eq. of ADP to **PDPA**-assembly pre-bound with a) 0.5 eq., b) 0.4 eq., c) 0.1 eq. of ATP (10% MeCN in aq. HEPES solution, c = 2 x 10^{-5} M).*

Another important observation from these graphs is the presence of lag phase, especially at lower eq. of pre-bound ATP, where the assembly remains CD silent despite the binding of ADP or PPi (Figure 5.10 a, b). For example, upon the addition of ADP, **H1**-assembly with 0.1 eq. of pre-bound ATP remains CD silent until 0.7 eq. of ADP is added, beyond which chirality induction sets in. This lag phase decreases with the increase of binding sites pre-occupied with ATP molecules and disappears completely when 0.5 eq. of ATP was added. Explanation to such a phenomenon is sought from the possibility that, initial ATP and other phosphate molecules bind preferentially to only one of the two binding sites of each chromophores in the **H1**-assembly, which does not give any CD signal as discussed above. Subsequent binding of multivalent guests to the second site is essential for the manifestation of **H2**-state and induction of chirality. However, the observation that chiral induction is absent till half of the binding sites in the assembly are occupied, irrespective of the eq. of pre-bound ATP molecules, prompt us to propose a preferential binding of the guests to one side of the **H1**-assembly at the initial stages. Although, the exact reason for such a preferential facial binding of the guest molecules is not clear at this moment, we believe it could be due the morphological constraints, where multi-layered 2D assembly of **H1**-state prevents the accessibility to all binding sites.
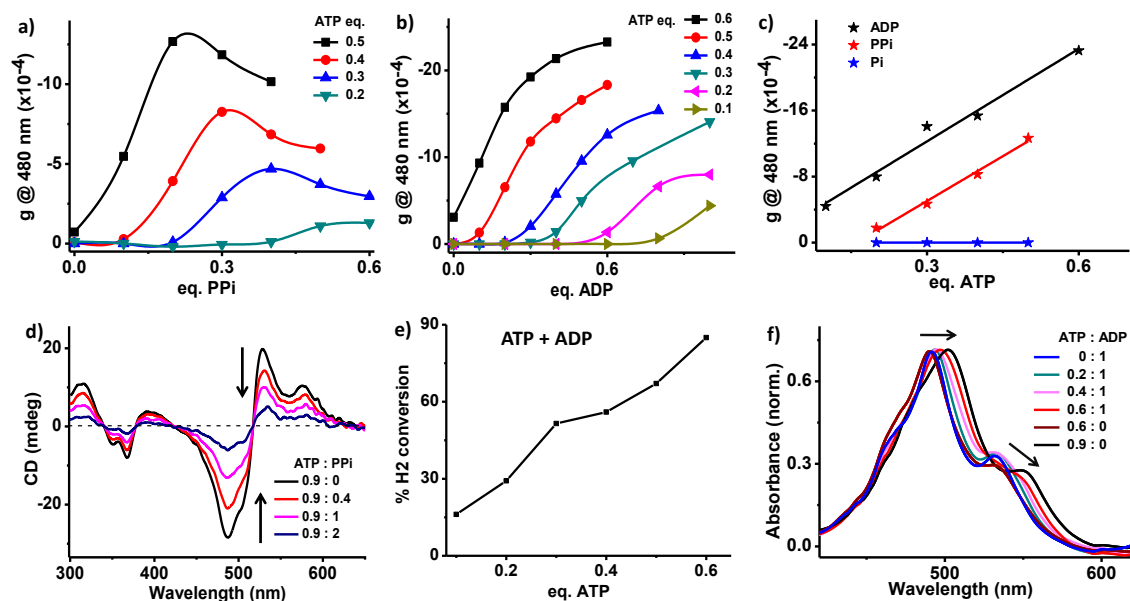
Figure 5.10. *a-c) Heterotropic allosteric experiments of **H1**-states containing varying fraction of ATP bound sites (0.1-0.5 eq.). Variation in anisotropy value or g-value of **PDPA** in ATP bound **H1**-state upon addition of a) PPi and b) ADP. c) Plot of ascending eq. of pre-bound ATP versus the maximum CD intensity attained for the **H2**-states with different heterotropic guests, which show a positive slope with PPi and ADP. The decrease in CD signal after reaching maximum value in a) is due to competitive replacement of ATP by PPi as clearly visible in d) where CD signal decreases upon addition of PPi to 0.9 eq. ATP bound **PDPA**. e) Shows the percentage **H2**-conversion upon addition of ADP to **H1**-state (calculated with respect to g-value of ATP bound **H2** with $g_{ATP(max)} = 27.3 \times 10^{-4}$). f) Change in the absorption spectra upon addition of 1 eq. ADP to **H1**-states created with varying eq. of ATP showing transition to **H2**-state. All measurements were in 10% MeCN in aq. HEPES solution, $c = 2 \times 10^{-5}$ M.*

  Thus, in the **H1**-assembly with 0.5 eq. of pre-bound ATP, binding sites at one face of the 2-D sheets are completely occupied. Further addition of any multivalent phosphate causes morphology transition to 1-D fibers, thereby setting in the allosteric mechanism with induced chirality. On the other hand, **H1**-assembly with 0.2 eq. of ATP, further required 0.4 eq. of ADP or PPi to completely occupy the binding sites on the exposed face of sheet, and hence they are CD silent. As expected, further addition of phosphates regulates the chirality induction, with less CD intensity. The final CD intensity of the **H2**-assembly, which reflects the induced *ee* in the helical stack formed during these experiments, directly correlates to the number of **PDPA** chromophores pre-bound with ATP at one site (Figure 5.10 c, e). In c) we notice that the conversion to **H2** state on PPi or ADP binding is not 100%, which can be due to inherent lower strength of ADP/PPi binding when compared to ATP and competitive replacement of ATP by

ADP/PPi. We see that at 0.6 eq. ATP, addition of ADP indeed leads of red shifted absorption expected of **H2**-state, but with lower absorbance (Figure 5.10f). This could be either due to inherent weaker association of ADP compared to ATP, which might affect the interchromophoric interactions leading to slightly lower effects. This is also supported by only 83% recovery of **H2**-state, when compared with the **H2** obtained from ATP alone as shown in Figure 5.10e).
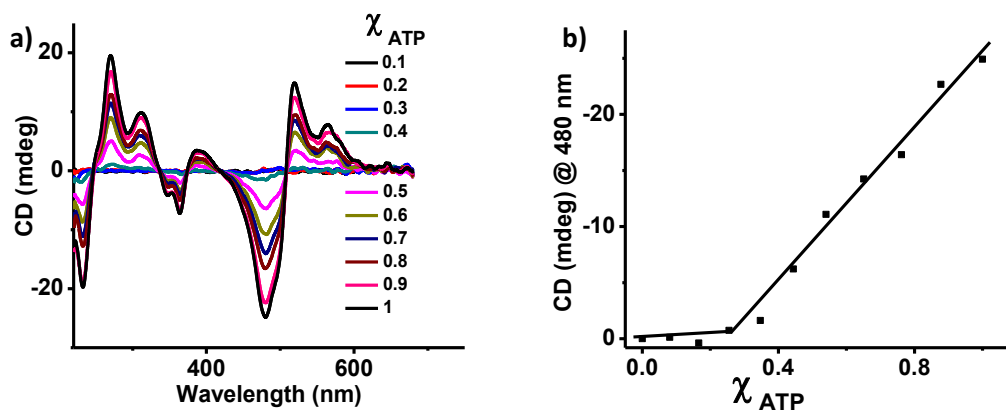
Figure 5.11. *Sergeant and soldiers like experiment of the **H2**-state of the **PDPA**-assembly performed with a mixture of ATP and PPi. a) CD signal with varying molar ratios of ATP-PPi b) shows respective plot of CD intensity against mole fraction of ATP monitored at 480 nm. (10% MeCN in aq. HEPES solution, c = 2 x 10^{-5} M). The initial lag in b) till χ_{ATP} = 0.3 is due to the allosteric effect of ATP binding, where initial eq. of ATP do not show any CD signal. However, the linear response in CD signal clearly suggests the absence of chiral amplification in the present system.*

5.5 Conclusions

In conclusion, we have demonstrated a new allosteric regulation design for modulating the supramolecular chirality of helical receptor assemblies, by the homotropic and heterotropic binding of adenosine phosphate guest molecules. Through chiral guest induced helicity into the 1-D assembly of PBI, we have shown both homotropic and heterotropic allosterically responsive supramolecular chirality in a single system, which finds no precedence. Detailed investigations revealed the crucial role of conformational reorganization from 2-D sheets to 1-D nanofibers being responsible for such allosteric effect. Such systems with highly cooperative response to biologically relevant molecules can allow amplified signalling of both chiral as well as achiral phosphates, whereas the unique heterotropic allosteric effects could be utilized further for the autoregulation of ATP.

5.6 Experimental Section

<u>**General Methods**</u>:

Transmission Electron Microscopy (TEM): TEM measurements were performed on a JEOL, JEM 3010 operated at 300 kV. Samples were prepared by placing a drop of the solution on carbon coated copper grids followed by drying at room temperature. The images were recorded with an operating voltage 300 kV. In order to get a better contrast, the samples were stained with uranyl acetate (1 wt % in water) before the measurements. For TEM, water was used instead of aq. HEPES solution to avoid masking of nanostructures due to HEPES deposition upon drying.

Optical Measurements: Electronic absorption spectra were recorded on a Perkin Elmer Lambda 900 UV-Vis-NIR Spectrometer and emission spectra were recorded on Perkin Elmer Ls 55 Luminescence Spectrometer. UV-Vis and emission spectra were recorded in 10 mm path length cuvettes. Fluorescence spectra of solutions were recorded with 470 nm and 570 nm excitation wavelength as per the requirement. Circular Dichroism measurements were performed on a Jasco J-815 spectrometer where the sensitivity, time constant and scan rate were chosen appropriately. Corresponding temperature dependent measurements were performed with a CDF – 426S/15 Peltier-type temperature controller with a temperature range of 263-383 K and adjustable temperature slope.

Sample Preparation: All samples for spectroscopic measurements were prepared by injecting the stock solution of **PDPA** (solvent MeCN) into required volume of solvent (aq. HEPES buffer in MeCN, wherever applicable). To that required amount of phosphates were injected and the solutions were mixed by manual shaking before measurements.

Aq. HEPES buffer was prepared by making 10 mM solution of the compound in water.

Phosphates stock solutions were prepared in 10^{-2} M concentration by dissolving the required amount of compound in HEPES buffer solution.

Materials: All chemicals / solvents were purchased from the commercial sources and were used as such. Spectroscopic grade solvents were used for all optical measurements.

Legends in graphs represent molar eq. with respect to **PDPA**.

Synthesis: PDPA was synthesized and characterized according to the literature procedure.[10a]

5.7 References and Notes

1. a) A. R. A. Palmans and E. W. Meijer, *Angew. Chem. Int. Ed.*, **2007**, *46*, 8948; b) A. E. Rowan and R. J. M. Nolte, *Angew. Chem. Int. Ed.*, **1998**, *37*, 63; c) E. Yashima, K. Maeda, H. Iida, Y. Furusho and K. Nagai, *Chem. Rev.*, **2009**, *109*, 6102; d) M. M. Green, K.-S. Cheon, S.-Y. Yang, J.-W. Park, S. Swansburg and W. Liu, *Acc. Chem. Res.*, **2001**, *34*, 672; e) M. Fujiki, J. R. Koe, K. Terao, T. Sato, A. Teramoto and J. Watanabe, *Polym. J.*, **2003**, *35*, 297; f) A. Lohr and F. Würthner, *Isr. J. Chem.*, **2011**, *51*, 1052; g) V. K. Praveen, S. S. Babu, C. Vijayakumar, R. Varghese and A. Ajayaghosh, *Bull. Chem. Soc. Jpn.*, **2008**, *81*, 1196; h) D. K. Smith, *Chem. Soc. Rev.*, **2009**, *38*, 684; i) Y. Wang, J. Xu, Y. Wang and H. Chen, *Chem. Soc. Rev.*, **2013**, *42*, 2930.

2. a) Z. Huang, S.-K. Kang, M. Banno, T. Yamaguchi, D. Lee, C. Seok, E. Yashima and M. Lee, *Science*, **2012**, *337*, 1521; b) Y. Nakano, A. J. Markvoort, S. Cantekin, I. A. W. Filot, H. M. M. ten Eikelder, E. W. Meijer and A. R. A. Palmans, *J. Am. Chem. Soc.*, **2013**, *135*, 16497; c) B. W. Messmore, P. A. Sukerkar and S. I. Stupp, *J. Am. Chem. Soc.*, **2005**, *127*, 7992; d) M. Banno, T. Yamaguchi, K. Nagai, C. Kaiser, S. Hecht and E. Yashima, *J. Am. Chem. Soc.*, **2012**, *134*, 8718; e) V. Percec, A. E. Dulcey, M. Peterca, M. Ilies, M. J. Sienkowska and P. A. Heiney, *J. Am. Chem. Soc.*, **2005**, *127*, 17902; f) F. García and L. Sánchez, *J. Am. Chem. Soc.*, **2012**, *134*, 734; g) A. Gopal, M. Hifsudheen, S. Furumi, M. Takeuchi and A. Ajayaghosh, *Angew. Chem. Int. Ed.*, **2012**, *51,* 10505; h) K. Toyofuku, M. A. Alam, A. Tsuda, N. Fujita, S. Sakamoto, K. Yamaguchi and T. Aida, *Angew. Chem. Int. Ed.*, **2007**, *119*, 6596; i) J. Kumar, T. Nakashima, H. Tsumatori and T. Kawai, *J. Phys. Chem. Lett.*, 2**014**, *5*, 316; j) A. Lohr and F. Würthner, *Angew. Chem. Int. Ed.*, **2008**, *47*, 1232; k) I. Danila, F. Riobé, F. Piron, J. Puigmartí-Luis, J. D. Wallis, M. Linares, H. Ågren, D. Beljonne, D. B. Amabilino and N. Avarvari, *J. Am. Chem. Soc.*, **2011**, *133*, 8344; l) U. Rösch, S. Yao, R. Wortmann and F. Würthner, *Angew. Chem. Int. Ed.*, **2006**, *45*, 7026; m) H. C. Fry, J. M. Garcia, M. J. Medina, U. M. Ricoy, D. J. Gosztola, M. P. Nikiforov, L. C. Palmer and S. I. Stupp, *J. Am. Chem. Soc.*, **2012**, *134,* 14646; n) Ž. Tomović, J. van Dongen, S. J. George, H. Xu, W. Pisula, P. Leclère, M. M. J. Smulders, S. De Feyter, E. W. Meijer and A. P. H. J. Schenning, *J. Am. Chem. Soc.*, **2007**, *129*, 16190; o) F. Aparicio, B. Nieto-Ortega, F. Nájera, F. J. Ramírez, J. T. López Navarrete, J. Casado and L. Sánchez, *Angew. Chem. Int. Ed.*, **2014**, *53*, 1373; p) A. Ajayaghosh, C. Vijayakumar, R. Varghese and S. J. George, *Angew. Chem. Int. Ed.*, **2006**, *45*, 456; q) A. Ajayaghosh, R. Varghese, S. Mahesh and V. K. Praveen, *Angew. Chem. Int. Ed.*, **2006**, *45*, 7729; r) W. Jin, T. Fukushima, M. Niki, A. Kosaka, N. Ishii and T. Aida, *Proc. Natl. Acad.*

Sci. U. S. A., **2005**, *102*, 10801; s) K. Sato, Y. Itoh and T. Aida, *Chem. Sci.*, **2014**, *5*, 136; N. Ousaka, Y. Takeyama and E. Yashima, *Chem. Sci.*, **2012**, *3*, 466.

3. a) P. G. A. Janssen, J. Vandenbergh, J. L. J. van Dongen, E. W. Meijer and A. P. H. J. Schenning, *J. Am. Chem. Soc.*, **2007**, *129*, 6078; b) M.-a. Morikawa, M. Yoshihara, T. Endo and N. Kimizuka, *J. Am. Chem. Soc.*, **2005**, *127*, 1358; c) H. Fenniri, B.-L. Deng and A. E. Ribbe, *J. Am. Chem. Soc.*, **2002**, *124*, 11064; d) A. R. A. Palmans, J. A. J. M. Vekemans, E. E. Havinga and E. W. Meijer, *Angew. Chem., Int. Ed. Engl.*, **1997**, *36*, 2648; e) S. J. George, Z. Tomovic, A. P. H. J. Schenning and E. W. Meijer, *Chem. Commun.*, **2011**, *47*, 3451; f) S. J. George, Ž. Tomović, M. M. J. Smulders, T. F. A. de Greef, P. E. L. G. Leclère, E. W. Meijer and A. P. H. J. Schenning, *Angew. Chem. Int. Ed.*, **2007**, *46*, 8206; g) J. Lin, M. Surin, D. Beljonne, X. Lou, J. L. J. van Dongen and A. P. H. J. Schenning, *Chem. Sci.*, **2012**, *3*, 2732; h) T. H. Rehm, M. R. Stojkovic, S. Rehm, M. Skugor, I. Piantanida and F. Würthner, *Chem. Sci.*, **2012**, *3*, 3393; i) A. Ajayaghosh, P. Chithra and R. Varghese, *Angew. Chem. Int. Ed.*, **2007**, *46*, 230.

4. a) E. Yashima, K. Maeda and Y. Okamoto, *Nature*, **1999**, *399*, 449; b) S. J. George, R. de Bruijn, Ž. Tomović, B. Van Averbeke, D. Beljonne, R. Lazzaroni, A. P. H. J. Schenning and E. W. Meijer, *J. Am. Chem. Soc.*, **2012**, *134*, 17789; c) P. A. Korevaar, S. J. George, A. J. Markvoort, M. M. J. Smulders, P. A. J. Hilbers, A. P. H. J. Schenning, T. F. A. De Greef and E. W. Meijer, *Nature*, **2012**, *481*, 492; d) A. Mammana, A. D'Urso, R. Lauceri and R. Purrello, *J. Am. Chem. Soc.*, **2007**, *129*, 8062; e) W. Zhang, W. Jin, T. Fukushima, N. Ishii and T. Aida, *J. Am. Chem. Soc.*, **2013**, *135*, 114; f) F. Helmich, C. C. Lee, A. P. H. J. Schenning and E. W. Meijer, *J. Am. Chem. Soc.*, **2010**, *132*, 16753; g) R. Lauceri, G. F. Fasciglione, A. D'Urso, S. Marini, R. Purrello and M. Coletta, *J. Am. Chem. Soc.*, **2008**, *130*, 10476; h) I. De Cat, Z. Guo, S. J. George, E. W. Meijer, A. P. H. J. Schenning and S. De Feyter, *J. Am. Chem. Soc.*, **2012**, *134*, 3171; i) J.-S. Zhao, Y.-B. Ruan, R. Zhou and Y.-B. Jiang, *Chem. Sci.*, **2011**, *2*, 937; j) K. Shimomura, T. Ikai, S. Kanoh, E. Yashima and K. Maeda, *Nat. Chem.*, **2014**, *6*, 429.

5. a) E. Yashima, T. Matsushima and Y. Okamoto, *J. Am. Chem. Soc.*, **1995**, *117*, 11596; b) F. Riobe, A. P. H. J. Schenning and D. B. Amabilino, *Org. Biomol. Chem.*, **2012**, *10*, 9152; c) T. Ikeda, O. Hirata, M. Takeuchi and S. Shinkai, *J. Am. Chem. Soc.*, **2006**, *128*, 16008; d) W.-S. Li, D.-L. Jiang, Y. Suna and T. Aida, *J. Am. Chem. Soc.*, **2005**, *127*, 7700; e) C. Zhao, Q.-F. Sun, W. M. Hart-Cooper, A. G. DiPasquale, F. D. Toste, R. G. Bergman and K. N. Raymond, *J. Am. Chem. Soc.*, **2013**, *135*, 18802.

6. a) J.-P. Changeux and S. J. Edelstein, *Science*, **2005,** *308,* 1424; b) A. Whitty, *Nat. Chem. Biol.* **2008**, *4*, 435; c) C. A. Hunter and H. L. Anderson, *Angew. Chem. Int. Ed.*, **2009**, *48*, 7488.

7. a) S. Shinkai, M. Ikeda, A. Sugasaki and M. Takeuchi, *Acc. Chem. Res.*, **2001**, *34*, 494; b) M. Takeuchi, M. Ikeda, A. Sugasaki and S. Shinkai, *Acc. Chem. Res.*, **2001**, *34*, 865; c) E. M. Pérez, L. Sánchez, G. Fernández and N. Martín, *J. Am. Chem. Soc.*, **2006**, *128*, 7172; d) M. Takeuchi, T. Imada and S. Shinkai, *Angew. Chem. Int. Ed.*, **1998**, *37*, 2096; e) M. Ikeda, M. Takeuchi, A. Sugasaki, A. Robertson, T. Imada and S. Shinkai, *Supramol. Chem.*, **2000**, *12*, 321.

8. a) T. Noguchi, T. Shiraki, A. Dawn, Y. Tsuchiya, L. T. N. Lien, T. Yamamoto and S. Shinkai, *Chem. Commun.*, **2012**, *48*, 8090; b) G. M. Cockrell, Y. Zheng, W. Guo, A. W. Peterson, J. K. Truong and E. R. Kantrowitz, *Biochemistry*, **2013***, 52*, 8036.

9. L. A. Fothergill-Gilmore and P. A. M. Michels, *Prog. Biophys. Mol. Biol.*, **1993**, *59*, 105.

10. a) X. Chen, M. J. Jou and J. Yoon, *Org. Lett.*, **2009**, *11*, 2181; b) L. Yan, Z. Ye, C. Peng and S. Zhang, *Tetrahedron*, **2012**, *68*, 2725; c) M. Kumar, N. Jonnalagadda and S. J. George, *Chem. Commun.*, **2012**, *48*, 10948.

11. The intensity ratio of the two most intense band was 0.94, which is high compared to known PBI monomers, indicating the existence of weak interchromophoric interactions even in MeCN at this concentration.

12. This was calculated from the emission quenching data shown in Figure 6.1b, where emission of MeCN solution was taken as 100 % monomers and completely aggregated species to be non-fluorescent (zero in intensity).

13. ATP's three site binding should have saturated all site at 0.66 eq., however, we observe CD saturation at 0.9 eq. ATP which could be due to inability of few ATP to bind via all three sites.

14. X. Zhang, D. Görl, V. Stepanenko and F. Würthner, *Angew. Chem. Int. Ed.*, **2014**, *53*, 1270.

15. Allosteric control of helicity was seen only with ATP and not with AMP or ADP probably due to its multivalent interactions compared to ADP and AMP. Usually only multivalent ligands are known to show such effects. Also preliminary investigations with single stranded DNA (which is a polymeric analogue of AMP) with **PDPA** also shows allosteric control over chirality, confirming the role of multivalent host guest interactions and ruling out any specific interaction with ATP being responsible for the allosterism.

16. AMP also did not induce heterotropic allosteric effects.

17. Handedness of the stacks are dictated by the strength of guest ligation.

CHAPTER-6

Towards Chiroptical Functionality

Chapter-6.1   *Induction and Imprinting of Circularly Polarized Luminescence by Chiral Auxiliary Approach*

Chapter-6.2   *Supramolecular Clippers for Controlling Photo-Physical Processes via Pre-Organized Chromophores*

Chapter-6.1

Induction and Imprinting of Circularly Polarized Luminescence by Chiral Auxiliary Approach

Abstract

Circularly polarized luminescence (CPL) from assemblies of chiral π-conjugated molecules has been investigated in great detail. Here we present guest induced CPL as a novel approach for the construction of helical electronic excited state in the assembly of achiral molecules. Coronene bisimide and perylene bisimide functionalized with dipicolylethylenediamine (DPA) based molecular recognition unit show adenosine phosphate binding induced CD signal. The chiral and fluorescent nature of these aggregates were most suited for CPL measurements, which showed high luminescence dissymmetric factor i.e. g_{lum}, even in dilute solutions. Moreover, enzyme assisted removal of chiral guest molecules from the helical stacks allows the imprinting of chiral excited state in the assembly of achiral monomers, termed as "CPL memory". Detailed spectroscopic investigations reveal the role of supramolecular reorganization in obtaining such imprinted CPL. Thus, we conceptualize this guest induced CPL in assembly of achiral π-conjugated fluorophores, as a unique approach for variety of CPL based chirotechnological applications.
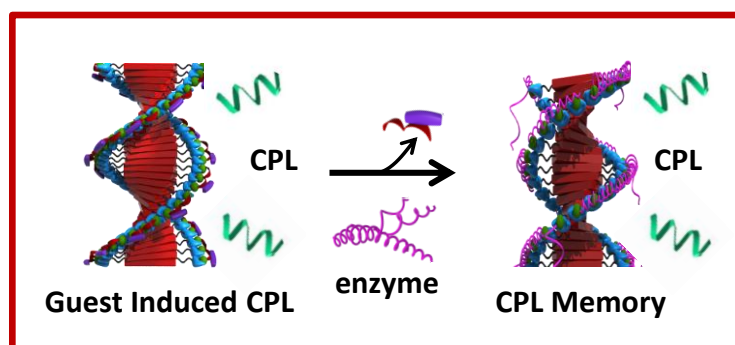
Manuscript based on this work is under preparation.

6.1.1 Introduction

Macromolecular helical assemblies, constructed from inherently chiral molecules, have been well investigated as structural mimics of biomolecules and as model systems to understand the homochirality in nature.[1, 2] In this regard, helical polymers and supramolecular assemblies of achiral monomeric unit, obtained by chiral auxiliary approach, have attracted immense attention for various chiroptical applications.[3] Such systems have been utilized for the construction of helical metastable state (chiral memory), by removal of chiral guest molecules from the helical assembly of achiral molecules.[4] Another application of these helical assemblies is their excited state chirality, leading to CPL emission.[5] Such studies provide insights into the helical organization of molecules in their electronic excited states.[6] Although, this has been demonstrated with many chiral fluorophores,[7] guest induced CPL into the assembly of achiral π-conjugated fluorophores is unprecedented. Moreover, such a design can be utilized for imprinting CPL in the assembly of achiral molecules in a so called "CPL memory", by post synthetic removal of chiral guest molecules.
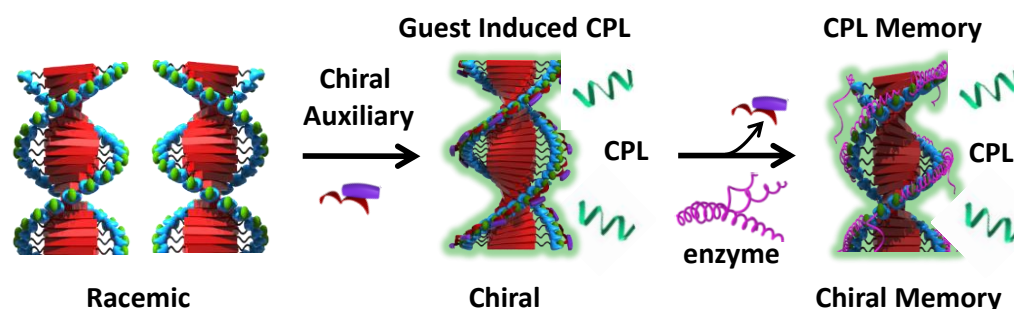

Scheme 6.1.1. *Schematic illustration of guest induced CPL and "CPL Memory" in the assembly of achiral π-conjugated fluorophores.*

For a helical assembly of chromophores to show CPL, the aggregates must be fluorescent. This is a serious limitation as aggregation is known to quench the fluorescence of molecules.[8] In this chapter, we investigate the CPL emission from the helical organization of dipicolylethylenediamine (DPA) functionalized achiral coronene bisimide (**ZnCPA**) and perylene bisimide (**PDPA**) derivatives (Scheme 6.1.1). These molecules show induced helical organization upon interaction with homochiral adenosine phosphates, resulting in a bisignated CD signal. Interestingly, binding to phosphate leads to enhanced emission in **ZnCPA** assembly and a new emission band in **PDPA** assembly, both of which render the aggregates fluorescent, making the system suitable for CPL study. These chromophores show phosphate induced CPL emission with luminescence dissymmetric factor (g_{lum}) comparable with the well studied assembly of chiral fluorophores. Moreover, as demonstrated in Chapter 4.2, we have used an enzyme (CIAP) for competitive removal of chiral auxiliary, wherein **PDPA** assemblies

continues to show CPL emission, leading to "CPL memory" effect (Scheme 6.1.1). Thus, we present a unique system with guest induced chiral assembly, which are fluorescent to show CPL, whereas the removal of chiral phosphate retains its emission to allow investigation of imprinted CPL and study their excited state stereomutation kinetics.
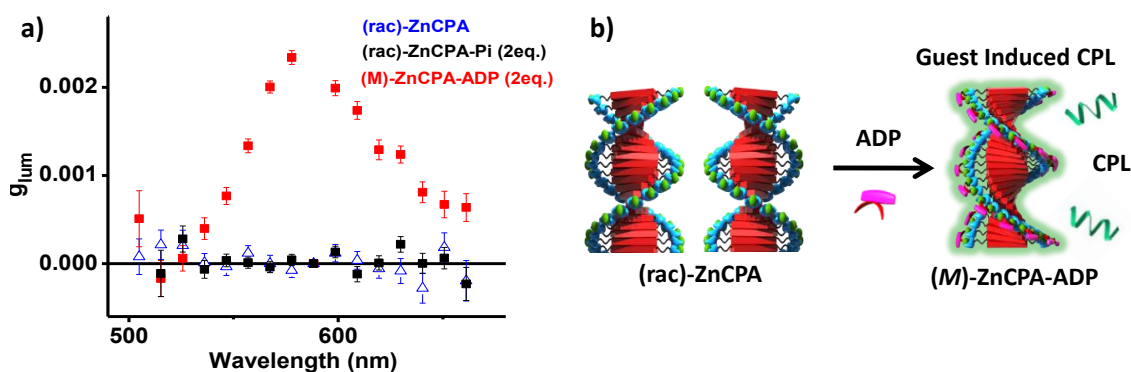
6.1.2 Chiral Guest Induced CPL
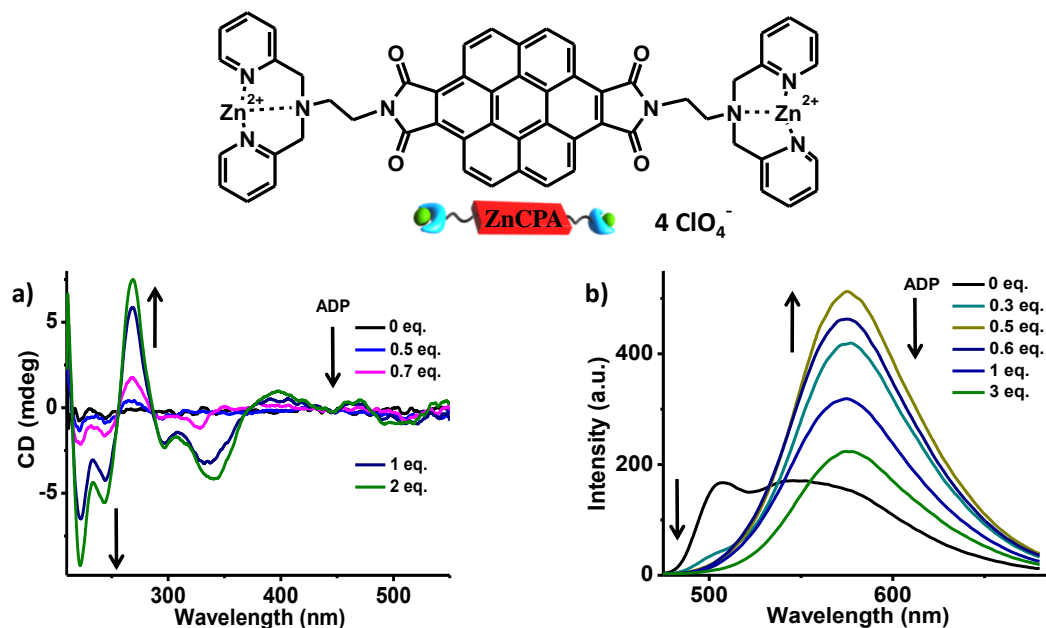
Figure 6.1.1. *Molecular structure of **ZnCPA** along with its schematic representation. Changes in a) CD spectra and b) emission spectra (λ_{ex}=350 nm) of **ZnCPA** upon titration with ADP (70% aq. HEPES in MeCN, 2 x 10^{-5} M).*[9]

     The coronene bisimide derivative **ZnCPA** was synthesized as described in Chapter 4 (Section 4.1.6). This bolaamphiphilic molecule was completely soluble in solvents like MeCN, DMF and self-assembled in water through hydrophobic and aromatic-aromatic interactions. Therefore, all spectroscopic studies were performed in appropriate composition of MeCN – aq. HEPES buffer (10 mM solution in water). Through spectroscopic investigations, we have previously shown that these molecules form typical J-type aggregates by slipped packing of chromophores (Chapter 4.1.1). Binding of homochiral guests like ADP to **ZnCPA** stacks induced a left-handed helical assembly (*M*)-**ZnCPA**-ADP, as evident from the negative bisignated CD signal, negative at 343 nm and positive at 268 nm, with a zero crossing at 286 nm (Figure 6.1.1a, 30% MeCN in aq. HEPES, c = 2 x 10^{-5} M). This confirms the potential of molecular recognition design for binding of ADP leading to efficient chirality transfer into assembly of achiral **ZnCPA**. For such a system with guest induced helical assembly of fluorophore to show circularly polarized luminescence (CPL), these aggregates must be

fluorescent. Binding of ADP to **ZnCPA** stacks results in quenching of monomeric emission at 506 nm along with enhancement of aggregate band at 575 nm (Figure 6.1.1b). As discussed in previous chapter (Section 4.1.2), such a turn on emission has been attributed to prevention of photo electron transfer (PET) upon interaction of DPA substituted chromophores with adenosine phosphates. Unlike usual fluorophores, which show aggregation induced quenching of emission, binding of ADP leads to formation of fluorescent nanofibers (Chapter 4, Figure 4.1.10), making it suitable for CPL investigations.

Chiral nature of emission or helical assembly of fluorophores which is in chiral environment even in their electronic excited state, can be characterized by CPL. It is usually measured as luminescence dissymmetric factor i.e. $|g_{lum}| = 2(I_L-I_R)/I_L+I_R$, where I_L+I_R are fluorescence intensities of left and right circularly polarized light (LCP and RCP respectively). **ZnCPA** stacks upon binding to 2 eq. ADP i.e. ZnCPA-ADP, show a strong positive CPL signal indicating preferential emission of LCP over RCP (Figure 6.1.2, 70% aq. HEPES in MeCN, 2 x 10^{-5} M). The fluorescence anisotropy value, g_{lum} obtained was 2.3 x 10^{-4}, which is comparable to most self-assembled chiral fluorophores.[5] Moreover, similar experiments done without any phosphates or in presence of achiral guest molecules like Pi (PO_4^{3-}) do not show any significant CPL signal, ruling out the contribution from any scattering based artifacts. Thus, it clearly demonstrate the guest induced chiral organization of achiral **ZnCPA,** in the electronic ground state (as shown by CD signal (Figure 6.1.1a) as well as excited state (shown by CPL measurements), an unprecedented report in the self-assembly of π-conjugated systems.

Figure 6.1.2. *a) CPL spectra of **ZnCPA** upon binding to 2 eq. of Pi (PO_4^{3-}) and ADP. b) Schematic representation of chiral guest induced CPL in assembly of achiral chromophores.*

6.1.3 CPL Memory

Having demonstrated the chiral guest induced CPL in the assembly of achiral chromophores, the next challenging task was the retention of this preferential emission even after removal of chiral information in a so called "CPL memory". In Chapter 4.2, we have

already established the construction of imprinted helicity in the assembly of achiral monomers, by the detachment of bound ADP upon addition of enzyme (calf intestinal alkaline phosphatase - CIAP). These enzymes (CIAP) were shown to act as polyvalent anionic scaffold for competitive replacement of ADP and as molecular chaperone for the stabilization of chiral memory. Such an imprinted helical assembly was probed by CD signal and is due to retention of chiral organization of achiral chromophores in the ground state. Thus, we investigated if such a system could also retain its organization in the excited state and emit CPL. However, to be able to exhibit the CPL memory, the imprinted helical system must be fluorescent (schematic of Figure 6.1.3). Thus, emission spectra of (*M*)-**ZnCPA**-ADP were monitored upon addition of enzyme. We notice that the highly fluorescent (*M*)-**ZnCPA**-ADP instantaneously quenches its emission upon removal of ADP by enzyme addition (Figure 6.1.3). This is expected as the enhancement in emission was due to ADP binding induced prevention of PET, which would restart after phosphate removal (Section 4.2.3, Figure 4.2.6).
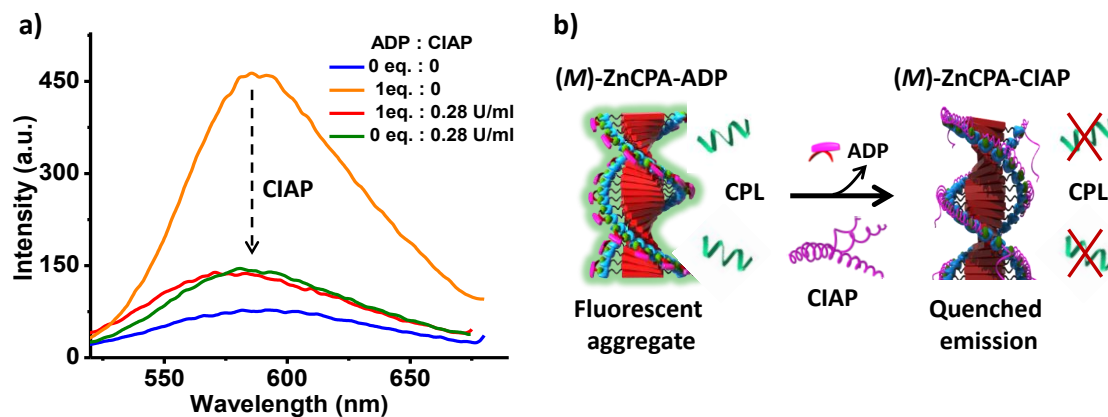
Figure 6.1.3. *a) Variation in fluorescence spectra upon addition of CIAP (0.28 U/ml) to (M)-**ZnCPA**-ADP (1 eq.) (90% aq. HEPES in MeCN, 10^{-5} M, λ_{ex}=350 nm). b) Pictorial representation of enzyme binding induced ADP removal and emission quenching.* [9]

Thus, a simple design for "CPL memory" would require a system which undergoes chiral guest binding induced supramolecular reorganization leading to fluorescent helical assembly. We have already shown in chapter 5 that DPA functionalized perylenebisimide (**PDPA**) shows ATP binding induced allosteric regulation of supramolecular chirality. Binding to ATP shows a positive bisignated CD signal, positive at 518 nm followed by negative at 480 nm (Figure 6.1.4a). Interestingly, fluorescence spectra upon ATP titration shows emergence of a new red shifted band at 665 nm (Figure 6.1.4b). Through detailed spectroscopic investigations, we have already established the role of conformational reorganization upon ATP binding, leading to transition from non-fluorescent **H1**-state to fluorescent **H2**-state (Chapter 5, Section 5.3). These results indicate that the fluorescence at 665 nm is due to formation of **H2**-

state, and ATP is merely a structure directing unit. Therefore, this can be an ideal system to study the concept of excited state chiral memory, where we envisage that removal of ATP from the **H2**-state would continue to retain its helical organization both in the ground state and excited state.
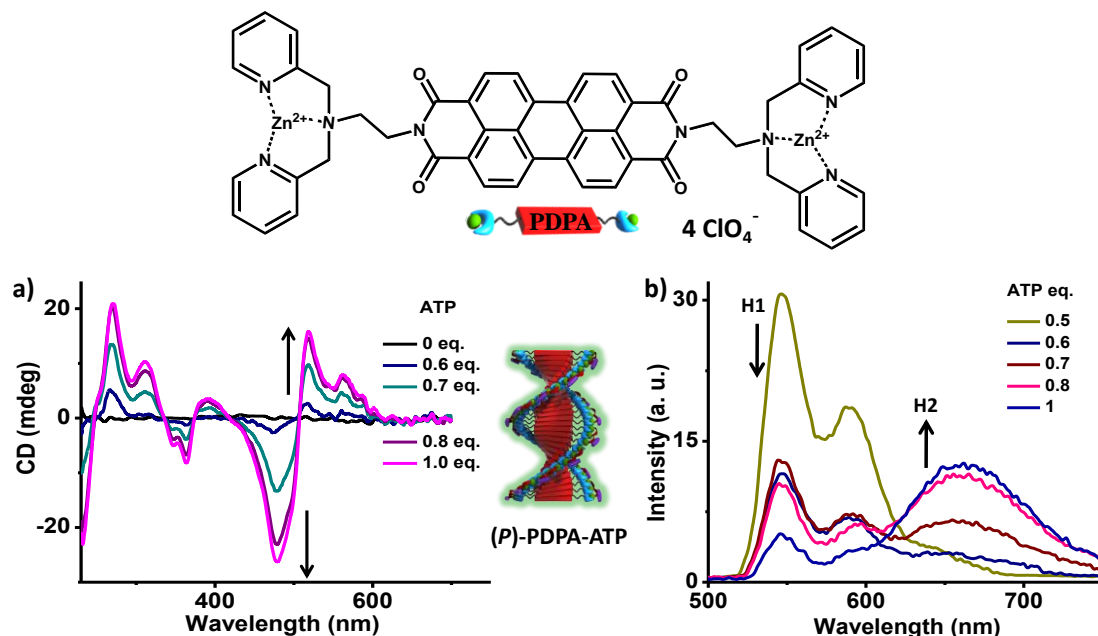

*Figure 6.1.4. Molecular structure of **PDPA** and variation in a) CD spectra and b) emission spectra (λ_{ex}=470 nm) of **PDPA** upon ATP titration (90% aq. HEPES in MeCN, 2 x 10^{-5} M).* [10]

We first probed into the CPL emission property of these assemblies. ATP bound helical assembly (*P*)-**PDPA**-ATP (90% aq. HEPES in MeCN, 2 x 10^{-5} M) showed a positive CPL signal with maximum g_{lum} = 5 x 10^{-3} (Figure 6.1.5a). Such an intense CPL intensity indicates efficient transfer of chirality from the chiral guest to the assembly of achiral fluorophore in the excited state. To prove that the CPL signal is indeed due to the formation of ATP bound fluorescent **H2**-state, we repeated the same experiment upon interaction of AMP to **PDPA** i.e. (*M*)-**PDPA**-AMP. We see that (*M*)-**PDPA**-AMP does not show any significant CPL signal. This could be easily explained based on AMP binding induced CD and fluorescence characteristics. As already discussed in Chapter 2 (Section 2.5), binding of AMP to **PDPA** results in negative bisignated CD signal (Figure 6.1.6a). Interestingly, emission spectra show quenching of monomeric emission without the appearance of any new band. These data clearly confirm that (*M*)-**PDPA**-AMP are non-fluorescent aggregates and thus they cannot show any differential emission (CPL). With all these experiments, it is clear that (*P*)-**PDPA**-ATP is a unique system which can be very useful in understanding the excited state chiral memory.
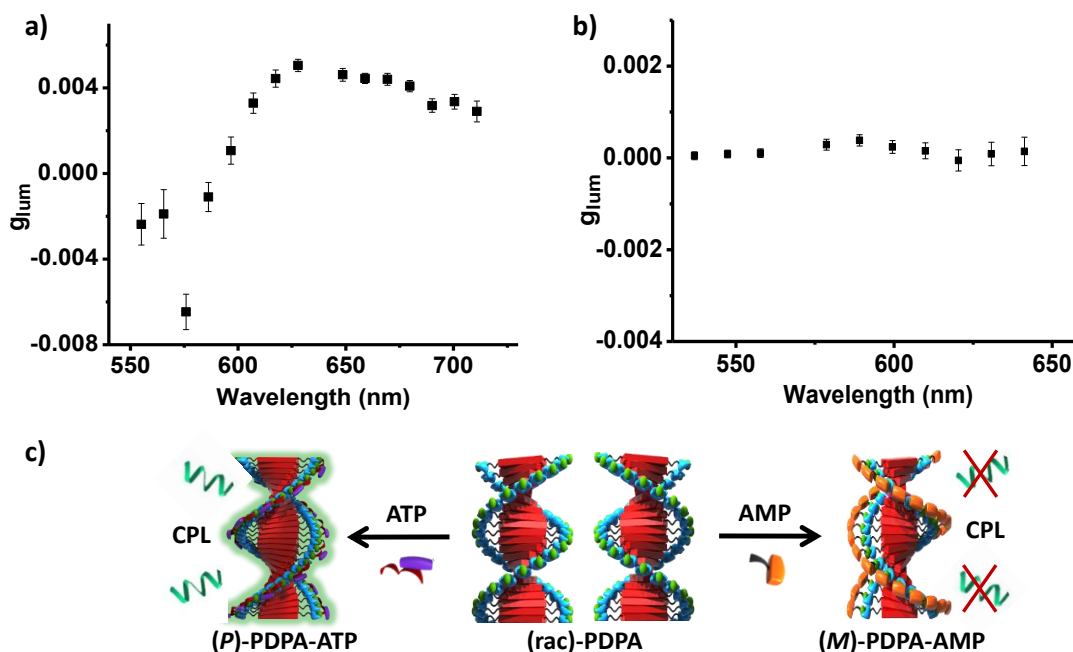
Figure 6.1.5. *CPL spectra of a) (P)-**PDPA**-ATP (3 eq.) and b) (M)-**PDPA**-AMP (1 eq.) (90% aq. HEPES in MeCN, 2 x 10^{-5} M). c) Schematic representation of the two processes.*
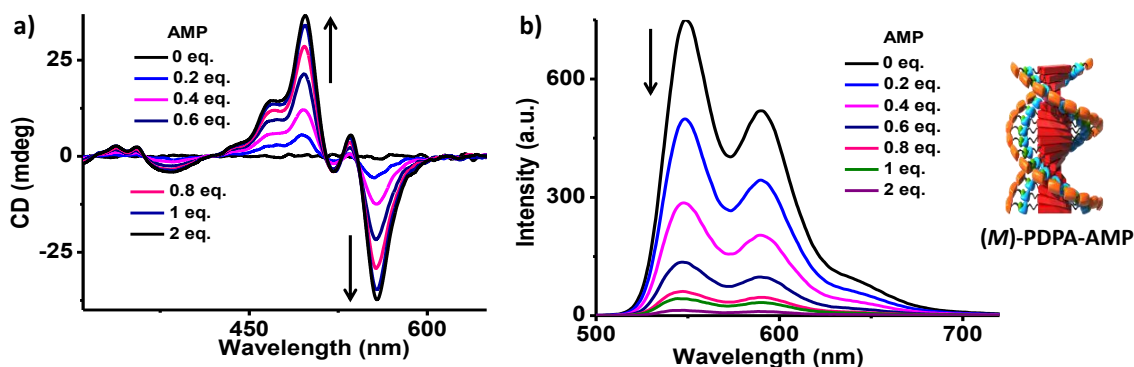
Figure 6.1.6. *Variation in a) CD spectra and b) emission spectra (λ_{ex}=470 nm) of **PDPA** upon titration with AMP (90% aq. HEPES in MeCN, 2 x 10^{-5} M).*[10]

Following our well established enzyme approach for fast removal of chiral phosphate (as shown in Chapter 4.2 and Figure 6.1.3), we first probed the ground state imprinted chirality based on CD signal. Thus, time dependent variation in CD signal of (*P*)-**PDPA**-ATP was monitored at 477 nm upon addition of CIAP (90% aq. HEPES in MeCN, 2 x 10^{-5} M, [CIAP] = 0.56 U/ml). We notice that the helical stacks take a finite amount of time for complete racemization (Figure 6.1.7 a, b). Thus, although CIAP instantaneously (within seconds) removes ATP from the stacks, the assembly retains its chiral organization in the ground state in a metastable helical memory. CD spectra monitored after complete stereomutation shows no signal, confirming the racemization of stacks, which in the present case is due to transition from

H2 to **H1** state of assembly. (Figure 6.1.7c). Moreover, absorption spectral changes clearly indicate the conformational transformation during the racemization process. As shown before (Chapter 5, Figure 5.2), ATP binding leads to a bathochromic jump in the absorption maxima (499 nm to 514 nm and 535 nm to 564, Figure 6.1.7d). These have been assigned to **H1**- to **H2**-state transformation upon ATP binding. Interestingly, after complete racemization i.e. from (*P*)-**PDPA**-CIAP to (*rac*)-**PDPA**-CIAP, we see a blue shift in absorption spectra (514 nm to 500 nm and 564 nm to 550 nm, Figure 6.1.7c). Moreover, the final absorption spectrum resembles an **H1**-state of **PDPA**. Thus, we confirm that the racemization process is indeed a result of transition from **H2**- to **H1**- state.
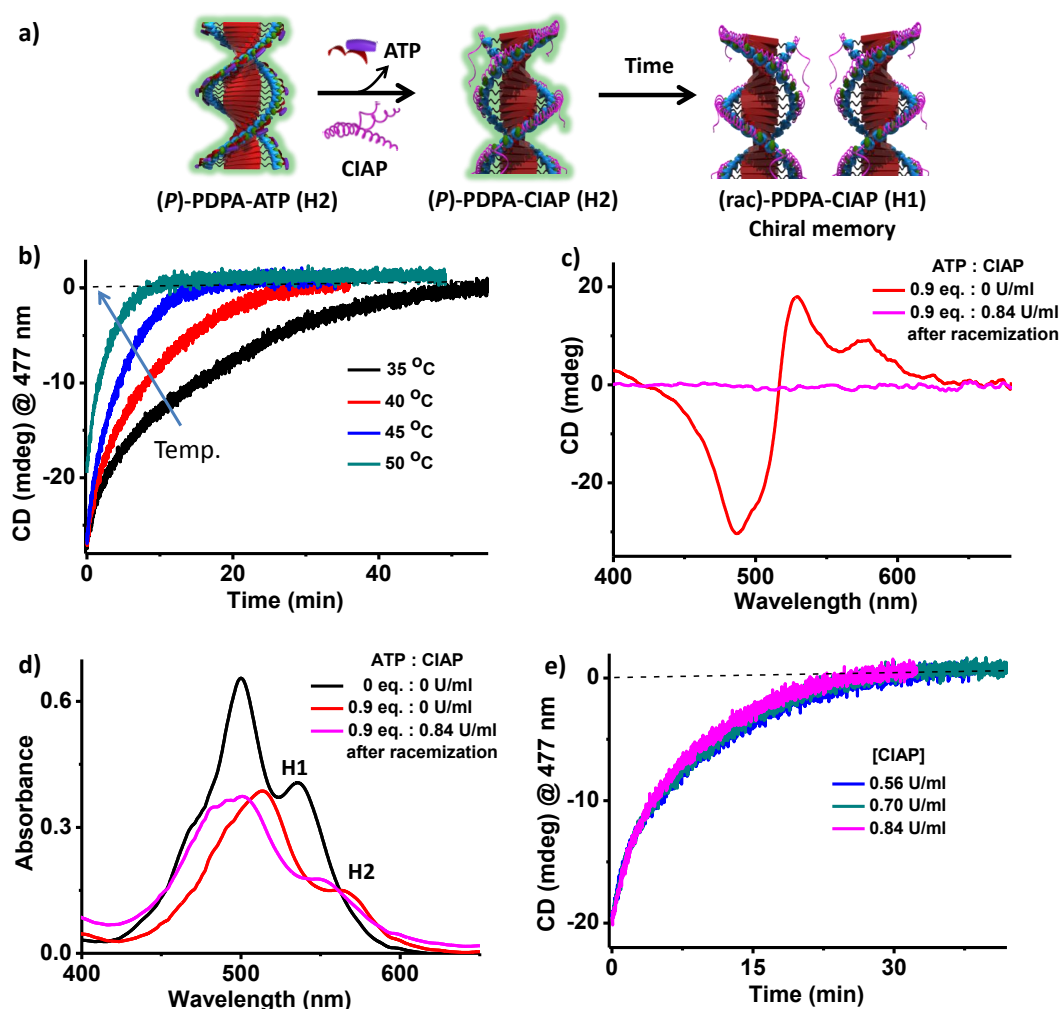
Figure 6.1.7. *a) Schematic representation of CIAP binding induced chiral memory in **PDPA** assembly. b) Time dependent changes in CD signal of (P)-**PDPA**-ATP upon addition of CIAP (0.56 U/ml) at various temperatures. Change in c) CD spectra and d) absorption spectra of (P)-**PDPA**-ATP upon racemization in presence of CIAP (0.84 U/ml) at 40 °C. e) Time dependent variation in CD intensity of (P)-**PDPA**-ATP (0.9 eq.) with varying concentration of enzyme at 40 °C (90% aq. HEPES in MeCN, 2 x 10^{-5} M).*

The racemization kinetics of the helical memory was probed at various temperatures. CD signal of (*P*)-**PDPA**-CIAP (chiral memory) was monitored upon increasing temperature from 35 °C to 50 °C (90% aq. HEPES in MeCN, 2 x 10^{-5} M, [CIAP] = 0.56 U/ml, Figure 6.1.7b). We observe a faster decay at higher temperatures, clearly confirming the activation energy mediated process. Moreover, when the racemization kinetics were probed at varying concentration of enzyme, we do not see any change in their stereomutation rate (90% aq. HEPES in MeCN, 2 x 10^{-5} M, 40 °C, Figure 6.1.7e). Rate of racemization being independent of CIAP concentrations clearly proves that it is not an enzyme catalysed process (as conclusively demonstrated in section 4.2.3). This once again confirms the fact that enzyme is not active as a catalyst for phosphate hydrolysis, but acts as a guest for competitive replacement of bound phosphate.[11]
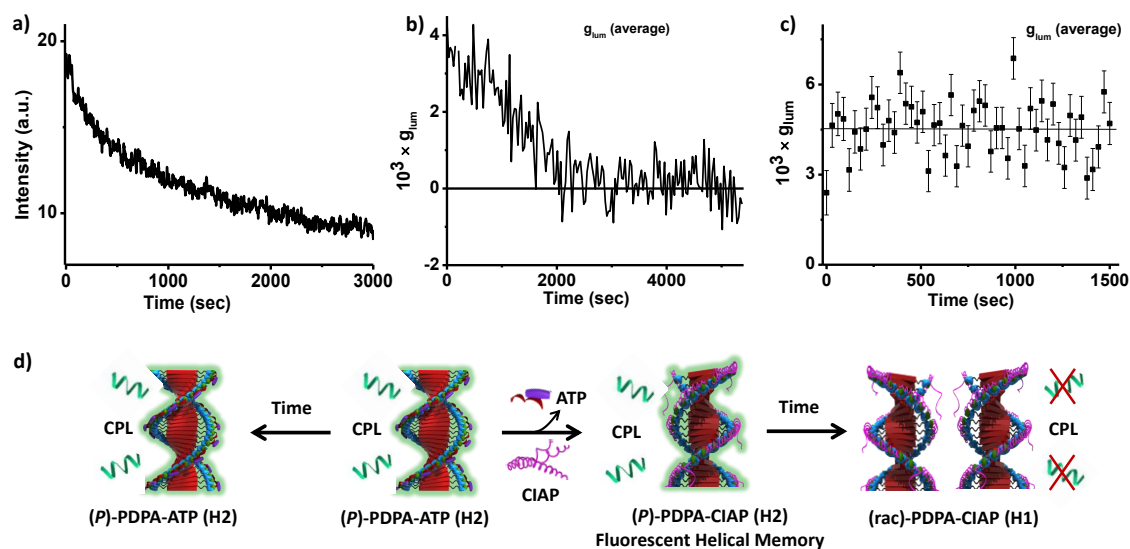
Figure 6.1.8. *Time dependent variation in a) fluorescence intensity (665 nm, λ_{ex}=570 nm), CPL signal b) with 0.70 U/ml CIAP and c) without CIAP (90% aq. HEPES in MeCN, 2 x 10^{-5} M). Emission in a) does not completely quench mainly due to partial overlap of monomeric emission.*

Results thus far have shown that (*P*)-**PDPA**-ATP form right-handed helical assembly leading to fluorescent **H2**-assembly. This chiral auxiliary i.e. ATP could be easily removed for the construction of ground state helical memory (*P*)-**PDPA**-CIAP. Now, for the construction of CPL memory, we need to first prove that the assembly retains its fluorescence even after removal of ATP by enzyme addition. Thus, emission intensity of (*P*)-**PDPA**-CIAP (90% aq. HEPES in MeCN, 2 x 10^{-5} M, 25 °C, [CIAP] = 0.70 U/ml, 0.9 eq. ATP, λ_{ex}=570 nm) was monitored as a function of time (Figure 6.1.8a). Finite kinetics involved in the emission decay clearly indicates that the **H2**-state emission is retained even after ATP detachment.[12] Finally,

when time dependent CPL was measured upon addition of CIAP, we see that it also follows the same pattern of decay as that of steady state emission (Figure 6.1.8 b) (90% aq. HEPES in MeCN, 2 x 10^{-5} M, 25 °C, [CIAP] = 0.70 U/ml, 0.9 eq. ATP). Also, time dependent CPL measured without CIAP do not show any change in signal intensity (Figure 6.1.8c), confirming that the racemization process is responsible for the slow decay of CPL in presence of enzyme. Thus, we demonstrate an unprecedented report of CPL memory in the assembly of achiral π-conjugated fluorophores.

6.1.4 Conclusion

To conclude, we have presented a new design strategy for the CPL emission from the assembly of achiral molecules. Adenosine phosphate recognition driven chiral induction for the CPL emission from the assembly of π-conjugated system is unprecedented and the strategy could be generalized by demonstrating it in both **PDPA** and **ZnCPA** derivatives. Moreover, the g_{lum} obtained is comparable to literature report of CPL emission in assembly of chiral monomers, confirming the efficient induction of helicity in the electronic excited state. Finally, we have also shown "CPL memory" in our system, where the stacks of achiral molecules continue to emit CPL, even after removal of chiral guest molecules. Such a unique system holds great potential in CPL based light emitting technologies and display materials.

6.1.5 Experimental Section

General Methods:

Optical Measurements: Electronic absorption spectra were recorded on a Perkin Elmer Lambda 900 UV-Vis-NIR Spectrometer and emission spectra were recorded on Perkin Elmer Ls 55 Luminescence Spectrometer. UV-Vis and emission spectra were recorded in 10 mm path length cuvette. Fluorescence spectra of solutions were recorded with 350 nm excitation wavelength. Circular Dichroism measurements were performed on a Jasco J-815 spectrometer where the sensitivity, time constant and scan rate were chosen appropriately. Corresponding temperature dependent measurements were performed with a CDF – 426S/15 Peltier-type temperature controller with a temperature range of 263-383 K and adjustable temperature slope.

Circularly Polarized Luminescence Measurements: Circularly polarized luminescence spectra were measured on a home-built setup that uses a photoelastic modulator and a multichannel photon-counting detection system. The incident light was depolarized by passing it through an optical fiber. The emission was detected in an in-line geometry to avoid artifacts resulting from linear polarization. CPL error bars represent standard deviations in the

measurement, estimated from repeated sampling of the dissymmetry factor for circular polarization in luminescence g$_{lum}$.

Materials: All chemicals / solvents were purchased from the commercial sources and were used as such. Spectroscopic grade solvents were used for all optical measurements.

Commercially available CIAP was 2.8 units per mg and stock solution of CIAP was prepared by dissolving 1 mg of CIAP in 80 μl of aq. HEPES buffer. For each measurement, appropriate μl of this stock solution was added into 2.5 ml of required solution.

Synthesis of **ZnCPA** was peformed as reported in chapter 4.1 (Scheme 4.1.1). **PDPA** was synthesized following a reported procedure.[13]

6.1.6 References and Notes

1. a) A. R. A. Palmans and E. W. Meijer, *Angew. Chem. Int. Ed.*, **2007**, *46*, 8948; b) A. E. Rowan and R. J. M. Nolte, *Angew. Chem. Int. Ed.*, **1998**, *37*, 63; c) E. Yashima, K. Maeda, H. Iida, Y. Furusho and K. Nagai, *Chem. Rev.*, **2009**, *109*, 6102; d) M. M. Green, K.-S. Cheon, S.-Y. Yang, J.-W. Park, S. Swansburg and W. Liu, *Acc. Chem. Res.*, **2001**, *34*, 672; e) M. Fujiki, J. R. Koe, K. Terao, T. Sato, A. Teramoto and J. Watanabe, *Polym. J.*, **2003**, *35*, 297; f) A. Lohr and F. Würthner, *Isr. J. Chem.*, **2011**, *51*, 1052; g) V. K. Praveen, S. S. Babu, C. Vijayakumar, R. Varghese and A. Ajayaghosh, *Bull. Chem. Soc. Jpn.*, **2008**, *81*, 1196; h) D. K. Smith, *Chem. Soc. Rev.*, **2009**, *38*, 684; i) Y. Wang, J. Xu, Y. Wang and H. Chen, *Chem. Soc. Rev.*, **2013**, *42*, 2930.

2. a) Z. Huang, S.-K. Kang, M. Banno, T. Yamaguchi, D. Lee, C. Seok, E. Yashima and M. Lee, *Science*, **2012**, *337*, 1521; b) Y. Nakano, A. J. Markvoort, S. Cantekin, I. A. W. Filot, H. M. M. ten Eikelder, E. W. Meijer and A. R. A. Palmans, *J. Am. Chem. Soc.*, **2013**, *135*, 16497; c) M. Banno, T. Yamaguchi, K. Nagai, C. Kaiser, S. Hecht and E. Yashima, *J. Am. Chem. Soc.*, **2012**, *134*, 8718; d) A. Gopal, M. Hifsudheen, S. Furumi, M. Takeuchi and A. Ajayaghosh, *Angew. Chem. Int. Ed.*, **2012**, *51,* 10505; e) K. Toyofuku, M. A. Alam, A. Tsuda, N. Fujita, S. Sakamoto, K. Yamaguchi and T. Aida, *Angew. Chem. Int. Ed.*, **2007**, *119*, 6596; f) U. Rösch, S. Yao, R. Wortmann and F. Würthner, *Angew. Chem. Int. Ed.*, **2006**, *45,* 7026; g) Ž. Tomović, J. van Dongen, S. J. George, H. Xu, W. Pisula, P. Leclère, M. M. J. Smulders, S. De Feyter, E. W. Meijer and A. P. H. J. Schenning, *J. Am. Chem. Soc.*, **2007**, *129*, 16190; h) F. Aparicio, B. Nieto-Ortega, F. Nájera, F. J. Ramírez, J. T. López Navarrete, J. Casado and L. Sánchez, *Angew. Chem. Int. Ed.*, **2014**, *53*, 1373; i) A. Ajayaghosh, C. Vijayakumar, R. Varghese and S. J. George, *Angew. Chem. Int. Ed.*, **2006**, *45*, 456; j) A. Ajayaghosh, R. Varghese, S. Mahesh and V. K. Praveen, *Angew. Chem. Int.*

Ed., **2006**, *45*, 7729; k) W. Jin, T. Fukushima, M. Niki, A. Kosaka, N. Ishii and T. Aida, *Proc. Natl. Acad. Sci. U. S. A.*, **2005**, *102*, 10801.

3. a) H. Fenniri, B.-L. Deng, and A. E. Ribbe, *J. Am. Chem. Soc.,* **2002**, *124*, 11064; b) S. J. George, Ž. Tomović, M. M. J. Smulders, T. F. A. de Greef, P. E. L. G. Leclère, E. W. Meijer and A. P. H. J. Schenning, *Angew. Chem. Int. Ed.,* **2007**, *46*, 8206; c) J. Xiao, J. Xu, S. Cui, H. Liu, S. Wang and Y. Li, *Org. Lett.,* **2008**, *10*, 645; d) K. Toyofuku, Md. A. Alam, A. Tsuda, N. Fujita, S. Sakamoto, K. Yamaguchi and T. Aida, *Angew. Chem. Int. Ed.,* **2007**, *46,* 6476; e) A. R. A. Palmans, J. A. J. M. Vekemans, E. E. Havinga and E. W. Meijer, *Angew. Chem. Int. Ed. Engl.*, **1997**, *36*, 2648; f) S. J. George, Ž. Tomović, A. P. H. J. Schenning and E. W. Meijer, *Chem. Commun.,* **2011**, *47*, 3451; g) N. Katsonis, H. Xu, R. M. Haak, T. Kudernac, Ž. Tomović, S. J. George, M. Van der Auweraer, A. P. H. J. Schenning, E. W. Meijer, B. L. Feringa and S. D. Feyter, *Angew. Chem. Int. Ed.*, **2008**, *47*, 4997; h) S. Ghosh, X-Q. Li, V. Stepanenko and F. Würthner, *Chem. Eur. J.*, **2008**, *14*, 11343.

4. a) P. A. Korevaar, S. J. George, A. J. Markvoort, M. M. J. Smulders, P. A. J. Hilbers, A. P. H. J. Schenning, T. F. A. De Greef and E. W. Meijer, *Nature,* **2012**, *481*, 492; b) S. J. George, R. de Bruijn, Ž. Tomović, B. Van Averbeke, D. Beljonne, R. Lazzaroni, A. P. H. J. Schenning and E. W. Meijer, *J. Am. Chem. Soc.*, **2012**, *134*, 17789; c) F. Helmich, C. C. Lee, A. P. H. J. Schenning and E. W. Meijer, *J. Am. Chem. Soc.*, **2010**, *132*, 16753; d) I. D. Cat, Z. Guo, S. J. George, E. W. Meijer, A. P. H. J. Schenning and S. D. Feyter, *J. Am. Chem. Soc.,* **2012***, 134,* 3171; e) A. Mammana, A. D'Urso, R. Lauceri and R. Purrello, *J. Am. Chem. Soc.*, **2007**, *129*, 8062.

5. a) H. Maeda and Y. Bando, *Pure Appl. Chem.*, **2013***,85*, 1967; b) J. C. Y. Ng, J. Liu, H. Su, Y. Hong, H. Li, J. W. Y. Lam, K. S. Wong and B. Z. Tang, *J. Mater. Chem. C,* **2014**, *2*, 78; c) J. Kumar, T. Nakashima, H. Tsumatori and T. Kawai, *J. Phys. Chem. Lett.*, 2**014**, *5*, 316; d) J. Kumar, T. Nakashima, H. Tsumatori, M. Mori, M. Naito and T. Kawai, *Chem. Eur. J.,* **2013**, *19*, 14090; e) J. Liu, H. Su, L. Meng, Y. Zhao, C. Deng, J. C. Y. Ng, P. Lu, M. Faisal, J. W. Y. Lam, X. Huang, H. Wu, K. S. Wong and B. Z. Tang, *Chem. Sci.*, **2012**, *3*, 2737; f) H. Tsumatori, T. Nakashima and T. Kawai, *Org. Lett.,***2010***, 12*, 2362; g) Y. Kawagoe, M. Fujiki and Y. Nakano, *New J. Chem.*, **2010**, *34*, 637.

6. a) F. S. Richardson and J. P. Riehl, *Chem. Rev.*, **1977**, *77*, 773; b) F. C. Spano, Z. Zhao and S. C. J. Meskers, *J. Chem. Phys.*, **2004**, *120*, 10594; c) J. P. Riehl, *Chem. Rev*., **1986**, *86*, 1.

7. a) R. Carr, N. H. Evans and D. Parker, *Chem. Soc. Rev.,* **2012**, *41*, 7673; b) U. Tohgha, K. K. Deol, A. G. Porter, S. G. Bartko, J. K. Choi, B. M. Leonard, K. Varga, J. Kubelka, G. Muller and M. Balaz, *ACS Nano*, **2013**, *7*, 11094; c) K. D. Oyler, F. J. Coughlin and S.

Bernhard, *J. Am. Chem. Soc.*, **2007**, *129*, 210; d) J. L. Lunkley, D. Shirotani, K. Yamanari, S. Kaizaki and G. Muller, *J. Am. Chem. Soc.*, **2008**, *130*, 13814.

8. a) Y. Hong, J. W. Y. Lama and B. Z. Tang, *Chem. Commun.,* **2009**, 4332; b) Y. Hong, J. W. Y. Lam and B. Z. Tang, *Chem. Soc. Rev.*, **2011**, *40*, 5361.

9. This figure is adapted from chapter 4.2.

10. This figure is adapted from chapter 5.

11. A critical amount of CIAP is required for complete replacement of ATP, beyond which any further increase in CIAP concentration has no role to play.

12. Emission intensity does not completely go to zero even at longer time scale (Figure 6.1.8a), which can be due to slight overlap with the monomeric emission. So the residual emission is expected to be originating from the monomers.

13. X. Chen, M. J. Jou and J. Yoon, *Org. Lett.*, **2009**, *11*, 2181.

Chapter-6.2

Supramolecular Clippers for Controlling Photo-Physical Processes via Pre-Organized Chromophores

Abstract

In this chapter, a novel supramolecular clipping design for influencing the photo-physical properties of functional molecular assemblies, by the pre-organization (clipping) of chromophores, is described. Several chromophores end-functionalized with molecular recognition units were designed, which serve as handles to appropriately position these systems upon non-covalent interactions with multivalent guest molecules (supramolecular clippers). Towards this goal we have synthesized 1,5-Dialkoxynaphthalene (DAN) and Naphthalenediimide (NDI) functionalized with dipicolyl-ethylenediamine (DPA) motif. These molecules could pre-organize upon non-covalent clipping with adenosine di/tri phosphates resulting in pre-associated excimers and mixed (co- facial) charge-transfer assemblies. Chiral guest binding could also induce supramolecular chirality not only into their individual chromophoric assembly, but also into the hetero CT organization, as seen from the strong Circular Dichroism (CD) signal of the CT transition. The unique ability of the present design to influence the intermolecular interactions by changing the binding strength of clippers further make them very attractive for controlling the bimolecular photo-physical processes.
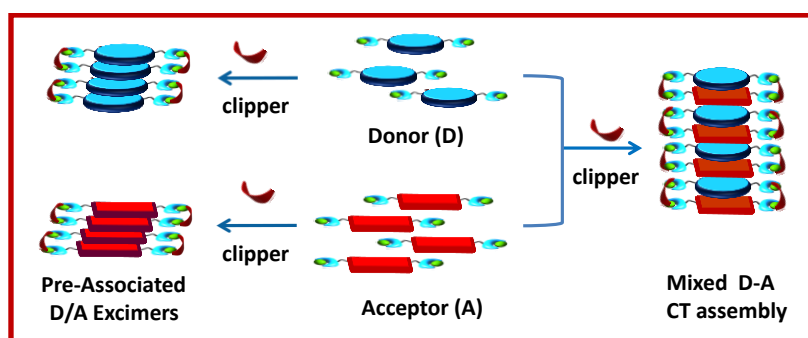
6.2.1 Introduction

Pre-organization of chromophores plays a very important role in various bi-molecular photophysical and photochemical processes, mainly due to the short-lived nature of the electronic excited states. In this regard, small ditopic receptor molecules that can simultaneously bind two chromophores using non-covalent interactions provide an elegant "supramolecular clipping" design for pre-assembling the chromophores in a reversible manner. Topochemical [2+2] cycloaddition reaction represents a class of bimolecular photochemical reaction, where relative orientation of reactant olefins is critically important.[1] In this respect, hydrogen bonding,[2] halogen bonding[3] and metal-coordination interactions[4] have been extensively used to clip and to pre-orient olefins in a geometrically suitable organization. Thus, it allows topochemical control in solid-state photo-cycloaddition reactions, resulting in near-perfect regio- and stereo-specific product. To date, however, the application of this supramolecular clipping approach to control various intermolecular photo-physical processes has been surprisingly unexplored, despite the remarkable potential of tuning the functional properties of resulting molecular assemblies.

Pre-associated excimer and mixed (alternate) charge transfer (CT) complex formation (homo and hetero bimolecular process, respectively) are two important photophysical processes, which demand inter-chromophoric preorganization in the ground-state. Pre-associated excimers, unlike typical excimers, are stable excited state dimers with relatively long life-time. These are formed due to the co- facial organization of chromophores in the ground state as observed in certain crystalline and self-assembled phases.[5] On the other hand, mixed CT complexes are face-to-face hetero chromophoric dimers formed between aromatic donor (D) and acceptor (A) molecules and are of great significance as a versatile supramolecular motif[6] and for applications in organic electronics.[7]

Pre-associated excimer: There are a few reports of pre-associated excimer formation in certain class of chromophores. For example, we have reported them in various Naphthalenediimide (**NDI**) derivatives. **NDI-Bola** was synthesized as shown in Scheme 6.2.4.[5b] **NDI-Bola** highly soluble in MeOH and self-assembled in presence of water due to hydrophobic interactions. Interestingly, we notice the evolution of a red shifted excimeric emission band at 513 nm (λ_{ex} = 350 nm) (Figure 6.2.1a), which enhances upon further aggregation by increasing percentage of water in methanol (MeOH). Usually chromophores are known to show aggregation induced quenching of emission, whereas here we show a new strategy for aggregation induced enhanced emission (AIEE) by formation of pre-associated excimer. These molecules self-assemble to form nanoparticles with an average diameter of 100 nm. As expected, these organic nanoparticles were retaining its emission as seen from the confocal fluorescent microscopic

imaging. These formed green fluorescent organic nanoparticles due to pre-associated excimer emission.
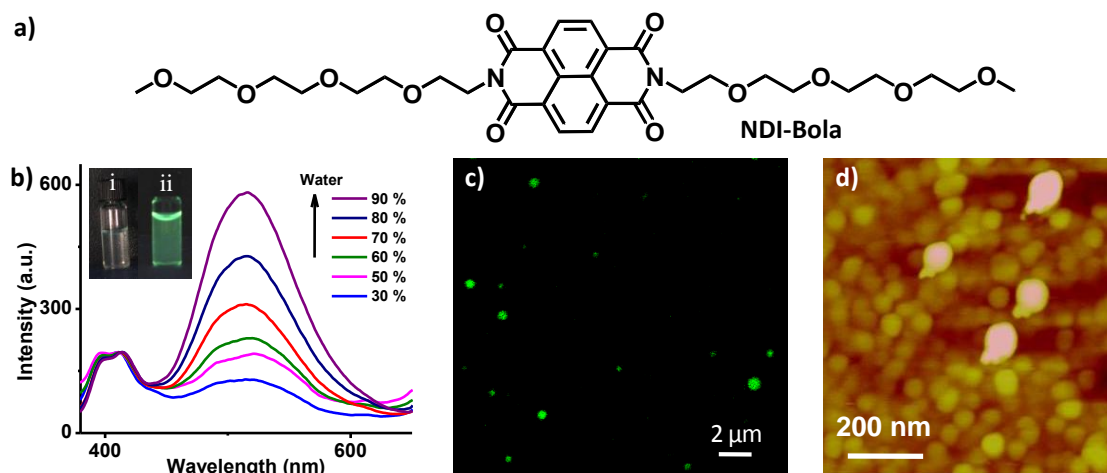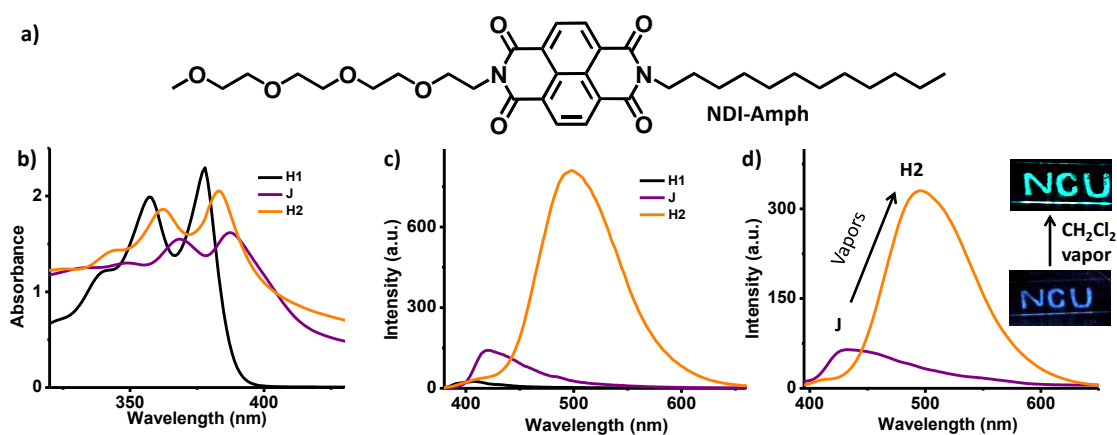

Figure 6.2.1. *a) Molecular structure of* **NDI-Bola***, b) steady-state emission spectra ($\lambda_{ex} = 350$ nm, normalized at 411 nm) in water-methanol solvent mixtures (1 x 10^{-3} M). All the spectra were recorded with front face geometry in 1 mm path length cuvette to minimize self-absorption. Inset in b) show the photographs of* **NDI-Bola** *in i) methanol and ii) water under UV illumination. Spherical aggregates of* **NDI-Bola** *as imaged under c) fluorescent confocal microscope and d) tapping mode AFM (10^{-3} M solution in 90% (v/v) water in methanol).*

Another report of such excimeric emission was shown in amphiphilic **NDI-Amph** (Figure 6.2.2a), which was synthesized as shown in Scheme 6.2.5.[5c] The weak blue emission of self-assembled film turned into enhanced green fluorescence upon exposure to vapors of organic solvents like $CHCl_3$, CH_2Cl_2, THF etc. (inset: Figure 6.2.2 d). Through detailed spectroscopic investigations, the exsistence of complex self-assembly processes accompanying three different states of assembly were observed (Figure 6.2.2 b-d). All photophysical studies were done at various percentage of water in MeOH with 1% $CHCl_3$. At 0% water the molecules self-assemble in the **H1** state with very weak emission (Figure 6.2.2c). On increasing water composition to 60%, a bathochromic shift of absorption spectra along with enhanced red shifted emission indicates the transformation from an **H1** state to **J** state of assembly. On further increase in water till 70%, we notice the evolution of a broad featureless emission band at 500 nm along with blue shift of the absorption spectra (Figure 6.2.2 b, c). Such an emission is characteristic of excimer formation in NDI derivatives and blue shift in absorption spectra indicates the formation of a different **H2** aggregate. Thus, when vapochromic behavior was probed with fluorescence spectroscopy, we notice the transformation from a **J** state to **H2** excimeric state upon exposure of **NDI-Amph** film with vapors of CH_2Cl_2 (Figure 6.2.2d). Such

a turn on of fluorescence was due to formation of pre-associated excimer and could be utilized as a turn on organic vapor sensor.

Figure 6.2.2. *a) Molecular structure of **NDI-Amph** and steady state b) absorption spectra, c) emission spectra (λ_{ex} = 350 nm) of three different states, i.e. **H1** , **J** and **H2** of **NDI-Amph** in 0%, 60%, 70% water in MeOH with 1% CHCl$_3$ respectively (c = 1 x 10^{-4} M). d) Emission spectra of **NDI-Amph** films (λ_{ex} = 350 nm) upon exposure to saturated vapors of CH$_2$Cl$_2$ and inset shows the visual changes in fluorescence of a **NDI-Amph** film upon exposure to CH$_2$Cl$_2$ vapors (illuminated with 365 nm UV light, the letters NCU is the abbreviation for New Chemistry Unit).*

In both these cases and many others reported in literature,[5] we observe the excimer formation, but there is no rational approach known yet to control such processes.

Charge transfer complex: Mixed stack charge-transfer (MS-CT) assemblies have been constructed via macromolecular,[8] supramolecular amphiphilic,[9] and host-guest designs.[10] In all such approaches, the alternate assembly of donor-acceptor were reported with varying association constants. For example, we have introduced coronene and NDI based novel D-A CT pairs (Figure 6.2.3). These formed strong CT complex in water with high association constants. Through systematic structural variation of the NDI at imide substitution, a structure property correlation has been established. Association constant measurements indicated that the **CS:NDI-DC** forms stronger CT compared to **CS: NDI-Bola**. Detailed studies clearly established the role of secondary forces like electrostatic interactions and amphiphilic organization in stabilizing the CT co-assembly. Thus we have shown simple ways to control the strength of CT interactions as well as to tune the supramolecular organization in solution leading to 1-D charge transfer nanofibers.
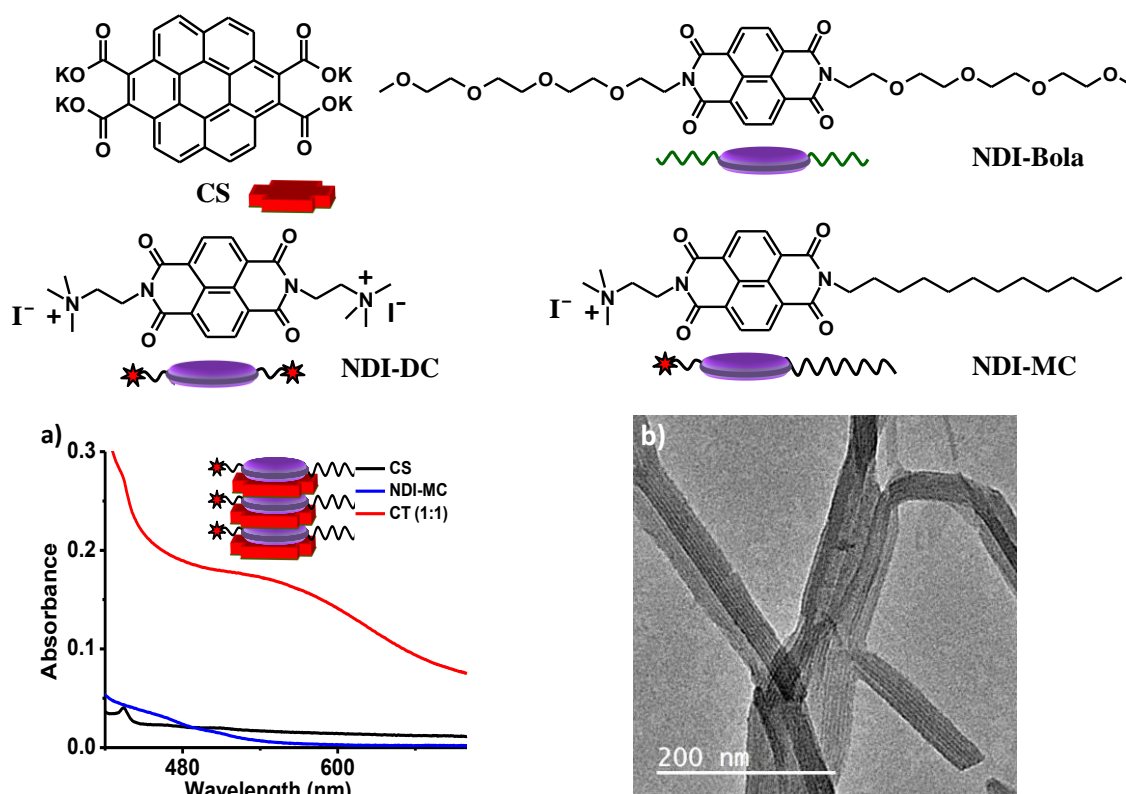
Figure 6.2.3. *Chemical structure of coronene based donor and NDI based acceptors. a)*
*Evolution of CT absorption band upon **CS:NDI-MC** 1:1 CT co-assembly (10^{-4} M, 90% water in*
MeOH, l=10mm). Inset in a) shows the schematic representation of alternate D-A CT co-
*assembly and b) shows the corresponding TEM image of **CS:NDI-MC** CT nanofibers.*

Thus we see that there are many reports of excimer and charge-transfer complex formation. However, it is still challenging to design a general supramolecular pinning strategy which can provide essential pre-organization of chromophores for the formation of excimer and mixed charge transfer complex.

In this chapter, we describe a novel molecular design where, the supramolecular clippers drive the pre-organization of chromophores in solution and thus dictating the bimolecular photo-physical processes of resulting assemblies (Scheme 6.2.1). As a proof of this concept, we have designed chromophores end-functionalized with molecular recognition units, which serve as handles to position these molecules upon non-covalent interactions with multivalent guest molecules (supramolecular clippers).
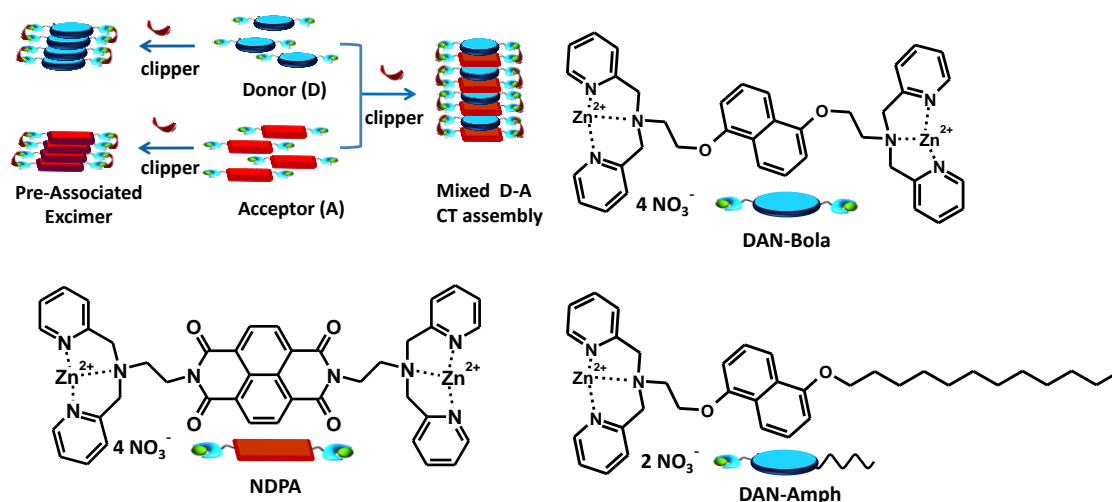
Scheme 6.2.1. *Chemical structures and schematic representations of DPA functionalized chromophores, **NDPA**, **DAN-Bola** and **DAN-Amph**. Top left: Pictorial representation of the supramolecular clipping approach for the homo and hetero pre-organization of D and A chromophores, which results in pre-associated excimer and alternate (mixed) D-A charge-transfer based assembly, respectively. Supramolecular clippers are multivalent guest molecules which binds specifically to the molecular recognition units of the chromophores.*

Dipicolylethylenediamine (DPA) motif is a well-known receptor for the selective binding of phosphate guest molecules and thus has been extensively used in the design of molecular phosphate sensors.[11] Hence, we have functionalized various chromophores with DPA units so that multivalent phosphates like AMP, ADP, ATP and PPi can be used as clipper molecules for the pre-organization of these chromophores. In this study, DPA derivatives of dialkoxynaphthalene (**DAN**-**Bola**) and naphthalenediimide (**NDPA**) were designed (Scheme 6.2.1) which on binding with multivalent phosphates resulted in strong pre-associated excimer, indicating the clipping action. In addition, phosphate clipping induced CT complexation between DPA functionalized NDI and DAN, a well-known donor-acceptor (D-A) pair,[12] is also demonstrated, thus proving the potential of this design for heterogeneous bi-component self-assembly (Scheme 6.2.1). Detailed photophysical and NMR studies further indicate that phosphate clipping also promotes higher order self-assembly of both homo and hetero-chromophoric systems, in agreement with our previous results.[13] In addition, amphiphilic DPA functionalized DAN derivative (**DAN-Amph**) provided insights into the crucial role of phosphate clipping for controlling these photophysical processes even in pre-aggregated assemblies.

6.2.2 Synthesis and Characterization
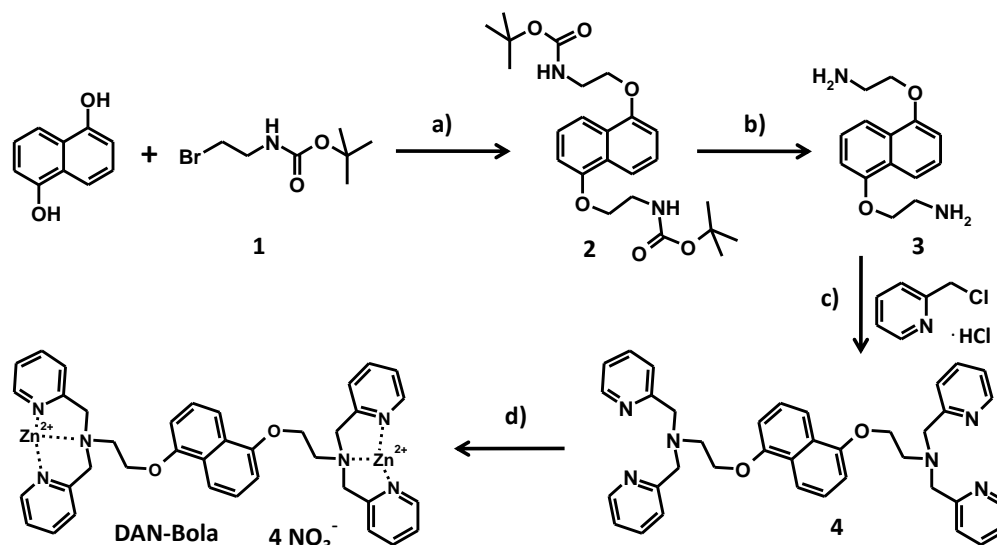
Scheme 6.2.2. *Chemical pathway for the synthesis of **DAN-Bola**. Reagents and conditions: (a) K_2CO_3, dry MeCN, 85 °C, 15 h; (b) TFA, DCM, 0 °C, 2 h; (c) 5M aq. NaOH, overnight; (d) $CHCl_3/MeOH$, $Zn(NO_3)_2.6H_2O$, 2 h.*

The synthesis of **DAN-Bola** and **DAN-Amph** were carried out following a multistep pathway as shown in Schemes 6.2.2 and 6.2.3, respectively (Section 6.2.7). **DAN-Bola** synthesis started with the alkylation of 1,5-dihydroxynaphthalene with BOC (tert-butyloxycarbonyl) protected bromoethylenediamine (**1**), which was then followed by the deprotection with TFA (trifluoroaceticacid) to yield diamine **3**. Electrophilic substitution on **3** with 2-(chloromethyl) pyridinehydrochloride gave **4**, which was then complexed with Zn^{2+} to yield the desired compound **DAN-Bola** (Scheme 6.2.2). For the synthesis of **DAN-Amph**, statistical alkylation of 1,5-dihydroxynaphthalene with **1** and dodecyl bromide was carried out to obtain **5** (Scheme 6.2.3). Further steps followed similar procedures as described for **DAN-Bola**. **NDPA** was synthesized based on a reported procedure.[14] All compounds were completely characterized by $^1H/^{13}C$ NMR and high resolution mass spectrometry (HRMS). Bolaamphiphilic derivatives, i.e. **NDPA** and **DAN-Bola**, were completely soluble in water and therefore all measurements were performed in aq. HEPES buffer (10 mM aq. HEPES solution). On the other hand, the amphiphilic derivative **DAN-Amph** was completely soluble in THF and was expected to trigger a surfactant-like self-assembly in water. Hence all the investigations of **DAN-Amph** were carried out in various solvent compositions of aq. HEPES in THF.
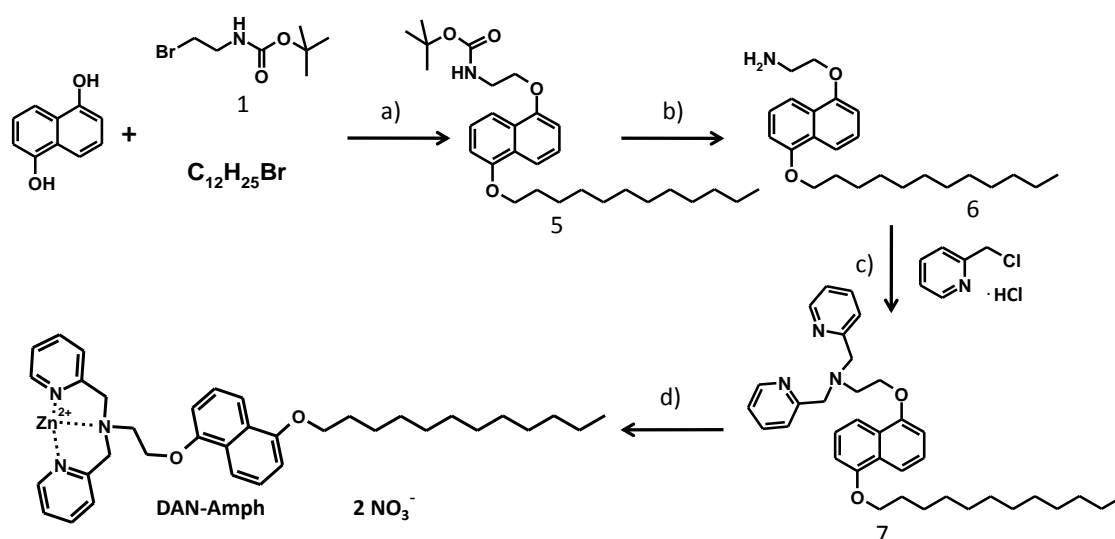
Scheme 6.2.3. *Chemical pathway for the synthesis of* **DAN-Amph.** *Reagents and conditions: (a) K_2CO_3, dry MeCN, 85 °C, 20 h; (b) TFA, DCM, 0 °C, 2 h; (c) 5M aq. NaOH, DCM, 15 h; (d) $CHCl_3/MeOH$, $Zn(NO_3)_2.6H_2O$, 4 h.*

6.2.3 Clipping Induced Pre-associated Excimer

We studied the phosphate clipping of individual D and A chromophores by probing their optical properties. **DAN-Bola** being molecularly soluble in water shows three sharp absorption bands at 297 nm, 312 nm and 325 nm in aq. HEPES buffer (c = 8 x 10^{-5} M). Upon binding with increasing eq. of adenosine triphosphate (ATP), a trivalent clipper molecule, gradual bathochromic shift (2 nm) along with decrease in absorbance and slight scattering at higher wavelengths were observed. These are clear signature of J-type inter-chromophoric organization in dialkoxy-naphthalene derivatives (Figure 6.2.4a).[15] Quite surprisingly, the corresponding emission spectra showed a gradual decrease in the monomeric emission at 342 nm, with simultaneous evolution of a significantly bathochromic emission band at 472 nm, which is 130 nm red-shifted compared to the monomeric emission, passing through an isoemissive point at 389 nm (Figure 6.2.4b). Such red shifted broad emission band with high fluorescence intensity and without any vibrational features is characteristic of excimer emission, well known in NDI, naphthalene or pyrene derived chromophores.[16] However, to our knowledge, this is the only report of excimer emission in dialkoxy naphthalene derivatives.
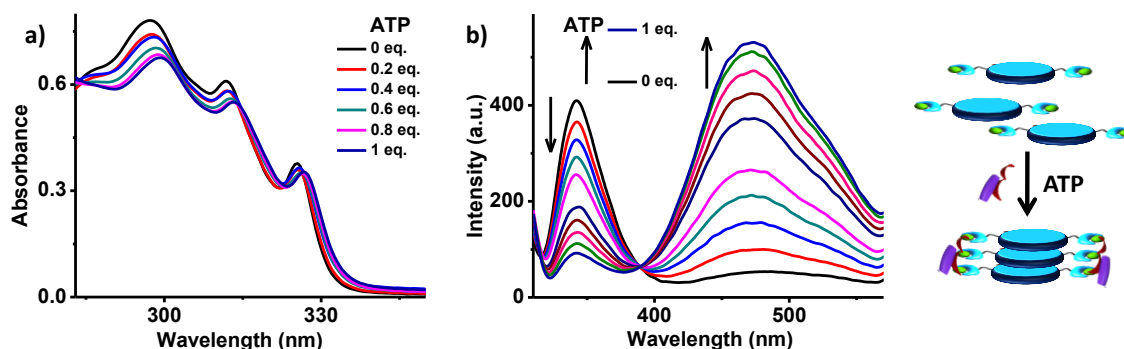
Figure 6.2.4. *a) Absorption and b) emission (λ_{ex}=300 nm) spectral changes of **DAN-Bola** upon titration with ATP. All measurements were done in 10 mM aq. HEPES buffer, c = 8 x 10^{-5} M in 10 mm cuvette. Schematics on the right-hand side show the molecular clipping process for pre-associated excimer.*

To probe into the nature of this excimer emission, excitation spectra were collected at monomeric (355 nm) and excimeric (480 nm) emission. Excitation spectra collected at 350 nm (without ATP, Figure 6.2.5a) appears like monomeric absorption of **DAN-Bola.** But, upon ATP binding, spectra collected at 490 nm is red shifted (4 nm) and broadened compared to the one collected at 350 nm (Figure 6.2.5a), characteristic of pre-associated excimer.[17] Thus providing an unambiguous proof of clipping induced pre-organization of chromophores in the ground state. Time correlated single photon counting studies were also done to characterize the excimer emission. Monitoring at 480 nm (excimer band) upon excitation at 310 nm showed biexponential decay with life-times of, τ_1=4.93 ns (33%) and τ_2=1.72 ns (67%) (Figure 6.2.5b). Such a high lifetime also indicates excited state stabilization through excimer formation.
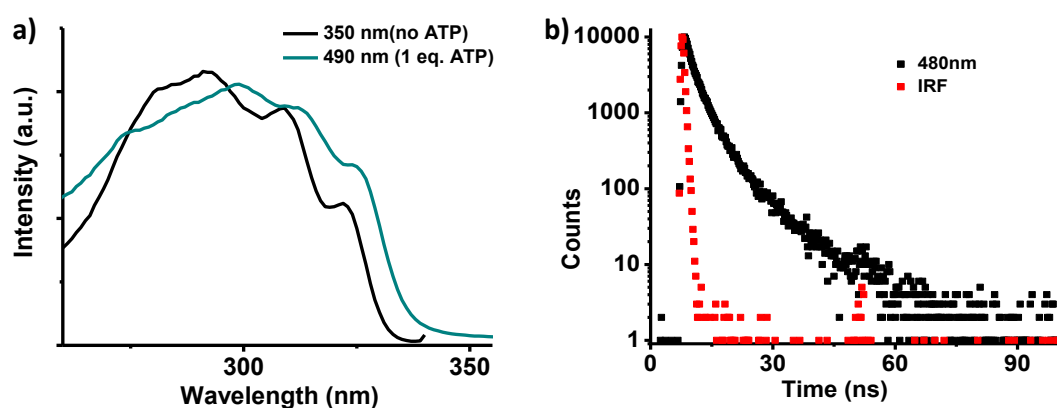

Figure 6.2.5. *a) Comparative excitation spectra collected at monomeric emission as well as excimeric emission for **DAN-Bola** with and without ATP. Fluorescence lifetime decay profile of **DAN-Bola** (λ_{ex}=310 nm) with 1 eq. ATP, monitored at excimeric emission. All measurements were in aq. HEPES buffer, c = 8 x 10^{-5} M (IRF=Instrument response function).*

In addition, binding of other multivalent phosphates like ADP or PPi ($P_2O_7^{4-}$) also showed excimer formation with varying degree of enhancement in 472 nm emission (Figure 6.2.6). On the other hand, addition of AMP, which is a monovalent phosphate, showed negligible excimer emission compared to others indicating the requirement of multivalent molecules for supramolecular clipping action.
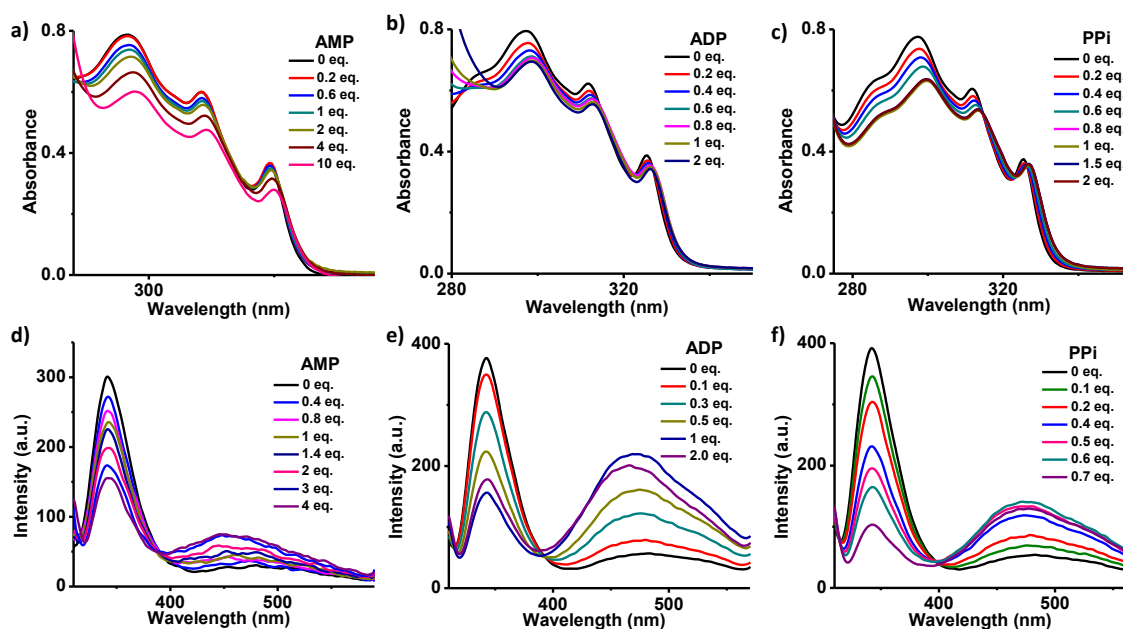
Figure 6.2.6. *Changes in absorption spectra upon titration of **DAN-Bola** with (a) AMP, (b) ADP and (c) PPi, whereas (d), (e) and (f) shows respective fluorescence spectra ($\lambda_{ex}=300$ nm). All measurements were done in 10 mM aq. HEPES buffer, c = 8 x 10^{-5} M in 10 mm cuvette.*

Similarly, binding of pyrophosphate clipper to **NDPA** (c = 8 x 10^{-5} M) also resulted in their aggregation, marked by the changes in absorption spectra. With increasing eq. of PPi, λ_{max} of **NDPA** showed a red shift from 383 nm to 385 nm with broadening of absorption bands and reversal of their peak intensity ratio (I_{0-0}/I_{0-1} from 1.2 to 0.77, Figure 6.2.7a).[18] Emission spectra showed decrease in the monomeric emission at 411 nm with concomitant evolution of a red shifted broad band centred at 485 nm (Figure 6.2.7b), similar to the observation in **DAN-Bola**. This highly emissive band has been assigned to pre-associated excimer formation by **NDPA**, as evident from their excitation spectra (Figure 6.2.7c)[5, 17] which show a new red shifted aggregate band. This is shown to have originated from the clipping of chromophores upon selective PPi binding.[14, 19] Thus, preassociated nature of excimer emission and the unique ability of multivalent phosphates to induce excimeric emission validate our design of guest induced pre-organization through supramolecular clipping of chromophores.
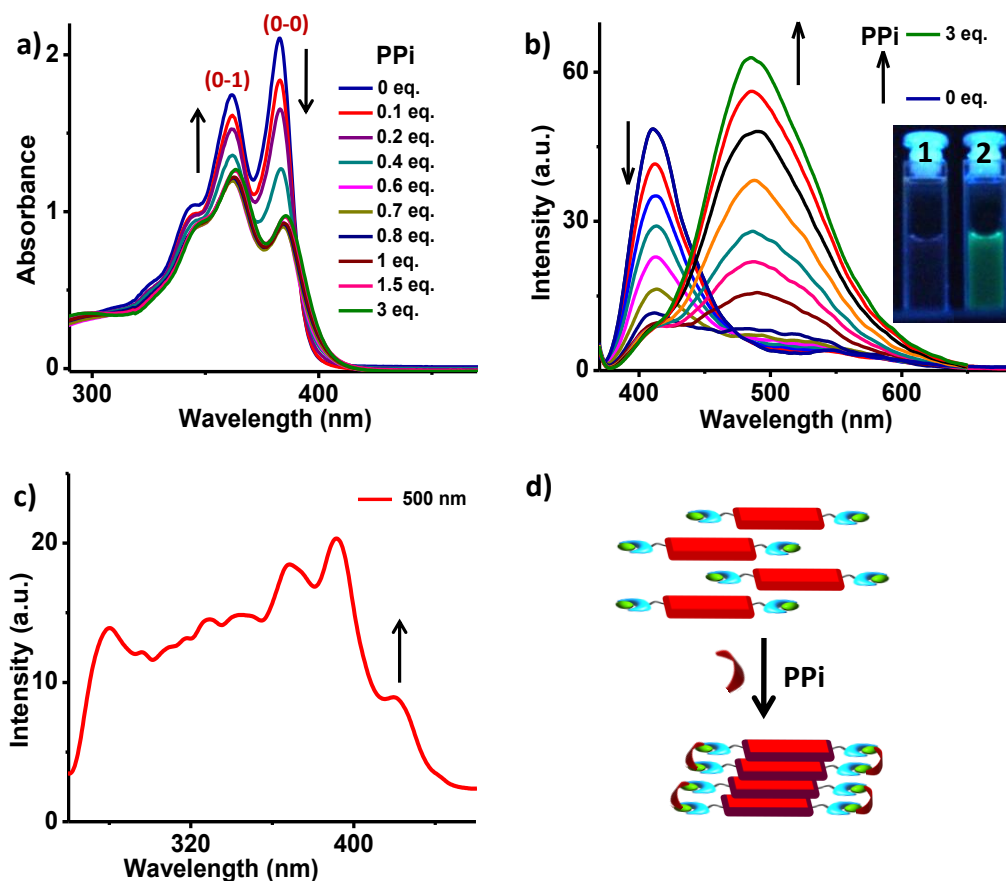
Figure 6.2.7. *a) and b) show respective changes in absorption and fluorescence (λ_{ex}=350 nm) spectra of **NDPA** on binding with PPi. Inset in b) shows photographs of **NDPA** solution 1) without and 2) with PPi under UV illumination (365 nm). c) Excitation spectra collected at excimeric emission for **NDPA** with 0.7 eq. PPi demonstrating its pre-associated (aggregated) nature. All measurements were done in 10 mM aq. HEPES buffer, c = 8 x 10^{-5} M in 10 mm cuvette. Schematics on the right hand side show the molecular clipping process for pre-associated excimer.*

Our previous studies with DPA-functionalized molecules have shown that molecular recognition of multivalent guest molecules results in one-dimensional self-assembly of chromophores, probably through simultaneous clipping at two or more consecutive binding sites, resulting in supramolecular stitching of chromophores along the stacking direction (Chapter 2).[13] Using dynamic light scattering and transmission electron microscopy experiments we have shown that supramolecular clipping of **NDPA** results in extended assembly rather than terminating the growth at dimeric or tetrameric level. Inter-chromophoric interactions are known to decrease the emission intensity of various chromophores, including NDI and DAN derivatives.[20] In the present investigation, it is evident that even though phosphate binding induces self-assembly of both these derivatives, emission is enhanced and

retained in their assembly through aggregation induced enhanced emission (AIEE) mechanism[21] i.e. via formation of pre-associated excimer as shown in other NDI derivatives (Figure 6.2.1, 6.2.2).[5] Thus, phosphate binding induced clipping of chromophores presents a simple and rational approach for the construction of fluorescent (AIEE) assemblies.

To investigate the role of clipping induced pre-organization and general scope of our excimer design strategy, we have synthesized amphiphilic DAN derivative, **DAN-Amph**, which exists as free molecules in THF and self-assembles in the presence of water due to hydrophobic and aromatic-aromatic interactions. Unlike **DAN- Bola** which could aggregate only in presence of phosphates, interchromophoric interactions in **DAN-Amph** could be achieved without phosphates in presence of polar solvents like water.
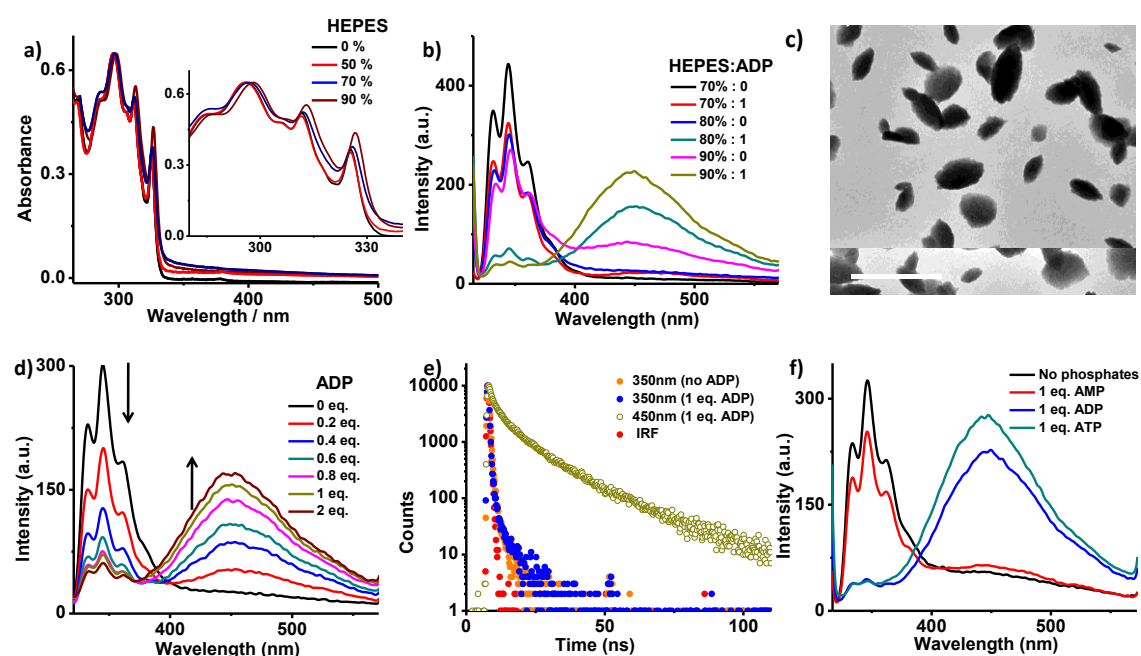
Figure 6.2.8. *a) Normalized absorption spectra of **DAN-Amph** with varying HEPES composition in THF, whereas b) shows solvent dependent emission (λ_{ex}=300 nm) changes on binding to 1 eq. of ADP. Inset in a) shows the corresponding zoomed in portion showing aggregation features in absorption. c) TEM images of self-assembled **DAN-Amph** with 1 eq. ATP. d) Emission spectra of **DAN-Amph** (λ_{ex}=300 nm) upon titration with ADP and e) fluorescence lifetime decay profile of **DAN-Amph** (λ_{ex}=310 nm) with no ADP and 1 eq. ADP, monitored at monomeric (350 nm) and excimeric emission (450 nm). f) Comparative emission spectra of **DAN-Amph** (λ_{ex}=300 nm) with various adenosine phosphates (1 eq. each). d)–f) were recorded in 90% HEPES in THF. All measurements were done in 10 mm cuvette, c =7 x 10^{-5} M.*

On increasing the percentage of HEPES, **DAN-Amph** begins to aggregate as seen from the slight red shift in the absorption maxima and appearance of scattering along with decrease in monomeric emission (Figure 6.2.8 a, b). Formation of higher order assembly upon phosphate binding in 90% HEPES was evident from TEM analysis, which showed the presence of short nanostructures (Figure 6.2.8c). However, significant excimer emission could not be observed even in 90% HEPES in THF solvent mixture (Figure 6.2.8b). Remarkably, upon titration with ADP (90% HEPES in THF, c = 7×10^{-5} M), the monomeric emission (345 nm) further decreases with the emergence of a new red shifted band at 450 nm (Figure 6.2.8d), which is assigned to excimer formation (*vide supra*). This suggests that even in pre-assembled chromophores, molecular clipping has the unique role of inducing appropriate pre-organization in the ground-state required for excimer formation. Characterization of excimer emission was again probed with time resolved fluorescence measurements. Fluorescence decay profile of **DAN-Amph** without ADP (90% HEPES in THF, c = 7×10^{-5} M) monitored at 350 nm (λ_{ex} = 310 nm), shows very fast decay as expected of monomeric species (Figure 6.2.8e). Upon binding with ADP, monitoring the emission at 350 nm again shows similar very short lived species indicative of monomeric species. Monitoring at excimeric band (450 nm) showed a triexponential decay with lifetimes of τ_1 = 16.82 ns (27%), τ_2 = 5.44 ns (27%) and τ_3 = 1.07 ns (46%). Existence of such high lifetimes proves the pre-associated nature of this excimer emission.

Further emission studies of **DAN-Amph** with 1 eq. of bound ADP in various solvent compositions showed that the excimer intensity increases with HEPES percentage in THF (Figure 6.2.8b) i.e. 90% HEPES solution showed higher excimer intensity compared to 80% or 70% HEPES composition. Also there is weak emission at 450 nm even without ADP as seen in 90% HEPES mixture. These two facts indicate that pronounced aggregation of chromophores (at higher HEPES percentages) can indeed assist in the pre-orientation of chromophores, but it cannot be a substitute for phosphate binding in inducing the excimer formation. In addition, a comparison among various phosphate binding shows that excimer emission is highest for stronger binding guest ATP, and least for AMP (weakest binding), whereas ADP falls in between (Figure 6.2.8f), thus providing a simple means for controlling the intermolecular interactions and the emission properties.

With this we have shown the phosphate binding induced clipping for excimer formation in **NDPA, DAN-Bola** and **DAN-Amph** derivatives. This justifies the broader scope of dipicolylethylenediamine functionality based design strategy for guest induced pre-organization of chromophores leading to excimer formation.

## 6.2.4 Clipping Induced Donor-Acceptor Co-assembly

Having established the role of clipping in pre-organizing individual chromophores, we extended it to the hetero-dimerization of D and A molecules for the construction of mixed CT assemblies. Several molecular designs have been utilized in literature for obtaining effective CT between DAN and NDI derivatives,[8,12] a well studied donor-acceptor (D-A) pair. Since pre-organization of D and A chromophores in a face-to-face manner is a prerequisite for these mixed (alternate) CT complexes, we investigate the potential of present molecular clipping design for co-facial D-A alternate assembly.
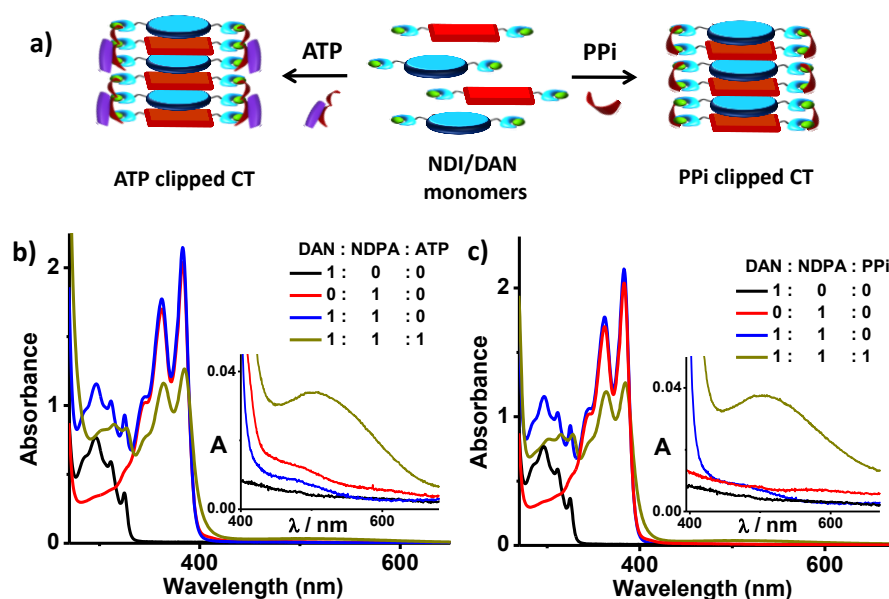
Figure 6.2.9. *a) Schematic representation of ATP/PPi clipped mixed CT stack formation of DPA functionalized NDI (A) and DAN (D) chromophores. Absorption spectra of **NDPA** (NDI), **DAN-Bola** (DAN) and their 1:1 CT complex upon binding of b) ATP, c) PPi. Insets show the corresponding zoomed in portions of absorption spectra near CT transition region. All measurements were performed in 10 mM aq. HEPES buffer, c = 8 x 10^{-5} M in 10 mm cuvette. Low intensity band at 475 nm seen in the absence of ATP (blue curve) is due to noise and not a CT band.*

Thus co-assembly of **NDPA** and **DAN-Bola** (aq. HEPES buffer, 8×10^{-5} M) was investigated in presence of multivalent phosphates, to study the role of guest binding in hetero pre-organization. As shown above, both these chromophores show absorption and emission features of molecularly dissolved state in the absence of any binding phosphates. When these chromophores were mixed in 1:1 molar ratio in the absence of any clippers, the absorption features of individual D and A were retained, indicating no interaction between the D-A pair (Figure 6.2.9b). In addition, absence of any new low-energy absorption band, corresponding to

CT transition, clearly rules out formation of any D-A complex. Remarkably, addition of 1 eq. of ATP to the solution of D and A mixture, showed a clear change in the absorption spectral features. Apart from inducing aggregation to these chromophores, binding of ATP resulted in the appearance of a new red-shifted broad band at 510 nm, characteristic of ground state CT complex formation between NDI-DAN D-A pair.[8,12] Similar experiments with other divalent phosphates, such as PPi and ADP, also resulted in alternate D-A complex as evident from the red shifted absorption band (Figure 6.2.9c, Figure 6.2.11a). Monitoring the emission spectra also corroborates with the formation of clipping induced charge-transfer complex formation. For example, emission spectra of a 1:1 mixture of **NDPA** and **DAN-Bola** with clipping phosphates (ATP), upon excitation at 300 nm showed significant quenching of monomeric or excimeric emissions of both the components, characteristic of charge-transfer interactions (Figure 6.2.10a). On the other hand, as expected, binding of monovalent AMP did not show any characteristics of CT formation, due to their inability to clip the chromophores together (Figure 6.2.11a). ATP binding induced 1:1 CT complex formed extended supramolecular assembly, as evident from the TEM analysis which showed short nanostructures (Figure 6.2.10b).
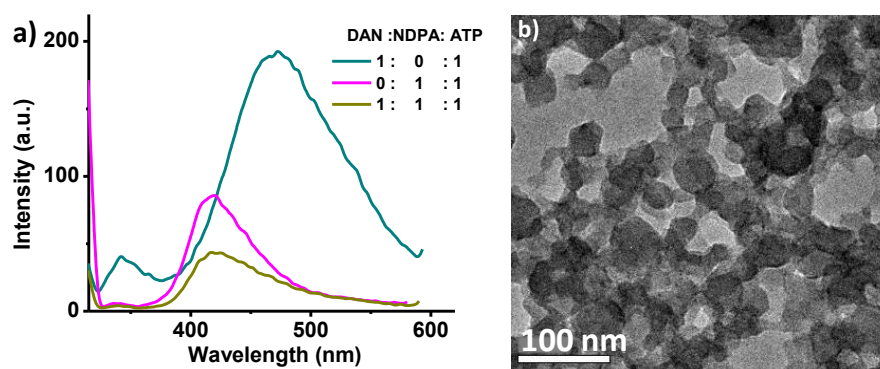
Figure 6.2.10. a) Steady state emission spectra of NDPA, DAN-Bola and their 1:1 complex upon binding of ATP (λ_{ex}=300 nm) (c = 8 x 10^{-5} M in aq HEPES buffer). Quenching of monomeric and excimeric emission proves CT formation. b) Nanostructures formed by 1:1 D-A assembly of DAN-Bola (D) and NDPA (A) with 1 eq. ATP (c = 8 x 10^{-5} M in water).

Interestingly, comparing the CT band intensity at 510 nm with different binding phosphates showed that the strength of CT complexation is highest for ATP followed by ADP whereas AMP with only one binding site fails to induce CT formation (Figure 6.2.11a). This is in agreement with the higher binding strength of ATP through three point clipping compared to its lower analogues like ADP and AMP, due to multivalent interactions. Thus, it is evident that the role of phosphate clipping is very crucial in providing appropriate organization and association energy for CT complexation in the present system. Moreover, supramolecular

clipping provides a unique and very simple handle to control and tune the strength of CT complexation between same D-A pair without any tedious structural modifications; but just by changing the clipper molecules. A simple strategy like presented here, for tuning the strength of CT provides an additional dimension to their potential use in various applications in organic electronic and ferroelectric materials.[22]
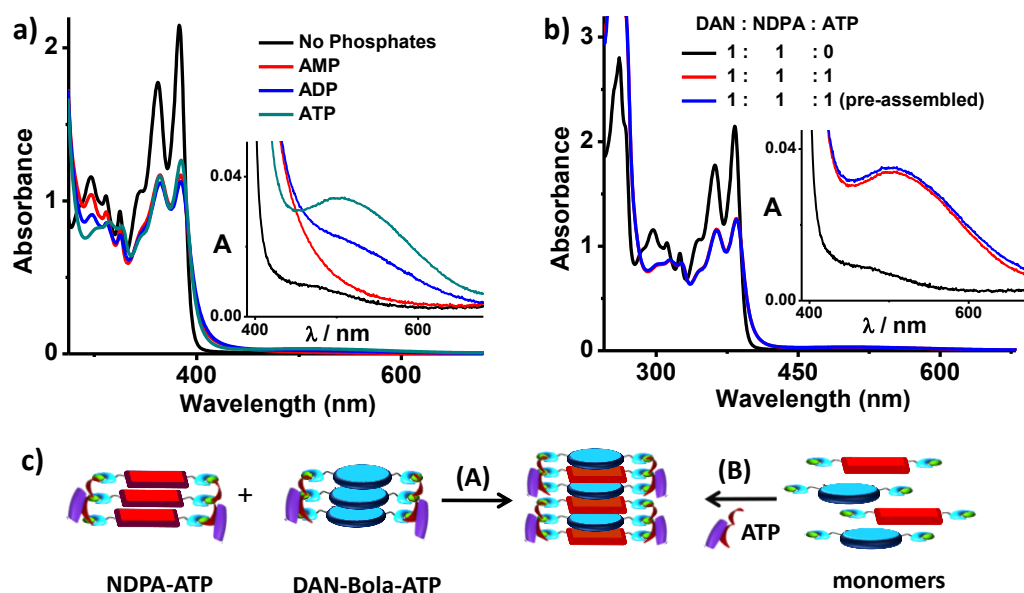

Figure 6.2.11. *Absorption spectra of **NDPA**, **DAN-Bola** and their 1:1 complex upon binding with a) all three adenosine phosphates showing comparative strengths of 1:1 CT formation.[23] b) Shows the comparison of CT formation between mixing of pre-assembled stacks of D and A molecules using ATP (method (A)) with that of in situ construction by the addition of ATP to a mixture of D and A monomers (method (B)). c) Schematic representation of these two methods is shown in c). Insets show the corresponding zoomed in portion of absorption spectra near CT transition region. All measurements were done in 10 mM aq. HEPES buffer, c = 8 x 10^{-5} M, 10 mm cuvette.*

We further investigated the dynamic nature of the chromophores and phosphate clipping in these supramolecular aggregates using CT as a probe. For that, we have mixed the individual stacks of both **NDPA** and **DAN-Bola**, which are pre-assembled with 1 eq. of ATP and monitored the kinetics of CT band formation. Interestingly, charge-transfer band due to the formation of alternate D-A assembly was fully attained within seconds, suggesting a very fast dynamics of all the components in this assembly (Figure 6.2.11b). This was further confirmed by similar experiments with other guests like ADP and PPi. Insight into phosphate binding induced extended aggregation of mixed D-A chromophores was provided by NMR measurements. In the absence of any clipping guests, 1:1 mixture of **NDPA** and **DAN-Bola** did

not show any shift or broadening of their characteristic peaks, indicating the existence of non-interacting monomeric chromophores. However, complete broadening of the peaks was observed on guest binding, confirming the formation of extended aggregates (Figure 6.2.12, Figure 6.2.13).
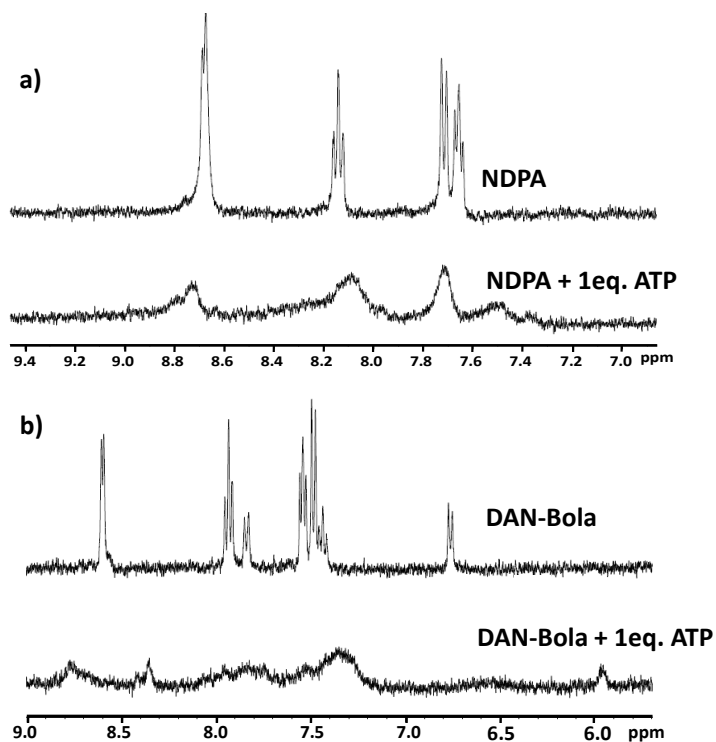
Figure 6.2.12. *Partial ^1H NMR spectra showing changes in the aromatic region of a)* **NDPA** *and b)* **DAN-Bola** *with and without ATP. All measurements were done in D_2O, $c = 3 \times 10^{-4}$ M.*
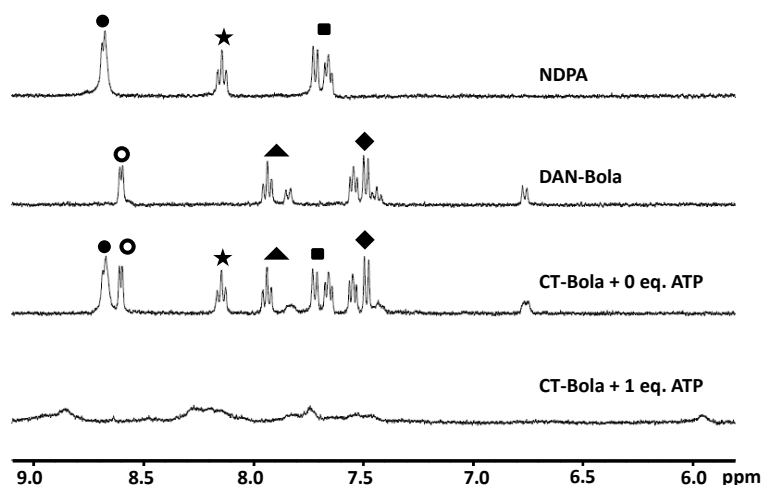
Figure 6.2.13. *Partial ^1H NMR spectra showing changes in the aromatic region of* **NDPA**, **DAN-Bola** *along with their 1:1 complex with and without ATP. All measurements were done in D_2O, $c = 3 \times 10^{-4}$ M.*

Chiral Organization of Mixed Charge-Transfer Chromophores

An interesting feature of the supramolecular clippers used in the present study is their molecular chirality, which can be expressed in stacked chromophores and helically bias their pre-organization during clipping action. This would result in the expression of supramolecular chirality to excitonically coupled chromophores and mixed D-A assemblies. Although, chiral clipping induced helical assembly has been reported in polymeric[24] and one-dimensional supramolecular assembly,[25] chirality induction in charge-transfer coupling between alternatively stacked D and A molecules using supramolecular clipping design is not yet reported.
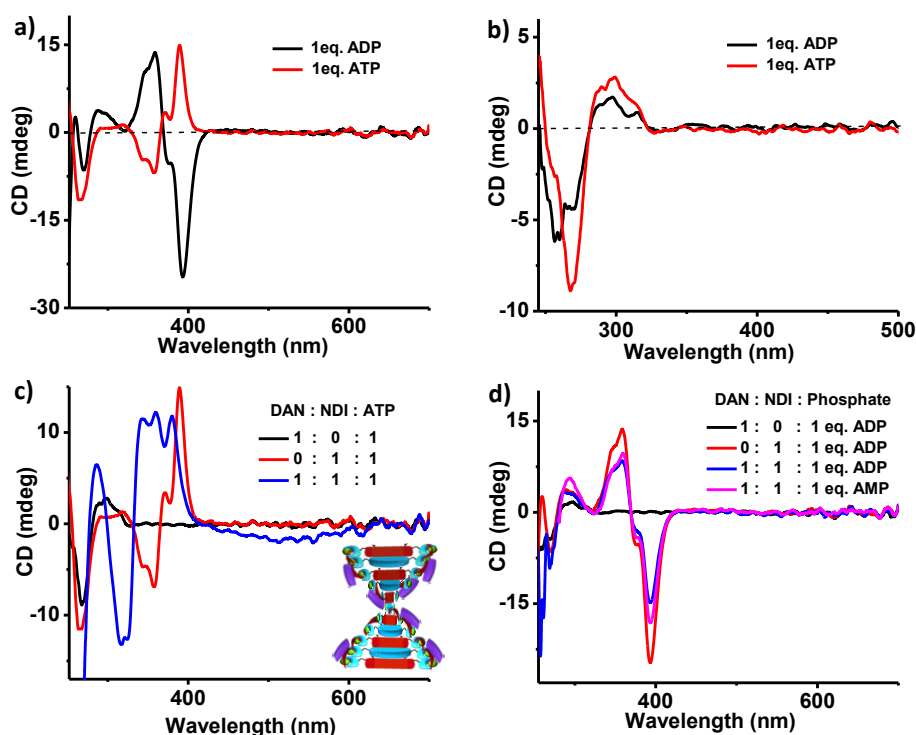
Figure 6.2.14. *CD spectra of a)* ***NDPA*** *and b)* ***DAN-Bola*** *with 1 eq. of ADP and ATP, and their 1:1* ***DAN-Bola:NDPA*** *co-assembly formed with chiral guests c) ATP, d) ADP and AMP. Inset in c) shows schematic illustration of CT based helical co-assembly. All measurements were done in 10 mM aq. HEPES buffer, c = 8 x 10^{-5} M in a 10 mm cuvette.*

Motivated by this, we have further probed the chiroptical properties of the present phosphate clipped chromophoric stacks. Chiral clipping of **NDPA** by ATP and ADP biases the organization of chromophores in right- and left-handed helical organizations, respectively as reported in Chapter 2.[13] This differential bias in organization and the presence of excitonically coupled chromophores upon phosphate clipping were signalled by the oppositely bisignated circular dichroism (CD) spectral features. (Figure 6.2.14a). On the other hand, binding of ATP or ADP to **DAN-Bola** resulted in a positive bisignated CD signal, with 299 nm and 267 nm as

the positive and negative maxima respectively, again suggesting the expression of helical bias to the chromophoric organization (Figure 6.2.14b). These CD signals were significantly distinct compared to that of individual ATP or ADP clippers, though a partial contribution from them cannot be ruled out. Having confirmed the chirality induction into individual organization of D and A chromophores, we further looked at the role of chiral clippers in biasing their co-assembled CT state. Interestingly, binding of 1 eq. of ATP to a 1:1 mixture of **NDPA** and **DAN-Bola** chromophores (aq. HEPES buffer, c = 8 x 10^{-5} M), showed a strongly coupled bisignated CD signal (Figure 6.2.14c). The signal obtained is distinctly different when compared with that of individually organized NDI and DAN chromophores, as evident from the broadening of CD signal in the 350 nm range, with shift in the CD zero crossing point from 365 nm to 332 nm, suggesting the chiral co-organization of D-A complex. In addition, a broad monosignated CD band with a maximum at 500 nm was observed, which lies in the absorption region of characteristic CT transition. These observations clearly confirm the presence of strong excitonically coupled and helically organized mixed CT assemblies. Such chiral CT complexes displaying strong CD signals are seldom reported in literature[26] and the present system provides the only report of clipping induced chirality in CT complexes. Similar experiments performed on binding of ADP/AMP with the D and A chromophoric mixture, failed to show any such features in the CD signal, but rather retained the individual CD signatures of DAN and NDI (Figure 6.2.14d), reiterating the weak or insignificant CT formation as reflected in the intensity of CT band in their absorption spectra (Figure 6.2.11a).

6.2.5 Conclusions

We have demonstrated a new design strategy for the pre-organization of chromophores to modulate their photophysical properties based on supramolecular clippers. Dipicolylethylenediamine (DPA) motif, a well known receptor for phosphate groups, was utilized as the molecular recognition unit, whereas multivalent adenosine phosphates were used as supramolecular clippers.

As a proof of principle, we synthesized 1,5-dialkoxynaphthalene (DAN) functionalized with DPA motif which could pre-organize upon non-covalent binding with adenosine di/tri phosphates. Phosphate clipping led to aggregation induced pre-associated excimer formation in DAN assemblies, hitherto unknown in various DAN derivatives. This design could be generalized by extending it to the excimer formation in DPA functionalized Naphthalenediimide (NDI) derivative as well. Detailed spectroscopic studies, with self-aggregating amphiphilic, DPA appended DAN derivative, revealed the unique task of phosphate clippers in providing the appropriate pre-organization of chromophores for excimer formation.

Adenosine phosphate clipping was also applied for the heterogeneous assembly of donor and acceptor chromophores, as shown by clipping induced charge transfer (CT) complex formation. DAN and NDI, a well known donor-acceptor pair could be arranged in a co-facial manner only in presence of these phosphates.

Apart from controlling the photophysical properties, phosphate clippers, being chiral, also induced helical bias to the homo- and hetero-chromophoric assemblies, as evident from the chiroptical studies. Chirality induction in the CT transition by the helical organization of the donor-acceptor co-assembly is seldom achieved and would be of great interest in chirotechnological applications.

It is evident that clipping induced modulation of chromophoric organization was primarily responsible for the observed bimolecular photophysical properties in the present systems. Remarkably, this design also allows the modulation of inter-chromphoric interactions by varying the binding strength of clipper molecules. Thus we believe that the supramolecular clipping approach presented here holds great promise in controlling various interchromophoric phenomena like energy/electron transfer, which can be investigated in future.

6.2.6 Experimental Section

General Methods:

Transmission Electron Microscopy (TEM): TEM measurements were performed on a JEOL, JEM 3010. Samples were prepared by placing a drop of the solution on carbon coated copper grids followed by drying at room temperature. The images were recorded with an operating voltage 300 kV. In order to get a better contrast samples were stained with uranyl acetate (1 wt % in water) before the measurements. For TEM, water was used instead of aq. HEPES solution to avoid masking of nanostructures due to HEPES deposition upon drying.

Atomic Force Microscopy (AFM): AFM measurements were performed on a Veeco diInnova SPM operating in tapping mode regime. Micro - fabricated silicon cantilever tips doped with phosphorus and with a frequency between 235 and 278 kHz and a spring constant of 20-40 Nm^{-1} were used. The samples were prepared by drop casting 10^{-3} M solution of **1** in 90% (v/v) water in methanol on glass substrate and dried in air followed by vacuum drying at room temperature.

Optical Measurements: Electronic absorption spectra were recorded on a Perkin Elmer Lambda 900 UV-Vis-NIR Spectrometer and emission spectra were recorded on Perkin Elmer Ls 55 Luminescence Spectrometer. UV-Vis and emission spectra were recorded in 10 mm path length cuvettes. Fluorescence spectra of solutions were recorded with 350 nm or 300 nm excitation wavelength. Circular Dichroism measurements were performed on a Jasco J-815

spectrometer where the sensitivity, time constant and scan rate were chosen appropriately. CD spectra were smoothened using adjacent averaging method.

Confocal Microscopy Imaging: Confocal Microscopy imaging was done at room temperature using a Zeiss LSM 510 META laser scanning confocal microscope. The microscope objective of 63X (NA 1.4) and 20X (NA 0.5) were employed. Sample was prepared by sealing the solution between two glass plates.

NMR Measurements: NMR spectra were obtained with a Bruker AVANCE 400 (400 MHz) Fourier transform NMR spectrometer with chemical shifts reported in parts per million (ppm) with respect to solvent residual peak .

High-Resolution Mass-Spectrometry (HR-MS): HRMS measurements were performed with Agilent Technologies Q-TOF-LCMS system, 6538 instrument. Measurements were done in ESI mode (positive mode).

Matrix-assisted laser desorption ionization time-of-flight (MALDI-TOF): MALDI-TOF spectra were obtained on a Bruker ultraflex 2 MALDI-TOF mass spectrometer with α-cyano-4-hydroxycinnamic acid matrix.

Single Photon Counting Spectrometer: Fluorescence decay was recorded in a timecorrelated single-photoncounting spectrometer of Horiba-Jobin Yvon with 310 nm nanosecond LED.

Sample Preparation: All samples for spectroscopic measurements were prepared by injecting the aqueous stock solution of **NDPA** or **DAN-Bola** into required volume of aq. HEPES buffer (HEPES - (4-(2-hydroxyethyl)-1-piperazineethanesulfonic acid). For **DAN-Amph** THF stock solution was injected into required volume of aq. HEPES-THF composition. To these appropriate amount of phosphates were injected and the solution was mixed by manual shaking before measurements.

For CT measurements, both the stock solutions of D and A were mixed and then introduced into appropriate solvents followed by phosphate addition.

For pre-complex dynamic CT experiment shown in Figure 6.2.11b, individual **NDPA** and **DAN-Bola** were separately pre-complexed with 1 eq. of ATP and then the two solutions were mixed together.

Materials: N,N-Bis(2-pyridylmethyl)ethane-1,2-diamine was synthesized based on reported procedure.[27] All other chemicals were purchased from the commercial sources and were used as such. Spectroscopic grade solvents were used for all optical measurements.

Synthesis and Procedures
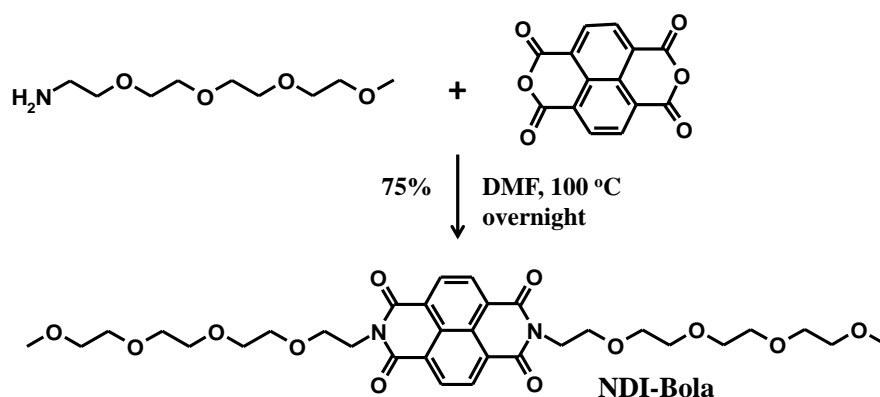
Scheme 6.2.4. Chemical pathway for the synthesis of NDI-Bola.

Synthesis of **NDI-Bola:** 0.53 g (2 mmol) of 1,4,5,8–naphthalenetetracarboxylic dianhydride and 0.91 g (4.37 mmol) of methoxytetraethylene-glycolamine[28] in 15 ml DMF was heated at 110 °C for 12 h. After the removal of DMF, the reaction mixture was extracted with $CHCl_3$ and washed with water. Organic layer was dried with anhydrous Na_2SO_4 and solvent was removed under vacuum. Silica gel column chromatography (100-200 mesh, eluent 5% MeOH in $CHCl_3$) followed by precipitation in diisopropyl ether gave 0.97 g of **NDI-Bola** in 75% yeild. ^{1}H NMR δ_H (400 MHz; $CDCl_3$; Me_4Si): 8.75 (s, 4H, ArH), 4.46 (t, J=7 Hz, 4H, N-CH_2), 3.85 (t, J=7 Hz, 4H, N-CH_2CH_2), 3.5-3.7 (m, 24H, CH_2), 3.35 (s, 6H, O-CH_3) ; ^{13}C NMR δ_C (100 MHz, $CDCl_3$): 163.01, 131.12, 126.92, 126.79, 72.06, 70.76, 70.71, 70.63, 70.28, 67.94, 59.14, 39.76 ; MALDI-TOF MS m/z: 669.37 [M+Na^{+}], HRMS (TOF-MS ES+): m/z: calcd for $C_{32}H_{42}N_2O_{12}Na^+$: 669.2635 [M+Na^{+}], found: 669.2440.
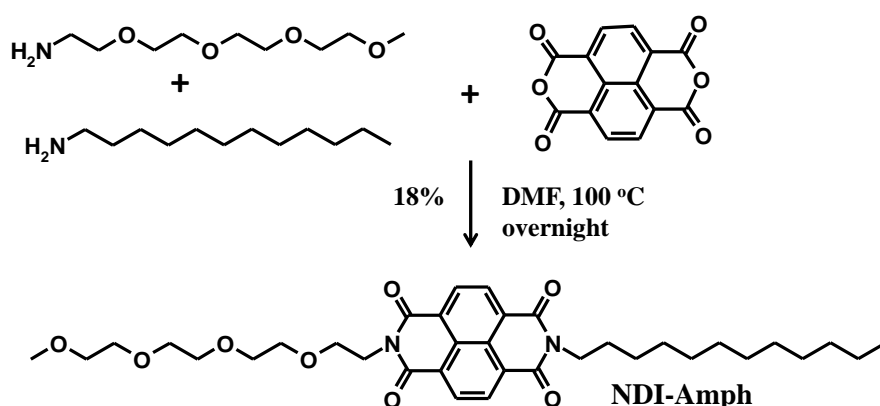
Scheme 6.2.5. Chemical pathway for the synthesis of NDI-Amph.

Synthesis of **NDI-Amph:** 0.97 g (3.645 mmol) of 1,4,5,8–naphthalenetetracarboxylic dianhydride, 0.91 g (4.37 mmol) of methoxytetraethylene-glycolamine[28] and 0.81 g (4.37

mmoles) of dodecylamine were taken in 25 ml DMF and heated at 110 °C for 24 h. Upon cooling the reaction mixture DMF was removed under vacuum. The reaction mixture was extracted with CHCl$_3$ and washed with water. Organic layer was dried with anhydrous Na$_2$SO$_4$ and solvent was removed under vacuum. Silicagel column chromatography (100-200 mesh, eluent 5 - 10% MeOH in CHCl$_3$) gave **NDI-Amph** (0.32 g, 14% yield) along with Boloamphiphilic product[5b] (0.43 g, 18% yield) and the di-dodecyl derivative. ^{1}H NMR δ_H (400 MHz; CDCl$_3$; Me$_4$Si): 8.75 (s, 4H, ArH), 4.45 (t, J=6 Hz, 2H, N-CH$_2$ of tetraethyleneglycol {TEG}), 4.18 (t, J=7.6 Hz, 4H, N-CH$_2$ of dodecyl), 3.84 (t, J=5.6 Hz, 2H, N-CH$_2$CH$_2$ of TEG), 3.70-3.49 (m, 12H, CH$_2$ of TEG), 3.35 (s, 3H, O-CH$_3$); 1.77-1.25 (m, 20H, CH$_2$ of dodecyl), 0.87 (t, J=7 Hz, CH$_3$ of dodecyl); ^{13}C NMR δ_C (100 MHz, CDCl$_3$): 163.05, 162.95, 131.13, 131.05, 126.93, 126.88, 126.85, 126.71, 72.07, 70.76, 70.71, 70.63, 70.29, 67.95, 59.14, 41.16, 39.75, 32.05, 29.77, 29.76, 29.73, 29.66, 29.47, 28.23, 27.24, 22.82, 14.24 ; ESI- MS m/z: 647.55 [M+Na]$^+$, HRMS (TOF-MS ESI+): m/z: calcd for C$_{35}$H$_{48}$N$_2$O$_8$Na$^+$: 647.3308 [M+Na]$^+$, found: 647.3127.

NDPA and compound **1** was synthesized following the reported procedure and was characterized accordingly.[14]

Synthesis of **DAN-Bola** was peformed according to Scheme 6.2.2. Procedures are given below.

Synthesis of 2: 300 mg (1.87 mmol) of 1,5-Dihydroxynaphthalene and 2 g of dry K$_2$CO$_3$ along with 10 mL of dry MeCN were stirred for 10 minutes at 50 °C. To this solution 1.05 g (4.68 mmol) of **1** in 5 mL of dry MeCN was added and whole solution was refluxed for 15 h under inert atmosphere. MeCN was evaporated under low pressure and the residue obtained was dissolved in CH$_2$Cl$_2$. This solution was filtered to remove insoluble K$_2$CO$_3$ and filtrate obtained was extracted with water and brine. The organic layer was dried over Na$_2$SO$_4$ and evaporated. Compound was purified by column chromatography (Silica gel, 100-200 mesh, eluent 5% MeOH in CHCl$_3$) to obtain 320 mg of pure product in 38% yield. ^{1}H NMR δ_H (400 MHz; CDCl$_3$; Me$_4$Si) : 7.84 (d, 2H, J = 8.4 Hz), 7.36 (t, 2H, J = 8 Hz), 6.84 (d, 2H, J = 7.6 Hz), 4.19 (t, 4H, J = 4.8 Hz), 3.68 (q, 4H, J = 4.8 Hz), 1.45 (s, 18H); MS (EI): m/z: calcd for C$_{24}$H$_{34}$N$_2$O$_6$: 446.5 [M]$^+$, found : 446.

Synthesis of 3: 10 mL of trifluoroacetic acid (TFA) was dissolved in 10 mL of DCM and the solution was stirred at 0 °C. 300 mg (0.67 mmol) of **2** was dissolved in 10 mL of DCM and was added to the above solution dropwise over 20 minutes. The reaction mixture was stirred at 0 °C for 1 hr and at rt for 1 hr. TLC was checked to confirm the completion of reaction. TFA and DCM were removed under low pressure and the residue was dissolved in DCM. The whole solution was neutralized with 2 M NaOH solution and the product was washed with water and extracted with DCM. Organic layer was dried over Na$_2$SO$_4$ and solvent was removed. Product

was characterized with NMR and proceeded to next step without any further purification. ^{1}H NMR δ_H (400 MHz; CDCl$_3$; Me$_4$Si): 7.86 (d, 2H, J = 8.4 Hz), 7.36 (t, 2H, J = 8 Hz), 6.86 (d, 2H, J = 7.6 Hz), 4.17 (t, 4H, J = 5.2 Hz), 3.22 (t, 4H, J = 5.2 Hz).

Synthesis of 4: 120 mg (0.48 mmol) of crude **3** and 400 mg (2.43 mmol) of 2-(Chloromethyl)pyridinehydrochloride along with 20 mL of 5 M aq. NaOH solution was stirred at room temperature overnight. Some precipitate formation was observed and to make sure that everything undergoes complete substitution, 10 mL of DCM was added and the whole solution was stirred for another 3 h. The reaction mixture was extracted with DCM and organic layer was dried over anhydrous Na$_2$SO$_4$. DCM was removed at reduced pressure and the compound obtained was purified by neutral alumina column, initially with 1% MeOH in CHCl$_3$ which removed most of the impurities and later increased polarity to 3% MeOH in CHCl$_3$ to give pure compound 93 mg in 32% yield. ^{1}H NMR (400 MHz, CDCl$_3$, TMS) : δ 8.53 (td, 4H, J = 1.2 Hz, 4.8 Hz), δ 7.79 (d, 2H, J = 8.4 Hz), δ 7.61 (m, 8H), δ 7.29 (t, 2H, J = 8 Hz), δ 7.15 (m, 4H), δ 6.76 (d, 2H, J = 7.6 Hz), δ 4.27 (t, 4H, J = 5.6 Hz), δ 4.07 (s, 8H), δ 3.24 (t, 4H, J = 5.6 Hz); ^{13}C NMR δ_C (100 MHz, CDCl$_3$): 159.3, 154.4, 149.1, 136.8, 126.8, 125.2, 123.3, 122.3, 114.6, 105.4, 66.4, 61.0, 53.5; HRMS (ESI): m/z: calcd for C$_{38}$H$_{39}$N$_6$O$_2$: 611.3129 [M+H]$^+$, found : 611.3253.

Synthesis of DAN-Bola: 50 mg (0.08 mmol) of **4** was dissolved in 4 mL of CHCl$_3$. 60 mg (0.2 mmol) of Zn(NO$_3$)$_2$.6H$_2$O was dissolved in 1 mL of MeOH and was added drop wise to the above solution. The whole solution was stirred at room temperature for 2 h during which the reaction mixture turned turbid. This mixture was filtered and the residue was washed with excess CHCl$_3$ (to remove unreacted **4**) followed by washing with cold MeOH (to remove excess Zn(NO$_3$)$_2$.6H$_2$O). The residue obtained was dried under high vacuum which weighed 50.5 mg (62% yield). ^{1}H NMR (400 MHz, D$_2$O) : δ 8.51 (d, 4H, J = 4.8 Hz), δ 7.93 (t, 4H, J = 7.6 Hz), δ 7.84 (d, 2H, J = 8.4 Hz), δ 7.54 (t, 4H, J = 6.4 Hz), δ 7.47 (m, 6H), δ 6.77 (d, 2H, J = 7.6 Hz), δ 4.66 (d, 4H, J = 16 Hz), δ 4.33 (m, 8H), δ 3.39 (br, 4H); ^{13}C NMR δ_C (100 MHz, D$_2$O): 154.59, 153.03, 147.36, 140.97, 125.97, 125.87, 124.77, 124.62, 114.39, 106.25, 64.33, 58.21, 53.45; HRMS (ESI): m/z: calcd for C$_{38}$H$_{39}$N$_6$O$_2$: 611.3129 [M+H-2Zn(NO$_3$)$_2$]$^+$, found : 611.3241.

Synthesis of **DAN-Amph** was performed according to Scheme 6.2.3 in the main text. Procedures are given below.

Synthesis of 5: 1.3 g (8.16 mmol) of 1,5 Dihydroxynaphthalene and 4 g of dry K$_2$CO$_3$ along with 30 mL of dry MeCN were stirred for 10 minutes at 50 °C. A solution of 2.19 g (9.8 mmol) of **1** and 2.3 g (9.22 mmol) of dodecylbromide in 10 mL of dry MeCN was added to the above mixture and the whole solution was refluxed for 20 h under inert atmosphere. This solution was

cooled to room temperature and MeCN was evaporated at low pressure. The obtained residue was dissolved in CHCl$_3$ and filtered to remove insoluble K$_2$CO$_3$ and the filtrate obtained was extracted with water. The organic layer was dried over Na$_2$SO$_4$ and evaporated. Compound was purified by column chromatography (Silica gel, 100-200 mesh, eluent 2% MeOH in CHCl$_3$) to obtain 790 mg of desired unsymmetrical product **5** in pure form (21% yield) along with two other symmetrical by products. ^{1}H NMR (400 MHz, CDCl$_3$, TMS) : δ 7.88 (d, 1H, *J* = 8.4 Hz), δ 7.80 (d, 1H, *J* = 8.4 Hz), δ 7.37 (d, 1H, *J* = 7.6 Hz), δ 7.34 (d, 1H, *J* = 7.6 Hz), δ 6.84 (d, 1H, *J* = 7.2 Hz), δ 6.82 (d, 1H, *J* = 7.2 Hz), δ 4.19 (t, 2H, *J* = 4.8 Hz), δ 4.12 (t, 2H, *J* = 6.4 Hz), δ 3.68 (m, 2H), δ 1.92 (m, 2H), δ 1.5 - 1.2 (m, 18H), δ 0.88 (t, 3H, *J* = 6.8 Hz); ^{13}C NMR δ$_C$ (100 MHz, CDCl$_3$): 155.95, 154.78, 154.05, 126.85, 126.53, 125.32, 124.95, 114.83, 113.72, 105.49, 68.23, 67.58, 40.26, 31.92, 29.67, 29.61, 29.44, 29.35, 29.31, 28.40, 26.27, 22.70, 14.12; MS (EI): m/z: calcd for C$_{29}$H$_{45}$NO$_4$: 471.6 [M]$^+$, found : 471.

Synthesis of 6: 20 mL of TFA was dissolved in 20 mL of DCM and stirred at 0 °C. A solution of **5** (790 mg, 1.67 mmol) in 20 mL DCM was added dropwise to the above solution over 30 minutes and the reaction mixture was stirred at 0 °C for 1 hr and room temperature for 1 hr. DCM and TFA were removed from the reaction mixture at low pressure. The obtained residue was dissolved in CH$_2$Cl$_2$ and extracted with 2 M NaOH to neutralize excess TFA in the mixture. After extraction with CH$_2$Cl$_2$ – water, organic layer was dried over anhydrous Na$_2$SO$_4$ and CH$_2$Cl$_2$ was evaporated to obtain **6** in crude form. NMR was obtained to confirm the product and it was used for the next step without further purification. ^{1}H NMR (400 MHz, CDCl$_3$, TMS) : δ 7.87 (d, 1H, *J* = 8.4 Hz), δ 7.83 (d, 1H, *J* = 8.4 Hz), δ 7.35 (m, 2H), δ 6.85 (d, 1H, *J* = 7.2 Hz), δ 6.83 (d, 1H, *J* = 7.2 Hz), δ 4.16 (t, 2H, *J* = 5.2 Hz), δ 4.12 (t, 2H, *J* = 6.4 Hz), δ 3.22 (t, 2H, *J* = 5.2 Hz), δ 1.92 (m, 2H), δ 1.6 - 1.2 (m, 18H), δ 0.88 (t, 3H, *J* = 6.8 Hz).

Synthesis of 7: 380 mg (1.02 mmol) of crude **6** was dissolved in 10 mL of DCM. 402 mg (2.45 mmol) of 2-(Chloromethyl)pyridinehydrochloride along with 20 mL of 5 M aq. NaOH solution was added to the above solution and stirred at room temperature for 15 h. The reaction mixture was extracted with DCM and organic layer was dried over anhydrous Na$_2$SO$_4$. DCM was removed at low pressure and the compound obtained was purified by silica gel column chromatography (100-200 mesh, eluent: 5% to 10% MeOH in CHCl$_3$). This was followed by size exclusion chromatography (Biobeads, S-X3; CHCl$_3$ as the solvent) to obtain pure compound in 17% yield (100 mg). ^{1}H NMR (400 MHz, CDCl$_3$, TMS) : δ 8.54 (td, 2H, *J* = 1.2 Hz, 4.8 Hz), δ 7.84 (d, 1H, *J* = 8.4 Hz), δ 7.79 (d, 1H, *J* = 8.4 Hz), δ 7.60 (m, 4H), δ 7.32 (t, 1H, *J* = 8 Hz), δ 7.30 (t, 1H, *J* = 8 Hz), δ 7.12 (m, 2H), δ 6.82 (d, 1H, *J* = 7.2 Hz), δ 6.75 (d, 1H, *J* = 7.2 Hz), δ 4.25 (t, 2H, *J* = 5.6 Hz), δ 4.12 (t, 2H, *J* = 6.8 Hz), δ 4.03 (s, 4H), δ 3.19 (t, 2H, *J* = 5.2 Hz), δ 1.91 (m, 2H), δ 1.6 – 1.2 (m, 18H), δ 0.88 (t, 3H, *J* = 7.2 Hz); ^{13}C NMR δ$_C$ (100 MHz, CDCl$_3$): 159.85, 154.88, 154.51, 149.14, 136.80, 127.01, 125.27, 125.10, 123.18, 122.15,

114.53, 114.25, 105.46, 105.41, 68.39, 66.61, 61.26, 53.60, 32.07, 29.85, 29.82, 29.79, 29.77, 29.70, 29.60, 29.50, 26.43, 22.84, 14.26; HRMS (ESI): m/z: calcd for $C_{36}H_{47}N_3O_2$: 554.3741 $[M+H]^+$, found : 554.3829.

Synthesis of DAN-Amph: 50 mg (0.09 mmol) of **7** was dissolved in 5 mL of $CHCl_3$. 30 mg (0.1 mmol) of $Zn(NO_3)_2.6H_2O$ was dissolved in 1 mL of MeOH and was added drop wise to the above solution. The whole solution was stirred at room temperature for 4 h during which the reaction color turned slightly dark. The solvent was completely removed at low pressure and the residue was redissolved in $CHCl_3$ followed by filteration (to remove excess $Zn(NO_3)_2.6H_2O$). The filtrate obtained was dried under high vacuum which weighed 50 mg (almost quantitative yield). ^{1}H NMR (400 MHz, $CDCl_3$, TMS) : δ 8.84 (br, 2H), δ 7.83 (d, 1H, $J = 8.4$ Hz), δ 7.68 (m, 3H), δ 7.41 (m, 3H), δ 7.19 (m, 3H), δ 6.87 (d, 1H, $J = 7.6$ Hz), δ 6.46 (d, 1H, $J = 7.6$ Hz), δ 4.56 (br, 2H), δ 4.38 (br, 2H), δ 4.24 (br, 2H), δ 4.14 (t, 2H, $J = 6.4$ Hz), δ 3.28 (br, 2H), δ 1.93 (m, 2H), δ 1.5 − 1.2 (m, 18H), δ 0.88 (t, 3H, $J = 6.8$ Hz); ^{13}C NMR δ_C (100 MHz, $CDCl_3$): 155.15, 153.80, 152.94, 149.10, 140.20, 127.20, 126.80, 126.38, 125.69, 125.10, 113.33, 107.70, 105.51, 105.29, 68.48, 32.07, 29.83, 29.80, 29.78, 29.70, 29.60, 29.50, 29.45, 26.43, 22.84, 14.26; HRMS (ESI): m/z: calcd for $C_{36}H_{47}N_3O_2$: 554.3741 $[M+H-Zn(NO_3)_2]^+$, found : 554.3834.

6.2.7 References and Notes

1. a) G. M. J. Schmidt, *Pure Appl. Chem.,* **1971**, *27*, 647; b) D. Braga and F. Grepioni, *Angew. Chem. Int. Ed.,* **2004**, *43*, 4002; c) A. Vidonne and D. Philp, *Eur. J. Org. Chem.,* **2009**, 593.

2. a) B. R. Bhogala, B. Captain, A. Parthasarathy and V. Ramamurthy, *J. Am. Chem. Soc.,* **2010**, *132*, 13434; b) M. Nagarathinam, A. M. P. Peedikakkal and J. J. Vittal, *Chem. Commun.,* **2008**, 5277; c) N. Shan and W. Jones, *Tetrahedron Lett.,* **2003**, *44*, 3687; d) X. Gao, T. Friščić and L. R. MacGillivray, *Angew. Chem. Int. Ed.,* **2004**, *43*, 232; e) L. R. MacGillivray, J. L. Reid and J. A. Ripmeester, *J. Am. Chem. Soc.,* **2000**, *122*, 7817.

3. T. Caronna, R. Liantonio, T. A. Logothetis, P. Metrangolo, T. Pilati and G. Resnati, *J. Am. Chem. Soc.,* **2004**, *126*, 4500.

4. a) M. Nagarathinam and J. J. Vittal, *Angew. Chem. Int. Ed.,* **2006**, *45*, 4337; b) N. L. Toh, M. Nagarathinam and J. J. Vittal, *Angew. Chem. Int. Ed.,* **2005**, *44*, 2237; c) T. Wu, L.-H. Weng and G.-X. Jin, *Chem. Commun.*, **2012**, *48*, 4435; d) I. G. Georgiev and L. R. MacGillivray, *Chem. Soc. Rev.*, **2007**, *36*, 1239.

5. a) N. S. S. Kumar, S. Varghese, C. H. Suresh, N. P. Rath and S. Das, *J. Phys.Chem. C,* **2009**, *113*, 11927; b) M. Kumar and S. J. George, *Nanoscale,* **2011**, *3*, 2130; c) M. Kumar

and S. J. George, *Chem. Eur. J.,* **2011**, *17*, 11102; d) S. Basak, J. Nanda and A. Banerjee, *Chem. Commun.*, **2013**,*49*, 6891.

6. a) B. V. V. S. P. Kumar, K. V. Rao, T. S. Soumya, S. J. George and M. Eswaramoorthy, *J. Am. Chem. Soc.,* **2013**, *135*, 10902; b) D. Jiao, J. Geng, X. J. Loh, D. Das, T.-C. Lee and O. A. Scherman, *Angew. Chem. Int. Ed.*, **2012**, *51*, 9633; c) J. F. Stoddart, *Chem. Soc. Rev.,* **2009**, *38*, 1802; d) L. Fang, M. A. Olson, D. Benítez, E. Tkatchouk, W. A. Goddard and J. F. Stoddart, *Chem. Soc. Rev.,* **2010**, *39*, 17.

7. a) L. Zhu, Y. Yi, Y. Li, E.-G. Kim, V. Coropceanu and J.-L. Brédas, *J. Am. Chem. Soc.,* **2012**, *134*, 2340; b) J. Guasch, L. Grisanti, M. Souto, V. Lloveras, J. V.-Gancedo, I. Ratera, A. Painelli, C. Rovira and J. Veciana, *J. Am. Chem. Soc.,* **2013**, *135*, 6958; c) A. Jain, K. V. Rao, U. Mogera and A. A. Sagade, S. J. George, *Chem.-Eur. J.,* **2011**, *17*, 12355; d) M. Sakai, H. Sakuma, Y. Ito, A. Saito, M. Nakamura and K. Kudo, *Phys. Rev. B,* **2007**, *76*, 045111; e) A. A. Sagade, K. V. Rao, U. Mogera, S. J. George, A. Datta and G. U. Kulkarni, *Adv. Mater.,* **2013**, *25*, 559; f) A. A. Sagade, K. V. Rao, S. J. George, A. Datta and G. U. Kulkarni, *Chem. Commun.,* **2013**, *49*, 5847; g) A. Girlando, A. Painelli, C. Pecile, G. Calestani, C. Rizzoli and R. M. Metzger, *J. Chem. Phys.,* **1993**, *98*, 7692.

8. a) S. Ghosh and S. Ramakrishnan, *Angew. Chem. Int. Ed.,* **2004**, *43*, 3264; b) S. De and S. Ramakrishnan, *Chem. Asian J.,* **2011**, *6*, 149; c) R. S. Lokey and B. L. Iverson, *Nature,* **1995**, *375*, 303.

9. a) C. Wang, Z. Wang and X. Zhang, *Acc. Chem. Res.,* **2012**, *45*, 608; b) X. Zhang and C. Wang, *Chem. Soc. Rev.,* **2011**, *40*, 94; c) K. V. Rao, K. Jayaramulu, T. K. Maji and S. J. George, *Angew. Chem. Int. Ed.*, **2010**, *49*, 4218; d) K. V. Rao and S. J. George, *Chem. Eur. J.,* **2012**, *18*, 14286; e) M. Kumar, K. V. Rao and S. J. George, *Phys. Chem. Chem. Phys.,* **2014**, *16*, 1300; f) K. V. Rao, K. Jalani, K. Jayaramulu, U. Mogera, T. K. Maji and S. J. George, *Asian J. Org. Chem.*, **2013**, *3*, 161.

10. a) Y. Liu, Y. Yu, J. Gao, Z. Wang and X. Zhang, *Angew. Chem. Int. Ed.,* **2010**, *49*, 6576; b) J. Zhang, Y. Liu, B. Yuan, Z. Wang, M. Schönhoff and X. Zhang, *Chem. Eur. J.,* **2012**, *18*, 14968.

11. a) S. K. Kim, D. H. Lee, J.-I. Hong and J. Yoon, *Acc. Chem. Res.,* **2009**, *42*, 23; b) T. Sakamoto, A. Ojida and I. Hamachi, *Chem. Commun.,* **2009**, 141.

12. a) A. Das, M. R. Molla, A. Banerjee, A. Paul and S. Ghosh, *Chem. Eur. J.,* **2011**, *17*, 6061; b) J. J. Reczek, K. R. Villazor, V. Lynch, T. M. Swager and B. L. Iverson, *J. Am. Chem. Soc.,* **2006**, *128*, 7995; c) S. A. Vignon, T. Jarrosson, T. Iijima, H.-R. Tseng, J. K. M. Sanders and J. F. Stoddart, *J. Am. Chem. Soc.,* **2004**, *126*, 9884.

13. M. Kumar, N. Jonnalagadda and S. J. George, *Chem. Commun.,* **2012**, *48*, 10948.

14. H. N. Lee, Z. Xu, S. K. Kim, K. M. K. Swamy, Y. Kim, S.-J. Kim and J. Yoon, *J. Am. Chem. Soc.,* **2007**, *129*, 3828.

15. A. Das and S. Ghosh, *Chem. Eur. J.,* **2010**, *16*, 13622.

16. a) K. Jalani, M. Kumar and S. J. George, *Chem. Commun.,* **2013**, *49*, 5174; b) M. Licchelli, A. O. Biroli and A. Poggi, *Org. Lett.,* **2006**, *8*, 915; c) E. C. Lim, *Acc. Chem. Res.,* **1987**, *20*, 8.

17. F. M. Winnik, *Chem. Rev.,* **1993**, *93*, 587..

18. a) S. V. Bhosale, S. V. Bhosale and S. K. Bhargava, *Org. Biomol. Chem.,* **2012**, *10*, 6455.; b) B. Narayan, C. Kulkarni and S. J. George, *J. Mater. Chem. C*, **2013**, *1*, 626..

19. As shown earlier in ref no. 14 adenosine phosphate binding fails to show excimeric emission.

20. a) M. Kasha, H. R. Rawls and M. A. EL-Bayoumi, *Pure Appl. Chem.*, **1965**, *11*, 371.; b) Y. Hong, J. W. Y. Lama and B. Z. Tang, *Chem. Commun.,* **2009**, 4332.

21. Y. Hong, J. W. Y. Lam and B. Z. Tang, *Chem. Soc. Rev.,* **2011**, *40*, 5361.

22. a) A. S. Tayi, A. K. Shveyd, A. C.-H. Sue, J. M. Szarko, B. S. Rolczynski, D. Cao, T. J. Kennedy, A. Sarjeant, C. L. Stern, W. F. Paxton, W. Wu, S. K. Dey, A. C. Fahrenbach, J. R. Guest, H. Mohseni, L. X. Chen, K. L. Wang, J. F. Stoddart and S. I. Stupp, *Nature,* **2012**, *488*, 485; b) S. Horiuchi and Y. Tokura, *Nature Mater.,* **2008**, *7*, 357; c) J. J. Tan, Z. Ma, W. Xu, G. Zhao, H. Geng, C. Di, W. Hu, Z. Shuai, K. Singh and D. Zhu, *J. Am. Chem. Soc.,* **2013**, *135*, 558.

23. Higher eq. of phosphate did not have any effect on the intensity of CT band.

24. E. Yashima, K. Maeda and Y. Okamoto, *Nature,* **1999**, *399*, 449.

25. a) S. J. George, R. de Bruijn, Ž. Tomović, B. V. Averbeke, D. Beljonne, R. Lazzaroni, A. P. H. J. Schenning and E. W. Meijer, *J. Am. Chem. Soc.,* **2012**, *134*, 17789; b) T. Ma, C. Li and G. Shi, *Langmuir,* **2008**, *24*, 43; c) K. P. Nandre, S. V. Bhosale, K. V. S. R. Krishna, A. Gupta and S. V. Bhosale, *Chem. Commun.*, **2013**, *49*, 5444; d) A. A. Sobczuk, Y. Tsuchiya, T. Shiraki, S.-ichi Tamaru and S. Shinkai, *Chem. Eur. J.,* **2012**, *18*, 2832.

26. a) T. Mori, Y. H. Ko, K. Kim and Y. Inoue, *J. Org. Chem,* **2006**, *71*, 3232; b) T. Mori and Y. Inoue, *Angew. Chem. Int. Ed.,* **2005**, *44*, 2582; c) Y. Tatewaki, T. Hatanaka, R. Tsunashima, T. Nakamura, M. Kimura and H. Shirai, *Chem. Asian J.,* **2009**, *4*, 1474.

27. S. Mizukami, S. Okada, S. Kimura and K. Kikuchi, *Inorg. Chem.*, 2009, **48**, 7630.

28. R. Voicu, R. Boukherroub, V. Bartzoka, T. Ward, J. T. C. Wojtyk and D. D. M. Wayner, *Langmuir*, 2004, **20**, 11713.

CURRICULUM VITAE

Mohit kumar was born on April 24, 1986 in Munger, Bihar (India). He completed his B.Sc. (Chemistry Hons.) from Sri Sathya Sai University, Puttaparthi in 2007, where he continued to finish his M.Sc degree in Chemistry in 2009. There after he joined Jawaharlal Nehru Centre for Advanced Scientific Research as a Ph.D. student in 2009, under the guidance of Prof. Subi J. George. His research work at Supramolecular Chemistry Laboratory focused on the dynamic self-assembly of chromophores and guest induced chirality in functional supramolecular polymers.